

VOL. 17 NO. 3/4 JUNE 1968  
COMPLETING VOLUME 17  
PUBLISHED MONTHLY

JOURNAL OF

# ELECTROANALYTICAL CHEMISTRY AND INTERFACIAL ELECTROCHEMISTRY

International Journal devoted to all Aspects  
of Electroanalytical Chemistry, Double Layer  
Studies, Electrokinetics, Colloid Stability, and  
Electrode Kinetics.

EDITORIAL BOARD:

- J. O'M. BOCKRIS (Philadelphia, Pa.)  
G. CHARLOT (Paris)  
B. E. CONWAY (Ottawa)  
P. DELAHAY (New York)  
A. N. FRUMKIN (Moscow)  
L. GIERST (Brussels)  
M. ISHIBASHI (Kyoto)  
W. KEMULA (Warsaw)  
H. L. KIES (Delft)  
J. J. LINGANE (Cambridge, Mass.)  
J. LYKLEMA (Wageningen)  
G. W. C. MILNER (Harwell)  
R. H. OTTEWILL (Bristol)  
J. E. PAGE (London)  
R. PARSONS (Bristol)  
C. N. REILLEY (Chapel Hill, N.C.)  
G. SEMERANO (Padua)  
M. VON STACKELBERG (Bonn)  
I. TACHI (Kyoto)  
P. ZUMAN (Prague)

E L S E V I E R



## GENERAL INFORMATION

See also Suggestions and Instructions to Authors which will be sent free, on request to the Publishers.

### *Types of contributions*

- (a) Original research work not previously published in other periodicals.
- (b) Reviews on recent developments in various fields.
- (c) Short communications.
- (d) Bibliographical notes and book reviews.

### *Languages*

Papers will be published in English, French or German.

### *Submission of papers*

Papers should be sent to one of the following Editors:

- Professor J. O'M. BOCKRIS, John Harrison Laboratory of Chemistry,  
University of Pennsylvania, Philadelphia 4, Pa. 19104, U.S.A.  
Dr. R. H. OTTEWILL, Department of Chemistry, The University, Bristol 8, England.  
Dr. R. PARSONS, Department of Chemistry, The University, Bristol 8, England.  
Professor C. N. REILLEY, Department of Chemistry,  
University of North Carolina, Chapel Hill, N. C. 27514, U.S.A.

Authors should preferably submit two copies in double-spaced typing on pages of uniform size. Legends for figures should be typed on a separate page. The figures should be in a form suitable for reproduction, drawn in Indian ink on drawing paper or tracing paper, with lettering etc. in thin pencil. The sheets of drawing or tracing paper should preferably be of the same dimensions as those on which the article is typed. Photographs should be submitted as clear black and white prints on glossy paper. Standard symbols should be used in line drawings, the following are available to the printers:



All references should be given at the end of the paper. They should be numbered and the numbers should appear in the text at the appropriate places.

A summary of 50 to 200 words should be included.

### *Reprints*

Fifty reprints will be supplied free of charge. Additional reprints (minimum 100) can be ordered at quoted prices. They must be ordered on order forms which are sent together with the proofs.

### *Publication*

The *Journal of Electroanalytical Chemistry and Interfacial Electrochemistry* appears monthly and four volumes will appear in 1968.

Subscription price: \$ 70.00 or Sfr. 304.00 per year; \$ 17.50 or Sfr. 76.00 per volume; plus postage. Additional cost for copies by air mail available on request. For advertising rates apply to the publishers.

### *Subscriptions*

Subscriptions should be sent to:

ELSEVIER SEQUOIA S.A., P.O. Box 851, 1001 Lausanne 1, Switzerland

## SUR LA VALIDITE DE L'APPROXIMATION DE NERNST EN REGIME TRANSITOIRE LINEAIRE POUR UNE ELECTRODE A DISQUE TOURNANT

JEAN MICHEL COUEIGNOUX

*Direction des Etudes et Techniques Nouvelles, 361 Avenue du Président Wilson, 93 La Plaine Saint-Denis (France)*

DANIEL SCHUHMANN

*Laboratoire d'Electrolyse du C.N.R.S., Place Aristide Briand, 92 Bellevue (France)*

(Reçu le 9 septembre, 1967)

### INTRODUCTION

Dans une précédente note<sup>1</sup>, il a été montré que la formule classique de l'impédance de diffusion, dite formule de Warburg, prévoyant une valeur infinie à fréquence nulle, n'est pas valable aux très basses fréquences. L'impédance de diffusion ne se calcule simplement, par voie analytique, qu'en admettant l'approximation de Nernst, c'est-à-dire en négligeant la convection dans une couche limite de diffusion d'épaisseur finie,  $\delta$ .

LEVICH<sup>2</sup> a montré la légitimité de cette approximation en régime permanent pour une électrode à disque tournant, mais elle restait problématique en régime transitoire linéaire, lorsqu'un courant variable de faible amplitude est superposé au courant continu.

La formule proposée dans réf. 1 a été vérifiée expérimentalement<sup>3</sup> et a permis de retrouver à 10% la valeur de  $\delta$  déterminée d'après la théorie en régime permanent. Si l'essentiel de cet écart provient de la formule, celle-ci ne peut servir qu'à titre de première approximation; l'état actuel de la technique permet en effet de mesurer des impédances électrochimiques avec une précision très supérieure. On ne peut envisager d'utiliser les propriétés du transport en régime transitoire de diffusion finie que si l'on dispose de valeurs théoriques plus précises.

D'autre part, l'impédance de diffusion dépend seulement de la valeur prise à l'électrode par la variation de concentration de la substance électro-active. La vérification de la formule ne renseigne pas sur la validité de l'approximation pour les autres points de la couche de diffusion. La détermination numérique de la distribution permet de le faire et aussi d'établir une table précise pour le spectre de l'impédance. Le présent article est consacré à la résolution de ce problème pour le seul système connu qui assure une distribution de concentration devant l'électrode, identique en tous les points de celle-ci, le disque tournant<sup>2</sup>.

### RÉSOLUTION

L'équation fondamentale pour décrire cette distribution est:

$$\frac{\partial c}{\partial t} = D \frac{\partial^2 c}{\partial y^2} - v_y \frac{\partial c}{\partial y} \quad (1)$$

la solution étant déterminée par les conditions aux limites:

$$y \rightarrow \infty; \quad c \rightarrow c_\infty \quad (2)$$

$$J = -zFD \left( \frac{\partial c}{\partial y} \right)_{y=0} \quad (3)$$

$c$  est la concentration de la substance électroactive,  $c_\infty$  sa valeur d'équilibre,  $D$  le coefficient de diffusion,  $y$  la distance à l'électrode à disque tournant,  $v_y$  la composante de vitesse suivant l'axe correspondant,  $z$  le nombre d'électrons échangés dans la réaction,  $F$  le faraday et  $J$  la densité du courant traversant l'électrode.

Pour une réaction irréversible par exemple, ou pour une grande surtension,  $J$  est donné par l'expression:

$$J = k(c)_{y=0} \exp(bV) \quad (4)$$

où  $k$  et  $b$  sont des constantes et  $V$  la surtension.

Si l'on superpose à la surtension continue  $\bar{V}$ , une tension alternative de faible amplitude,  $\Delta V = |\Delta V| \exp(j\omega t)$ , il apparaît des composantes alternatives  $\Delta J$  et  $\Delta c$  pour la densité de courant et la concentration, telles que l'on ait, d'après (1), (2), (3) et (4):

$$j\omega \Delta c = D \frac{\partial^2 \Delta c}{\partial y^2} - v_y \frac{\partial \Delta c}{\partial y} \quad (5)$$

$$y \rightarrow \infty, \quad \Delta c \rightarrow 0 \quad (6)$$

$$\Delta J = -zFD \left( \frac{\partial \Delta c}{\partial y} \right)_0 \quad (7)$$

$$\Delta J = kb(\bar{c})_{y=0} \exp(b\bar{V}) \Delta V + k(\Delta c)_{y=0} \exp(b\bar{V}) \quad (8)$$

$\bar{c}$  représentant la solution stationnaire du système (1)-(4).

D'après (8), on a:

$$\frac{\Delta V}{\Delta J} = [kb(\bar{c})_{y=0} \exp(b\bar{V})]^{-1} - \frac{1}{b(\bar{c})_{y=0}} \left( \frac{\Delta c}{\Delta J} \right)_{y=0} \quad (9)$$

$\Delta V / \Delta J$  représente l'impédance faradique et le deuxième terme de (9) sa composante appelée impédance de diffusion. Les variations avec la fréquence  $\omega/2\pi$  de cette impédance sont proportionnelles à celles de  $-(\Delta c / \Delta J)_{y=0}$  qu'il s'agit de déterminer.

On se ramène à un problème n'impliquant que des variables et des paramètres sans dimension en posant:

$$x = \left( \frac{\Omega}{\nu} \right)^{\frac{1}{2}} y, \quad Pr = \frac{\nu}{D}, \quad v_y = H(x) \cdot (\nu \Omega)^{\frac{1}{2}} \quad (10)$$

comme pour le problème en régime permanent<sup>2</sup>, puis:

$$\nu = \frac{\omega \nu}{\Omega D}, \quad -\frac{\Delta c}{\Delta J} zFD \left( \frac{\Omega}{\nu} \right)^{\frac{1}{2}} = X(x, Pr, \nu) \quad (11)$$

$\Omega$  représentant la vitesse de rotation du disque et  $\nu$  la viscosité cinématique de la solution électrolytique.

Les composantes de la vitesse du liquide au voisinage du disque tournant ont été déterminées par VON KARMAN<sup>4</sup> et COCHRAN<sup>5</sup> sous forme de développements en série suivant les puissances de  $x$  ou de  $\lambda = \exp(-Ax)$  si  $A = H(x=\infty)$ . L'évaluation numérique des coefficients a été améliorée depuis<sup>6-7</sup>. Nous avons défini  $H(x)$  à l'aide des nouvelles valeurs. En limitant les développements en  $x^6$  ou  $\lambda^6$  et en choisissant 0.66 comme abscisse de changement de formule, nous avons pu obtenir  $H$  à quelques  $10^{-5}$  près.

Posons  $X = Y - jZ$ . Le problème numérique est la résolution d'un système du 4ème ordre d'équations différentielles aux conditions aux limites et à coefficients non constants:

$$Y'' - Pr H(x) Y' - \nu Z = 0$$

$$Z'' - Pr H(x) Z' + \nu Y = 0$$

$$Y'(0) = 1; \quad Z'(0) = 0 \text{ et } Y(\infty) = Z(\infty) = 0$$

La résolution est effectuée à partir des formules de discréétisation classiques:

$$Y'_i = (Y_{i-1} + Y_{i+1})/2h \text{ et } Y''_i = (Y_{i-1} - 2Y_i + Y_{i+1})/h^2$$

On détermine d'abord l'abscisse  $x_\infty$  pour laquelle les conditions à l'infini sont vérifiées à une constante arbitrairement petite près (à  $Pr$  fixé,  $x_\infty$  varie très peu avec  $\nu$ ), puis on résout le système sur  $[0, x_\infty]$  avec le nombre de pas choisi.

L'erreur maximale est obtenue en fin de table, pour les fortes valeurs de  $\nu$ , quand la courbure à l'origine est la plus forte. Ces mêmes considérations de courbure expliquent que  $Z(0, \nu)$  soit obtenu de manière plus précise que  $Y(0, \nu)$ .

Nous avons donc étudié, pour ces grandes valeurs de  $\nu$ , comment l'erreur varie avec le nombre de pas  $N$ . Les résultats obtenus à l'ordinateur montrent que les deux composantes de l'impédance  $Y(0, \nu)$  et  $Z(0, \nu)$  varient linéairement avec  $1/N$  pour  $N$  compris entre 550 et 3,000.  $Y(0, \nu)$  est fonction croissante de  $1/N$  et  $Z(0, \nu)$  fonction décroissante.

Le calcul a donc été effectué deux fois pour toutes les valeurs de  $\nu$  et de  $Pr$  choisies, une fois avec  $N=550$  et l'autre avec  $N=900$ . L'erreur sur le résultat de l'extrapolation à  $N$  infini suivant la loi décrite peut être estimée grossièrement au cinquième de l'écart entre ce résultat et celui du calcul pour  $N=900$ .

Les solutions numériques pour  $\nu=0$  peuvent être comparées aux résultats acquis concernant le régime permanent car on peut vérifier que  $X(0, 0)$  est inversement proportionnel à  $\bar{J}$ . La théorie de LEVICH a été améliorée par NEWMAN<sup>8</sup> qui a tenu compte des trois premiers termes du développement de  $H(x)$ . Il trouve:

$$\frac{\bar{J}}{zF(C_\infty - C_0)(\Omega\nu)^{\frac{1}{2}}} = \frac{0.62048 Pr^{-\frac{2}{3}}}{1 + 0.2980 Pr^{-\frac{1}{3}} + 0.14514 Pr^{-\frac{2}{3}}} = f(Pr) \quad (12)$$

et constate un accord à mieux que 1/1000 pour  $Pr$  supérieur à 100 entre les valeurs données par (12) et celles obtenues numériquement. Nous trouvons un accord du même ordre pour  $Pr=100, 1,000$  et  $10,000$  entre les valeurs de  $X(0, Pr, 0)$ , déterminées numériquement, et celles d'après l'expression  $Pr f(Pr)^{-1}$  déduite de (12).

Il reste à comparer les valeurs numériques de  $X$  pour  $v$  différent de zéro avec les grandeurs correspondantes obtenues en adoptant l'approximation Nernst. L'épaisseur effective  $\delta$  de la couche de diffusion est définie rigoureusement par:

$zFD(C_\infty - C_0)/\bar{J}$ . On a donc:

$$\delta = \left(\frac{\nu}{\Omega}\right)^{\frac{1}{2}} X(0, Pr, 0) \quad (13)$$

L'onde de concentration est donnée par l'expression (1):

$$zFD \frac{\Delta C}{\Delta J} = \left(\frac{D}{j\omega}\right)^{\frac{1}{2}} \text{Sh}\left[\left(\frac{j\omega}{D}\right)^{\frac{1}{2}} (y - \delta)\right] / \text{Ch}\left[\left(\frac{j\omega}{D}\right)^{\frac{1}{2}} \delta\right] \quad (14)$$

D'après (13), (14) et (11), il faut donc comparer  $X(x, Pr, v)$  et:

$$X_1 = + \frac{\text{Sh}\{(jv)^{\frac{1}{2}}[-x + X(0, Pr, 0)]\}}{(jv)^{\frac{1}{2}} \text{Ch}[(jv)^{\frac{1}{2}} X(0, Pr, 0)]} \quad (15)$$

La Table 1 donne les parties réelle et imaginaire de  $X(0, Pr, v) = Y_0 - jZ_0$ ,

TABLE 1

$Pr = 100$

$v$	$Y_0 \cdot 10^4$	$\Delta Y \cdot 10^4$	$Y_1 \cdot 10^4$	$Z_0 \cdot 10^4$	$\Delta Z \cdot 10^4$	$Z_1 \cdot 10^4$
0	3723.3	0	3723.3	0	0	0
1	3710.0	0.17	3713.8	196.5	6	171.5
2	3618	1.7	3686	384	7.5	334
3	3609	4.5	3640	562	9	502
4	3528	6	3578	727	12	656
5	3429	10	3502	877	17	798
6	3320	12	3415	1007	17	928
7	3202	15	3318	1118	17	1045
8	3079	18	3215	1211	18	1148
10	2833	23	2998	1308	20	1314
12.5	2546	26	2724	1438	17	1450
15	2292	31	2467	1470	16	1524
17.5	2078	33	2236	1463	14	1552
20	1900	34	2034	1434	11	1548
22.5	1753	35	1860	1400	10	1523
25	1631	35	1712	1351	8	1487
30	1442	34	1479	1263	6	1397
35	1304	34	1309	1181	4	1303
40	1200	34	1183	1110	3	1215
45	1118	34	1088	1049	2.5	1137
50	1051	34	1013	996	2	1068
60	948	34	906	911	2	956
70	873	32	831	843	1.5	871
80	812	32	776	790	1.5	804
90	763	32	733	744	1	752
100	721	33	697	706	1	709
120	656	33	640	645	1	644
150	582	34	576	577	1	575
170	545	35	542	542	1	541
200	500	37	500	500	1	499
300	494	38	408	409	1.5	408
400	348	39	353	354	1.5	354
500	307	41	316	317	2	316

TABLE 1 (Continué)  $Pv = 1000$ 

$v$	$Y_0 \text{ } 10^4$	$\Delta Y \text{ } 10^4$	$Y_1 \text{ } 10^4$	$Z_0 \text{ } 10^4$	$\Delta Z \text{ } 10^4$	$Z_1 \text{ } 10^4$	$v$	$Y_0 \text{ } 10^4$	$\Delta Y \text{ } 10^4$	$Y_1 \text{ } 10^4$	$Z_0 \text{ } 10^4$	$\Delta Z \text{ } 10^4$	$Z_1 \text{ } 10^4$
0	1662.2	0	1662.2	0	0	0	75	1030	11.5	1104	658	5	680
0.1	1662.2	0	1662.2	1.7	0	1.5	80	990	12	1061	659	5	687
1	1662.0	0	1662.0	16.9	0	15.3	85	952	12	1020	657	4	692
2	1661.4	0	1661.5	34.3	0.4	30.6	90	917	12	981	654	3.6	693
5	1656.4	0.3	1658.0	86.0	1.6	76.3	100	854	12	910	644	3	691
7	1651.0	0.5	1654.0	119.0	2.3	106.5	110	800	12	847	630	2	683
10	1639.8	0.7	1645.5	168.2	3	151.2	130	712	12	743	600	2	657
13	1625	1	1634.2	217.5	3.5	195	150	646	12	662	567.5	1.5	624
16	1607	1.3	1620.2	264.5	4.5	237.5	170	594	12	600	538	1.5	591
20	1578	2	1598	322.5	5.5	292	200	530	12	530	498.8	1	543.7
23	1552	3	1578	361.5	5.5	330.5	220	506	12	494	476.2	0.8	515.4
26	1526	3.5	1557	401	6.5	367.5	250	470	12	453	447.0	0.7	478.0
29	1496	4	1533	436	7	402	300	423	12	405	408.3	0.7	427.9
32	1466	5	1508.5	468	7	435	350	389	12	372	378.0	0.7	389.7
35	1435	5.5	1482.5	497	7.5	465.5	400	362	12	347	353.7	0.7	360.0
38	1402	7	1455	523	7.5	494	450	340	12	328	333.2	0.4	336.4
41	1373	7	1427	546	7.5	520	500	321.5	12	312	316.2	0.4	317.3
44	1338	7	1400	567	7.5	544	700	270	12	266	267.3	0.4	266.3
47	1305	7.5	1370	585	7.5	566	1000	227	11	224	223.8	0.4	223.3
50	1272	8.5	1340	600	7	585.5	2000	162	9	158	158.3	0.4	158.1
55	1220	9	1291	621	6.5	614							
60	1168	10	1242	636	6	637							
65	1120	10	1195	647	6	655							
70	1074	11	1148	654	5.5	670							

 $Pv = 10,000$ 

$v$	$\Delta Y_0 \text{ } 10^4$	$\Delta Y \text{ } 10^4$	$Y_1 \text{ } 10^4$	$Z_0 \text{ } 10^4$	$\Delta Z \text{ } 10^4$	$Z_1 \text{ } 10^4$
0	758.7	0	758.7	0	0	0
10	758.3	0	758.4	16.4	0.3	14.5
25	755.9	0.1	756.6	40.7	0.7	36.3
50	747.7	0.3	750.4	80.2	1.3	71.8
75	734.6	0.7	740.4	113.5	2	106.0
100	717.5	1	727	152	2.5	138
125	696.5	1.5	710.5	177	3	168
150	673.5	2	691.5	209.5	3	195
175	648.5	2.5		226	3	
200	623	3	648.5	251	3	240
250	572	3.5	602.5	278.5	3	273
300	523	4.5	556	288	3	295
350	480	4.5	512	300	2.5	308.5
400	441	5	471.5	301	2	315
450	408	5	435.5	298	1.5	316.5
500	380	5	403	292	1.5	314.5
600	335	5	350	278	1	303.5
700	300	5	309	262.5	0.7	288
800	275	5	278	248.5	0.5	272.5
900	255	5	253.5	235.1	0.3	256.9
1000	238	5	234.5	223.6	0.3	242.6
1100	225	5	219.5	213.4	0.3	229.7
1200	214	5	207	204.4	0.3	218.2
1300	205	5	196.5	196.2	0.2	207.9
1500	189	5	180.5	182.7	0.2	190.5
1700	176	5	168	171.4	0.1	176.6
2000	162	5	155	158.0	0.1	160.5
2200	154	5	148	150.7	0.1	152.0
2500	144	5	140	141.3	0	141.7
2700	138	5	134	136.0	0	136.0
3000	131	5	128	129.0	0	128.7
4000	113	5	112	111.7	0	111.8
6000	92	5	91.3	91.2	0	91.3

déterminées par extrapolation à  $N$  infini, les écarts  $\Delta Y$  et  $\Delta Z$  définis plus haut et les composantes de  $X_1(0, Pr, v) = Y_1 - jZ_1$ , en fonction de  $v$ , pour les trois valeurs de  $Pr$  étudiées, 100, 1,000 et 10,000.

La valeur centrale correspond aux solutions aqueuses dans les conditions normales.  $Pr$  varie rapidement avec la température suivant une loi du type  $\exp(W/RT)$ ,  $W$  étant une constante. Le calcul effectué pour les deux autres valeurs de  $Pr$  renseigne sur la variation de comportement à prévoir aux températures supérieures ou inférieures à la normale pour les solutions aqueuses. Il permet aussi de prévoir le comportement de solutions non aqueuses, de viscosité supérieure ou inférieure à celle de l'eau.

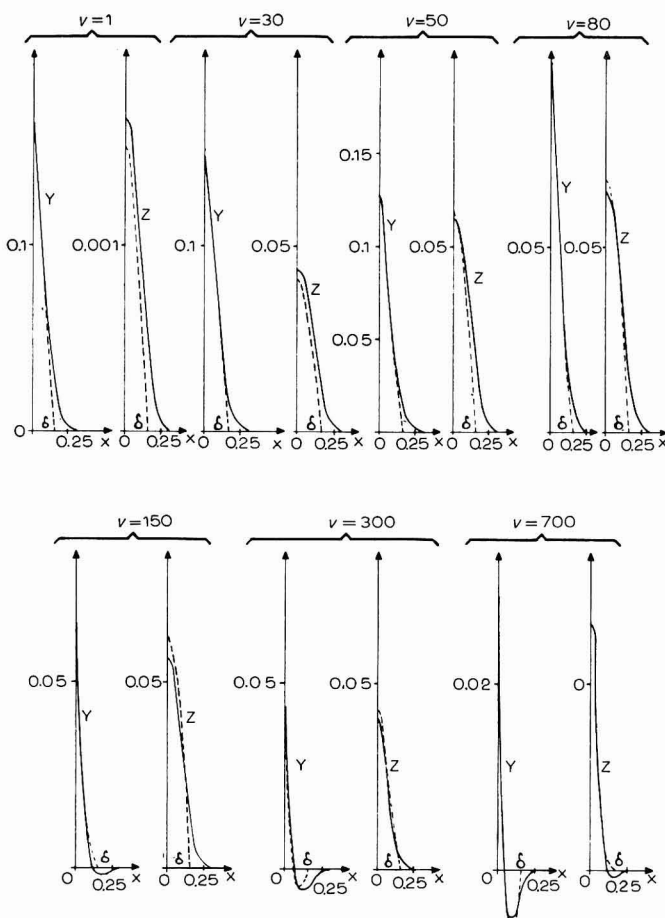


Fig. 1.

La Fig. 1 représente, pour quelques valeurs de  $v$  et pour  $Pr = 1,000$ , les variations en fonction de  $x$ , de  $X(x, Pr, v) = Y_x - jZ_x$  calculées avec  $N = 900$  et celles de  $X_1(x, Pr, v) = Y_{1x} - jZ_{1x}$  (en traits discontinus).

## DISCUSSION ET CONCLUSION

La figure montre que la distribution des variations de concentration, calculée en utilisant l'approximation de Nernst, est exacte à mieux que 10% près pour la partie réelle, et à 20% près pour la partie imaginaire, dans deux premiers tiers de la couche de diffusion au contact de l'électrode; mais cette distribution devient ensuite très erronée puisque les deux composantes ne s'annulent au millième près qu'à une distance de l'électrode égale environ au double de l'épaisseur "effective" de la couche de diffusion  $\delta$ .

La comparaison des valeurs données dans la table montre que l'erreur sur une composante de l'impédance de diffusion, entraînée par l'approximation de Nernst, est de l'ordre de 10% (sauf pour  $v=0$  naturellement); l'erreur diminue pour les plus grandes valeurs de  $v$ .

Si l'on introduit une autre fréquence réduite  $u$ , telle que  $u=vX^2(0, Pr, 0)$ , on retrouve l'expression proposée précédemment<sup>1</sup>, l'impédance étant proportionnelle à  $\text{th}(\sqrt{ju})/\sqrt{ju}$ . Le tableau permet de constater que l'erreur relative sur une des composantes de l'impédance est inférieure à 5% environ, pour les trois valeurs de  $Pr$ , dès que  $u$  est supérieur à 12.5.

Le but principal de ce travail était l'obtention d'une table donnant les composantes de l'impédance. L'erreur relative obtenue peut être estimée à quelques millièmes en milieu de table, et à un pour cent en fin de table; ceci est inférieur aux erreurs expérimentales usuelles dans l'état actuel de la technique. La table permet ainsi de prévoir, avec une précision suffisante, la variation relative de l'impédance quand la fréquence varie, à condition de connaître seulement les grandeurs qui définissent la fréquence réduite: la viscosité de la solution, la vitesse de rotation du disque et le coefficient de diffusion de la substance électroactive. Les deux premières peuvent être mesurées avec précision. La comparaison entre les valeurs issues de tables et les valeurs expérimentales pourrait inversement fournir une nouvelle méthode pour déterminer le coefficient de diffusion sans avoir besoin de connaître l'aire réactionnelle. Elle pourrait se comparer avantageusement à l'autre méthode électrochimique, basée sur la mesure de l'impédance dans le seul domaine de fréquence où la formule de Warburg est vérifiée<sup>9</sup>.

De plus, comme on peut le voir facilement, si on connaît la surtension à l'électrode et la concentration, la valeur absolue de l'impédance, pour une fréquence donnée, permettrait d'accéder précisément à cette aire réactionnelle. Une telle méthode pour déterminer ce dernier paramètre serait applicable aux systèmes à surtension de transfert négligeable devant la surtension de concentration et pourrait ainsi compléter une autre méthode proposée précédemment<sup>10</sup>.

## RÉSUMÉ

On détermine numériquement comment la composante transitoire de la concentration d'une substance électroactive varie au voisinage d'une électrode à disque tournant soumise à une polarisation comprenant une composante alternative de faible amplitude. On peut ainsi évaluer l'erreur due à l'approximation de Nernst en régime transitoire. On donne, avec une erreur inférieure au pour cent, l'impédance de diffusion en basse fréquence, sous forme de tables reliant les variations de paramètres

sans dimension. On discute la possibilité d'utiliser ces tables pour mesurer les coefficients de diffusion et les aires réactionnelles.

#### SUMMARY

The numerical variation of the transient component of the concentration of a electroactive substance in the vicinity of a rotating disc electrode subjected to a polarising potential on which is imposed an altering component of small amplitude, is determined. The error due to the Nernst approximation in a transient system can then be evaluated. The diffusion impedance at low frequencies is given, with an error of less than 1%, in the form of Tables relating the variation of the dimensionless parameters. The possibility of using these Tables for measuring diffusion coefficients and reactive areas is discussed.

#### BIBLIOGRAPHIE

- 1 D. SCHUHMANN, *Compt. Rend.*, 262 (1966) 624.
- 2 V. G. LEVICH, *Hydrodynamique Physicochimique* (en russe), trad. en anglais, Prentice Hall, 1962.
- 3 I. EPELBOIN, M. KEDDAM ET J. C. LESTRADE, *Compt. Rend.*, 263 (1966) 1110.
- 4 I. VON KARMAN, *Z. Angew. Math. Mech.*, 1 (1921) 244.
- 5 W. G. COCHRAN, *Proc. Cambridge Phil. Soc.*, 30 (1934) 365.
- 6 E. M. SPARROW ET J. L. GREGG, *J. Heat Transfer*, 81C (1959) 249.
- 7 E. R. BENTON, *J. Fluid Mech.*, 24 (1966) 781.
- 8 J. NEWMAN, *J. Phys. Chem.*, 70 (1966) 1327.
- 9 F. PERDU, Thèse, Paris, 1967.
- 10 M. BONNEMAY, E. LEVART ET E. POIRIER D'ANGE D'ORSAY, *Compt. Rend.*, 260 (1965) 2493.

*J. Electroanal. Chem.*, 17 (1968) 245-252

## CURRENT-TIME CURVES IN CONTROLLED-POTENTIAL ELECTROLYSIS AND THE RATES OF REACTIONS OF INTERMEDIATES

STEWART KARP\*† AND LOUIS MEITES‡

*Department of Chemistry, Polytechnic Institute of Brooklyn, Brooklyn, New York (U.S.A.)*

(Received August 28th, 1967)

### INTRODUCTION

The first description of the current-time curve obtained during a controlled-potential electrolysis was that written by LINGANE<sup>1,2</sup>. For the half-reaction



occurring under such conditions that the rate of the backward process is negligible, he showed that

$$-\frac{dC_o^b}{dt} = \beta_o^* C_o^b = i/nFV \quad (2)$$

where  $\beta_o^*$  is a first-order electrolytic rate constant whose value depends on both the mass-transfer coefficient of O and the rate of the electron-transfer process<sup>3</sup>, while  $C_o^b$  denotes the concentration of O in the bulk of the solution at the instant under consideration. More complex mechanisms have since been considered by others<sup>4–12</sup>, who have uniformly written

$$i = FV \sum_j \beta_j^* n_j C_j^b \quad (3)$$

to describe the total current at any instant. This draws no distinction between an electroactive substance present originally and one formed as an intermediate during the course of the reaction.

Equation (3) is an unreliable basis for predicting current-time curves, for it often misrepresents the shapes of the concentration profiles for electroactive intermediates. This has been privately recognized for some time<sup>13</sup>, but was not stated in print until MASON<sup>14</sup> did so after the completion of the present work. MASON considered the mechanism:



with special emphasis on the possibility of isolating the intermediate, I. To write eqn. (3) for this mechanism, as was done by GELB AND MEITES<sup>10</sup>, implies that in-

\* This paper is based on a thesis submitted on July 11, 1966, by STEWART KARP to the Faculty of the Polytechnic Institute of Brooklyn in partial fulfilment of the requirements for the Ph.D. degree.

† Present address: Department of Chemistry, Long Island University, Brookville, N.Y. 11548 U.S.A.

‡ To whom correspondence and requests for reprints should be addressed.

creasing the stirring efficiency will increase the current at any instant near the beginning of the electrolysis because it increases the rate of mass transfer of I from the bulk of the solution to the surface of the working electrode. In fact, it has exactly the opposite effect because it increases the rate at which I is lost to the bulk of the solution. Thus eqn. (3) here conceals the tacit assumption that the intermediate cannot undergo further reduction immediately upon being formed, but must instead be swept into the bulk of the solution before it becomes reducible. It is equivalent to supposing that the mechanism is really an ECE mechanism



in which the rate of the intervening chemical step, though much larger than the rate of bulk depletion, is so small that no appreciable fraction of the I formed at the electrode surface is converted into the reducible species, J, until after it has escaped from the diffusion layer.

For the mechanism:



eqn. (3) predicts that increasing the stirring efficiency will increase the fraction of the intermediate I that undergoes further reduction to R instead of dimerizing to yield the electrolytically inert product, D<sup>8</sup>. In fact, however, the effect is to increase the rate at which I is carried away from the electrode surface, where the further reduction can take place, into the bulk of the solution, where it is likely to dimerize before it can return to the electrode surface and be reduced. Here, too, eqn. (3) contains the tacit assumptions that the intermediate I must undergo some chemical transformation before it can be further reduced, and that the rate of this transformation is small by comparison with the rate of mass transfer across the diffusion layer.

In general, eqn. (3) will traduce the facts whenever an electroactive intermediate can be consumed to any appreciable extent, either by further reduction or by any homogeneous reaction, in the time that it requires to traverse the entire thickness of the diffusion layer and escape therefrom into the bulk of the solution. This paper presents the results obtained by examining a number of common mechanisms in the light of these ideas. No *a priori* assumptions about the rates of either heterogeneous or homogeneous processes have been made, and the extents of homogeneous reactions occurring within the diffusion layer are taken into account.

#### GENERAL CONSIDERATIONS

Three assumptions are made in the following treatment:

i. Concentration gradients within the solution being electrolyzed are confined to a thin layer of solution at the surface of the working electrode, and the volume of

this layer is so much smaller than that of the bulk of the solution that the quantity of any substance contained in it can be described by a steady-state equation.

2. Mass transfer within this layer takes place by diffusion alone.

Although these assumptions are formally equivalent to the Nernst diffusion-layer hypothesis, they are also consistent with LEVICH's proof<sup>15</sup> that the mass-transfer-controlled steady-state flux at the surface of an electrode in a turbulent solution is given by an equation of the form:

$$f_{x=0} = DAC^b/c$$

in which the parameter  $c$ , though a complex function of the kinematic viscosity and turbulence of the solution and the diffusion coefficient  $D$  of the electroactive species, none the less has the dimensions of distance, as does the "thickness",  $\delta$ , of the Nernst diffusion layer. This amounts to regarding the value of  $\delta$  as a distance that is equivalent to the thickness of the diffusion-turbulence-damping region. It appears here as a convenient algebraic symbol for an experimentally determinable parameter.

3. Because the volume of the diffusion layer is so small, the concentration gradients within it are established instantaneously, and at any instant are the same as they would be in a steady-state electrolysis with the same current and the same bulk and surface concentrations. This implies that the time required to establish the concentration gradients at the start of the electrolysis can be neglected, and that the shapes (though of course not the slopes) of the concentration profiles are invariant with time.

#### RESULTS AND DISCUSSION

##### *Case I*

To illustrate the application and consequences of these assumptions we shall first discuss the simple case represented by eqn. (1). The current at any instant is given by:

$$i = nFAk_0C_0^0 \quad (7)$$

where  $A$  is the area of the electrode,  $k_0$  is the heterogeneous rate constant for electron transfer to ions or molecules of O at the surface of the electrode, and  $C_0^0$  is the concentration of O at the electrode surface at the instant under discussion. The rate of change of the concentration of O at any place within the diffusion layer

$$\left( \frac{\partial C_0}{\partial t} \right) = D_O \left( \frac{\partial^2 C_0}{\partial x^2} \right) \quad (0 \leq x \leq \delta) \quad (8)$$

may be equated to zero by the above hypotheses, yielding the ordinary differential equation:

$$\frac{d^2 C_0}{dx^2} = 0 \quad (0 \leq x \leq \delta) \quad (9)$$

with the boundary conditions  $C_0 = C_0^0$  at  $x = 0$  and  $C_0 = C_0^b$  at  $x = \delta$ . At the electrode surface, the flux of O is equal to the rate at which it is reduced:

$$D_O A \left( \frac{d C_0}{d x} \right)_{x=0} = A k_0 C_0^0 \quad (x = 0) \quad (10)$$

while the rate at which O is transferred from the bulk of the solution into the diffusion layer is given by

$$-\left(\frac{dN_O}{dt}\right)_{x>\delta} = -V \left(\frac{dC_O^b}{dt}\right) = D_O A \left(\frac{dC_O}{dx}\right)_{x=\delta} \quad (11)$$

Combining this with eqns. (9) and (10) yields:

$$C_O^0 = \beta_O V C_O^b / (A k_O + V \beta_O) \quad (12)$$

and

$$C_O^b = C_O^{b,0} \exp\{-[\beta_O A k_O / (A k_O + V \beta_O)] t\} \quad (13)$$

where  $C_O^{b,0}$  is the initial bulk concentration of O and  $\beta_O = D_O A / V \delta$ . DELAHAY<sup>16</sup> has described the reasons why it is imprudent to attempt *a priori* calculations of the mass transfer coefficient,  $\beta_O$ , or *a posteriori* correlations of it with variations of  $D$ ,  $A$ , or the stirring efficiency, and no quantitative interpretation of it is recommended or implied here. What is demanded of it is that it be constant throughout any one electrolysis and, for some purposes such as the evaluation of  $\alpha n_a$  by means of eqn. (19), that it be reproducible from one electrolysis to another and independent of potential under otherwise identical conditions. There is much experimental proof that both of these demands are satisfied within the precisions of careful measurements in properly designed experiments, and its use for the present purpose therefore seems amply justified.

Combining eqns. (12), (13), and (7) gives

$$i = [\beta_O n F V A k_O C_O^{b,0} / (A k_O + V \beta_O)] \exp\{-\beta_O A k_O / (A k_O + V \beta_O) t\} \quad (14)$$

There are two extreme cases. On the plateau of the wave, where  $k_O \gg V \beta_O / A$ , eqns. (12) and (13) yield:

$$C_O^0 = (V \beta_O / A k_O) C_O^{b,0} \exp(-\beta_O t) \quad (15)$$

so that the concentration of O at the surface of the electrode is always extremely small, while eqn. (14) becomes

$$i = \beta_O n F V C_O^{b,0} \exp(-\beta_O t) = i^0 \exp(-\beta_O t) \quad (16)$$

At the foot of the wave, however,  $k_O \ll V \beta_O / A$ , so that eqn. (12) becomes very nearly

$$C_O^0 = C_O^{b,0} \quad (17)$$

while eqn. (14) becomes

$$i = n F A k_O C_O^{b,0} \exp\{-(A k_O / V) t\} \quad (18)$$

The potential-dependent rate constant,  $\beta_O^*$ , may be defined by writing

$$\beta_O^* = \beta_O A k_O / (A k_O + V \beta_O) \quad (19)$$

Combining this with eqn. (14) yields the familiar result

$$i = \beta_O^* n F V C_O^{b,0} \exp(-\beta_O^* t) \quad (20)$$

at any potential whatever, providing that the rate of the backward reaction remains negligible. Because

$$k_O = k_{O,s} \exp[\alpha n_a F (E^{0'}_{O,R} - E) / RT] \quad (21)$$

where  $k_{0,s}$  is the standard heterogeneous rate constant for the reduction of O, it is easily shown that

$$E = \left( E^{0'}_{O,R} + \frac{RT}{\alpha n_a F} \ln \frac{Ak_{0,s}}{V\beta_O} \right) - \frac{RT}{\alpha n_a F} \ln \frac{\beta_O^*}{\beta^* - \beta_O} \quad (22)$$

while integration of eqn. (20) yields the expected description of the quantity of electricity consumed in an exhaustive electrolysis:

$$Q_\infty = \int_0^\infty i dt = nFVC_O^{b,0} \quad (23)$$

Equation (22) provides a convenient description of the difference between the half-wave potentials in voltammetry with stirred-pool electrodes, and in polarography<sup>17,18</sup>. The former,  $E_{1/2,v}$ , is the potential at which, neglecting changes of bulk composition during the voltammetric scan, the current described by eqn. (14) is half that described by eqn. (16), both at  $t=0$ . This corresponds to  $Ak_0 = V\beta_O$  so that  $\beta_O^* = \beta_O/2$ . Combining this with eqn. (22) and with the equation<sup>19</sup> for the polarographic half-wave potential,  $E_{1/2,dme}$ , for a totally irreversible process yields, at 25°,

$$E_{1/2,dme} - E_{1/2,v} = (0.05916/\alpha n_a) \log (1.349 \beta_O V t^{1/2} / D_O^{1/4} A) \quad (24)$$

where  $t$  is the drop time at the polarographic half-wave potential.

For the reduction of 2 mM hydrogen peroxide from 0.25 F potassium dihydrogen phosphate–0.25 F disodium hydrogen phosphate,  $E_{1/2,dme}$  was found to be  $-0.71$  V vs. the silver–silver chloride–saturated potassium chloride reference electrode when  $t$  was 4.5 sec, while the value  $\alpha n_a = 0.185 \pm 0.005$  was obtained from the slopes of appropriate log plots. A number of controlled-potential electrolyses were performed with  $V = 300$  cm<sup>3</sup>,  $\beta_{H_2O_2} = 5.5 \cdot 10^{-3}$  sec<sup>-1</sup>, and  $A = 49$  cm<sup>2</sup>, and  $\beta_{H_2O_2}^*$  was found by interpolation to be half as large as  $\beta_{H_2O_2}$  at  $-1.27$  V vs. the same reference electrode. Using KERN's value<sup>20</sup> of  $1.7 \cdot 10^{-5}$  cm<sup>2</sup>/sec for the diffusion coefficient of hydrogen peroxide, eqn. (24) predicts  $E_{1/2,dme} - E_{1/2,v} = 0.44$  V, in fairly close agreement with the experimental value, 0.56 V. Closer agreement is not to be expected because  $\alpha n_a$  could rarely remain constant throughout the whole range of potentials included in such a comparison. The use of eqn. (19) provides values of  $k_0$  at potentials quite different from those attainable polarographically and might be convenient in studies of the double-layer effect.

### Case II

For the stepwise reduction represented by eqns. (4), the current at any instant is given by

$$i = FA(n_1 k_0 C_O^0 + n_2 k_1 C_I^0) \quad (25)$$

where  $k_0$  and  $k_1$  are the heterogeneous rate constants for the first and second electron-transfer steps, respectively, at the potential employed. To simplify the results we shall assume that the electrolysis is performed at a potential where O yields its limiting current, so that the reduction of O is mass-transfer-controlled. Then  $k_0 \gg V\beta_O/A$  and  $\beta_O^* = \beta_O$ . Mass transfer of I within the diffusion layer can be described by writing:

$$\frac{d^2C_I}{dx^2} = 0 \quad (0 \leq x \leq \delta) \quad (26)$$

At the electrode surface,

$$k_O C_{O^0} - k_I C_{I^0} + D_I \left( \frac{dC_I}{dx} \right)_{x=0} = 0 \quad (x = 0) \quad (27)$$

Integrating eqn. (26) with the boundary conditions,  $C_I = C_{I^0}$  at  $x = 0$  and  $C_I = C_{I^b}$  at  $x = \delta$ , and combining the result with eqn. (27) yields:

$$C_{I^0} = (A k_O C_{O^0} + \beta_I V C_{I^b}) / (A k_I + V \beta_I) \quad (28)$$

The rate of mass transfer between the bulk of the solution and the diffusion layer is given by:

$$V \frac{dC_I^b}{dt} = -D_I A \left( \frac{dC_I}{dx} \right)_{x=\delta} \quad (x = \delta) \quad (29)$$

Equations (26), (27), and (29) are analogous to eqns. (9), (10), and (11). Combining them, and setting the initial bulk concentration of I equal to zero, gives:

$$C_{I^b} = C_{O^b,0} [\exp\{-\{\beta A k_I / (A k_I + V \beta)\} t\} - \exp(-\beta t)] \quad (30)$$

and

$$i = \beta F V C_{O^b,0} \left[ n_1 \exp(-\beta t) + \frac{n_2 A k_I}{A k_I + V \beta} \exp\left(-\frac{\beta A k_I}{A k_I + V \beta} t\right) \right] \quad (31)$$

if  $\beta_O = \beta_I = \beta$ . The corresponding expression when  $\beta_O$  and  $\beta_I$  are unequal is:

$$i = F V C_{O^b,0} \left\{ \beta_O n_1 + \frac{\beta_O n_2 A k_I}{A k_I + V \beta_I} \exp(-\beta_O t) \right. \\ \left. + \frac{\beta_O \beta_I^2 n_2 A k_I V}{(A k_I + V \beta_I)[(\beta_I - \beta_O) A k_I - \beta_O \beta_I V]} \left[ \exp(-\beta_O t) - \exp\left(-\frac{\beta_I A k_I}{A k_I + V \beta_I} t\right) \right] \right\} \quad (32)$$

Defining

$$\beta_I^* = \beta_I A k_I / (A k_I + V \beta_I) \quad (33)$$

by analogy with eqn. (19), this becomes

$$i = \beta_O F V C_{O^b,0} \left( n_1 + \frac{\beta_I^*}{\beta_I} n_2 \right) \exp(-\beta_O t) \\ + \frac{\beta_O (\beta_I^*)^2 n_2 F V^2 C_{O^b,0}}{A k_I (\beta_I^* - \beta_O)} [\exp(-\beta_O t) - \exp(-\beta_I^* t)] \quad (34)$$

On the rising part of the second wave, where  $k_I$  does not greatly exceed  $V \beta_I / A$ , a plot of  $\ln i$  vs.  $t$  must be concave upward. Much of the I formed at the electrode surface will escape into the bulk of the solution during the initial part of the electrolysis, and its reduction will be slow enough to continue for some time after all of the O has been consumed. Values of  $\beta_I^*$  at various potentials in this region, obtained at identical mass-transfer rates, can be calculated from the slopes of the more slowly decaying portions of the segmented plots of  $\ln i$  vs.  $t$ . Values of  $A k_I$  can be extracted from these and used to compute  $\alpha n_a$  with the aid of eqn. (21). Letting  $Q_1$  and  $Q_2$  be the current integrals corresponding to the first and second segments, respectively, eqn. (32) yields:

$$Q_1/Q_2 = 1 + 2(\beta_O - \beta_I)A k_I/\beta_O \beta_I V \quad (35)$$

when  $n_1 = n_2$ . The ratio of the current integrals is equal to the ratio of the quantities of electricity actually consumed in the two half-reactions only if the electrolysis is performed at a potential very near the foot of the wave of I.

The current-time curves obtained during controlled-potential electroreductions of oxygen from air-saturated solutions containing 0.25 F potassium dihydrogen phosphate and 0.25 F disodium hydrogen phosphate at mercury working electrodes were in substantial agreement with these predictions. Electrolyses were performed in the cell shown in Fig. 1, which was designed so as to minimize the point-to-point

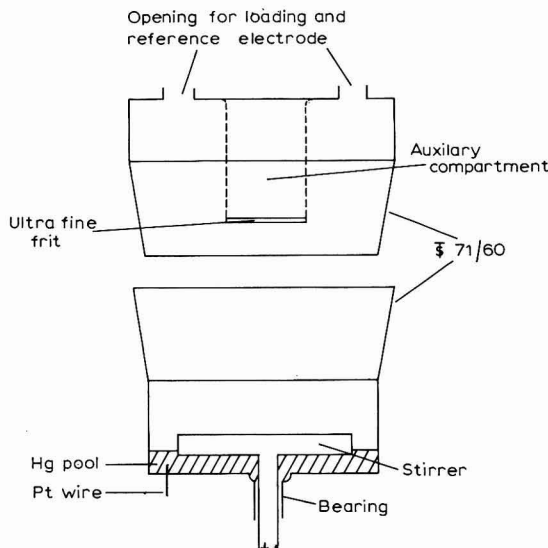


Fig. 1. All-glass cell for controlled-potential electrolysis with a mercury-pool working electrode.

variations in the potential of the working electrode that result from asymmetrical placement of the auxiliary electrode<sup>21,22</sup>. By filling the cell to the brim and stoppering it tightly, it was possible to electrolyze a known volume of solution out of contact with any gaseous phase while achieving values of  $\beta$  in the vicinity of  $1 \cdot 10^{-2} \text{ sec}^{-1}$ . In a cell of similar design that included provision for de-aeration, measurements of the potential at various different points on the surface of the working electrode, made with the stirrer blades raised about 1 cm above this surface, showed no detectable variation even with currents of 300 mA in 0.1 F potassium chloride or of 500 mA in 1 F potassium chloride.

Plots of  $\ln i$  vs.  $t$  at potentials on the rising part of the second wave had the expected segmented shape. In a typical electrolysis at  $-1.08 \text{ V}$  vs. the silver-silver chloride-saturated potassium chloride electrode, dissection in the customary way<sup>10,23</sup> gave lines having slopes of  $-6.75 \cdot 10^{-3}$  and  $-0.444 \cdot 10^{-3} \text{ sec}^{-1}$ . At more negative potentials, the slope of the second segment increased, while that of the first remained the same within experimental error, and at  $-1.49 \text{ V}$  only a single straight line was obtained. The total quantity of electricity consumed was always in good agreement with that calculated from the concentration of oxygen in these solutions ( $0.176 \pm 0.002$

$mM$ , as determined by the Winkler method) by taking  $(n_1+n_2)=4$ . On extracting values of  $Ak_{H_2O_2}$  from the slopes of the second segments of plots of  $\ln i$  vs.  $t$  and plotting  $\log Ak_{H_2O_2}$  against the potential of the working electrode, a straight line was obtained with a slope corresponding to  $\alpha n_a=0.32$  for the reduction of hydrogen peroxide. As was mentioned in connection with eqn. (24), this pertains to a range of potentials much more negative than the one in which the previously cited polarographic value was obtained; the difference between the two values is easily attributed to the double-layer effect. At  $-1.08$  V, where eqn. (35) predicts  $Q_1/Q_2=1.07$  with the appropriate values of the experimental parameters, the graphical dissection led to a value of  $1.11$ .

At a potential where both O and I yield their limiting currents,  $k_I \gg V\beta_I/A$  and  $\beta_I^*=\beta_I$ , and either eqn. (32) or eqn. (34) becomes, for  $\beta_O \neq \beta_I$

$$i = FVC_O^{b,0} \left\{ \beta_O(n_1+n_2) \exp(-\beta_O t) + \frac{\beta_O \beta_I^2 n_2 V}{Ak_I(\beta_I - \beta_O)} [\exp(-\beta_O t) - \exp(-\beta_I t)] \right\} \quad (36)$$

As the second term within the braces will be negligibly small regardless of the relative values of  $\beta_O$  and  $\beta_I$ , a plot of  $\ln i$  vs.  $t$  must be linear under these conditions, as was stated by MASON<sup>14</sup>. The corresponding result when  $\beta_O=\beta_I=\beta$  is most readily obtained from eqn. (31):

$$i = \beta FVC_O^{b,0} (n_1+n_2) \exp(-\beta t) \quad (37)$$

### Case III

If the mechanism is:



so that the intermediate I can either undergo a pseudo-first-order irreversible homogeneous transformation (for which the rate constant is  $k_2$ ) into an electrolytically inert product P, or undergo further reduction (for which the heterogeneous rate constant is  $k_I$  at the potential employed), the fundamental equations are:

$$\frac{dC_I}{dt} = D_I (\frac{d^2C_I}{dx^2}) - k_2 C_I = 0 \quad (0 \leq x \leq \delta) \quad (39)$$

within the diffusion layer,

$$k_O C_O^0 - k_I C_I^0 + D_I \left( \frac{dC_I}{dx} \right)_{x=0} = 0 \quad (x=0) \quad (27)$$

at the surface of the electrode, and

$$V \frac{dC_I^b}{dt} = -D_I A \left( \frac{dC_I}{dx} \right)_{x=\delta} - V k_2 C_I^b \quad (x=\delta) \quad (40)$$

in the bulk of the solution and at the boundary between this and the diffusion layer. To write eqn. (27) for this mechanism is equivalent to saying that, even though the reaction described by eqn. (38b) may occur to an appreciable extent in the diffusion layer as a whole, it cannot do so at the plane in immediate contact with the surface of the electrode. These equations yield:

$$C_I = \frac{C_{I^0} - C_{I^0} \cosh \alpha}{\sinh \alpha} \sinh \left( \frac{k_2}{D_I} \right)^{\frac{1}{2}} x + C_{I^0} \cosh \left( \frac{k_2}{D_I} \right)^{\frac{1}{2}} x \quad (0 \leq x \leq \delta) \quad (41a)$$

in which

$$\alpha = (k_2 D_I)^{\frac{1}{2}} A / V \beta_I \quad (41b)$$

The concentration profile is not linear. Assuming that the rate of reduction of O is mass-transfer-controlled and that  $\beta_O = \beta_I = \beta$ , we obtain:

$$C_I^b = \{H/(G-\beta)\} [\exp(-\beta t) - \exp(-Gt)] \quad (42a)$$

where

$$G = k_2 + \alpha \beta \left\{ \frac{V \alpha \beta \sinh \alpha + A k_I \cosh \alpha}{A k_I \sinh \alpha + V \alpha \beta \cosh \alpha} \right\} \quad (42b)$$

$$H = \frac{\beta C_{O^b,0}}{[k_I/(k_2 D_I)^{\frac{1}{2}}] \sinh \alpha + \cosh \alpha} \quad (42c)$$

The current at any instant is given by eqn. (25), which becomes

$$i = \beta F C_{O^b,0} \left[ \left( n_1 + \frac{n_2 k_I}{k_I + (k_2 D_I)^{\frac{1}{2}} \coth \alpha} \right) V \exp(-\beta t) + \frac{n_2 A k_I H^2}{(G-\beta)(\beta C_{O^b,0})^2} [\exp(-\beta t) - \exp(-Gt)] \right] \quad (43)$$

which of course approaches eqn. (31) as  $k_2$  approaches zero. If  $k_2$  is very small, I accumulates in the bulk of the solution and its concentration there eventually becomes larger than it is at the electrode surface, so that a plot of  $\ln i$  vs.  $t$  is concave upward as in Case II. On the other hand, if  $k_2$  is very large, little or no I can escape from the diffusion layer, and any that does escape cannot survive long enough to return to the electrode surface and undergo further reduction. Hence eqn. (33) approaches eqn. (16) as  $k_2$  increases without limit. The total quantity of electricity consumed is given by:

$$Q_\infty = F C_{O^b,0} \left[ \left( n_1 + \frac{n_2 k_I}{k_I + (k_2 D_I)^{\frac{1}{2}} \coth \alpha} \right) V + \frac{n_2 A k_I}{G \{ [k_I/(k_2 D_I)^{\frac{1}{2}}] \sinh \alpha + \cosh \alpha \}^2} \right] \quad (44)$$

Consequently, the apparent value of  $n$ , which is defined by

$$n_{app} = Q_\infty / F V C_{O^b,0} \quad (45)$$

lies between  $n_1$  and  $(n_1 + n_2)$  for all finite values of  $k_2$ , in agreement with *a priori* expectation.

#### Case IV

For the ECE mechanism described by eqns. (5), the fundamental equations for the intermediate I are:

$$D_I (d^2 C_I / dx^2) - k_2 C_I = 0 \quad (0 \leq x \leq \delta) \quad (39)$$

where  $k_2$  is the pseudo-first-order homogeneous rate constant for the transformation of I into J, within the diffusion layer,

$$k_O C_{O^0} + D_I \left( \frac{dC_I}{dx} \right)_{x=0} = 0 \quad (x = 0) \quad (46)$$

at the surface of the electrode, and

$$V \frac{dC_I^b}{dt} = -D_I A \left( \frac{dC_I}{dx} \right)_{x=\delta} - V k_2 C_I^b \quad (x = \delta) \quad (40)$$

in the bulk of the solution. Equation (40), like eqn. (27) in Case III, ignores the extent of the homogeneous reaction at the plane in immediate contact with the electrode. The bulk concentration of the intermediate I is given by:

$$C_I^b = \{h/(g-\beta)\} [\exp(-\beta t) - \exp(-gt)] \quad (47a)$$

where

$$g = k_2 + \alpha \beta \tanh \alpha \quad (47b)$$

and

$$h = \beta C_O^{b,0} / \cosh \alpha \quad (47c)$$

if the reduction of O to I is mass-transfer-controlled and if O and I have identical mass-transfer coefficients,  $\beta$ . The parameter  $\alpha$  is defined by eqn. (41b).

Meanwhile, for J

$$D_J (d^2 C_J / dx^2) + k_2 C_I = 0 \quad (0 \leq x \leq \delta) \quad (48)$$

and

$$V \frac{dC_J^b}{dt} = -D_J A \left( \frac{dC_J}{dx} \right)_{x=\delta} + V k_2 C_J^b \quad (x = \delta) \quad (49)$$

Combining eqn. (48) with the solution of eqn. (39) yields an equation relating  $C_J$  to  $x$  within the diffusion layer, and from this, together with eqn. (49) and descriptions of the time-dependences of  $C_I^b$  and  $C_I^0$ , we obtain:

$$\begin{aligned} C_J^b = & \frac{h}{\beta-g} \left[ \left( 1 - \frac{\beta \operatorname{sech} \alpha}{\beta-g} - \beta t \cosh \alpha + \frac{(\beta-k_2)t \sinh \alpha}{\alpha} \right) \exp(-\beta t) \right. \\ & \left. - \left( 1 - \frac{\beta \operatorname{sech} \alpha}{\beta-g} \right) \exp(-gt) \right] \end{aligned} \quad (50)$$

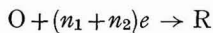
on assuming that the reduction of J, like that of O, is mass-transfer-controlled. The current at any instant is given by:

$$\begin{aligned} i = & \beta F V C_O^{b,0} \left\{ \left[ n_1 + \left( 1 - \frac{\tanh \alpha}{\alpha} \right) n_2 - \frac{n_2 \beta t}{g-\beta} \left( \beta - \frac{(\beta-k_2) \tanh \alpha}{\alpha} \right) \right] \exp(-\beta t) \right. \\ & \left. - \frac{n_2 \beta g}{(g-\beta)^2 \cosh^2 \alpha} [\exp(-\beta t) - \exp(-gt)] \right\} \end{aligned} \quad (51)$$

As expected, this yields

$$Q_\infty = (n_1 + n_2) F V C_O^{b,0} \quad (52)$$

on integration. What is of more interest is that the current-time curve may be fairly complex. Typical plots of  $\ln i$  vs.  $t$  are shown in Fig. 2. They were computed with the aid of a program written by Mr. ROBERT RODGERS, whose help is gratefully acknowledged. They approach linearity if  $k_2/\beta$  is either very large or very small. In the former case, very little J escapes from the diffusion layer and the overall half-reaction



proceeds without visible intermediate steps: although the plot of  $\ln i$  vs.  $t$  is slightly concave downward even if  $k_2/\beta$  is as large as  $10^3$ , it would seem to be too optimistic to conclude that the chemical steps could be detected under such extreme conditions. The value  $k_2/\beta = 10^2$  is a more realistic estimate of the upper limit of the value of  $k_2$  for any intervening chemical step that could be identified with certainty by this technique. At the other extreme, when  $k_2/\beta$  is very small, the transformation of I into J in the bulk of the solution will be very slow, and the reduction of J will give rise to small and slowly decreasing currents that may be difficult to separate from the continuous faradaic current at the same potential.

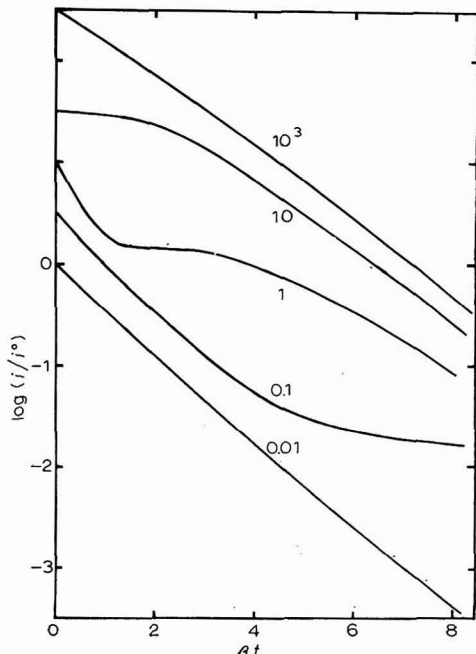


Fig. 2. Plots of  $\log (i/i_0)$  vs.  $t$  for the ECE mechanism (Case IV), calculated from eqn. (51). It is assumed that both O and J yield their limiting currents at the potential employed, that  $\beta_0 = \beta_O = \beta_J = \beta = 10^{-3}$  sec $^{-1}$ , and that  $D_O = D_I = D_J = 10^{-6}$  V/A cm $^2$ /sec. The value of  $k_2/\beta$  for each curve is given by the number beside it. The ordinate scale pertains to the lowermost curve, for which  $k_2/\beta = 0.01$ . Each successive curve above this is shifted upward 0.5 unit with respect to the ordinate axis.

#### CONCLUSIONS

Although the present treatment of Case II gives a result considerably different from that of GELB AND MEITES<sup>10</sup>, the curves in Fig. 2 for  $0.1 \leq k_2/\beta \leq 10$  in Case IV are virtually indistinguishable from theirs. It is easy to see why this is so. Taking the Nernstian definition of  $\beta$  at face value, the time,  $\tau$ , that elapses between the instant at which an ion or molecule of an electrolytically inert substance is formed at the surface of the electrode and the instant at which it escapes from the diffusion layer into the bulk of the solution, is given by:

$$\tau = D(A/\beta V)^2 \quad (53)$$

The fraction of it that can undergo any chemical reaction having the pseudo-first-order rate constant  $k$ , during this interval, may be described by writing

$$1 - \exp(-k\tau) = 1 - \exp\left[-\frac{k}{\beta} \frac{D}{\beta} \left(\frac{A}{V}\right)^2\right] \quad (54)$$

For ordinary values of  $D$ ,  $A$ , and  $V$  this indicates that only about 2 or 3% of the intermediate will be consumed in the diffusion layer even if  $k/\beta$  is as large as  $10^2$ , and in that event, as was argued in the preceding paragraph, there is only a marginal chance that the chemical reaction can be detected at all. In short, the extent of a chemical reaction in the diffusion layer is not worth taking into account if the reaction is slow enough to detect. Under such circumstances the use of eqn. (3) is fully justified.

On the other hand, as MASON showed, this is not true when the intermediate is electroactive, for the rate of its further reduction may then be so large that it can never leave the diffusion layer as eqn. (3) assumes it to do. In this case, the use of eqn. (3) is unjustifiable except at potentials very near the foot of the wave of the intermediate, where the heterogeneous rate constant for its reduction is so small that almost all of it can be carried away from the electrode surface before it can be reduced. Otherwise, the complications of the treatment outlined here must be undertaken in describing any mechanism involving successive electron-transfer steps.

#### SUMMARY

Taking into account the rates at which intermediates are reduced at the surface of the working electrode or consumed by chemical reactions in the bulk of the solution or in the diffusion layer, equations are written for the current-time curves obtained in controlled-potential electrolysis for several common consecutive and branched mechanisms, including the ECE mechanism. The implications of the traditional equation,

$$i = \sum_j \beta_j^* n_j F V C_j b,$$

where  $\beta_j^*$  is the potential-dependent electrolytic rate constant for the reduction of the  $j$ th electroactive species and  $C_j b$  is its bulk concentration, and the conditions under which this is and is not in acceptable agreement with the much more complicated exact equations obtained here, are examined in detail.

#### REFERENCES

- 1 J. J. LINGANE, *J. Am. Chem. Soc.*, 67 (1945) 1916.
- 2 J. J. LINGANE, *Electroanalytical Chemistry*, Interscience Publishers, Inc., New York, 2nd ed., 1958, pp. 224-228.
- 3 L. MEITES, *J. Electroanal. Chem.*, 7 (1964) 337.
- 4 L. MEITES AND S. A. MOROS, *Anal. Chem.*, 31 (1959) 23.
- 5 D. H. GESKE AND A. J. BARD, *J. Phys. Chem.*, 63 (1959) 1057.
- 6 A. J. BARD AND J. S. MAYELL, *J. Phys. Chem.*, 66 (1962) 2173.
- 7 S. A. MOROS AND L. MEITES, *J. Electroanal. Chem.*, 5 (1963) 105.
- 8 L. MEITES, *J. Electroanal. Chem.*, 5 (1963) 270.
- 9 A. J. BARD AND E. SOLON, *J. Phys. Chem.*, 67 (1963) 2326.
- 10 R. I. GELB AND L. MEITES, *J. Phys. Chem.*, 68 (1964) 630.
- 11 R. I. GELB AND L. MEITES, *J. Phys. Chem.*, 68 (1964) 2599.

- 12 Y. ISRAEL AND L. MEITES, *J. Electroanal. Chem.*, 8 (1964) 99.
- 13 A. J. BARD, personal communication, 1963.
- 14 J. G. MASON, *J. Electroanal. Chem.*, 11 (1966) 462.
- 15 V. G. LEVICH, *Physicochemical Hydrodynamics*, Prentice-Hall, Inc., Englewood Cliffs, N. J., 1962, pp. 139-154.
- 16 P. DELAHAY, *New Instrumental Methods in Electrochemistry*, Interscience Publishers, Inc., New York, 1954, pp. 225-227.
- 17 D. J. ROSIE AND W. D. COOKE, *Anal. Chem.*, 27 (1955) 1360.
- 18 L. SPRITZER, B. S. in Chem. Thesis, Polytechnic Institute of Brooklyn, 1967.
- 19 L. MEITES AND Y. ISRAEL, *J. Am. Chem. Soc.*, 83 (1961) 4903.
- 20 D. M. H. KERN, *J. Am. Chem. Soc.*, 76 (1954) 4208.
- 21 G. L. BOOMAN AND W. B. HOLBROOK, *Anal. Chem.*, 35 (1963) 1793.
- 22 J. E. HARRAR AND I. SHAIN, *Anal. Chem.*, 38 (1966) 1148.
- 23 H. K. FICKER AND L. MEITES, *Anal. Chim. Acta*, 26 (1962) 172.

*J. Electroanal. Chem.*, 17 (1968) 253-265



## ADSORPTION OF POTENTIAL-DETERMINING IONS AT THE SILICA-AQUEOUS ELECTROLYTE INTERFACE AND THE ROLE OF SOME CATIONS

TH. F. TADROS AND J. LYKLEMA

*Laboratory for Physical and Colloid Chemistry, De Dreijen 6, Wageningen (The Netherlands)*

(Received December 11th, 1967)

Studies on the structure of electrical double layers at phase boundaries have proved useful for a number of purposes, notably in the fields of electrode kinetics, electrokinetics and colloid stability. As a result, the properties of the double layer on a number of relatively "simple" systems like mercury or silver iodide are now reasonably well understood.

In this article some properties of the double layer on silica are discussed. Studies of this kind can be useful for soil chemistry or may provide a clue to the understanding of the operative mechanism of glass electrodes. Moreover, they have the additional advantage that the effect of the nature of the charge-carrying material on the double-layer properties can be investigated by comparing the double-layer properties with those on mercury or silver iodide.

The starting point of our discussion is a number of surface charge *vs.* pH curves. Plots of this type have been obtained previously by SEARS<sup>1</sup>, BOLT<sup>2</sup>, HESTON, ILER AND SEARS<sup>3</sup> and LI AND DE BRUYN<sup>4</sup>. In the following study these results have been extended. The specific surface area was determined by two independent methods, a counter charge–surface charge balance was set up and analytically checked and special attention has been paid to the effect of the nature of the counter ion.

### EXPERIMENTAL

#### Materials

The silica powder was a B.D.H. precipitated sample used without further treatment. Electron micrographs showed particles of irregular shape although some spherical ones could be detected. The diameter of the particles lies roughly between 500 and 1000 Å.

All salts were of AnalaR-grade and were used without further purification. Standard solutions were always checked gravimetrically. Distilled water was boiled in a nitrogen atmosphere to expel CO<sub>2</sub>, before use.

#### Surface area

This was determined by two independent methods, *viz.*, by the BET nitrogen gas adsorption method and by negative adsorption (VAN DEN HUL AND LYKLEMA<sup>5</sup>). The surface area determined by the first method was 56 m<sup>2</sup>/g whereas the surface area determined by negative adsorption of sulphate<sup>6</sup> was 35 ± 2 m<sup>2</sup>/g. This discrepancy

is not surprising because negative adsorption "sees" only the outer surface<sup>5</sup>, whereas the BET method measures all surface irregularities larger than the cross section of a nitrogen molecule. Indeed, a  $t$ -plot according to DE BOER *et al.*<sup>7</sup> (Fig. 1) shows that at relative pressures of about 0.35, surface pores of average radius below 20 Å are filled. After completion of the capillary condensation, the BET nitrogen adsorption measures an outer surface of about 40 m<sup>2</sup>/g which agrees reasonably well with the negative adsorption area. Our experimental surface charges are based on the BET (N<sub>2</sub>) inner surface area.

#### The point of zero charge (p.z.c.)

In order to calculate the absolute surface charge density of silica from the adsorption isotherms, the p.z.c. should be known. The precise location of the p.z.c. of silica is still an open question, although most authors agree that it is low; values

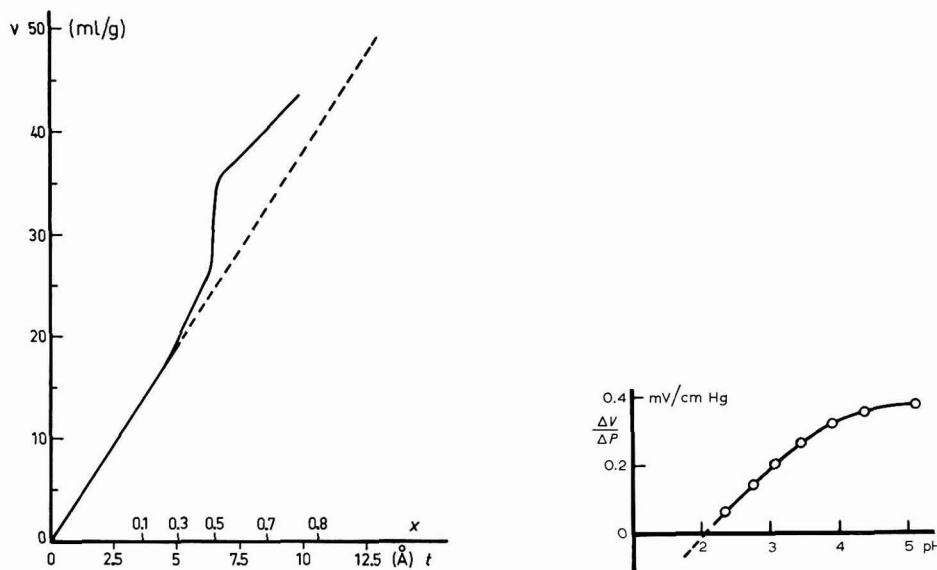


Fig. 1.  $t$ -Plot for  $\text{SiO}_2$ .

Fig. 2. Determination of the isoelectric point of  $\text{SiO}_2$  in  $10^{-3} \text{ N KCl}$  from streaming potential measurements.

between pH 1 and 3.7 have been tabulated by PARKS<sup>8</sup> for various forms of  $\alpha$ - $\text{SiO}_2$  (quartz), silica sols and gels. The wide range obtained by various authors might be due to differences in surface treatment and/or presence of cationic impurities. For the present silica powder, the isoelectric point (I.E.P.) has been established by the streaming potential technique using an apparatus essentially the same as that employed by BUCHANAN AND HEYMANN<sup>9</sup>. Streaming potentials were measured by a Keithley amplifier, Type 603. Figure 2 shows the variation as a function of pH of  $\Delta V/\Delta P$  (mV/cm Hg) for plugs in equilibrium with  $10^{-3} \text{ N KCl}$ . The values of  $\Delta V/\Delta P$  were obtained as the slopes of the straight lines obtained when  $V$  was plotted against

P. Streaming potentials could not be measured at pH-values below 2.3 owing to the large amounts of acid needed to lower the pH further. Moreover, it was not possible to measure streaming potentials in higher electrolyte concentrations (say  $10^{-2}$  or  $10^{-1} \text{ N}$ ). The data obtained when extrapolated to zero show that the I.E.P. is located at  $\text{pH} \sim 2$  in  $10^{-3} \text{ N KCl}$ . Unfortunately, the lack of data on the acid side of the I.E.P. makes the extrapolation procedure inaccurate. An indication about the shift of the p.z.c. to higher pH-values as the electrolyte concentration increases, can be obtained from the titration curves, as will be shown later.

#### *Determination of charge vs. pH curves*

The basic technique consists of the potentiometric titration of a silica suspension in aqueous electrolyte solutions ( $\text{LiCl}$ ,  $\text{NaCl}$ ,  $\text{KCl}$ ,  $\text{CsCl}$  or  $(\text{C}_2\text{H}_5)_4\text{NCl}$ ) of various ionic strengths ( $10^{-3}$ – $10^0$ ) with  $\text{H}^+$  or  $\text{OH}^-$  ions using a glass and a silver-silver chloride electrode for pH determination. A sample of electrolyte solution of the same volume and concentration as the silica sol is then titrated with acid or alkali. The difference between the amounts of  $\text{OH}^-$  or  $\text{H}^+$  ions that produce a given pH in the silica suspension and the corresponding pH in the blank sample of the electrolyte gives the amount of  $\text{OH}^-$  or  $\text{H}^+$  ions adsorbed by the surface. The surface charge is defined throughout as,

$$\sigma_0 = F(\Gamma_{\text{H}^+} - \Gamma_{\text{OH}^-}) \quad (1)$$

where  $\Gamma_{\text{H}^+}$  and  $\Gamma_{\text{OH}^-}$  are the numbers of equivalents of  $\text{H}^+$  and  $\text{OH}^-$  ions, respectively, adsorbed/ $\text{cm}^2$ .

Silver-silver chloride electrodes were prepared electrolytically<sup>10</sup>. The average reading of at least 4 electrodes was used; individual readings differed always by less than 0.2 mV. Potentials were measured at  $20 \pm 0.05^\circ$  using a Vibret pH-meter (Electronic Instruments, England) with a precision of better than 0.2 mV. The electrodes were standardised using a number of NBS buffer solutions<sup>11</sup>.

The titration vessel was completely gas-tight and nitrogen purified from  $\text{O}_2$  and  $\text{CO}_2$  was passed to avoid contamination of  $\text{CO}_2$  from the atmosphere. After each addition of acid or alkali, the e.m.f. of the cell was measured at intervals of time (5–15 min) until a constant potential ( $\pm 0.2$  mV at the low pH-value and  $\pm 0.5$  mV at the high pH-values) was measured, indicating attainment of equilibrium (within 30–60 min up to  $\text{pH} \sim 9$  and 60–90 min at higher pH-values).

In the case of tetraethylammonium chloride as the indifferent electrolyte, the reference electrode was linked to the solution via a salt bridge containing  $1.75 \text{ M }$   $\text{KNO}_3$  +  $0.25 \text{ M }$   $\text{NaNO}_3$  to suppress the liquid junction. The liquid junctions were realised with so-called van Laar capillaries<sup>12</sup>.

#### *Sodium ion adsorption measurements*

In order to check the charge balance of the electrical double layer, counter ion ( $\text{Na}^+$ ) adsorption in  $10^{-2}$  and  $10^{-3} \text{ N}$  solutions was measured simultaneously with  $\text{OH}^-$  ion adsorption.  $\text{Na}^+$  concentrations were determined with an Eppendorf flame photometer (with an accuracy of  $\pm 2\%$ ). The accuracy of the determinations depends to a large extent on the ratio between  $\text{Na}^+$  ion adsorption and that remaining in solution, so that in the higher  $\text{NaCl}$  concentrations, the amount of  $\text{SiO}_2$  used for adsorption was increased.

### *Determination of SiO<sub>2</sub>*

In a few instances, the concentration of SiO<sub>2</sub> dissolved during the titration was determined using the molybdate method described by MULLIN AND RILEY<sup>13</sup>.

### RESULTS

#### *Reversibility of the adsorption process and effect of sol concentration*

The reversibility of the adsorption process was tested by titrating a silica suspension at constant ionic strength, of an indifferent electrolyte, with OH<sup>-</sup> ions to pH  $\sim$  8.5 and reversing the titration with H<sup>+</sup> ions. Small deviations were observed which became less pronounced the more quickly the titration was carried out. These deviations could be quantitatively accounted for by dissolution of silica. Reversibility of adsorption was also realised at pH  $>$  8.5. The titration was carried out rapidly to minimise dissolution of SiO<sub>2</sub>.

The effect of sol concentration was studied by titrating different quantities of SiO<sub>2</sub> (2, 10, 20 g) in the same volume and at the same ionic strength of an indifferent electrolyte. No change in the amount of OH<sup>-</sup> adsorbed/gram of silica was observed, indicating that there is practically no effect of sol concentration upon the absolute surface charge density. BOLT<sup>2</sup>, and HESTON, ILER AND SEARS<sup>3</sup> working with "Ludox" have found the same phenomenon, although JØRGENSEN *et al.*<sup>14</sup> reported a very definite effect of the suspension concentration for quartz.

#### *Adsorption around the p.z.c.*

In principle, it is possible to obtain the p.z.c. from the intersection points of the  $\sigma_0$ -pH curves at various salt concentrations. However, owing to the low accuracy and the low slope in the acid region, these intersection points are not distinct. The best results have been obtained by studying the pH change upon addition of salt. We found a p.z.c. of about 3 in  $10^{-2} \rightarrow 10^{-1}$  N KCl and a p.z.c. of about 2.5 in  $10^{-3} \rightarrow 10^{-2}$  N KCl. The increase with increasing salt concentration would suggest specific adsorption of the chloride ion. The p.z.c. thus obtained is also somewhat higher than the I.E.P. obtained with the streaming potential technique.

The following  $\sigma_0$ -pH plots are based upon a p.z.c. of 3 (BOLT<sup>2</sup> used a value of 3.7 and LI AND DE BRUYN<sup>4</sup> used a value below 2). Fortunately, the precise value accepted for the p.z.c. is not critical for the calculated surface charge since around the p.z.c. the isotherms are almost horizontal.

#### *Adsorption isotherms*

Examples of  $\sigma_0$ -pH curves are given in Figs. 3 and 4 for KCl and (C<sub>2</sub>H<sub>5</sub>)<sub>4</sub>NCl as indifferent electrolytes. Plots with other alkali counter ions are of the same nature as that for KCl. Comparison of the present data in NaCl with the corresponding data obtained by BOLT<sup>2</sup> on "Ludox" and by LI AND DE BRUYN<sup>4</sup> on quartz, shows clearly that the surface charge density on the present silica sample is much higher, although the qualitative appearance of the curves is similar. The specific surface charge density can in some cases reach a magnitude of the order of 150  $\mu\text{C}/\text{cm}^2$  (see Fig. 3). With tetraethylammonium chloride as the indifferent electrolyte, the surface charge density is much lower (Fig. 4). Moreover, the distinct differences in surface charge density with change in electrolyte concentration were not observed in this

case. The effect of the nature of the indifferent electrolyte on the specific charge density is shown in Fig. 5 for 0.1 N concentrations. This figure shows a distinct increase of  $\text{OH}^-$  adsorption on silica in the order,  $(\text{C}_2\text{H}_5)_4\text{N}^+ < \text{Li}^+ < \text{Na}^+ < \text{K}^+ < \text{Cs}^+$ , at least at  $\text{pH} > 7$  (the data for NaCl are not shown in Fig. 5, to avoid overcrowding). The sequence for the alkali-metal cations agrees well with the order of affinity of

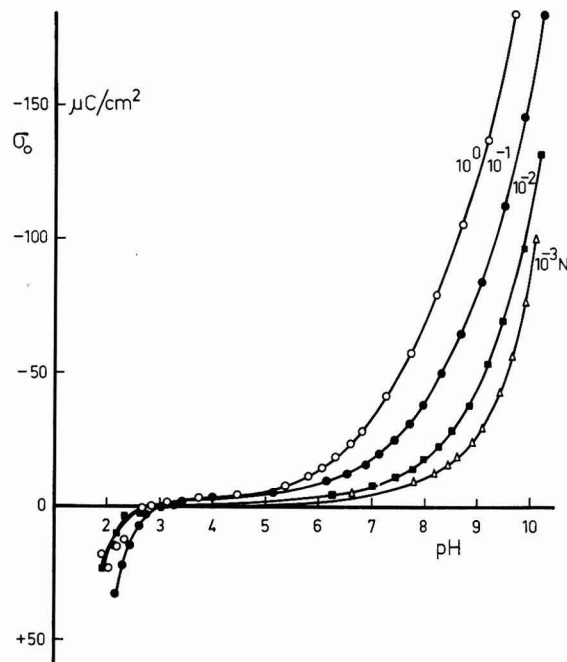


Fig. 3. Surface charge density as a function of pH for  $\text{SiO}_2$  in four different conc. of KCl.

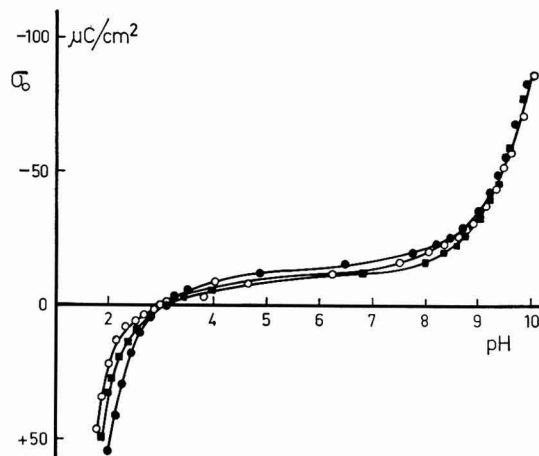


Fig. 4. Surface charge density as a function of pH for  $\text{SiO}_2$  in: (○),  $10^{-1}$ ; (●),  $10^{-2}$ ; (■),  $10^{-3}$  N  $(\text{C}_2\text{H}_5)_4\text{NCl}$ .

silica gel for these cations obtained by TIEN<sup>15</sup> using an accurate radiotracer method for the determination of equilibrium selectivity coefficients. The same sequence also has been obtained by LYKLEMA<sup>16</sup> on silver iodide, and by GRAHAME on mercury<sup>17</sup> although in the last case the differences were extremely small.

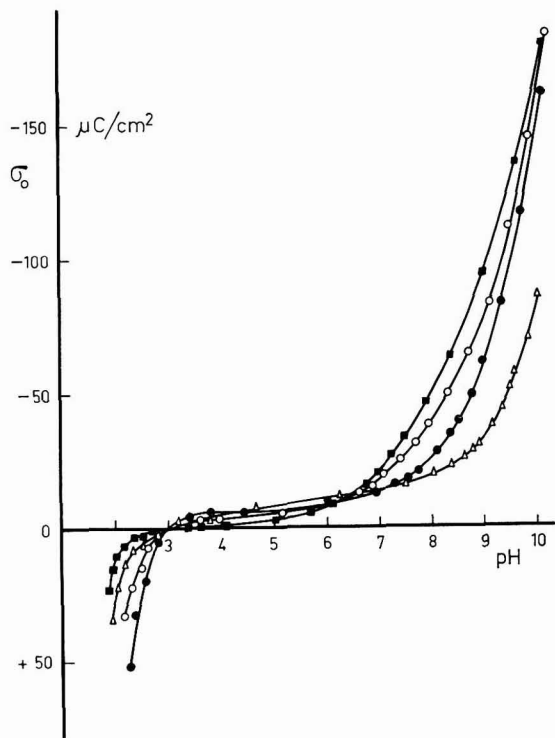


Fig. 5. Effect of the nature of the indifferent electrolyte on the surface charge density of  $\text{SiO}_2$  in  $10^{-1} \text{ N}$ : (■),  $\text{CsCl}$ ; (○),  $\text{KCl}$ ; (●),  $\text{LiCl}$ ; ( $\Delta$ ),  $(\text{C}_2\text{H}_5)_4 \text{NCl}$ .

#### DISCUSSION

The counter charge–surface charge balance can be illustrated from the data in Table I which shows the relative adsorption of  $\text{OH}^-$  and  $\text{Na}^+$  at various pH-values in  $10^{-3}$  and  $10^{-2} \text{ N}$   $\text{NaCl}$  together with the amount of silicate in solution (calculated on the assumption of the formation of monosilicic acid and taking the equilibrium value for its dissociation— $K = 10^{-9.8}$ —according to ROLLER AND ERVIN<sup>18</sup>). The negative adsorption of chloride, which, as will be shown below, is a small quantity especially in  $10^{-3}$  or  $10^{-2} \text{ N}$  electrolyte concentration, is neglected. The data of Table I indicate that the sum of  $(\text{Na}^+)_{\text{ads}}$  and  $(\text{silicate})$  compares well with the  $(\text{OH}^-)_{\text{ads}}$ .

Since the surface charge is partly neutralised by positive adsorption of counter ions and partly by negative adsorption of co-ions, it is of interest to calculate the contribution of each and compare the negative adsorption with that calculated from

theory and that directly measured. If the method described by LYKLEMA<sup>16</sup> is followed, the ionic components of charge at the silica/aqueous electrolyte interface can be calculated from the relation:

$$\sigma_{\pm} = \pm F \int \left( \frac{\partial \sigma_0}{\partial \mu_s} \right)_{pH} - \frac{\sigma_0}{2} \quad (2)$$

where  $\mu_s$  is the chemical potential of the indifferent salt and  $F$  is the Faraday. The integral can be evaluated from the data of Fig. 3 and this enables the calculation of  $\sigma_+$  and  $\sigma_-$  at various pH-values. It was found that the value of the negative adsorption

TABLE I

CHARGE BALANCE OF THE ELECTRICAL DOUBLE LAYER AT THE SILICA/AQUEOUS ELECTROLYTE INTERFACE

pH	(OH <sup>-</sup> ) <sub>ads.</sub>	(Na <sup>+</sup> ) <sub>ads.</sub>	(silicate)	(Na <sup>+</sup> ) + (silicate)
	(mequiv./g SiO <sub>2</sub> · 10 <sup>2</sup> )			
<i>10<sup>-3</sup> N NaCl</i>				
8.25	2.3	2.3	0	2.3
8.55	5.6	4.1	0.5	4.6
9.07	11.7	9.5	2.2	11.7
9.23	18.5	15.1	4.2	19.3
9.66	30.1	24.7	9.3	34.0
<i>10<sup>-2</sup> N NaCl</i>				
7.62	3.1	2.7	0	2.7
8.37	9.7	8.7	0.1	8.8
8.89	19.3	17.3	0.4	17.7
9.60	38.3	35.4	2.1	37.5

in 10<sup>-1</sup> N KCl increases with increase of pH and then attains a constant value of about 2  $\mu$ C/cm<sup>2</sup>, which agrees well with the corresponding value predicted by the diffuse double-layer theory (1.85  $\mu$ C/cm<sup>2</sup>). The directly measured negative adsorption gave a value of 1.62  $\mu$ C/cm<sup>2</sup>. The relative low value of the negative adsorption surface area is, of course, due to this relatively low value.

The process by which the surface charge is established on silica can be regarded as occurring in two steps: surface hydration with the formation of silanol groups followed by adsorption of OH<sup>-</sup> and dehydration leaving the surface with a negative charge. The data of Fig. 3 show that the surface charge thus formed is extremely high. At high pH and high salt content, there is no end to the charge build-up, the OH<sup>-</sup> adsorption increases beyond the surface density of silanol groups. On the other hand, electrokinetic potentials of silica are not particularly high<sup>4,19,20</sup>, neither is the SiO<sub>2</sub> sol particularly stable<sup>21</sup>. Consideration of these facts indicates that it is likely that negative groups as well as counter ions are present inside the solid matrix. Thus, most of the charge is neutralised by cations penetrating into the pores of the gel structure. The extent of penetration depends mainly on the size of the counter ion. This picture agrees well with the experimentally observed effect of the nature of the counter ion (Fig. 5) on OH<sup>-</sup> adsorption, which shows a distinct increase in the order, (C<sub>2</sub>H<sub>5</sub>)<sub>4</sub>N<sup>+</sup> < Li<sup>+</sup> < Na<sup>+</sup> < K<sup>+</sup> < Cs<sup>+</sup>. Thus, from a simple geometric effect which depends upon the ion volume as compared to pore size, it is expected that Cs<sup>+</sup> ions with the

smallest hydrated radius do fit better than  $\text{Li}^+$  ions, which have the highest hydrated radius of the alkali-metal cations\*. With a big and more hydrophobic cation such as  $(\text{C}_2\text{H}_5)_4\text{N}^+$ , which cannot fit readily in the pores of the gel structure, the surface charge density is much lower. This assumption does not mean that the possibility of a specific interaction effect between the cation and the negative  $\text{SiO}^-$  sites, *i.e.*, specific adsorption in the usual sense, is completely ruled out. This would also work in the order,  $\text{Li}^+ < \text{Na}^+ < \text{K}^+ < \text{Cs}^+$ . However, analysis by LYKLEMA<sup>23</sup> for the charge and potential distribution inside the gel has shown that the penetration depth (*i.e.*, ion volume as compared to pore size) is dominant over specific adsorption and this explains why there are only small differences in specificity between alkali-metal cations on mercury although quite a pronounced specificity is found in the case of a porous surface like that of  $\text{SiO}_2$ .

Tetraethylammonium chloride shows an anomalous behaviour in that the surface charge density is nearly independent of the salt concentration (Fig. 4). This can be due to the presence of  $(\text{C}_2\text{H}_5)_4\text{N}^+$  cations in the Stern layer only (*i.e.*, not inside the surface gel layer), leading to a lower potential,  $\psi_\delta$ , in the diffuse layer, and hence to a relatively insensitivity to changes in electrolyte concentration. Electrocapillary measurements on the surface of mercury using tetramethyl-, tetraethyl-, tetrapropyl- and tetrabutylammonium iodides<sup>24</sup> have shown evidence of specific adsorption of all tetraalkylammonium ions. Tetramethylammonium iodide also behaved anomalously on mercury. In the first place, the surface excesses were lower than those of the potassium ion on the cathodic side. In the second place, the surface excess was independent of the concentration of the salt, as was observed with tetraethylammonium ion on silica. It has been postulated<sup>24</sup> that the independence of surface excess with respect to the concentration of tetramethylammonium iodide on mercury might be due to the opposing effect of specific adsorption of cation and anion. However, the relatively low surface charge in the presence of tetraethylammonium salt is probably due to the fact that  $(\text{C}_2\text{H}_5)_4\text{N}^+$  ions are too big and/or too hydrophobic to diffuse into the surface pores.

In conclusion, the double-layer properties of silica are distinctly different from those on silver iodide or on mercury. The surface charge density is extremely high; nevertheless,  $\psi_\delta$  is comparable to  $\psi_\delta$  on silver iodide and this suggests that surface and counter charge extend inside the pores of the gel structure. This makes the affinity of cations to the gel largely dependent upon ion-volume to pore-size ratio a trend which was also observed experimentally.

#### ACKNOWLEDGEMENTS

The authors are indebted to Dr. H. J. VAN DEN HUL for the determination of the surface area of the silica sample and to the Ministry of Foreign Affairs, The Hague, for a fellowship for TH. F. TADROS during his study in the Netherlands.

\* TIEN<sup>15</sup> interpreted the interaction of alkali-metal cations with silica gel in terms of ion-exchange, physical adsorption and ion-exclusion from the small pores. However, MAATMAN<sup>22</sup> did not accept this picture since he calculated from a geometric effect, found at any solution-solid interface, that hydrated  $\text{Al}^{3+}$  ions of radius 5–7 Å (much larger than any of the alkali-metal cations) could enter the pores of all the gels used.

## SUMMARY

The specific surface charge density on a silica sample of known surface area was measured in the presence of LiCl, NaCl, KCl, CsCl and  $(\text{C}_2\text{H}_5)_4\text{NCl}$ . A counter-ion charge-surface charge balance was set up and analytically checked. Above pH  $\sim 7$ , the surface charge is much higher than on silver iodide or mercury. At a fixed ionic strength it increases in the order,  $(\text{C}_2\text{H}_5)_4\text{N}^+ < \text{Li}^+ < \text{Na}^+ < \text{K}^+ < \text{Cs}^+$ . Notwithstanding the high surface charge, the diffuse double-layer potential,  $\psi_0$ , is not particularly high. An explanation of these facts has been given on the basis of the presence of negative groups and cation penetration inside the pores of the gel layer, the extent of which depends to a large extent on the cation volume as compared to pore size.

## REFERENCES

- 1 G. W. SEARS, *Anal. Chem.*, 28 (1956) 1981.
- 2 G. H. BOLT, *J. Phys. Chem.*, 61 (1957) 1166.
- 3 W. M. HESTON JR., R. K. ILER AND G. W. SEARS, *J. Phys. Chem.*, 64 (1960) 147.
- 4 H. C. LI AND P. L. DE BRUYN, *Surface Sci.*, 5 (1966) 203.
- 5 H. J. VAN DEN HUL AND J. LYKLEMA, *J. Colloid Interface Sci.*, 23 (1967) 500.
- 6 H. J. VAN DEN HUL AND J. LYKLEMA, *J. Am. Chem. Soc.*, accepted for publication.
- 7 J. H. DE BOER, B. C. LIPPENS, B. G. LINSEN, J. C. P. BROEKHOFF, A. VAN DEN HEUVEL AND TH. J. OSINGA, *J. Colloid Interface Sci.*, 21 (1966) 405.
- 8 G. A. PARKS, *Chem. Rev.*, 65 (1965) 177.
- 9 A. S. BUCHANAN AND E. HEYMANN, *Proc. Roy. Soc. (London)*, A 195 (1948) 150.
- 10 A. S. BROWN, *J. Am. Chem. Soc.*, 56 (1934) 646.
- 11 R. G. BATES, *Determination of pH. Theory and Practice*, John Wiley and Sons, New York, 1964.
- 12 J. A. W. VAN LAAR, Thesis, State University of Utrecht, Netherlands, 1952.
- 13 J. B. MULLIN AND J. P. RILEY, *Anal. Chim. Acta*, 21 (1955) 162.
- 14 S. S. JØRGENSEN AND A. T. JENSEN, *J. Phys. Chem.*, 71 (1967) 745.
- 15 H. T. TIEN, *J. Phys. Chem.*, 69 (1965) 350.
- 16 J. LYKLEMA, *Trans. Faraday Soc.*, 59 (1963) 418.
- 17 D. C. GRAHAME, *J. Electrochem. Soc.*, 98 (1951) 343; 99 (1952) 273.
- 18 P. S. ROLLER AND G. ERVIN JR., *J. Am. Chem. Soc.*, 62 (1940) 461.
- 19 D. P. BENTON AND G. A. H. ELTON, *Trans. Faraday Soc.*, 49 (1953) 1213.
- 20 V. PRAVDIĆ AND M. MIRNIK, *Croat. Chem. Acta*, 30 (1958) 113.
- 21 R. K. ILER, *The Colloid Chemistry of Silica and Silicates*, Cornell University Press, Ithaca, N.Y., 1955, chap. V.
- 22 R. W. MAATMAN, *J. Phys. Chem.*, 69 (1965) 3196.
- 23 J. LYKLEMA, to be published.
- 24 M. A. V. DEVANATHAN AND M. J. FERNANDO, *Trans. Faraday Soc.*, 58 (1962) 368.



## RELAXATION OF ELECTRODE PROCESSES WITH SIMULTANEOUS CONSIDERATION OF DOUBLE-LAYER CHARGING AND FARADAIC CURRENT. PART I

KAREL HOLUB\*

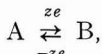
Department of Chemistry, New York University, New York, N. Y. 10003 (U.S.A.)

(Received October 17th, 1967)

It was recently shown by DELAHAY<sup>1-3</sup> that for some non-steady-state and periodic electrode processes it is necessary to take into account simultaneously the charging of the double layer and the faradaic process in the solution of the mass transfer problem. It was also pointed out that the current for non-steady-state or periodic electrode processes generally cannot be separated into two independent parts corresponding to the charging of a supposedly ideal polarized electrode and to the pure faradaic process, respectively. The combination of these ideas, which were originally developed on the basis of the model of charge separation and recombination, was formulated in the form of three general conditions for transport (diffusion) equations<sup>1,2</sup>. An explicit form of the time-derivatives appearing in the general equations was suggested<sup>4</sup> for small perturbations and was applied to the derivation of the electrode admittance with either any exchange current<sup>5</sup> or with an infinite exchange current<sup>6</sup>. The same approach is followed here for non-steady-state electrode processes, and the differences between this treatment and previous classical treatments are noted. A general formulation is given for any galvanostatic or potentiostatic perturbation of small amplitude and is then applied to specific cases.

### FORMULATION AND SOLUTION

We consider a charge transfer reaction,



which takes place on a plane electrode. The oxidized (A) and reduced (B) species correspond, for example, to a metal ion in solution and the metal in the corresponding amalgam-electrode. The formulation will be given for this case but the results are also valid when both A and B are soluble in solution. Furthermore, we assume that the changes of concentrations of constituents other than A and B can be completely neglected in the analysis of the mass transfer process.

The time-derivatives of the surface excesses ( $\Gamma$ ) of A and B, which appear in the first two general equations<sup>1,2</sup> are expressed as linear functions of the potential  $E$  and the concentrations of A and B for a finite exchange current (irreversible process). The time-derivative of the charge density of the electrode ( $q$ ), which appears

\* Present address: J. Heyrovsky Polarographic Institute, Opletalova 25, Prague 1, Czechoslovakia.

in the third general equation, is expressed in the same fashion. This procedure is identical with that already applied in the derivation of the electrode admittance<sup>5,6</sup> and is justified for perturbations of sufficiently small amplitude. Only two of the above three variables are needed when the exchange current is infinite (reversible processes). The expression for the faradaic current is linearized, as usual, and so is the Nernst equation for small perturbation. The model of the double layer used here is only approximate. Thus, surface excesses are reduced to surface concentrations; the surface concentrations are assumed to be in equilibrium with the potential and the volume concentrations at the electrode.

The problem is formulated for galvanostatic or potentiostatic pulse of any shape (for which the linear approximation is adequate) by the system of diffusion equations

$$\partial c_a / \partial t = D_a \partial^2 c_a / \partial x^2, \quad \partial c_b / \partial t = D_b \partial^2 c_b / \partial x^2 \quad (1)$$

with the following initial and boundary conditions

$$t=0: \quad i=0, \quad E=E_{eq} \quad (2)$$

$$\begin{aligned} t=0, \quad & \pm x \geq 0 \\ t>0, \quad & \pm x \rightarrow \infty \end{aligned} \left\{ \begin{array}{l} c_a = c_a^s \text{ (sign +)}, \quad c_b = c_b^s \text{ (sign -)}, \end{array} \right. \quad (3)$$

$$t>0, \quad x=0: \quad \begin{cases} D_a \partial c_a / \partial x - D_b \partial c_b / \partial x = d(\Gamma_a + \Gamma_b) / dt, \\ i = zF(-D_a \partial c_a / \partial x + d\Gamma_a / dt) + dq / dt, \end{cases} \quad (4)$$

$$t>0, \quad x=\infty: \quad \begin{cases} i_f = zF(-D_a \partial c_a / \partial x + d\Gamma_a / dt). \end{cases} \quad (5)$$

Notations are quite conventional and need not be described except that to note that  $i$  is the experimental current and  $i_f$  represents the faradaic current. Equation (5) is not a boundary condition for potentiostatic perturbation; this equation allows the calculation of  $i$  once the diffusion problem is solved. Note also that eqn. (6) holds for a finite exchange current; it should be replaced by the linearized Nernst equation for an infinite exchange current.

The time-derivatives of the  $\Gamma$ 's and  $q$  are introduced as indicated before, and the following notation is introduced: one of the superscripts,  $a$ ,  $b$ ,  $\eta$ , on the symbols  $q$ ,  $\Gamma_a$ ,  $\Gamma_b$  indicates the first derivatives of  $q$ ,  $\Gamma_a$  or  $\Gamma_b$  with respect to  $c_a$ ,  $c_b$  or  $E$ . The symbol  $\Gamma_\Sigma$  represents  $\Gamma_a + \Gamma_b$ , and the superscript notation is also used for  $\Gamma_\Sigma$ . Moreover, we have one of the two conditions

$$t>0: \quad i=i(t) \quad \text{for galvanostatic process} \quad (7)$$

$$t>0: \quad E=E(t) \quad \text{for potentiostatic process.} \quad (8)$$

We introduce

$$a = (c_a - c_a^s) / c_a^s, \quad b = (c_b - c_b^s) / c_b^s, \quad I = i \Gamma_\Sigma^a / (zFD_a c_a^s), \quad (9a)$$

$$v = v\eta, \quad v = (\partial c_b / \partial E) / c_b^s = -zF/(RT), \quad \eta = E - E_{eq}, \quad (9b)$$

$$T = D_a t / (\Gamma_\Sigma^a)^2, \quad X = x / \Gamma_\Sigma^a \quad (10)$$

and obtain (see list of symbols in Appendix)

$$\partial a / \partial T = \partial^2 a / \partial X^2, \quad \partial b / \partial T = D \partial^2 b / \partial X^2 \quad (11)$$

$$T=0: \quad v=0, \quad I=0, \quad (12)$$

$$\begin{aligned} T=0, \quad \pm X \geq 0 \\ T>0, \quad \pm X \rightarrow \infty \end{aligned} \left\{ \begin{array}{l} a=0 \text{ (sign +), } b=0 \text{ (sign -), } \\ \end{array} \right. \quad (13)$$

$$T>0, X=0: \quad \frac{\partial a/\partial X - RD\partial b/\partial X}{I = -\partial a/\partial X + h_a da/dT + h_b db/dT + h_\eta dv/dT}, \quad (14)$$

$$T>0, X=0: \quad \begin{cases} \frac{\partial a/\partial X - RD\partial b/\partial X}{I = -\partial a/\partial X + h_a da/dT + h_b db/dT + h_\eta dv/dT}, \\ -\sigma\partial a/\partial X + \sigma_a da/dT + \sigma_b db/dT + \sigma_\eta dv/dT = i_a a + i_b b + i_\eta v. \end{cases} \quad (15) \quad (16)$$

The following relationships hold in eqn. (16) for irreversible processes

$$\sigma=1, \quad \sigma_j=\gamma_j (j=a,b,\eta), \quad i_j (j=a,b,\eta) \text{ as defined in the Appendix.} \quad (17)$$

For reversible processes one has in eqn. (16)

$$\sigma=0, \quad \sigma_j=0 (j=a,b,\eta), \quad i_a=-\mu, \quad i_b=1, \quad i_\eta=-1. \quad (18)$$

If we choose for  $q$ ,  $\Gamma_a$ ,  $\Gamma_b$ , the independent variables  $c_a(x=0)$  and  $E$ , we have  $\gamma_a=1$ ,  $\gamma_b=0$ ,  $k_b=0$ ,  $h_b=0$ .

Finally we have

$$I=I(T) \quad \text{for galvanostatic, or} \quad (19)$$

$$v=v(T) \quad \text{for potentiostatic perturbation.} \quad (20)$$

The system for eqns. (11)–(20), as solved by Laplace transform, yields:

$$\hat{v} = \frac{\hat{I}}{\sqrt{s}} \cdot \frac{\begin{vmatrix} 1+\sqrt{s} & r+\gamma\sqrt{s} \\ \sigma\sqrt{s}+s\sigma_a-i_a & s\sigma_b-i_b \end{vmatrix}}{\begin{vmatrix} h_\eta\sqrt{s} & 1+h_a\sqrt{s} & h_b\sqrt{s} \\ \epsilon\sqrt{s} & 1+\sqrt{s} & r+\gamma\sqrt{s} \\ s\sigma_\eta-i_\eta & \sigma\sqrt{s}+s\sigma_a-i_a & s\sigma_b-i_b \end{vmatrix}}, \quad (21)$$

where  $\hat{v}$  and  $\hat{I}$  are Laplace transform of  $v$  and  $I$ , respectively. Equation (21) can also be written in the form:

$$\hat{v} = \hat{I} s^{-\frac{1}{2}} \sum_{j=0}^3 b_j s^{j/2} / \sum_{j=0}^4 a_j s^{j/2} \quad (22)$$

where the coefficients  $a_j$  and  $b_j$  can be easily calculated from eqn. (21).

For galvanostatic perturbations we write on the basis of eqn. (22) the expression for  $\hat{v}$  in a more convenient form

$$\hat{v} = \hat{I} \sum_{j=1}^4 [A_j / (\sqrt{s}(r_j + \sqrt{s}))] \quad (23)$$

where  $A_j$  can be calculated from eqn. (22) and from the  $r_j$ 's which are the roots of the equation:

$$a_4^{-1} \sum_{j=0}^4 a_j x^j = 0. \quad (24)$$

The expression for  $\hat{I}$  for potentiostatic perturbations, can be written on the basis of eqn. (22) in the form:

$$\hat{I} = \hat{v} [B_2 s + B_1 \sqrt{s} + B_0 + \sum_{j=1}^3 C_j / (\sqrt{s} + \varrho_j)], \quad (25)$$

where the coefficients  $B_k$  ( $k=0,1,2$ ) can be found from eqn. (22) and  $\varrho_j$  are the roots of the equation:

$$b_3^{-1} \sum_{j=0}^3 b_j x^j = 0. \quad (26)$$

Formulas (23) and (25) can be used directly for obtaining  $v$  and  $I$  for any admissible (within the linear approximation) kind of perturbation. The inverse transform is in general

$$v = \sum_{j=1}^4 A_j \int_0^T I(T-\tau) \exp(r_j^2 \tau) \operatorname{erfc}(r_j \sqrt{\tau}) d\tau, \quad (27)$$

$$\begin{aligned} I = & B_2 \frac{dv}{dT} + B_1 \frac{d}{dT} \int_0^T \frac{v(\tau)}{\sqrt{\pi(T-\tau)}} d\tau + B_0 v + \\ & \sum_{j=1}^3 C_j \int_0^T v(T-\tau) \left[ \frac{1}{\sqrt{\pi\tau}} - \varrho_j \exp(\varrho_j^2 \tau) \operatorname{erfc}(\varrho_j \sqrt{\tau}) \right] d\tau \end{aligned} \quad (28)$$

#### REVERSIBLE ELECTRODE PROCESSES

To treat reversible electrode processes we use eqn. (21) in which the coefficients are those of eqn. (18). We also introduce the following notation

$$\varrho = r/(1+\mu r), P = (1+\mu r)/(1+\mu\gamma), N = r/(\gamma + \varepsilon), M = 1/h_a, L = h_\eta MN/P\varrho \quad (29)$$

and deduce a result similar to eqn. (22), namely

$$\hat{v} = \hat{I} \frac{MN}{P\varrho} \cdot \frac{1}{\sqrt{s}} \cdot \frac{P + \sqrt{s}}{L(P + \sqrt{s})\sqrt{s} - (N + \sqrt{s})(M + \sqrt{s})}. \quad (30)$$

We obtain explicit forms of this result for potentiostatic or galvanostatic perturbations by introducing any particular perturbation and deducing the resulting inverse Laplace transform. Thus, for a galvanostatic perturbation

$$\hat{v} = \hat{I} \cdot K_1 \left\{ \frac{1}{\sqrt{s(x_1 + \sqrt{s})}} + \frac{K_2}{\sqrt{s(x_2 + \sqrt{s})}} \right\}, \quad (31)$$

where

$$K_1 = MN(x_1 - P)/[P\varrho(L - 1)(x_1 - x_2)], \quad K_2 = K_1(P - x_2)/(x_1 - P) \quad (32)$$

with

$$x_1 = \dot{p} + \sqrt{\dot{p}^2 + Q}, \quad x_2 = \dot{p} - \sqrt{\dot{p}^2 + Q}, \quad (33)$$

$$\dot{p} = [PL - (M + N)]/[2(L - 1)], \quad Q = MN/(L - 1). \quad (34)$$

Similarly we have for potentiostatic perturbation

$$\hat{I} = \hat{v}(P\varrho/MN) \{s(L - 1) - L_1\sqrt{s} - L_2\sqrt{s}/(P + \sqrt{s})\} \quad (35)$$

where

$$L_1 = M + N - P, \quad L_2 = MN - PL. \quad (36)$$

#### APPROXIMATE SOLUTION

We now solve the system of eqns. (11)–(20) by changing it into a system of integral equations. This approach yields an approximate solution which allows direct comparison with results obtained in classical treatments for  $T \rightarrow 0$ . This approach

also enables one to estimate an error affecting the approximate solution. We first introduce some notations. Let  $A$  be a matrix with  $n$  rows and  $n$  columns of elements  $a_{kl}$  and  $\mathbf{x}$  a column vector of  $n$  components  $x_k$ . The quantities  $\|A\|_\infty$  and  $\|\mathbf{x}\|$  are defined by the following

$$\|A\|_\infty = \max_k \sum_{l=1}^n |a_{kl}|, \quad \|\mathbf{x}\| = \max_k |x_k| \quad (37)$$

If we have<sup>7</sup> another vector  $\mathbf{y}$  given by the equation  $\mathbf{y} = A \cdot \mathbf{x}$  then

$$\|\mathbf{y}\| \leq \|A\|_\infty \|\mathbf{x}\|.$$

Let  $f(T)$  and  $g(T)$  be two functions, and let us denote by  $f*g$  the convolution integral

$$f*g = \int_0^T f(T-\tau)g(\tau)d\tau. \quad (38)$$

In the same way we denote by  $A*\mathbf{x}$  a vector  $\mathbf{y}$  whose components  $y_k$  are defined by the relation:

$$y_k = \sum_{l=1}^n a_{kl}*x_l \quad (39)$$

If  $a_{kl}$  or  $x_l$  is a function of  $t$ , we define  $\|A\|$  and  $\|\mathbf{x}\|$  for a given interval,  $0 \leq t \leq T$ , by the relations:

$$\|\mathbf{x}\| = \max_{t, 0 \leq t \leq T} |x_t|, \quad \|A\| = \max_{k, 0 \leq t \leq T} |a_{kt}*\mathbf{1}|. \quad (40)$$

Similarly we have for  $\mathbf{y} = A*\mathbf{x}$   $\|\mathbf{y}\| \leq \|A\| \cdot \|\mathbf{x}\|$ . By noting that we have at  $x=0$  (see eqns. (11) and (13))

$$(\partial a / \partial X)*\mathbf{1} = -(\mathbf{1} / \sqrt{\pi T})*a, \quad D(\partial b / \partial X)*\mathbf{1} = \sqrt{D / (\pi T)}*b \quad (41)$$

we deduce from eqn. (41) and eqns. (11)–(20) the following system of integral equations:

$$h_\eta v + h_a a + h_b b = I*\mathbf{1} - (\mathbf{1} / \sqrt{\pi T})*a, \quad (42a)$$

$$\varepsilon v + a + \gamma b = -(\mathbf{1} / \sqrt{\pi T})*a - (r / \sqrt{\pi T})*b, \quad (42b)$$

$$\gamma_\eta v + \gamma_a a + \gamma_b b = -(\mathbf{1} / \sqrt{\pi T})*a + i_a*a + i_b*b + i_\eta*v. \quad (42c)$$

We now write this system of integral equations in matrix formulation in a way which is different for galvanostatic and potentiostatic perturbations. In the first case,  $I*\mathbf{1}$  is a known function and we must find  $v$  (and perhaps also  $a$  and  $b$ ). Conversely,  $v$  is a known function for potentiostatic perturbation and we have to obtain  $I$  (and perhaps also  $a$  and  $b$ ). It is seen immediately from eqn. (42) that we can directly calculate just  $I*\mathbf{1}$  but this does not matter so much because we can measure the integral of the current during the perturbation just as well as the current. We denote for a galvanostatic perturbation

$$\mathbf{x} = \begin{pmatrix} v \\ a \\ b \end{pmatrix}, \quad \mathbf{y} = \begin{pmatrix} I*\mathbf{1} \\ 0 \\ 0 \end{pmatrix}, \quad (43)$$

$$G = \begin{pmatrix} h_\eta & h_a & h_b \\ \varepsilon & I & \gamma \\ \gamma_\eta & \gamma_a & \gamma_b \end{pmatrix}, \quad H_1 = \begin{pmatrix} 0 & I & 0 \\ 0 & I & \gamma \\ 0 & I & 0 \end{pmatrix}, \quad K_2 = \begin{pmatrix} 0 & 0 & 0 \\ 0 & 0 & 0 \\ i_\eta & i_a & i_b \end{pmatrix}, \quad (44)$$

$$K_1 = (I/\sqrt{\pi T}) \cdot H_1. \quad (45)$$

The system of integral equations can be now written in the simple form:

$$Gx = y - (K_1 - K_2) * x \quad (46)$$

where  $x$  is the vector to be found. If we assume that  $\det(G) \neq 0$ , we get from eqn. (42)

$$x = z - (M_1 - M_2) * x \quad (47)$$

$$\text{where } z = G^{-1}y, \quad M_j = G^{-1}K_j \quad (j=1,2). \quad (48)$$

Writing  $Ax$  instead of  $(M_1 - M_2) * x$ , we can rewrite the system of integral equations in eqn. (42) in the simplest form:

$$x = z - Ax. \quad (49)$$

The solution can be written simply in the form

$$x = (E - A + A^2 - A^3 + \dots + (-1)^n A^n + \dots)z \quad (50)$$

where  $E$  is the unit operator, *i.e.*,

$$Ex = z \quad (51)$$

If we take a finite number of terms in eqn. (50) we obviously obtain only an approximate solution<sup>7,8</sup>. If we take for example, as  $n$ -th approximate solution

$$x^{(n)} = (E - A + A^2 \mp \dots + (-1)^n A^n)z \quad (52)$$

we obtain the estimate of error

$$\|x - x^{(n)}\| \leq \frac{\|M_1 - M_2\|^{n+1}}{1 - \|M_1 - M_2\|} \|z\|. \quad (53)$$

This estimate is only useful for  $\|M_1 - M_2\| < 1$  but, in a given case, the solution of eqn. (50) is valid for any  $\|M_1 - M_2\|$ .

For the zero-th approximation,  $x^{(0)} = z$ , we deduce an estimate of the error from eqn. (53)

$$\|x - z\| \leq \sqrt{\frac{4T}{\pi}} \cdot \|G^{-1}H_1\| \frac{1 + \sqrt{\frac{\pi T}{4}} \cdot \frac{\|M_2\|_\infty}{\|G^{-1}H_1\|_\infty}}{1 - \left[ \sqrt{\frac{\pi T}{4}} \|G^{-1}H_1\|_\infty + T \|M_2\|_\infty \right]} \|z\|. \quad (54)$$

It is immediately seen from eqn. (54) that for  $T \rightarrow 0$  we have  $x \rightarrow z$  with an error of order  $\sqrt{T}$ .

For potentiostatic perturbation we write

$$x = \begin{pmatrix} I * I \\ a \\ b \end{pmatrix}, \quad y = \begin{pmatrix} -h_\eta v \\ -\varepsilon v \\ i_\eta * v - \gamma_\eta v \end{pmatrix} \quad (55)$$

$$K_2 = \begin{pmatrix} 0 & 0 & 0 \\ 0 & 0 & 0 \\ 0 & i_a & i_b \end{pmatrix}, \quad G = \begin{pmatrix} -I & h_a & h_b \\ 0 & I & \gamma \\ 0 & \gamma_a & \gamma_b \end{pmatrix} \quad (56)$$

and we use the same  $K_1$  and  $H_1$  as in eqns. (44) and (45).

We can now apply eqns. (45)–(54), keeping in mind that  $\mathbf{x}$ ,  $\mathbf{y}$ ,  $K_2$  and  $G$  have different meaning than for a galvanostatic perturbation. In particular, we have for the zero-th approximation,  $\mathbf{x}^{(0)} = \mathbf{z} = G^{-1}\mathbf{y}$ , and we again find that the exact solution  $\mathbf{x} \rightarrow \mathbf{x}^{(0)}$  with an error of order  $1/T$ .

#### COMPARISON WITH CLASSICAL FORMULATION

We compare the present results with those derived by the classical approach, *i.e.*, without consideration of the double-layer charging in the analysis of the diffusion problem. We start with galvanostatic perturbations, and let the current, in our notations, be given by

$$I = \begin{cases} 0, & T < 0 \\ I_1, & T > 0. \end{cases} \quad (57)$$

The dimensionless potential is given in classical treatment (denoted by the subscript  $c$ ) by:

$$v_c \rightarrow I_1 T \cdot (1/k_\eta) \quad \text{for } T \rightarrow 0. \quad (58)$$

We have in our treatment

$$v_N \rightarrow I_1 T \cdot (b_3/a_4) \quad \text{for } T \rightarrow 0 \quad (59)$$

where the subscript  $N$  indicates our values, and  $b_3$  and  $a_4$  are coefficients from eqn. (22). The limit given by eqn. (59) can easily be obtained from eqn. (27) after integration and by noting that

$$\sum_{j=1}^4 A_j = b_3/a_4.$$

The limit can be deduced directly from  $\mathbf{x} \rightarrow G^{-1}\mathbf{y}$  where  $\mathbf{x}$  and  $\mathbf{y}$  are defined by eqn. (43) and  $G$  by eqn. (44). We deduce from eqns. (58) and (59)

$$v_N : v_c = (k_\eta b_3/a_4) : 1 = \frac{k_\eta \begin{vmatrix} I & \gamma \\ \gamma_a & \gamma_b \end{vmatrix}}{\begin{vmatrix} k_\eta & k_a & k_b \\ \epsilon & I & \gamma \\ \gamma_\eta & \gamma_a & \gamma_b \end{vmatrix}} : 1. \quad (60)$$

The potential in both treatments is a linear function of time, but the proportionality constant is different. This coefficient, in the classical formulation, is proportional to  $1/k_\eta$ , *i.e.*, to the reciprocal of  $dq/dE$ . In the present treatment, the coefficient is proportional to a more involved expression containing  $d\Gamma/dc$ 's,  $dq/dc$ 's and  $dq/dE$ .

Results for large  $T$ 's are obtained as follows. We deduce from eqns. (23) or (27) and (57)

$$v = I_1 \sum_{j=1}^4 \frac{A_j}{r_j^2} \left[ -I + \frac{2r_j/T}{\sqrt{\pi}} + \exp(r_j^2 T) \operatorname{erfc}(r_j/T) \right]. \quad (61)$$

The last term approaches zero when  $\min_j |r_j| \sqrt{T} \gg 1$ , and the asymptotic expression of  $v$  is

$$v = I_1 \left\{ \frac{2}{\sqrt{\pi}} \frac{i_b - i_a r}{i_\eta r} \sqrt{T} - \frac{b_1 a_0 - b_0 a_1}{a_0^2} \right\} \quad (62)$$

This formula gives the same relation for the proportionality coefficient between  $\eta$  and  $t^{\frac{1}{2}}$  as the classical theory<sup>9</sup>. The difference between the two treatments appears in the constant term which is now more involved than in the classical treatment. It should be kept in mind that eqn. (61) is valid only when  $v$  is so small to be in the region of the linear approximation. Thus, there is a lower and upper value of  $T$  for which eqn. (62) can be applied. Finally, we note that eqn. (61) is formally the sum of four terms whereas the corresponding classical formula contains only two terms.

We now turn to the potentiostatic perturbation for which we have

$$v = \begin{cases} v_0, & T > 0; \quad v_0 \text{ is a constant} \\ 0, & T \leq 0. \end{cases} \quad (63)$$

The classical treatment<sup>10-13</sup> yields, with the present notations,

$$I = v_0 i_\eta \exp(i_\alpha^2 T) \operatorname{erfc}(-i_\alpha \sqrt{T}) \quad (64)$$

where

$$i_\alpha = i_a - i_b/r \quad (65)$$

The present treatment yields on the basis of eqns. (63) and (25) or (29)

$$I = v_0 \left\{ \frac{B_1}{\sqrt{\pi T}} + B_0 + \sum_{j=1}^3 \frac{C_j}{Q_j} [1 - \exp(Q_j^2 T) \operatorname{erfc}(Q_j \sqrt{T})] \right\}. \quad (66)$$

$|I| = \infty$  for  $T = 0$ , both for eqns. (64) and (66). The basic difference between eqns. (64) and (66) lies in the first term on the right-hand side of eqn. (66). We have for  $T \rightarrow 0$

$$I_N \rightarrow v_0 B_1 / \sqrt{\pi T} \quad (67)$$

whereas the classical solution gives

$$I_c \rightarrow v_0 i_\eta \quad (68)$$

We pursue the comparison between present and classical treatments by considering reversible processes. The classical treatment yields, with the present notations,

$$\hat{I} = \hat{v}(-\sqrt{s}\varrho + sk_\eta) \quad (69)$$

The limit according to classical theory

$$v_c \rightarrow I_1 T / k_\eta, \quad \text{for } T \rightarrow 0 \quad (70)$$

holds for a galvanostatic pulse [eqn. (57)] whereas the present treatment leads to

$$v_N \rightarrow I_1 (MN/P\varrho) \{T/(L-1)\}, \quad \text{for } T \rightarrow 0. \quad (71)$$

Both results coincide in the functional dependence on  $T$  at  $T \rightarrow 0$ , but the proportionality constants are different. Both treatments coincide completely for  $\min_j |x_j| \sqrt{T} \gg 1$ .

The formulas for potentiostatic perturbations and reversible processes are:

$$I_c = -v_0 \varrho / \sqrt{\pi T}, \quad (72)$$

$$I_N = -v_0 \varrho (PL_1/MN) \{ 1/\sqrt{\pi T} + (L_2/L_1) \exp(P^2 T) \operatorname{erfc}(P\sqrt{T}) \}. \quad (73)$$

Both  $I_c$  and  $I_N$  depend on  $T^{-\frac{1}{2}}$  at times  $T \ll L_1/(\sqrt{\pi} L_2)$  but with different proportionality coefficients.  $I_c$  and  $I_N$  coincide for  $P\sqrt{T} \gg 1$ .

Comparison between this and the previous approaches can also be extended to coulostatic perturbations<sup>14</sup>. We first substitute in eqn. (27) the coulostatic perturbation  $Q_1 \delta(T)$  for  $I(T)$  and integrate from  $-o$ . Thus

$$v = \sum_{j=1}^4 A_j Q_1 \exp(r_j^2 T) \operatorname{erfc}(r_j \sqrt{T}). \quad (74)$$

The classical formula is, with present notations,

$$v = \frac{Q_1}{k_\eta(z_1 - z_2)} \sum_{j=1}^2 Z_j \exp(z_j^2 T) \operatorname{erfc}(z_j \sqrt{T}) \quad (75)$$

where

$$Z_1 = -z_2, \quad Z_2 = z_1, \quad (76)$$

$$z_1 = -i_\alpha/2 + \sqrt{(\frac{1}{2}i_\alpha)^2 - i_\eta/k_\eta}, \quad z_2 = -i_\alpha/2 - \sqrt{(i_\alpha/2)^2 - i_\eta/k_\eta} \quad (77)$$

We again find the same behavior for  $T \rightarrow o$  but the constants to which the solutions converge are not the same. They are in the ratio  $(b_3/a_4):(1/k_\eta)$ , for this and classical treatments, respectively. The formulas coincide in the limits for  $\min_j |r_j| \sqrt{T} \gg 1$  and  $\min_j |z_j| \sqrt{T} \gg 1$ .

#### CONCLUSION

The classical formulation of non-steady-state electrode processes and the present approach compare as follows:

The same kind of functional dependence of the response on time prevails for short time in some cases but the proportionality constants are not the same, *e.g.*, linear overvoltage-time dependence for a single-step galvanostatic perturbation. Hence, previous analyses in which  $dq/dE$  was deduced by extrapolation to  $t=o$  for a galvanostatic step-perturbation are in error whenever conditions are such that the classical analysis is not applicable. In other cases, *e.g.*, potentiostatic single-step perturbation, the functional time-dependence is not the same in both treatments. Thus, the present treatment yields a current which varies inversely with time whereas the classical formulation gives a current approaching a constant for time tending to zero.

Both treatments coincide for long times, *i.e.*, whenever charging of the double layer becomes of little significance. Conditions for coincidence in the solutions are for irreversible processes:

$$\min_j |r_j| T^{\frac{1}{2}} \gg 1 \text{ for a single-step galvanostatic perturbation (see } r_j \text{ in eqn. (24))};$$

$$\min_j |\varrho_j| T^{\frac{1}{2}} \gg 1 \text{ for a single-step potentiostatic perturbation (see } \varrho_j \text{ in eqn. (26)).}$$

In the time-domain between the above two extreme regions the functional time-dependence is different in the two treatments.

## ACKNOWLEDGEMENT

This work was supported by the National Science Foundation. The author wishes to express his thanks to Professor DELAHAY for suggesting this work and for his kind interest in it.

## SUMMARY

Non-steady-state electrode processes are analyzed with simultaneous consideration of the double-layer charging and the faradaic process in the treatment of the diffusion problem. A treatment is given from a unified point of view for any galvanostatic or potentiostatic perturbation. The general formulas thus derived are applied to galvanostatic and potentiostatic step-perturbations and to one type of coulostatic perturbation. Differences from the results previously derived by the classical approach were found in the region where the double-layer charging influences the overall process.

## APPENDIX

*List of symbols*

All parameters given below are dimensionless with the exception of quantity  $\nu$  and the parameters  $f_1, f_2, f_3$ . The superscript,  $a, b$  or  $\eta$ , on the quantities  $q, \Gamma_a, \Gamma_b, \Gamma_\Sigma$ , denotes the partial derivative of these quantities with respect to  $c_a, c_b$ , or  $E$ . The subscript  $\Sigma$  denotes the sum  $\Gamma_\Sigma = \Gamma_a + \Gamma_b$ .

- |               |  |
|---------------|--|
| $D$           | $= D_b/D_a$  |
| $f_1$         | $= (\partial i_f / \partial c_a) / (zF)$             |
| $f_2$         | $= (\partial i_f / \partial c_b) / (zF)$             |
| $f_3$         | $= (\partial i_f / \partial E) / (zF)$               |
| $h_j$         | $= \gamma_j + k_j \quad (j=a,b,\eta)$                |
| $i_a$         | $= f_1 \Gamma_\Sigma^a / D_a$                        |
| $i_b$         | $= R f_2 \Gamma_\Sigma^a / D_a$                      |
| $i_\eta$      | $= f_3 \Gamma_\Sigma^a / (\nu c_a^s D_a)$            |
| $I$           | $= i \Gamma_\Sigma^a / (zFD_a c_a^s)$                |
| $k_a$         | $= q^a / (zF \Gamma_\Sigma^a)$                       |
| $k_b$         | $= R q^b / (zF \Gamma_\Sigma^a)$                     |
| $k_\eta$      | $= q^\eta / (zF \nu \Gamma_\Sigma^a c_a^s)$          |
| $Q$           | $= \Delta q / (zF c_a^s \Gamma_\Sigma^a)$            |
| $r$           | $= R/D$  |
| $R$           | $= c_b^s / c_a^s$                                    |
| $\varepsilon$ | $= \Gamma_\Sigma^\eta / (\nu c_a^s \Gamma_\Sigma^a)$ |
| $\gamma$      | $= R \Gamma_\Sigma^b / \Gamma_\Sigma^a$              |

$$\begin{aligned}\gamma_a &= \Gamma_a^a / \Gamma_{\Sigma}^a \\ \gamma_b &= R \Gamma_a^b / \Gamma_{\Sigma}^a \\ \gamma_\eta &= \Gamma_a^\eta / (\nu c_a^s \Gamma_{\Sigma}^a) \\ h_j &= \gamma_j + k_j \quad (j=a,b,\eta) \\ \mu &= (\partial c_b / \partial c_a) / R = 1 \\ \nu &= (\partial c_b / \partial E) / c_b^s = -zF / (RT)\end{aligned}$$

Constants  $a_j$  and  $b_j$  in eqn. (22)

The constants  $a_j$ ,  $b_j$  appearing in eqn. (22) can be derived from eqn. (21). These constants are listed here.

$$a_0 = -i_\eta r$$

$$\begin{aligned}a_1 &= - \begin{vmatrix} h_\eta & h_a & h_b \\ 0 & 1 & \gamma \\ i_\eta & i_a & i_b \end{vmatrix} + \varepsilon i_b - \gamma i_\eta \\ a_2 &= - \begin{vmatrix} h_\eta & h_a & h_b \\ \varepsilon & 1 & \gamma \\ i_\eta & i_a & i_b \end{vmatrix} - r(h_\eta - \gamma_\eta) \\ a_3 &= \begin{vmatrix} h_\eta & 1 & h_b \\ \varepsilon & 1 & \gamma \\ \gamma_\eta & 1 & \gamma_b \end{vmatrix} - r(h_\eta \gamma_a - h_a \gamma_\eta) \\ a_4 &= \begin{vmatrix} h_\eta & h_a & h_b \\ \varepsilon & 1 & \gamma \\ \gamma_\eta & \gamma_a & \gamma_b \end{vmatrix}\end{aligned}$$

$$b_0 = i_a r - i_b$$

$$b_1 = \gamma i_a - (r + i_b)$$

$$b_2 = \gamma_b - (r \gamma_a + \gamma)$$

$$b_3 = \gamma_b - \gamma \gamma_a$$

## REFERENCES

- 1 P. DELAHAY, *J. Phys. Chem.*, 70 (1966) 2067.
- 2 P. DELAHAY, *ibid.*, 70 (1966) 2373.
- 3 P. DELAHAY AND G. G. SUSBIELLES, *ibid.*, 70 (1966) 3150.
- 4 P. DELAHAY, K. HOLUB, G. G. SUSBIELLES AND G. TESSARI, *ibid.*, 71 (1967) 779.
- 5 K. HOLUB, G. TESSARI AND P. DELAHAY, *ibid.*, 71 (1967) 2612.
- 6 P. DELAHAY AND K. HOLUB, *J. Electroanal. Chem.*, 16 (1968) 131.
- 7 L. COLLATZ, *Functional Analysis and Numerical Mathematics*, Academic Press, New York, 1966.
- 8 B. VULIKH, *Introduction to Functional Analysis for Scientists and Technologists*, Addison-Wesley, Reading, Mass., 1963.
- 9 T. BERZINS AND P. DELAHAY, *J. Am. Chem. Soc.*, 77 (1955) 6448.
- 10 M. SMUTEK, *Proc. Polarograph. Congr.*, 1 (1952) 677.
- 11 T. KAMBARA AND I. TACHI, *Bull. Chem. Soc. (Japan)*, 25 (1952) 135.
- 12 P. DELAHAY, *J. Am. Chem. Soc.*, 75 (1953) 1430.
- 13 H. GERISCHER AND W. VIELSTICH, *Z. Physik. Chem., N.F.*, 3 (1955) 16.
- 14 P. DELAHAY, *J. Phys. Chem.*, 66 (1962) 2204.



## RELAXATION OF ELECTRODE PROCESSES WITH SIMULTANEOUS CONSIDERATION OF DOUBLE-LAYER CHARGING AND FARADAIC CURRENT. PART II

G. G. SUSBIELLES AND P. DELAHAY

*Department of Chemistry, New York University, New York, N. Y. 10003 (U.S.A.)*

(Received October 17th, 1967)

A general treatment of the relaxation of electrode processes was recently formulated by HOLUB<sup>1</sup> without *a priori* separation of faradaic and charging processes in the solution of the diffusion problem. The approach in his work was based on the three previously advanced general equations<sup>2</sup> and on the recently developed explicit form of the time-derivatives of the surface excesses and charge density on the electrode<sup>3</sup>. He expressed his result as a general current–overvoltage relationship in terms of Laplace transforms for any small perturbation. He also calculated upper limits for the difference between his results and those for a classical formulation for different perturbations of small amplitude. We summarize here the explicit forms of the current–overvoltage–time characteristics for various types of perturbation and point out the difference between this treatment and the classical formulation.

### GENERAL CURRENT–OVERVOLTAGE RELATIONSHIP IN LAPLACE TRANSFORM

HOLUB's general current–overvoltage relationship is:

$$\hat{v} = \frac{\hat{I}}{s^{\frac{1}{2}}} \begin{vmatrix} I + s^{\frac{1}{2}} & r + \gamma s^{\frac{1}{2}} \\ \sigma s^{\frac{1}{2}} + s\sigma_a - i_a & s\sigma_b - i_b \\ \hline h_\eta s^{\frac{1}{2}} & I + h_a s^{\frac{1}{2}} & h_b s^{\frac{1}{2}} \\ \epsilon s^{\frac{1}{2}} & I + s^{\frac{1}{2}} & r + \gamma s^{\frac{1}{2}} \\ s\sigma_a - i_\eta & \sigma s^{\frac{1}{2}} + s\sigma_a - i_a & s\sigma_b - i_b \end{vmatrix} \quad (1)$$

where  $s$  is the variable in the Laplace transform, and  $\hat{v}$  and  $\hat{I}$  are the Laplace transforms of dimensionless quantities,  $v$  and  $I$ , proportional to the overvoltage and the current density, respectively. These quantities and other notations are those of HOLUB<sup>1</sup>.

Equation (1) will be rewritten by transformation into partial fractions in two ways. The first of these forms, which expresses  $\hat{v}$  as a function of  $\hat{I}$ , applies to all types of perturbations considered here except potentiostatic control. The second form expresses  $\hat{I}$  as a function of  $\hat{v}$  and applies to potentiostatic perturbations. We start with the first form which is:

$$\hat{v} = \hat{I} \sum_{j=1}^4 \frac{M_j}{s^{\frac{1}{2}}(s^{\frac{1}{2}} + m_j)} \quad (2)$$

The  $m_j$ 's are the roots of the 4th-degree equation in  $s^{\frac{1}{2}}$  obtained by setting equal to zero the denominator of eqn (1). The resulting equation, solved for instance by the BROWN method<sup>4</sup>, has 4 roots of which 0, 2 or 4 may be complex. This equation may reduce to a 3rd-degree equation for particular values of the kinetic and double-layer parameters. There are then either 3 real roots, or 1 real plus 2 complex roots. Once  $m_j$  are computed, we determine the coefficients  $M_j$  of eqn (2) by expressing that this equation is identical with eqn. (1). No term in  $s^{\frac{1}{2}}$ , or of a higher degree, appears in eqn. (2) because the numerator of eqn. (1) contains terms in  $s^{\frac{1}{2}}$  raised to a power which is lower than, or at the most equal to, the highest power of the  $s^{\frac{1}{2}}$ -terms in the denominator of eqn. (1).

For a potentiostatic perturbation we express  $I$  as a function of  $v$  and we begin by writing eqn. (1) as:

$$\hat{I} = \hat{v} \frac{s^{\frac{1}{2}}(s^2 + S_1 s^{\frac{3}{2}} + S_2 s + S_3 s^{\frac{1}{2}} + S_4) \psi_1}{(s^{\frac{3}{2}} + R_1 s + R_2 s^{\frac{1}{2}} + R_3) \psi_2} \quad (3)$$

The explicit forms of the coefficients,  $S_j$ ,  $R_j$  and  $\psi_j$ , are simply obtained by calculating the determinants in eqn. (1). Equation (3) is now written in the form:

$$\begin{aligned} \hat{I} = v \frac{\psi_1}{\psi_2} & \left[ I + \frac{S_1 - R_1}{s^{\frac{1}{2}}} \right. \\ & \left. + \frac{[(S_2 - R_2) - R_1(S_1 - R_1)]s + [(S_3 - R_3) - R_2(S_1 - R_1)]s^{\frac{1}{2}} + [S_4 - (S_1 - R_1)R_3]}{s^{\frac{3}{2}}(s^{\frac{3}{2}} + R_1 s + R_2 s^{\frac{1}{2}} + R_3)} \right] \end{aligned} \quad (4)$$

or

$$\hat{I} = v \frac{\psi_1}{\psi_2} \left[ I + \frac{S_1 - R_1}{s^{\frac{1}{2}}} + \sum_{j=1}^3 \frac{N_j}{s^{\frac{1}{2}}(s^{\frac{1}{2}} + \varrho_j)} \right] \quad (5)$$

where  $-\varrho_j$  represents the roots of the 3rd-degree equation in  $s^{\frac{1}{2}}$  obtained by setting equal to zero the terms between parentheses in the numerator of eqn. (4). The coefficients  $N_j$  follow directly from identification of eqn. (4) with (5).

#### CURRENT-OVERTVOLTAGE-TIME RELATIONSHIP

We consider small perturbations for which a linearized current-overtoltage holds quite well and we obtain by inverse Laplace transform the following:

$$v = I \sum_{j=1}^4 \frac{M_j}{m_j^2} \left[ \exp(m_j^2 T) \operatorname{erfc}(m_j T^{\frac{1}{2}}) + 2m_j \left( \frac{T}{\pi} \right)^{\frac{1}{2}} - I \right] \quad (6)$$

(single-step galvanostatic perturbation)

$$v = I_1 \sum_{j=1}^4 \frac{M_j}{m_j^2} \left[ \exp(m_j^2 T) \operatorname{erfc}(m_j T^{\frac{1}{2}}) + 2m_j \left( \frac{T}{\pi} \right)^{\frac{1}{2}} - I \right]$$

$$+ (I_2 - I_1) \sum_{j=1}^4 \frac{M_j}{m_j^2} \left[ \exp[m_j^2(T - T_1)] \operatorname{erfc}[m_j(T - T_1)^{\frac{1}{2}}] + 2m_j \left( \frac{T - T_1}{\pi} \right)^{\frac{1}{2}} - I \right] \quad (7)$$

(double-step galvanostatic perturbation)

$$v = Q \sum_{j=1}^4 \frac{M_j}{m_j^2} \exp(m_j^2 T) \operatorname{erfc}(m_j T^{\frac{1}{2}}) \quad (8)$$

(coulostatic perturbation)

$$I = v \frac{\psi_1}{\psi_2} \left[ \delta + \frac{S_1 - R_1}{(\pi T)^{\frac{1}{2}}} + \sum_{j=1}^3 N_j \exp(\varrho_j^2 T) \operatorname{erfc}(\varrho_j T^{\frac{1}{2}}) \right] \quad (9)$$

(potentiostatic perturbation)

Notations in eqn. (7) are:  $I_1$  and  $I_2$  values of  $I$  for the first and second step, respectively;  $T_1$ -value of  $T$  at end of the first step. The symbol  $\delta$  in eqn. (9) represents the delta-function.

Equations (6)–(9) can be applied without difficulty when the roots  $m_j$  or  $\varrho_j$  are real. If these roots are complex, expanded forms of the function  $\exp(\lambda^2) \times \operatorname{erfc}(\lambda)$  are used<sup>5</sup> or values of this function are taken directly from tables<sup>6</sup>.

The condition for a horizontal tangent in the overvoltage-time plot, derived as in the classical treatment, is for a double-step galvanostatic perturbation

$$\frac{I_2}{I_1} = 1 - \frac{\sum_{j=1}^4 (M_j/m_j^2) \exp(m_j^2 T) \operatorname{erfc}(m_j T^{\frac{1}{2}})}{\sum_{j=1}^4 (M_j/m_j^2)} \quad (10)$$

#### EXPANSION FOR SMALL AND LARGE ARGUMENTS

The expansion of the above current–overvoltage–time relationships can immediately be written down for small or large arguments. The resulting relationships, which will not be given here, show the same time-dependence as for the classical treatment, except for potentiostatic perturbations. The coefficients in the expanded equations are of course different from those in the classical formulation. Some of these coefficients may vanish for particular combinations of the kinetic and double-layer parameters.

The difference between the expanded form for this treatment and the classical one for potentiostatic perturbations arises from the terms  $(S_1 - R_1)/(\pi T)^{\frac{1}{2}}$  in eqn. (9). Thus,  $I \rightarrow \infty$  for  $T = 0$  according to eqn. (9), whereas the current is finite at time zero in the classical treatment for a finite exchange current. The infinite value of  $I$  for  $T = 0$  is to be expected from the model from which eqn. (9) was derived. Thus, it was assumed that the variations of the surface excesses of reactant and product caused by perturbation of the potential were only diffusion-controlled. Hence, an ideal step-variation of potential results in an infinite current at  $T = 0$ . The delta-function in eqn. (9) corresponds to that part of the double-layer charging corresponding to all species except the reactant and product. Mass transfer was not considered for these species in our model. The delta-function would also appear in the classical treatment if a constant double-layer capacity were supposed to shunt the path for the faradaic current at the metal–electrolyte interface.

Finally, the functions  $\exp(\lambda^2) \operatorname{erfc}(\lambda)$  in eqns. (6)–(9) must approach unity for large arguments, and consequently all arguments must be positive. Hence the roots  $m_j$  or  $\varrho_j$ , if they are real, or the real parts of those roots if they are complex, must all

be negative ( $-m_j$  or  $-\varrho_j$  represents the roots). This condition imposes a restriction on the values of the partial differential coefficients of the surface excesses and charge density on the electrode.

#### COMPARISON WITH CLASSICAL TREATMENT

The foregoing treatment is of interest for fast processes with *specific* adsorption. Calculations were performed to ascertain the difference between this and the classical treatment for a single-pulse galvanostatic perturbation for data listed below. The difference was small even for an exchange current density of  $1 \text{ A cm}^{-2}$ . The data used here pertain approximately to a divalent cation in  $0.1 \text{ M}$  solution of a  $\text{I}-\text{I}$  supporting electrolyte at  $-0.5 \text{ V}$  *versus* the point of zero charge, *i.e.*, for a case with presumably strong non-specific adsorption. Data were:  $\partial q/\partial c_+^s = -0.2877 \text{ C cm mole}^{-1}$ ,  $\partial q/\partial c_M^s = 0$ ,  $\partial q/\partial E = 20 \mu\text{F cm}^{-2}$ ,  $\partial \Gamma_+/\partial c_+^s = 0.1382 \cdot 10^{-5} \text{ cm}$ ,  $\partial \Gamma_+/\partial c_M^s = 0$ ,  $\partial \Gamma_+/\partial E = 0.4584 \cdot 10^{-11} \text{ mole cm}^{-2} \text{ V}$ ,  $c_+^s = c_M^s = 10^{-6} \text{ mole cm}^{-3}$ ,  $D_+ = D_M = 10^{-5} \text{ cm}^2 \text{ sec}^{-1}$ . The above double-layer parameters were computed as before<sup>7</sup>, but by using lower absolute values of  $\phi_2$  and  $d\phi_2/dE$  than in the previous publication. We used here  $\phi_2 = -0.0518 \text{ V}$  and  $d\phi_2/dE = 0.055$ . We now believe, following SLUYTER's remark<sup>8</sup>, that the values of  $\phi_2$  and  $d\phi_2/dE$  previously used<sup>7</sup> were too high because they correspond to the supporting electrolyte alone. It is possible that we have used too low values of  $\phi_2$  and  $d\phi_2/dE$  here, and the matter could only be settled by experimental double-layer studies of a  $0.1 \text{ M}$  solution of a  $\text{I}-\text{I}$  supporting electrolyte containing a divalent cation ( $0.001 \text{ M}$  concentration range) which is not reduced at approximately  $-1 \text{ V}$  (vs. SCE), *e.g.*,  $\text{Ba}^{2+}$ . Classical double-layer measurements and calculation of  $\phi_2$  would then yield the coefficients that are needed to compare the present theory with the classical formulation in the case of strong non-specific adsorption.

This work was supported by the Office of Naval Research.

#### SUMMARY

Explicit forms of the response-time equation are given for the following relaxation methods: single-step and double-step galvanostatic, coulostatic and potentiostatic.

A numerical example shows that this treatment differs from the classical one only if there is marked specific adsorption of reactant and/or product.

#### REFERENCES

- 1 K. HOLUB, *J. Electroanal. Chem.*, 17 (1968) 277.
- 2 P. DELAHAY, *J. Phys. Chem.*, 70 (1966) 2373.
- 3 P. DELAHAY, K. HOLUB, G. G. SUSBIELLES AND G. TESSARI, *ibid.*, 71 (1967) 779.
- 4 J. M. McCORMICK AND M. G. SALVADORI, *Numerical Methods in Fortran*, Prentice-Hall, Englewood Cliffs, New Jersey, 1965, p. 60.
- 5 H. S. CARSLAW AND J. C. JAEGER, *Conduction of Heat in Solids*, Oxford University Press, New York, 1948, p. 372.
- 6 V. N. FADDEYEVA AND N. M. TERENTEV, *Tables of Values of the Function  $w(z) = \exp(-z^2) \cdot [1 + (2i/\pi)^{1/2} \int_0^z \exp t^2 dt]$  for Complex Argument*, English translation by D.C. FRY, Pergamon Press, London, 1961.
- 7 K. HOLUB, G. TESSARI AND P. DELAHAY, *J. Phys. Chem.*, 71 (1967) 2612.
- 8 J. H. SLUYTERS, M. SLUYTERS-REHBACH AND B. TIMMER, *J. Electroanal. Chem.*, 15 (1967) 452.

## BEMERKUNGEN ZUR METHODIK DER ORGANISCHEN POLAROGRAPHIE

L. HOLLECK, M. HEYROVSKÝ UND S. VAVŘIČKA

Chemisches Institut der Hochschule, Bamberg (Bundesrepublik Deutschland)

(Eingegangen am 31. Oktober, 1967)

Im Laufe der Untersuchungen der polarographischen Reduktion von *p*-Dinitrobenzol haben wir gefunden, dass diese Substanz weitaus grössere Ansprüche an die experimentelle Methodik stellt als die geläufigen Depolarisatoren. Da es sich dabei um Effekte handelt, die in der Polarographie von grundsätzlicher Bedeutung sind, wollen wir auf sie aufmerksam machen.

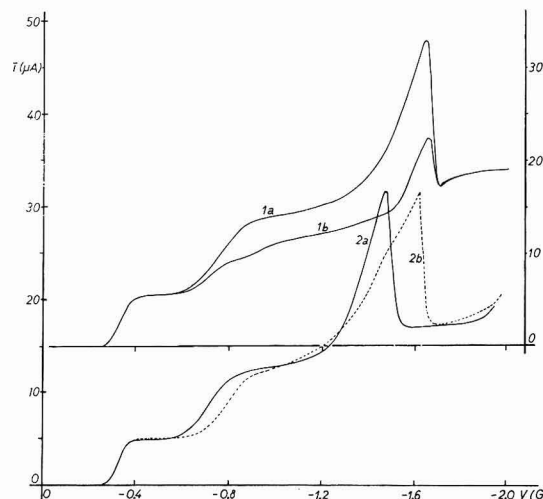


Abb. 1. Einfluss der Zusammensetzung der Pufferlösung auf die polarographische Strom-Spannungskurve von  $10^{-3} M$  *p*-Dinitrobenzol in wässrig-methanolischen Lösungen, 30%  $\text{CH}_3\text{OH}$ ; Tropfzeit,  $t_1 = 2.6$  sec. (konstant gehalten) pH = 8.25: (1a),  $\text{Na}_2\text{B}_4\text{O}_7 + \text{K}_2\text{HPO}_4$ ; (1b),  $\text{NaH}_2\text{PO}_4 + \text{Na}_2\text{HPO}_4$ . pH = 9: (2a),  $\text{NH}_3 + \text{NH}_4\text{Cl}$ ; (2b),  $\text{H}_3\text{BO}_3 + \text{NaOH} + \text{HCl}$ .

Es ist bekannt, dass reproduzierbare polarographische Kurven organischer Substanzen nur dann erhalten werden können, wenn man gut gepufferte Grundlösungen mit konstantem pH-Wert benutzt. Unsere Versuche haben jedoch gezeigt, dass diese Bedingung zwar nötig, aber nicht ausreichend ist. Die Gestalt der Kurven von *p*-Dinitrobenzol hängt nicht nur vom pH, sondern auch von der Zusammensetzung der Pufferlösung ab, was besonders im schwach alkalischen pH-Bereich bemerkbar ist (s. Abb. 1).

Wir schreiben diese Tatsache der verschiedenen Wirksamkeit der als Protonendonatoren fungierenden sauren Bestandteilen der Lösungen zu<sup>1,2</sup>.

Vergleicht man die Höhen der polarographischen Stufen bei verschiedenen

Potentialen und in Lösungen von verschiedenen pH-Werten, so hat man auch den Einfluss des Potentials auf die Tropfzeit in Betracht zu ziehen. Mit einer Auswirkung ist besonders im Falle von mehrelektronigen Reduktionen zu rechnen. Bei der 12-elektronigen Reduktion von *p*-Dinitrobenzol kann diese Korrektion der Stufenhöhe den Wert erreichen, welcher der Aufnahme eines Elektrons entspräche. Nichtberücksichtigung dieses Effektes führt u.U. zu falschen Schlüssen über den Chemismus bzw. Mechanismus der Elektrodenprozesse, weswegen es in solchen Fällen empfehlenswert ist, die Methode der mechanisch geregelten Tropfzeit anzuwenden. Es hat sich gerade im Falle des *p*-Dinitrobenzols gezeigt, dass es wichtig ist, mit konstant gehaltener Tropfzeit zu arbeiten, vor allem, wenn oberflächenaktive Stoffe zugegen sind. Bei Anwesenheit bzw. Zusatz solcher Substanzen wird mit der Grenzflächenspannung auch die Tropfzeit gegenüber der zusatzfreien Lösung geändert, was sich vor allem bei kinetischen und irreversiblen Prozessen im Kurvenverlauf (gewisse Veränderung der Kurvenlage und -steilheit) auswirkt. Diesen Einfluss könnte man irrtümlicherweise dem Eingriff der adsorbierbaren Substanzen in den Prozessablauf zuschreiben. In Abb. 2 sind Kurven von *p*-Dinitrobenzol wiedergegeben, die den Einfluss einer konstant gehaltenen Tropfzeit deutlich machen. Hierzu ist allerdings zu bemerken, dass in diesem Falle die Grösse des Effektes durch die Natur des die polarographische Strom-Spannungskurve bestimmenden komplizierten Reaktionsablaufs<sup>2</sup> gegeben ist.

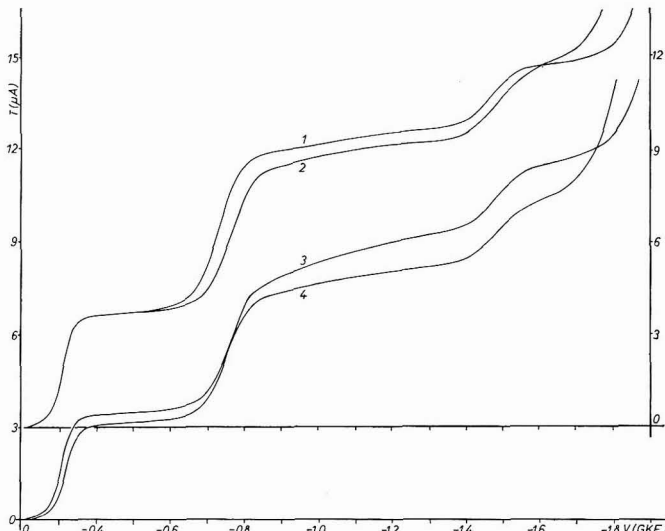


Abb. 2. Einfluss der konstant gehaltenen Tropfzeit auf die polarographischen Strom-Spannungskurven in Gegenwart oberflächenaktiver Substanz.  $5 \cdot 10^{-5} M$  *p*-Dinitrobenzol im Boratpuffer pH 9, 30%  $\text{CH}_3\text{OH}$ . Ungeregelte Tropfzeit: (1), ohne Gelatine; (2), mit 0.005% Gelatine. Konstant gehaltene Tropfzeit,  $t_1 = 2.3$  sec: (3), ohne Gelatine; (4), mit 0.005% Gelatine.

Wie bekannt, muss man in der Polarographie mit dem sogenannten Verarlungseffekt und gleichzeitig mit der Übertragung der Reaktionsprodukte von einem Tropfen auf den anderen rechnen. Diese Effekte machen sich besonders bemerkbar bei komplizierteren mehrelektronigen Vorgängen, wie z.B. bei der Reduktion von

*p*-Dinitrobenzol. Wie Abb. 3 zeigt, erscheint auf der polarographischen Kurve an dem sog. "ersten Tropfen" ein Maximum, das an dem "zweiten" und den folgenden Tropfen durch Übertragung der Reaktionsprodukte unterdrückt wird. Dem Einfluss dieser Übertragung schreiben wir auch den überraschenden Effekt schon geringer Änderungen der Quecksilberbehälterhöhe auf das Auftreten des Maximums (Abb. 4) zu. Dafür spricht die Tatsache, dass sich das Verschwinden des Maximums durch

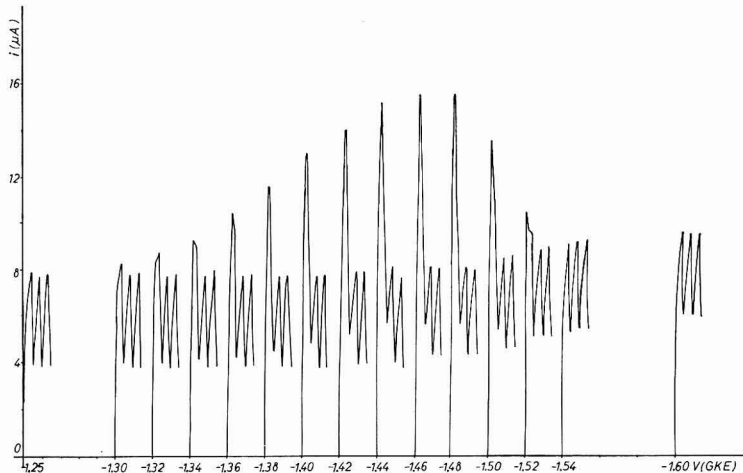


Abb. 3. Effekt der Übertragung von Reaktionsprodukten in den polarographischen Kurven.  $10^{-3} M$  *p*-Dinitrobenzol im Boratpuffer pH 9, 30%  $\text{CH}_3\text{OH}$ . Polarographische Strom-Zeitkurven mittels einer gewöhnlichen Kapillare bei verschiedenen Potentialen am ersten, zweiten und dritten Tropfen, mit dem Polarographen Polariter PO<sub>4</sub> (Firma Radiometer), Dämpfung 1, aufgenommen.

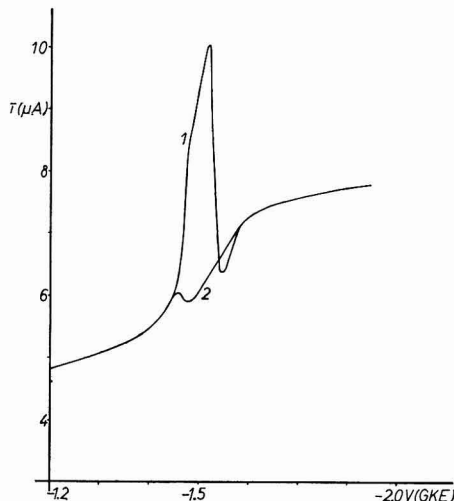


Abb. 4. Einfluss der Quecksilberbehälterhöhe auf das Auftreten des katalytischen Maximums.  $10^{-3} M$  *p*-Dinitrobenzol im Boratpuffer pH 8.9, 30%  $\text{CH}_3\text{OH}$ ; Tropfzeit konstant gehalten,  $t_1 = 1.9$  sec. Behälterhöhe: (1), 526; (2), 527 mm. Quecksilberausflussgeschwindigkeit unter 1 mg/sec, gewöhnliche vertikale Kapillare.

Erniedrigung des Quecksilberbehälters bei Verwendung einer den Übertragungseffekt weitgehendst beseitigenden Smolerschen Kapillare nicht erreichen lässt. Über die katalytische Natur dieses Maximums wurde an anderer Stelle berichtet<sup>1</sup>. Eine weitestgehende Beseitigung solcher Übertragungseffekte ist durch die Benützung der abgewinkelten Smolerschen Kapillare<sup>3</sup> erreichbar.

Die Aufklärung des gesamten Reduktionsablaufs—des Chemismus, wie des Elektrodenmechanismus—erfordert gerade bei vielelektronigen Prozessen mit ihren komplexen Geschehen infolge mannigfacher Einflüsse auf die primären und sekundären Elektrodenreaktionen, sowie die Wechselwirkung von Elektrolysen-Zwischen- und -Endprodukten mit dem Depolarisator bzw. den Lösungskomponenten—vielfach das Heranziehen weiterer, nicht-polarographischer Methoden. Gerade dann, wenn bei Benutzung der abgewinkelten Kapillare, gegenüber einer normalen vertikalen, ein grösserer Effekt im Kurvenverlauf auftritt, erscheint es angebracht, auch der Frage der chemischen Reaktionen von kathodischen Reduktionsprodukten das Augenmerk zuzuwenden. So tritt z.B. bei mikroskopischer Beobachtung der Elektrodenumgebung im Laufe der Reduktion von *p*-Dinitrobenzol eine braunrote Färbung auf<sup>4</sup>, die seinerzeit schon im Laufe von präparativen—potentiostatisch durchgeföhrten—Elektrolysen auftrat und die bei vollständiger Durchreduktion wieder verschwindet<sup>5</sup>. Die gleiche rote Färbung konnten wir beobachten, wenn die Reduktion

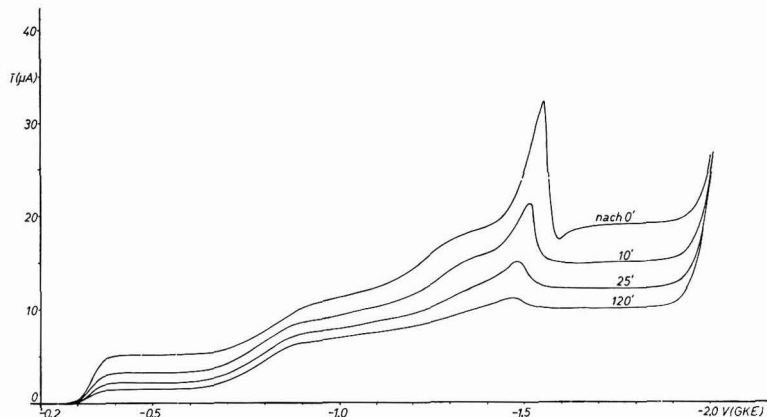


Abb. 5. Polarographische Verfolgung des zeitlichen Verlaufs der Reduktion von *p*-Dinitrobenzo mit H<sub>2</sub> an platiniertem Platinblech. 10<sup>-3</sup> M *p*-Dinitrobenzol im Boratpuffer, pH 9. Kurven nach angegebenen Zeitintervallen der Reduktion aufgenommen.

von *p*-Dinitrobenzol in schwach alkalischer Lösung mit Wasserstoff in Gegenwart eines platinierten Platinbleches durchgeführt wird. Dieses chemische Reduktionsverfahren, das nur einen minimalen Eingriff in das untersuchte System darstellt, lässt—wo anwendbar—auf einfache Art auch den Reduktionsprozess polarographisch verfolgen (Abb. 5) und kann als zusätzliche Methode zur Aufklärung von Reduktions-Chemismen, insbesondere die Verfolgung von Sekundärreaktionen mit herangezogen werden.

Für Forschungsmittel danken wir der Alexander-von-Humboldt-Stiftung sowie dem Bundesministerium für Wirtschaft bestens.

## ZUSAMMENFASSUNG

Am Beispiel der polarographischen Strom-Spannungskurven von *p*-Dinitrobenzol wird auf die Bedeutung gewisser beeinflussender Faktoren sowie bestimmter methodischer Massnahmen für die polarographische Untersuchung organischer Verbindungen hingewiesen, so der Zusammensetzung der Pufferlösungen (bei gleichem pH), der künstlich geregelten Tropfzeit und der Verwendung der geneigten Kapillare nach SMOLER. Vor allem bei komplizierteren Elektrodenprozessen kann sich die Übertragung von Elektrolysenprodukten von einem auf den anderen Tropfen im Kurvenverlauf stark auswirken, wie etwa in der Unterdrückung katalytischer Wasserstoffmaxima im Laufe der *p*-Dinitrobenzol-Reduktion. Als in speziellen Fällen zur Klärung von Reduktions-Chemismen anwendbare Zusatzmethode lässt sich die Reduktion durch Wasserstoff in Gegenwart eines platinierter Platinbleches, unter gleichzeitiger polarographischer Verfolgung des Reduktionsablaufs, anwenden.

## SUMMARY

Polarographic current-voltage curves for *p*-dinitrobenzene are given to illustrate the effect and significance of some experimental variables, *e.g.*, buffer composition (of the same pH), mechanically-regulated drop-time, and the use of SMOLER's bent capillary—in the study of organic compounds. The transfer of the electrolysis products from one drop to the other can—in case of complex electrode reactions—greatly affect the shape of the polarographic curve as, for example, in the suppression of the catalytic hydrogen maxima recorded in the course of reduction of *p*-dinitrobenzene.

Reduction by gaseous hydrogen in the presence of a platinized platinum plate and the simultaneous polarographic monitoring of the progress of reduction can—in special cases—be applied to clarify the reduction mechanism.

## LITERATUR

- 1 L. HOLLECK, S. VAVŘIČKA UND M. HEYROVSKÝ, *Z. Naturforsch.*, 22b (1967) 1226.
- 2 L. HOLLECK, in Vorbereitung.
- 3 J. SMOLER, *J. Electroanal. Chem.*, 6 (1963) 465.
- 4 L. HOLLECK, *Z. Anal. Chem.*, 224 (1967) 236.
- 5 L. HOLLECK UND H. SCHMIDT, *Z. Elektrochem.*, 59 (1955) 1039.



## DOUBLE-LAYER CAPACITY AT A PYROLYTIC GRAPHITE DISK ELECTRODE

HENRY H. BAUER<sup>a</sup>, MICHAEL S. SPRITZER<sup>b</sup> AND PHILIP J. ELVING

*The University of Michigan, Ann Arbor, Michigan (U.S.A.)*

(Received October 10th, 1966; in revised form October 28th, 1967)

An understanding of electrochemical reactions is frequently not attainable unless the structure of the electrical double-layer is understood. The nature of the double-layer at solid electrodes has not yet been adequately elucidated, knowledge about it being largely based on analogy with the well-characterized mercury electrodes; the present state of our understanding in this area has been comprehensively reviewed by DELAHAY<sup>1</sup>.

Primary difficulties with solid electrodes involve questions as to: (a) the reproducibility of the electrode surface and (b) the dependence of the apparent double-layer capacity on frequency. The aim of the present study was to investigate these questions in relation to the pyrolytic graphite electrode, which has in recent years proved useful in a variety of electrochemical studies; particular attention was given to electrode preparation and treatment.

The observed capacity was always to some extent dependent on the frequency at which the measurement was made. However, it is indicated that such an effect may be expected at any electrode, such as a disk, at which the distribution of current over the surface is not uniform.

### EXPERIMENTAL

#### *Polarization circuit*

Instrumentation for polarization by both alternating and direct voltages has been either fully manual, with corrections for  $iR$ -drop and other effects being calculated after the experiments have been made<sup>2</sup>, or fully controlled with both d.c. and a.c. signals held constant by electronic circuits, usually constructed of operational amplifiers<sup>3</sup>. The latter scheme has the disadvantage that, with readily available equipment, work is restricted to frequencies no higher than about 1000 Hz. Therefore, a "hybrid" arrangement (Fig. 1) was used in the present work, in which a.c. and d.c. circuits were connected in parallel across the cell.

The d.c. circuit was controlled by a conventional operational-amplifier control-loop<sup>4</sup>; the direct voltage was applied by potentiometer, E; capacitor  $C_2$  was used to

<sup>a</sup>Present address: Department of Chemistry, University of Kentucky, Lexington, Kentucky, U.S.A.

<sup>b</sup>Present address: Department of Chemistry, Villanova University, Villanova, Pennsylvania, U.S.A.

attenuate any a.c. picked up by the reference electrode; choke L ensured that a.c. applied between counter and working electrodes was not shunted through  $C_2$  to ground.

The a.c. circuit, supplied by an audio-frequency oscillator, was manually controlled. A parallel combination of resistance ( $R_p$ ) and capacitance ( $C_p$ ) decades was used for phase-angle measurement; phase shifts and cell impedances were measured as previously described<sup>5</sup>, using an oscilloscope. A 10-mV peak-to-peak voltage was maintained across the working electrodes by manual adjustment of  $R_1$  and of the oscillator amplitude-control. Capacitor  $C_1$  blocked the d.c. signal from the a.c. circuit.

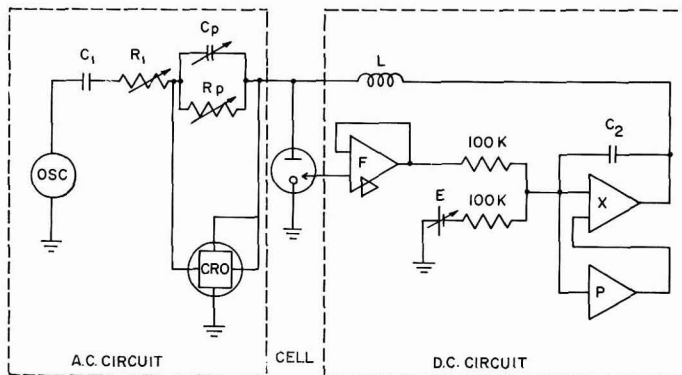


Fig. 1. Circuit for a.c. measurements. ( $C_1$ ), 0.01  $\mu\text{F}$ ; ( $C_2$ ), 2  $\mu\text{F}$ ; ( $C_p$ ), General Radio decade capacitor Type 1419-A; (CRO), Tektronix Model 502A dual-beam oscilloscope; (E), 0–10 V variable potential source; (F), stabilized follower; (L), United Transformer choke Type MQM-600; (OSC), Heathkit audio-frequency oscillator Model AG-8; (P), Philbrick K2-P operational amplifier; ( $R_1$ ), two 3/4-turn radio potentiometers in series, 5 k $\Omega$  and 1 M $\Omega$ ; ( $R_p$ ), General Radio decade resistor Type 1434-QC; (X), Philbrick K2-X operational amplifier.

### Cells

For runs in aqueous solution, a conventional H-cell was used with a saturated calomel electrode, SCE, as reference electrode, and an agar plug between compartments. The counter electrode, which was placed in the test-solution compartment, consisted of either a large mercury pool (area: 9.6 cm<sup>2</sup>) or a platinum gauze cylinder, 1 cm in diameter and 3 cm high (*ca.* 26 gauge wire). The three-compartment water-jacketted cell used for runs in pyridine solution has been described<sup>6</sup>; salt bridges were methyl cellulose gel-0.1 M Et<sub>4</sub>NClO<sub>4</sub> in pyridine. Runs in aqueous solution were at ambient room temperature (no significant effect of temperature changes of a few degrees on capacity has been reported); runs in pyridine solution were at 25°.

### Graphite electrode

Pyrolytic graphite electrodes (P.G.E.) made from 4-mm diameter cylinders sealed into glass tubing were prepared as previously described<sup>7</sup> with the graphite surface flush with the end of the glass tubing, as well as with several millimeters of graphite protruding from the tubing; in the latter case, the sides of the graphite cylinder were insulated. Shell Epon resin, Sears two-component epoxy resin, and polyethylene (obtained by melting polyethylene tubing in a low flame) were tried for sealing and insulation. Resurfacing was accomplished by polishing with a fine abrasive paper<sup>7</sup>.

or by cleaving about a millimeter of graphite from the electrode tip by means of a sharp scalpel. The most reproducible behavior was obtained with a "protruding" electrode, sealed and insulated with Sears epoxy resin and resurfaced by cleaving.

### Reagents

Aqueous potassium chloride (J. T. Baker) solutions were purified by treatment with charcoal (Darco G-60). Pyridine, argon for de-aeration, and tetraethylammonium perchlorate were obtained and treated as previously described<sup>6,8</sup>. The argon was equilibrated in the case of aqueous solutions by first being bubbled through water; for pyridine solutions, it was first passed through a column of Drierite and then through pyridine containing molecular sieves.

### MEASUREMENT APPROACH

The measuring technique involved determination of total cell impedance,  $Z$ , and phase angle,  $\phi$ , and calculation of the equivalent series resistance,  $R_s$  and capacity  $C_s$  (the apparent double-layer capacity), by simple transformation of the measured quantities. Thus,

$$Z^2 = R_s^2 + 1/\omega^2 C_s^2 \quad (1)$$

where  $\omega$  is the angular frequency of the applied alternating signal, and

$$\cot \phi = \omega R_s C_s \quad (2)$$

Combining eqns. (2) and (1),

$$Z^2 = R_s^2 + R_s^2 / \cot^2 \phi = R_s^2 / \cos^2 \phi \quad (3)$$

which permits  $R$  to be calculated directly from  $Z$  and  $\phi$  via

$$R_s = Z \cos \phi \quad (4)$$

$C$  can then be calculated, using eqn. (2), from

$$C_s = 1/\omega Z \sin \phi \quad (5)$$

If  $R_s$  and  $C_s$  are independent of frequency, support is given to a representation of the cell as being the double-layer capacity at the working (small) electrode in series with the solution resistance, and  $C_s$  and  $R_s$  can be taken to be measures of these quantities. However, if  $R_s$  and  $C_s$  change with frequency ("frequency dispersion"), such inferences cannot be drawn. It is worth emphasizing that, when the equivalent series circuit is inapplicable, use of  $C_s$  as a "double-layer capacity" involves an assumption whose validity does not necessarily improve as the frequency dispersion becomes less; it is the applicability or inapplicability that is significant, since any frequency dispersion points to a phenomenon that must be understood before  $C_s$ -values can be reliably used.

### REPRODUCIBILITY AND FREQUENCY DISPERSION

The reproducibility, nature, and magnitude of the frequency dispersion obtained on pyrolytic graphite electrodes (Tables 1 and 2) indicate that good reproducibility may be attained at a given electrode by rigorous control of the preparation and handling of the electrode (*cf.* subsequent discussion).

However, both the magnitude of the measured quantities and their variation with frequency are sensitive to the method of preparation of the electrode surface: compare data in Table 1 for a cleaved electrode and Table 2 for a polished electrode cathodized before the impedance measurements were made. Thus, one possible factor

TABLE 1

SERIES CAPACITY AND RESISTANCE AT A CLEAVED PYROLYtic GRAPHITE ELECTRODE<sup>a</sup>

Frequency (Hz)	$C_s^b$ ( $\mu F$ )			$R_s^b$ ( $\Omega$ )		
	(1)	(2)	(3)	(1)	(2)	(3)
50	2.09	2.36	2.34	256	279	285
125	1.85	2.13	2.14	129	146	143
250	1.76	1.96	2.60	81.8	90.5	96
500	1.61	1.78	1.78	56.6	62	58.1
1,250	1.53	1.54	1.80	36.7	37.6	31
2,500	1.43	1.42	2.05	30.8	28.5	39.4
5,000	1.31	1.21	1.27	26.6	23.2	22.2
12,500	1.26	1.12	1.07	23.4	17.6	17.8
25,000	1.20	1.03	1.83	22.4	15.8	15.8

<sup>a</sup>Electrode (diam. 4 mm) was sealed and covered by a polyethylene pressure-fitted sleeve. Soln. composition: 0.4 M KCl.

<sup>b</sup>Measurements were made at a potential of -0.5 V vs. SCE. The numbers in parentheses refer to the series of experiments made on the same electrode with resurfacing by cleaving between each series.

TABLE 2

SERIES CAPACITY AND RESISTANCE AT A GROUND PYROLYtic GRAPHITE ELECTRODE<sup>a</sup>

Frequency (Hz)	$C_s^b$ ( $\mu F$ )		$R_s^b$ ( $\Omega$ )	
	(1)	(2)	(1)	(2)
50	8.8	8.8	48.5	47.8
125	8.42	8.25	35.2	34.4
250	9.05	7.85	28.8	31
500	7.95	7.8	29	28.9
1,250	7.92	7.25	26.6	26.8
2,500	8.9	6.95	23.9	26.5
5,000	6.58	6.36	24.5	24.5
12,500	6.6	5.66	24.5	23.9
25,000	9.65		21	

<sup>a</sup>Electrode (diam. 4 mm) was sealed in a glass tube by polyethylene with its end flush with the glass; it was resurfaced by grinding. Soln. composition: 0.5 M KCl.

<sup>b</sup>Measurements were made at a potential of -0.5 V vs. SCE. In series (1), the soln. was pre-electrolyzed initially by cyclic scan to -1.0 V; in series (2), the soln. was similarly pre-electrolyzed before each measurement.

in the differences observed is the presence or absence of an "oxidized" surface. The P.G.E. normally has an "oxidized" surface that shows a different apparent capacity than the "reduced" surface<sup>9</sup>; the latter can be produced, e.g., by polarizing the electrode from 0 to -1.4 V vs. SCE at 10 mV sec<sup>-1</sup>. Therefore, if an "oxidized" electrode is held at a negative potential, the capacity would be expected to change with time. We have occasionally observed such effects, where the order of magnitude of the drift is about a 5% change in capacity in 15 min while the resistance remains constant or is

changed to a lesser extent; these changes appear to depend on applied electrode potential and on the frequency. No quantitative data bearing on this particular point were obtained; however, work is continuing on the study of the nature of the surface ("oxidized" or "reduced"), in particular by cyclic voltammetric investigations<sup>9</sup>.

Another possible factor in the small frequency dispersion that was persistently observed (*e.g.*, Tables 1 and 2) may have been penetration of the solution between the electrode and its insulation. For example, in one of a number of experiments that gave a much larger  $C_s$ -value at low frequencies (a factor of up to 4 over Table 2) together with a much greater degree of frequency dispersion (Table 3), the resin coating around

TABLE 3

EFFECT ON SERIES CAPACITY AND RESISTANCE OF SEEPAGE OF SOLUTION BETWEEN PYROLYtic GRAPHITE ELECTRODE AND ITS INSULATION<sup>a</sup>

Frequency (Hz)	$C_s$ <sup>b</sup> ( $\mu F$ )		$R_s$ <sup>b</sup> ( $\Omega$ )	
	(1)	(2)	(1)	(2)
50	27.9	33.8	199	164
125	30.9	29.9	101	103
250	22.9	24.1	77.2	74.9
500	22.5	18.2	89.3	75
1,250	4.55	4.75	53.4	52.5
2,500	3.26	3.38	37.7	37.3
5,000	1.75	1.92	31.7	31
12,500	1.70	1.70	23.8	23.8
25,000	1.69	1.60	21.7	21.1

<sup>a</sup>Electrode was encased in a two-component epoxy resin and was resurfaced by cleaving. Soln. composition: 0.4 M KCl.

<sup>b</sup>Measurements were made at a potential of -0.5 V *vs.* SCE. In series (1), a pool counter-electrode was used; in series (2), a platinum gauze cylinder counter electrode was used; the lack of any difference in the two series indicate that both counter-electrodes were equally effective.

the electrode became opaque and readily peeled away, evidently due to penetration of solution between electrode and resin. Continuous penetration is not necessarily involved, but merely the presence of a "wedge" of solution. The latter has been identified as a cause of frequency dispersion under some circumstances<sup>10-14</sup>; in fact, such an explanation is commonly invoked in a qualitative way to explain frequency dispersion, but quantitative support for the explanation is not usually available. At solid electrodes, roughness of the surface is another explanation commonly given for the observation of frequency dispersion.

Both explanations amount to the use of an equivalent circuit in which the lines of current flow have to be represented by a number of parallel paths, each with capacitive and resistive properties, whereas a lack of frequency dispersion permits the use of an equivalent circuit consisting of only one path for current flow, *viz.* through the capacity of the interface and the ohmic resistance of the solution in series. Thus, any physical situation in which the current density is not uniform over the surface of the electrode will result in frequency dispersion. In the following section, we discuss the possibility that such an effect is inherently present when a disk-shaped indicator electrode is used.

## ELECTRODE SHAPE AND FREQUENCY DISPERSION

Statements in the literature refer to the need for a symmetrical arrangement of electrodes if frequency dispersion is to be avoided, for example, in the work of GRAHAME:

"...Hanging droplet... not significantly different from d.m.e... with (large cupped Hg surfaces)... frequency effect always exceeded that... with droplets, and its magnitude depended critically upon the size and shape..." (p. 305 of ref. 10; cf. also column 1 of p. 307).

"...Generally... dispersion is greater on wires and sheets than on spheres... more difficult to satisfy the symmetry requirements..." (almost at end of ref. 15).

"... The necessity for smoothness and spherical symmetry (or any other symmetry which assure an equal flow of current to all points of the electrode surface)... Robertson... points out the enormous increase in the apparent series resistance... with platinum electrodes as the frequency is lowered... also noted by the writer... not only with platinum but also with other types of solid electrodes and to a lesser degree even with mercury. The effect with mercury has been... apparently explained... as being due to the creeping of the solution up the inner walls of the capillary... It is not clear that any similar explanation will suffice to explain the results observed with solid microelectrodes. The (series) capacity of a spherically symmetrical smooth solid electrode is virtually unaffected by the frequency... This fact can be used as a test for smoothness and symmetry of an electrode." (p. 353 of ref. 16).

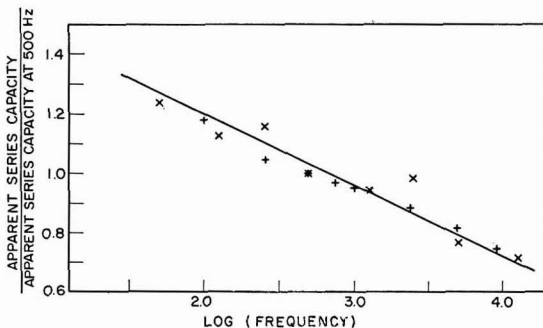


Fig. 2. Frequency dispersion of apparent double-layer capacity at planar disk-shaped working electrodes. (x), results obtained in the present study, taken from Tables 1 and 2; (+), results reported by GRANTHAM<sup>18</sup> at mercury. The line was calculated by assuming that all results follow the same relation.

In connection with our work, the question now arises whether a symmetrical arrangement of electrodes was achieved. We were not able to detect differences between the results obtained with a large mercury pool as counter electrode as compared with a large cylindrical platinum gauze counter electrode. Such a test is inconclusive, however, since the important feature is the current distribution at the disk-shaped working electrode, which could be very similar with the two counter-electrodes used. In point of fact, in a theoretical discussion of the distribution of direct current in electrodeposition, it has been shown that there are only three arrangements of electrodes in which it is possible to obtain an absolutely uniform current dis-

tribution over the electrodes: concentric spheres, concentric cylinders, and infinite parallel planes<sup>17</sup>. Thus, it seems that frequency dispersion will be inherently connected with the use of disk-shaped working electrodes.

Some support for this expectation may be found in data obtained at a plane mercury disk electrode<sup>18</sup>, where dispersion of the observed capacity with frequency was observed. Moreover, the magnitude of this dispersion is comparable to that found in the present work (*cf.* Fig. 2).

Given that a variation of measured capacity with frequency is the result of non-uniform distribution of current, an equivalent circuit would then be composed of a set of capacities and resistors,  $C_i$  and  $R_i$ , arranged so that there are parallel paths, each of which contains one  $C$  and the corresponding  $R$ . It is readily seen that in such an arrangement, extrapolation to sufficiently low frequencies will yield the sum of the individual capacities  $C_i$ ; sufficiently low frequencies require that all of the  $R_i$ -values will be small compared with the corresponding  $(1/2\pi f C_i)$  terms. The results in Table 2 may have approached this requirement; however, as mentioned, unresolved questions on the nature of the surface preclude further discussion at this stage of the significance of the numerical values obtained in these measurements.

#### EFFECT OF ELECTRODE POTENTIAL ON DOUBLE-LAYER CAPACITY

In studies where frequency dispersion is absent or ignored, measurements of the double-layer capacity are commonly made with signals of 1000 Hz or thereabouts. At solid electrodes<sup>19</sup>, the measured capacities generally are similar to those at mercury in that the capacity rises at both positive and negative polarizations and shows a more

TABLE 4

SERIES RESISTANCE AND CAPACITANCE AT A PYROLYtic GRAPHITE ELECTRODE OF A PYRIDINE SOLUTION OF TETRAETHYLAMMONIUM PERCHLORATE (0.1 M) AT 250 Hz

Potential <sup>a</sup> (V)	$R_s^b$ ( $\Omega$ )	$C_s^b$ ( $\mu F$ )
1.0	286	16.5
0.7	287	14.5
0.5	290	13.5
0.3	294	11.9
0.2	296	11.4
0.1	299	9.8
0	300	10.0
-0.1	302	11.2
-0.2	301	12.4
-0.3	294	11.7
-0.5	290	13.4
-0.7	289	15.0
-1.0	284	17.0

<sup>a</sup>Vs. N.Ag.E.: Ag/1 M  $AgNO_3$  in pyridine<sup>27</sup>.

<sup>b</sup>The values are averages of from one to five separate experiments, normalized for 10  $\mu F$  and 300  $\Omega$  at 0 V; the actual capacity at 0 V was about 60  $\mu F/cm^2$  of macroscopically measured surface.

TABLE 5

EFFECT OF APPLIED POTENTIAL ON SERIES CAPACITY AND RESISTANCE AT A PYROLYtic GRAPHITE ELECTRODE

Potential vs. S.C.E. (V)	$C_s$ ( $\mu F$ )	$R_s$ ( $\Omega$ )
+1.0	7.92	45.7
0.8	7.74	46.7
0.6	7.24	46.6
0.4	7.13	47.0
0.2	6.68	47.4
0.0	6.99	46.4
-0.1	6.68	47.4
0.2	6.58	48.2
0.3	6.60	48.1
0.4	6.57	48.2
0.5	6.68	47.4
0.6	7.02	46.5
0.8	7.38	46.3
1.0	8.05	46.3

<sup>a</sup>Electrode (diam. 4 mm) was sealed in a glass tube by polyethylene with its end flush with the glass; it was resurfaced by polishing. Soln. composition: 0.5 M KCl. Frequency: 1000 Hz.

or less pronounced minimum at intermediate potentials; the minimum capacity is sometimes taken as a measure of the potential of zero charge. In order to compare the behavior of the P.G.E. with that of other solid electrodes in this respect, measurements were made at a fixed frequency with changing electrode potential (Tables 4 and 5).

In aqueous KCl, the capacity appeared to show a very shallow minimum between *ca.* -0.2 and -0.4 V *vs.* SCE; in 0.1 M Et<sub>4</sub>NClO<sub>4</sub> in pyridine, a distinct minimum in the capacity lay close to 0 V *vs.* N.Ag.E.<sup>20</sup> In the latter system, polarization beyond -1.0 V produced an irreversible change in the electrode surface, *i.e.*, results obtained after such a polarization and a return to less negative potentials were scattered and unreproducible. In aqueous KCl solution, such behavior results from reduction of an "oxidized" surface (*cf.* previous discussion) or from the formation of hydrogen through discharge of protons<sup>21</sup>; the reactions, which may occur in pyridine to alter the graphite surface, have not yet been elucidated.

#### ACKNOWLEDGEMENTS

The authors thank the U.S. Atomic Energy Commission and the Horace H. Rackham School of Graduate Studies and the Institute of Science and Technology of The University of Michigan, which helped support the work described. They are indebted to Dr. WILBUR SHULTS for drawing their attention to the work of KASPER.

#### SUMMARY

The apparent double-layer capacity at pyrolytic graphite electrodes has been measured over a wide range of frequencies (50–25,000 Hz) in aqueous and in pyridine solutions. The capacity varied with frequency, as did the series resistance; various methods of preparation of the electrode surface were tried, but with no indication that the frequency-dependence could be eliminated along this line of approach to the problem.

It is suggested that the frequency dispersion may be at least in part an effect of electrode geometry since the distribution of current at a disk electrode is not uniform across the surface.

#### REFERENCES

- 1 P. DELAHAY, *Double Layer and Electrode Kinetics*, Interscience Publishers, New York, 1965.
- 2 B. BREYER AND H. H. BAUER, *Alternating Current Polarography and Tensammetry*, Interscience Publishers, New York, 1963, chap. 3.
- 3 D. E. SMITH, *Anal. Chem.*, 35 (1963) 1811.
- 4 W. L. UNDERKOFLER AND I. SHAIN, *Anal. Chem.*, 35 (1963) 1778.
- 5 H. H. BAUER AND P. J. ELVING, *J. Am. Chem. Soc.*, 82 (1960) 2091.
- 6 M. S. SPRITZER AND P. J. ELVING, work in progress.
- 7 W. R. TURNER AND P. J. ELVING, *Anal. Chem.*, 37 (1965) 207.
- 8 M. S. SPRITZER, J. M. COSTA AND P. J. ELVING, *Anal. Chem.*, 37 (1965) 211.
- 9 M. ROSEN, H. H. BAUER AND P. J. ELVING, work in progress.
- 10 D. C. GRAHAME, *J. Am. Chem. Soc.*, 68 (1946) 301.
- 11 V. I. MELIK-GAIKAZYAN, *Zh. Fiz. Khim.*, 26 (1962) 560 (translated by D. C. GRAHAME).
- 12 K. ROSENTHAL AND B. ERSHLER, *Zh. Fiz. Khim.*, 22 (1948) 1344 (translated by R. PARSONS).
- 13 E. A. UKSHE, N. G. BUKUN AND D. I. LEIKIS, *Russ. J. Phys. Chem. English Transl.*, 36 (1962) 1260.
- 14 D. I. LEIKIS, E. S. SEVASTYANOV AND L. L. KNOTS, *Russ. J. Phys. Chem. English Transl.*, 38 (1964) 997.

- 15 D. C. GRAHAME, *J. Electrochem. Soc.*, 99 (1952) 370C.
- 16 D. C. GRAHAME, *Ann. Rev. Phys. Chem.*, 6 (1955) 337.
- 17 C. KASPER, *Trans. Electrochem. Soc.*, 77 (1940) 353.
- 18 D. H. GRANTHAM, Ph. D. Thesis, Iowa State Univ., 1963; Univ. Microfilms, Order No. 63-2973.
- 19 A. N. FRUMKIN AND B. B. DAMASKIN, *Modern Aspects of Electrochemistry No. 3*, edited by J. O'M. BOCKRIS AND B. E. CONWAY, Butterworths, Washington, 1964, pp. 149-223.
- 20 A. CISAK AND P. J. ELVING, *J. Electrochem. Soc.*, 110 (1963) 160.
- 21 M. ROSEN AND P. J. ELVING, work in progress.

*J. Electroanal. Chem.*, 17 (1968) 299-307



## THE STANDARD POTENTIAL OF THE CALCIUM AMALGAM ELECTRODE

JAMES N. BUTLER

Tyco Laboratories, Inc., Waltham, Massachusetts 02154 (U.S.A.)

(Received October 30th, 1967)

### INTRODUCTION

Although a number of determinations of the potentials of calcium amalgam electrodes in aqueous solutions have been made<sup>1–5</sup>, no critical evaluation of this data presently exists, and in general it is ignored in compilations of thermodynamic data on the potential of the calcium electrode in aqueous solution<sup>6–8</sup>, or discredited as being unreliable<sup>9–11</sup>. However, recent experiments on the kinetics of the calcium amalgam electrode in aqueous calcium formate at high pH-values have shown that the electrode is apparently reversible<sup>12</sup>, in contrast to previous statements that it is irreversible<sup>10</sup>.

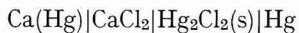
As we will show in this paper, the calcium amalgam electrode is apparently reversible in its behavior, and gives the same value of the standard potential under a wide variety of conditions. In addition, the standard potential of the calcium amalgam electrode is considerably more cathodic than that of sodium amalgam, in spite of the fact that the potentials of the pure metals are in the reverse order. We have used this property in our recent study of the activity coefficients of aqueous sodium chloride–calcium chloride electrolytes using sodium amalgam electrodes<sup>13</sup>.

Previous workers did not apply consistent corrections for activity coefficients to their data, did not in general extrapolate to infinite dilution, and did not in general apply any corrections for temperature, liquid junction potentials, or ion-pairing, where these were applicable. Thus in order to compare these data we recalculated them completely, beginning with the actual experimental measurements, and applying the most recent data on activity coefficients, liquid junction potentials, reference electrode potentials, and ion-pairing equilibria. The results are summarized below. We have divided this discussion into measurements involving cells without liquid junction, cells with liquid junction, and non-aqueous cells.

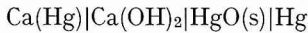
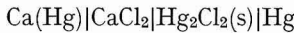
### DISCUSSION

#### *Cells without liquid junction*

The simplest measurement of the standard potential is made in a cell without liquid junction. Two sets of measurements have been made: TAMELE<sup>4</sup> used the cell:



and SHIBATA<sup>5</sup> used the cells:



Taking the  $\text{CaCl}_2$  cell as an example, we shall describe the method used for calculation. The potential of the cell is given by

$$E = E_{\text{ref}}^0 - E_{\text{Ca(Hg)}}^0 - \frac{RT}{2F} \ln \left\{ \frac{[\text{Ca}^{2+}][\text{Cl}^-]^2 \gamma^{\pm 3}}{X_{\text{Ca}} \gamma_{\text{Ca}}} \right\}.$$

The potential  $E$  is positive according to the IUPAC convention. The experimental measurements consist of the total concentration of  $\text{CaCl}_2$  ( $M$ ), the reference electrode standard potential,  $E_{\text{ref}}^0$ , the mole fraction of calcium in the amalgam ( $X_{\text{Ca}}$ ), the temperature  $T$ , and the measured potential  $E$ . To calculate a value of the amalgam standard potential, one must make assumptions about the activity coefficients of the ions and about the possibility of ion-pairing, and about the activity coefficient of calcium in the amalgam.

In the case of solutions containing only  $\text{CaCl}_2$  in water, ion-pairing is probably quite small<sup>11</sup> and we assumed that the ion-pair equilibrium constant,  $K_1$ , was 0.1 for all our calculations concerning  $\text{CaCl}_2$ :

$$[\text{CaCl}^+] = K_1 [\text{Ca}^{2+}] [\text{Cl}^-]$$

The activity coefficient of the ions was assumed to be given by the Davies equation:

$$\log \gamma_{\pm} = -A|Z_+ Z_-|V/I/(1+V/I) + 0.1|Z_+ Z_-|I$$

where

$$I = 2 [\text{Ca}^{2+}] + \frac{1}{2} [\text{CaCl}^+] + \frac{1}{2} [\text{Cl}^-]$$

is the ionic strength. This equation represents the experimental activity coefficients satisfactorily in dilute solutions, and provides a rational basis for calculating single-ion activity coefficients in the cells involving liquid junctions.

The activity coefficient of calcium in the amalgam was provisionally assumed to be unity, since there were no data or theory available which would predict this quantity. Since the amalgams are dilute, it was expected (by analogy with alkali-metal amalgams) that the activity coefficient of calcium would be within a few percent of unity. If the standard potential was found to vary with amalgam concentration, it could be extrapolated to zero concentration.

The standard potential of the calomel electrode was taken to be<sup>14</sup>

$$E_{\text{ref}}^0 = +0.27082 - 0.000254 (T - 15.0)$$

The amalgam standard potentials calculated from TAMELE's data, are plotted in Fig. 1.

Similar calculations were made for SHIBATA's measurements on the  $\text{Ca(OH)}_2$  cell. For this calculation, the ion-pairing constant was taken to be<sup>15</sup>  $K_1 = 10^{+1.20}$ , and the standard potential of the  $\text{HgO}/\text{Hg}$  electrode was taken to be<sup>16</sup>

$$E_{\text{ref}}^0 = +0.0977 - 0.000288 (T - 25.0)$$

The standard potentials are also plotted in Fig. 1.

With the exception of two points, all the data fit a single straight line (Fig. 1) giving  $E^0$  as a function of  $M$ . There does not appear to be any systematic trend with

temperature or with amalgam concentration, within the ranges covered, and there appear to be negligible differences between  $\text{CaCl}_2$  and  $\text{Ca}(\text{OH})_2$  as electrolyte. This latter observation is quite important, since the pH of the  $\text{CaCl}_2$  solution was probably about 6 or 7, and the pH of the  $\text{Ca}(\text{OH})_2$  solution was about 12. If there had been interference from the hydrogen evolution reaction, we would have expected the  $\text{CaCl}_2$  measurements to give  $E^0$ -values which were systematically more positive than the

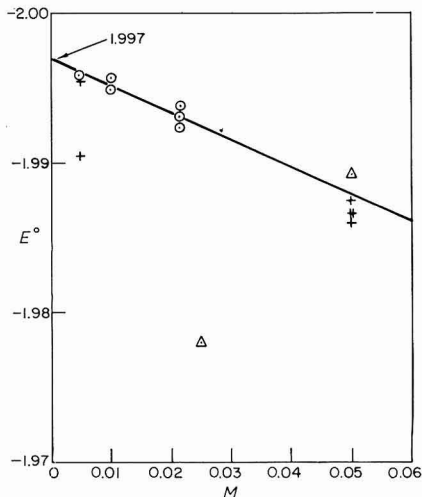


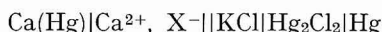
Fig. 1. Standard potential of  $\text{Ca}(\text{Hg})$  electrode. (○), SHIBATA ( $\text{Ca}(\text{OH})_2$ ); (△), SHIBATA ( $\text{CaCl}_2$ ); (+), TAMELE ( $\text{CaCl}_2$ ).

$\text{Ca}(\text{OH})_2$  measurements, both because of amalgam corrosion (which increases  $\text{Ca}^{2+}$  concentration near the electrode) and because of kinetic interference. Although the  $\text{CaCl}_2$  measurements of TAMELE are two or three millivolts more positive than those of SHIBATA, this difference is within experimental error. The fact that TAMELE's  $\text{CaCl}_2$  value at 0.005 M agrees with SHIBATA's  $\text{Ca}(\text{OH})_2$  value at the same concentration is perhaps the strongest evidence that the electrode potentials measured are indeed thermodynamic values.

The trend of calculated  $E^0$  with concentration simply reflects the use of the Davies equation as an extrapolation function; and extrapolation of the  $E^0$ -values to zero concentration gives a thermodynamic potential of  $-1.997 \pm 0.001$  V.

#### Cells with liquid junction

Almost one hundred measurements were made by DRUCKER AND LUFT<sup>2</sup> and by FOSBINDER<sup>1</sup>, using the cell:



In this cell, the nature of the anion has relatively little influence. FOSBINDER used  $\text{CaSO}_4$ ,  $\text{Ca}(\text{OH})_2$ ,  $\text{CaCl}_2$ , calcium lactate, and calcium acetate. DRUCKER AND LUFT used only  $\text{CaCl}_2$ . Their cell was slightly different, in that they used a normal calomel electrode connected to the  $\text{CaCl}_2$  solution by a 3 M KCl salt bridge. FOSBINDER used a saturated calomel electrode and a saturated KCl salt bridge. In either case, the poten-

tial of the cell is given by

$$E = E_{\text{ref}}^0 - E_{\text{Ca(Hg)}}^0 - \frac{RT}{2F} \ln \frac{[\text{Ca}^{2+}] \gamma_{2+}}{X_{\text{ca}} \gamma_{\text{ca}}} + E_j$$

For our calculations, we assumed (as before) that  $\gamma_{\text{ca}}$ , the activity coefficient of calcium in the amalgam, was unity and that the activity coefficient of the calcium ion was given by the Davies equation:

$$\log \gamma_{2+} = -4A/I(1+I) + 0.4I$$

$$I = 2[\text{Ca}^{2+}] + \frac{1}{2}[\text{CaX}^+] + \frac{1}{2}[\text{X}^-] \quad \text{for salts of the type CaX}_2$$

$$I = 2[\text{Ca}^{2+}] + 2[\text{SO}_4^{2-}] \quad \text{for CaSO}_4$$

The ion-pairing equilibrium constants used are given below:

<i>Ion pair</i>	<i>log K<sub>1</sub></i>	<i>Reference</i>
Ca <sub>2+</sub> -Cl <sup>-</sup>	-1	11
Ca <sup>2+</sup> -acetate	+0.77	17
Ca <sup>2+</sup> -OH <sup>-</sup>	+1.20	15
Ca <sup>2+</sup> -lactate	+1.42	18
Ca <sup>2+</sup> -SO <sub>4</sub> <sup>2-</sup>	+2.31	19

The combined potential of the reference electrode and liquid junction was taken to be the value given by IVES AND JANZ<sup>20</sup>

$$E_{\text{ref}}^0 + E_j = +0.283 - 0.0003(T - 25) \quad \text{for normal calomel}$$

$$= +0.2445 - 0.00066(T - 25) \quad \text{for saturated calomel}$$

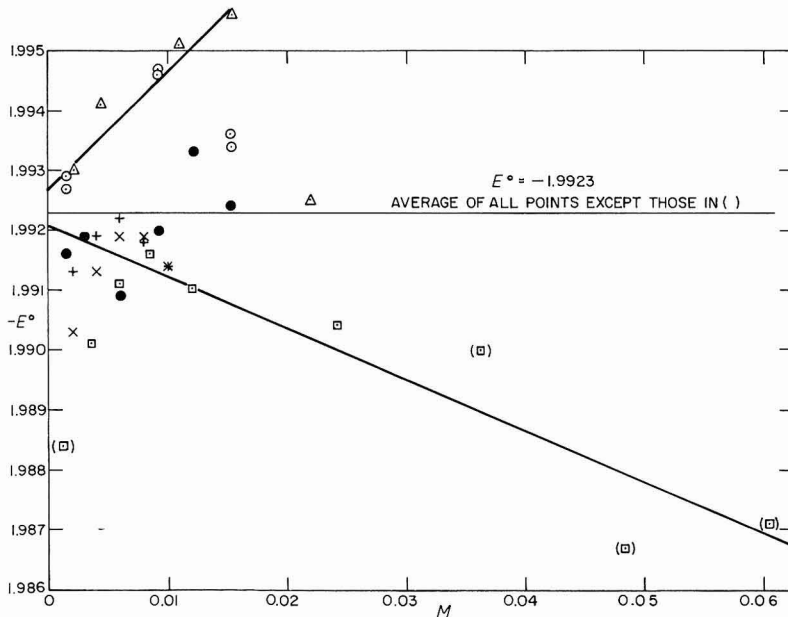


Fig. 2. Standard potential of Ca(Hg) electrode (data of FOSBINDER).  $10^3 X_{\text{ca}}:$  (□),  $\text{CaCl}_2, 0.75;$  (●),  $\text{CaSO}_4, 0.75;$  (○),  $\text{CaSO}_4, 0.60;$  (△),  $\text{Ca}(\text{OH})_2, 0.60;$  (+),  $\text{Ca lactate}, 0.60;$  (×),  $\text{Ca acetate}, 0.60.$

In calculating the activity coefficients, it was usually necessary to make several iterations, since the presence of the ion-pairs had a substantial influence on the ionic strength.

Figure 2 summarizes all the  $E^{\circ}$ -values for the calcium amalgam electrode which were calculated from FOSBINDER's data. Though one set of the  $\text{CaSO}_4$  data shows an upward trend with increasing concentration, and the  $\text{CaCl}_2$  data show a downward trend, all the data can be combined to give a standard potential

$$E^{\circ} = -1.992 \pm 0.001 \text{ V.}$$

This is 5 mV more positive than the value obtained from cells without liquid junction.

The data of DRUCKER AND LUFT<sup>3</sup> were less precise. Though the temperature varied substantially, there appeared to be no obvious trend with temperature. The slight trend of  $E^{\circ}$  with electrolyte concentration was accounted for by extrapolation to  $M=0$ . These extrapolated values are plotted in Fig. 3, along with all the other

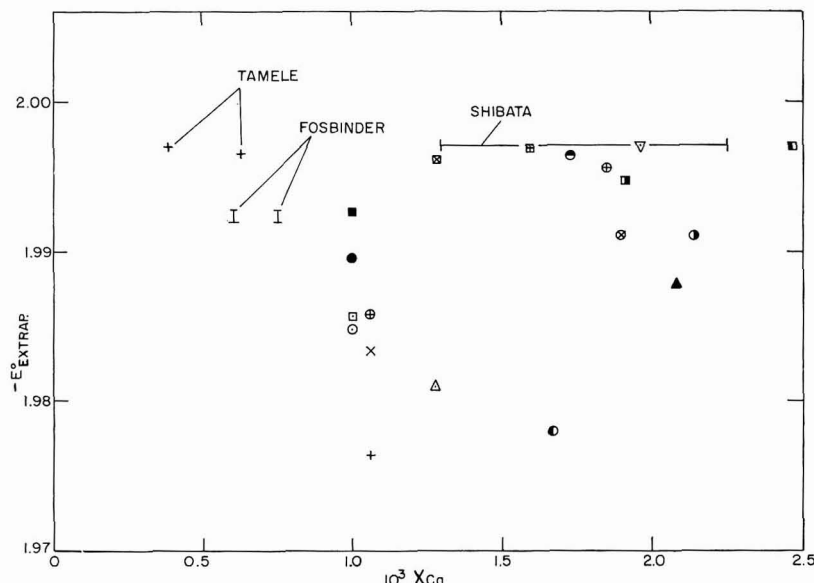


Fig. 3. Standard potential as a function of calcium amalgam concn. (all unmarked points: DRUCKER AND LUFT).

data, as a function of amalgam concentration. If the first two series of DRUCKER AND LUFT's data are ignored (since they show wide scatter) all the data from the four separate investigators lies between  $-1.992$  and  $-1.997$  V. There does not seem to be any trend with amalgam concentration, though a range of nearly a factor of ten was covered. This substantiates the assumption that  $\gamma_{\text{Ca}}=1$ .

DRUCKER AND LUFT's third series (which they consider to be the most accurate) gives an average potential

$$E^{\circ} = -1.996 \pm 0.001 \text{ V}$$

which agrees with the results from cells without liquid junction to within 1 mV.

In conclusion, the most reliable value for the standard potential of calcium amalgam (reference state: infinite dilution, mole fraction units for amalgam concentration, moles/l for electrolyte concentration) is

$$E^{\circ} = -1.996 \pm 0.002 \text{ V}$$

#### *Non-aqueous cells*

Although the thermodynamic potential of calcium amalgams apparently can be established in aqueous solutions with respect to standard reference electrodes, the potential of pure calcium is much too negative for any kind of electrochemical equilibrium to be established with an aqueous solution. The rapid corrosion and passivation problems cause entirely spurious potentials (much too positive) to be developed.

The standard potentials of the alkali metals have been measured by LEWIS and co-workers using the standard potential of the amalgams in aqueous solutions, and combining this information with the potential of a non-aqueous cell which has the amalgam as the positive electrode and the pure metal as the negative electrode. Such an approach should also work for calcium, and has been attempted on a number of occasions. However, the results obtained in this way for the standard potential of Ca have been discarded by the compilers of most tables of oxidation-reduction potentials<sup>6-9</sup>. The value given is -2.87 V, which was calculated by LATIMER<sup>21</sup> from the heat of dissolution of Ca in acid and the entropies of the hydrogen and calcium ions.

A much more important difficulty with the experimental measurements is the passivation of the calcium electrode. All the workers who have attempted measurements with the cell:



or similar non-aqueous cells, have remarked on the necessity for scraping the surface of the calcium electrode continuously in order to obtain a reproducible potential value. TAMELE<sup>4</sup> says: "The EMF of the non-aqueous cell was less constant. If not scratched, the value was about 0.6 volt and indistinct. During scraping the value rose to 0.88-0.90 volts and remained constant, varying slightly with the concentration of the calcium amalgam. After prolonged, very intensive scratching, the EMF fluctuated towards still greater values, which was most probably due to the warming of the rubbed surface. Owing to the instability of the calcium amalgam, the final determinations had to be obtained from the couple (aqueous and non-aqueous cells measured simultaneously) to ensure the same concentration of amalgam in both amalgam electrodes."

DRUCKER AND LUFT<sup>2</sup> said: "First we tried to make the measurement in a closed container but a remarkable case of passivity occurred, which has already been described by Tamele. A voltage of only 0.4 volts or less is observed when the calcium is completely immersed, but nevertheless no surface reaction is visible on the completely shiny metal. If one grinds the surface with a roughened glass or with carbondum, approximately 0.8 volts are obtained. Even a slight vibration of the electrode already dispenses with the passivity—for instance, hitting it against the glass wall. During the measurements, stirring was introduced, and the metal rod was always vibrating slightly against the glass wall. Under these circumstances, the voltage

dropped only very slowly, and reached its highest value immediately after renewal of the amalgam surface. Stopping the stirring caused the voltage to drop immediately to 0.4 volts, after which it decreased slowly. Stirring again caused the original value to appear once more."

It appears from DRUCKER AND LUFT's illustration that their measurements were carried out in an open beaker. No mention was made of using a drybox or other inert-atmosphere facility. The fact that these measurements gave a lower potential difference may be explained by atmospheric contamination with oxygen or water or both.

SHIBATA<sup>5</sup> said: "The difficulty lies in the following points: (1) When the calcium amalgam is brought into contact with water, decomposition begins, which lowers the concentration of calcium in the amalgam. (2) in the process of measuring the EMF between calcium and calcium amalgam, the surface of the calcium is oxidized, even though it is immersed in the organic solvent, so that the EMF is noticeably lowered... The vessel is made out of thick glass and is polished with rough sand. The reason for this is to keep a new surface of calcium continually exposed by rubbing the calcium electrode on the rough surface... When rubbing stops, the potential falls (from 0.895 volts) to 0.84 or lower. If the calcium electrode is not covered with de-Khotinsky cement, an unpolished spot is exposed to the solution, and in this case the observed value falls to 0.4 volts. If the diameter of the end is too large (*i.e.*, 7 mm), then the potential also falls because of the unpolished parts; but an end which is too small also gives an unstable value."

Again, the apparatus diagram implies that the experiments were done in an open beaker, and no indication of an inert-atmosphere facility is given.

It is clear from these experiments that passivation of the calcium surface is an important problem, but the fact that no real attempt was made to exclude oxygen or water-vapor from the system may have made the errors much larger than they need to be.

In Table 1, we have summarized all the experiments performed to date, including some early measurements by CAMBI<sup>22</sup>, some measurements by SMYRL<sup>23</sup> and our own preliminary measurements<sup>24</sup>. The quantity,  $\Delta E^0$ , listed in the last column of the table, was calculated from the equation

$$\Delta E^0 = E_{\text{Ca(Hg)}}^0 - E_{\text{Ca}}^0 = E + (RT/2 F) \ln X_{\text{Ca}} \gamma_{\text{Ca}}$$

As before, we have assumed that the activity coefficient of calcium in the amalgam is unity. The concentration of calcium ion in the electrolyte does not enter the calculation, but in most cases, the non-aqueous solution was saturated with the calcium salt.

From the observations quoted above, we expect that the highest values obtained for  $\Delta E^0$  are probably most nearly correct, since both factors introducing systematic error (corrosion and passivation of the solid calcium) tend to decrease the measured potential below its thermodynamic value. Thus we choose  $\Delta E^0 = 0.813$  (SHIBATA's highest value) to be the best of the presently available experimental values. Several other measurements tend to confirm this, but are slightly lower: CAMBI (0.791), TAMELE (0.782), SHIBATA (0.803), and our own measurements (0.789). We believe now, in the light of all these studies, that it may be possible to obtain a

TABLE I

POTENTIAL BETWEEN CALCIUM AMALGAM AND SOLID CALCIUM  
 $\text{Ca(s)}|\text{Ca}^{2+}$ , non-aqueous solution| $\text{Ca(Hg)}$

Workers	Year	Salt	Concn. (M)	Solvent	$X_{\text{Ca}}$ in amalgam	T (°C)	E	$\Delta E^0$
CAMBI <sup>22</sup>	1914	$\text{CaCl}_2$	0.25	MeOH	0.0148 (satd.)	-80	0.502	0.467
		$\text{CaCl}_2$	0.25	MeOH	0.01	-80	0.811	0.773
CAMBI <sup>22</sup>	1915	$\text{CaCl}_2$	0.35	MeOH	0.01	-80	0.829	0.791
		$\text{CaI}_2$	0.0093	pyridine	0.01	+25	0.149	0.089
TAMELE <sup>4</sup>	1924	$\text{CaI}_2$	satd.?	pyridine	0.000385	17.5	0.88 0.90	0.782 0.802
DRUCKER AND LUFT <sup>2</sup>	1926	$\text{CaI}_2$	satd.	pyridine	0.00126	17	0.843	0.759
SHIBATA <sup>5</sup>	1931	$\text{CaI}_2$	satd.	pyridine	0.00133	15	0.895	0.813
		$\text{CaI}_2$	satd.?	EtOH	0.00133	16	0.885	0.803
SMYRL <sup>23</sup>	1966	$\text{CaCl}_2$	0.0288	DMSO	0.0051	25	0.310	0.242
			0.0551	DMSO	0.0051	25	0.316	0.248
HUSTON AND BUTLER <sup>24</sup>	1967	$\text{CaCl}_2$	0.010	propylene carbonate	0.000148 0.000136	25	0.802 0.876	0.789 0.762

more nearly thermodynamic value for  $\Delta E^0$  by being extremely careful to eliminate oxygen and water from our non-aqueous electrolyte, and by introducing freshly-prepared amalgam and freshly-polished solid Ca simultaneously into the electrolyte. If the potential is read as a function of time during the first few minutes of cell operation, it may be possible to extrapolate to zero time and obtain a better measurement than has formerly been possible.

Let us now compare the value of the standard potential of calcium obtained by LATIMER with the value calculated from the best available experimental data. Since the amalgam concentrations used in both the aqueous and non-aqueous studies were roughly the same, the assumption of unit activity coefficient for calcium in the amalgam should not introduce appreciable error. The standard potential of the amalgam in aqueous solution we have already established as:

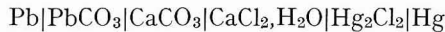
$$E_{\text{Ca(Hg)}}^0 = -1.996 \pm 0.002 \text{ V}$$

and in our discussion above, we proposed that the difference in standard potentials between the amalgam and solid calcium was greater than 0.813 V. This implies that

$$E_{\text{Ca}}^0 = -2.809 \text{ V}$$

or some more negative value. LATIMER's calculated value is -2.87 V, and to obtain this experimentally,  $\Delta E^0$  would have to be larger than 0.87 V. A value this high has not yet been obtained, but might be possible to obtain with extreme care.

As a final note, we must report that recent measurements<sup>25</sup> of the cell:



when combined with other thermodynamic data, have yielded the value  $E^0_{\text{Ca}} = -2.868$  V, which supports LATIMER's calculated value.

## ACKNOWLEDGEMENTS

This work was supported by the U.S. Department of the Interior, Office of Saline Water. The author thanks Dr. J. C. SOHM for a most stimulating discussion.

## SUMMARY

Experimental data in the literature on the potentials of calcium amalgam electrodes in aqueous solutions have been critically evaluated, and the standard potential of the amalgam in aqueous solutions found to be  $-1.996 \pm 0.002$  V vs. the standard hydrogen electrode. The standard state of calcium in the amalgam was infinite dilution, mole fraction scale, and, within experimental error, the activity coefficient of calcium in the amalgam was unity over the range from 0–0.25 mole %.

## REFERENCES

- 1 R. J. FOSBINDER, *J. Am. Chem. Soc.*, 51 (1929) 1345–56.
- 2 C. DRUCKER AND F. LUFT, *Z. Physik. Chem.*, 121 (1926) 307–29.
- 3 L. MEITES, *Polarographic Techniques*, Interscience, New York, 1965.
- 4 M. TAMELE, *J. Phys. Chem.*, 28 (1924) 502–5.
- 5 F. L. E. SHIBATA, *J. Sci. Hiroshima Univ.*, A1 (1931) 147–57.
- 6 F. D. ROSSINI, *Selected Values of Thermodynamic Properties*, Nat. Bur. Std. U.S., Circ. 500, 1950.
- 7 W. M. LATIMER, *Oxidation Potentials*, Prentice-Hall, New Jersey, 1952.
- 8 L. G. SILLÉN AND A. E. MARTELL, *Stability Constants*, The Chemical Society, London, 1964.
- 9 G. CHARLOT, D. BÉZIER AND J. COURTOT, *Selected Constants: Oxidation–Reduction Potentials*, Pergamon Press, London, 1958.
- 10 R. A. ROBINSON, *Trans. Faraday Soc.*, 36 (1940) 735–38.
- 11 H. S. HARND AND B. B. OWEN, *The Physical Chemistry of Electrolytic Solutions*, Reinhold, New York, 1958.
- 12 J. C. SOHM, private communication.
- 13 J. N. BUTLER AND R. HUSTON, *J. Phys. Chem.*, 71 (1967) 4479.
- 14 S. R. GUPTA, G. J. HILLS AND D. J. G. IVES, quoted in D. J. G. IVES AND G. J. JANZ, *Reference Electrodes*, Academic Press, New York, 1961, p. 138.
- 15 R. G. BATES, V. E. BOWERS, R. G. CANHAM AND J. E. PRUE, *Trans. Faraday Soc.*, 55 (1959) 2062.
- 16 W. J. HAMER AND D. N. CRAIG, *J. Electrochem. Soc.*, 104 (1957) 206.
- 17 C. A. COLEMAN-PORTER AND C. B. MONK, *J. Chem. Soc.*, (1952) 4363.
- 18 C. W. DAVIES AND C. B. MONK, *Trans. Faraday Soc.*, 50 (1954) 132.
- 19 R. P. BELL AND J. H. B. GEORGE, *Trans. Faraday Soc.*, 49 (1953) 619.
- 20 D. J. G. IVES AND G. J. JANZ, *Reference Electrodes*, Academic Press, New York, 1961, pp. 160–161.
- 21 W. M. LATIMER, *J. Phys. Chem.*, 31 (1927) 1267.
- 22 L. CAMBI, *Atti Reale Accad. Lincei, Ser. 5, Rend. Classe Sci. Fis. Mat. Nat.*, 24 (1915) 817–22.  
ibid., 23 (1914) 601–11.
- 23 W. H. SMYRL, Thesis, University of California, 1966.
- 24 R. HUSTON AND J. N. BUTLER, unpublished data.
- 25 B. JAKUSEWSKI AND S. TANIEWSKA-OSINSKA, *Roczniki Chem.*, 36 (1962) 329.



## THE OXYGEN ELECTRODE IN MOLTEN SALTS. POTENTIOMETRIC MEASUREMENTS

N. S. WRENCH\* AND D. INMAN\*\*

*Chemistry Department, City University, London, E.C.1 (England)*

(Received November 2nd, 1967)

### INTRODUCTION

The oxide concentration in molten salts is important in determining the acid–base characteristics of melts, since according to the Lux–Flood definition of an acid–base reaction in molten salts,



In order to determine the oxide concentration it is necessary to establish an oxygen electrode at an inert electrode. The oxygen electrode reaction is usually written as:



and the Nernst Equation for this reaction at an inert electrode is given by:

$$E = E^{\circ}_{\text{O}_2/\text{O}^{2-}} + (RT/4F) \ln ([\text{O}_2]/[\text{O}^{2-}]^2) \quad (2)$$

Several attempts have been made to establish reversible oxygen electrodes but these have been mainly confined to oxyanionic melts<sup>1–4</sup>. LAITINEN AND BHATIA<sup>5</sup> attempted to establish an oxygen electrode on carbon in molten lithium chloride–potassium chloride (LiCl–KCl) eutectic but were not successful; they did however show that certain electrodes of the second kind— $\text{M}_x\text{M}_y\text{O}_z\text{O}^{2-}$ —responded reversibly to the oxide-ion concentration. LITTLEWOOD AND ARGENT<sup>6</sup> found that the potential of a platinum electrode in NaCl–KCl (in air) gave an anomalous slope when plotted as a function of Na<sub>2</sub>O concentration. SHAMS EL DIN AND EL HOSARY<sup>7</sup> have used a platinum electrode in LiCl–KCl containing oxide as an indicator electrode for acid–base titrations. Plots of potential against the logarithm of the oxide-ion concentration in the absence of acid did not give the correct slope.

This paper reports a study of the potential behaviour of gold and platinum electrodes in a LiCl–KCl melt containing dissolved oxide and hydroxide, and the effects of varying the oxygen partial pressure above the melt.

### EXPERIMENTAL

#### *Apparatus*

A molten salt thermostat was used instead of the more conventional wire-wound furnace. This thermostat enabled the temperature to be controlled to  $\pm 0.2^\circ$  at 450°.

\* Present address: Central Electricity Research Laboratories, Leatherhead, Surrey, England.

\*\* Present address: Metallurgy Department, Imperial College, London, S.W.7, England.

The cell envelope was a Pyrex-glass tube closed at one end and fitted with a B55 socket at the other end. A water-cooled brass head was inserted in this socket; a vacuum and gas-tight seal was obtained by two O-rings. Electrodes and gas delivery tubes passed through the head by means of glass syringes. The melt ( $\sim 50$  ml) was contained in a gold crucible. Before an experiment, the crucible was cleaned in nitric-sulphuric acid, washed in distilled water and dried at  $120^\circ$ . The electrodes, gold and platinum wires 0.5 mm diam., were cleaned in the same way. The gases nitrogen, oxygen and argon, were obtained from cylinders and purified by the usual techniques.

The electrochemical cell consisted of the electrode under investigation and a silver-silver chloride reference electrode similar to that described by BOCKRIS *et al.*<sup>10</sup>. In this work no attempt was made to produce glass membranes of resistances below  $5000\ \Omega$  and the bulb thickness was about 0.5 mm. Potential measurements were made using either a Radiometer PH4 meter or a Vibron high impedance millivoltmeter used in conjunction with a Tinsley 3887B potentiometer.

The attack on the Pyrex bulbs by the basic melt did not appear to affect the potential measurements significantly, as the following observations show. Two identical reference electrodes placed in the same solution took up potentials within 1 mV of each other in 2 h. This potential difference did not become greater than 5 mV in 24 h which indicated that any asymmetry potentials were relatively small. The reproducibility of the oxygen electrode potentials was about  $\pm 20$  mV and therefore the errors introduced by the reference electrode could be neglected.

### Chemicals

The solvent, LiCl-KCl, was purified by pre-electrolysis under vacuum<sup>8</sup>. The criterion of purity of the melt was that the "residual time" of a potential-time curve obtained under galvanostatic conditions was negligible compared with the transition time to be expected when a solute was present. Analysis of samples of the melt by titration of an aqueous extract to pH 4.5 showed that the residual oxide concentration was less than  $5 \cdot 10^{-4}\ M$ .

Lithium oxide was prepared by a modification of the method described by BRAVO<sup>9</sup>. Lithium hydroxide,  $\text{LiOH} \cdot \text{H}_2\text{O}$ , was dried in a stream of nitrogen at  $150^\circ$ . The anhydrous LiOH was placed in a gold crucible and heated under vacuum to  $675^\circ$  to effect decomposition. The apparatus was dismantled in the dry box where the  $\text{Li}_2\text{O}$  was removed to, and stored in, a desiccator over soda-lime and magnesium perchlorate.

AnalaR potassium hydroxide was used after storage over magnesium perchlorate. The water content was determined by analysis.

### RESULTS AND DISCUSSION

The applicability of eqn. (2) to an oxygen electrode consisting of oxygen bubbling around platinum or gold wires immersed in LiCl-KCl containing dissolved  $\text{Li}_2\text{O}$ , was studied. Measurements were also made in solutions of KOH. All experiments were carried out at  $450^\circ$ .

The potential values obtained were converted to the 1 M Pt/Pt<sup>2+</sup> scale using the equation:

$$E_{(\text{Pt})} = E_{(\text{Ag})} + 0.1434 \log (\text{Ag}^+) - 0.743 \text{ V}$$

where  $(\text{Ag}^+)$  is the concentration of silver ions in the reference bulb in mole l<sup>-1</sup> and

$E_{(Ag)}$  is the potential of the oxygen electrode relative to the silver reference electrode.

The electrode potentials of gold and platinum in the pure eutectic under a nitrogen atmosphere were  $-0.90$  V and  $-0.86$  V, respectively. These potentials were only reproducible to  $\pm 0.1$  V. When oxygen gas was admitted to the cell, these potentials rapidly became more positive. After about one hour the potentials became steady, on gold:  $0.40 \pm 0.04$  V, and platinum:  $-0.36 \pm 0.04$  V. If nitrogen gas was now readmitted to the system, the electrode potentials did not return to their original values but only changed in a negative direction by about  $0.1$  V. Readmission of oxygen established the previous potential.

When  $\text{Li}_2\text{O}$  was added to the pure eutectic through which nitrogen was bubbling, the potential of both gold and platinum electrodes became more negative. When bubbling was stopped, the potential drifted slowly in a positive direction. No really stable and reproducible potentials were obtained for the  $\text{Li}_2\text{O}$  solute under either a static or bubbling atmosphere. The potential of a platinum electrode was generally about  $0.25$  V negative of that of a gold electrode.

When oxygen was bubbled into a melt containing oxide that had been held in nitrogen, the electrode potentials immediately became more positive. The potential change was of about the same magnitude, irrespective of the concentration of  $\text{Li}_2\text{O}$ . For gold this change was  $0.68$  V, and for platinum  $0.94$  V. It was also noted that the potentials of partly immersed electrodes were  $0.02$  V more positive than those of totally immersed electrodes in both nitrogen and oxygen atmospheres.

Attempts to investigate the variation of electrode potential with oxygen partial pressure were not conclusive. A gold or platinum electrode placed in a melt containing oxide under oxygen at one atmosphere pressure took up a steady reproducible potential. When the oxygen pressure was reduced by pumping down the system in stages, no stable potentials were established. The electrode potential drifted in a negative direction at each reduction in pressure. A pressure change of one order of magnitude produced a maximum potential change of  $0.02$  V rather than  $0.036$  V as required by eqn. (2).

Potential measurements with respect to oxide concentration under oxygen at one atmosphere pressure were more successful. At very low  $\text{Li}_2\text{O}$  concentrations, both gold and platinum electrodes took up to one hour to reach equilibrium. Gold electrodes were  $0.05$  V more positive than platinum electrodes. When a concentration of about  $2 \cdot 10^{-2} M$  oxide was reached, the potential of both gold and platinum electrodes changed in a negative direction by  $0.35$  V. The exact concentration at which this occurred was difficult to determine; no really satisfactory potential readings being obtained in the concentration range  $1 \cdot 10^{-2}$ – $2.5 \cdot 10^{-2} M$  oxide. Additions of  $\text{Li}_2\text{O}$  to give concentrations above  $2.5 \cdot 10^{-2} M$  produced rapid changes in electrode potential. Gold and platinum electrodes took up the same potential to  $\pm 2$  mV. Figure 1 shows the results of two experiments. The slope of the plot is  $0.140$  V. This figure corresponds, at  $450^\circ$ , to a pre-logarithmic factor of  $RT/F$ , and not  $RT/2F$  as predicted by eqn. (2).

This result clearly indicates that reaction (1) does not describe the behaviour of either the oxygen (gold) electrode or the oxygen (platinum) electrode in  $\text{LiCl}-\text{KCl}$  melts containing  $\text{Li}_2\text{O}$ . Also, the variation of the electrode potentials with a change in the partial pressure of oxygen was not that of a "reversible" electrode. The effect of admitting oxygen to systems initially under an inert atmosphere indicates that an irreversible process takes place. The most likely process is the surface oxidation of the

"inert" electrode. It has been shown that thick oxide films can form on platinum in molten nitrates<sup>11</sup> and oxide films have also been observed on gold and platinum in molten carbonates at 600°<sup>1</sup>. The extent of the surface oxidation of the electrodes used in these measurements was studied using cathodic galvanostatic pulses<sup>12</sup>. The results showed that gold electrodes under nitrogen were less highly "oxidised" than electrodes under oxygen. Platinum electrodes were also shown to be "oxidised".

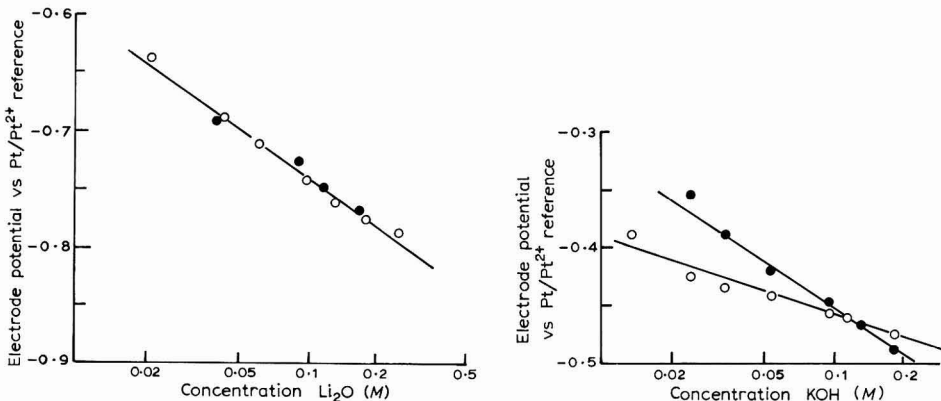


Fig. 1. Plot of potentials of gold and platinum electrodes *vs.* lithium oxide concn. in LiCl-KCl at 450° in oxygen atm. Points represent results from separate expts.; measurements on gold and platinum electrodes indistinguishable.

Fig. 2. Plot of potentials of (○), gold and (●), platinum electrodes *vs.* potassium hydroxide concn. in LiCl-KCl at 450° in oxygen atm.

The potential-determining process on this type of electrode has been discussed by several workers. JANZ AND SAEGUSA<sup>1</sup>, studying the O<sub>2</sub>(Au) and O<sub>2</sub>(Pt) electrodes in molten carbonates at 600°, described the electrodes as "relatives of the metal-metal oxide type". The O<sub>2</sub>(Pt) electrode in an unbuffered KNO<sub>3</sub> melt was found to give an *RT/F* slope<sup>13</sup>. The authors thought that small traces of moisture in the melt would give rise to OH<sup>-</sup> ions and the platinum would then function as a hydroxide electrode. In the present work, additions of potassium hydroxide produced a very complex concentration-electrode potential behaviour. Initially, the additions of KOH produced positive changes in potential at a platinum electrode; this was followed as the concentration was increased, by the expected negative change. The potential behaviour of gold electrodes was similar but the potential maximum was less pronounced. Figure 2 shows a plot of potential against the logarithm of concentration of KOH for gold and platinum electrodes. The pre-logarithmic factors are: gold, *RT/2F* and platinum, *RT/F*. The reproducibility of the results was not as good as that obtained with Li<sub>2</sub>O. The variation of the oxygen partial pressure over the melts did not produce any well-defined potential changes. This result suggests that the explanation given by SHAMS EL DIN<sup>13</sup> cannot be applied to this work.

If the electrode is functioning as an electrode of the second kind, *e.g.*, Pt, PtO/O<sup>2-</sup>, the potential-determining processes are as follows:



and the potential is given by:

$$E = E^0_{\text{Pt}^{2+}, \text{Pt}} + (RT/2F) \ln K_{sp} - (RT/2F) \ln (O^{2-}) \quad (5)$$

where  $K_{sp}$  is the solubility product of PtO.

A similar scheme can be written for the gold-gold oxide electrode. Both schemes lead to a pre-exponential factor of  $RT/2F$ , and not  $RT/F$  as found. It was observed that gold and platinum electrodes took up the same potential; this behaviour is unexpected if they function as electrodes of the second kind. The free energies of formation of PtO and  $\text{Au}_2\text{O}_3$  at  $450^\circ$  are approximately,  $-2.6$  kcal and  $+44$  kcal.

Sodium peroxide<sup>7</sup> and potassium hydroxide<sup>14</sup> have been used as sources of oxide ion. It is assumed that sodium peroxide decomposes to give oxide and oxygen. This appears to be doubtful, particularly if oxygen is present. STERN<sup>15</sup> reported finding up to 1% peroxide in oxide solutions in sodium chloride at  $900^\circ$ . In the present work, aqueous extracts of the solidified melt were analysed by iodometric titration and peroxide was found to be present. It was also shown that potassium hydroxide did not decompose completely when added to LiCl-KCl at  $450^\circ$ <sup>21</sup>.

Consideration of the Gibbs' free energies of formation at  $450^\circ$  shows that oxides in addition to  $M_2\text{O}$  (where M is an alkali metal) are likely to be stable (Table 1). Lux *et al.*<sup>16</sup> have shown that oxygen reacts with molten hydroxides in the temperature range  $400^\circ$ - $600^\circ$  to give peroxides. A recent study of molten hydroxides by current-potential curves has indicated that, depending upon the acid-base conditions, the ions  $\text{O}^{2-}$ ,  $\text{O}_2^{2-}$  and  $\text{O}_2^-$  and dissolved oxygen, can be present in the melt<sup>17,18</sup>. PIZZINI

TABLE 1

FREE ENERGIES OF FORMATION OF VARIOUS OXIDES AT  $450^\circ$ 

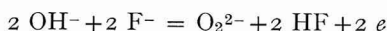
Oxide	$\Delta G$ (kcal/mole of M)	Oxide	$\Delta G$ (kcal/mole of M)
$\text{Li}_2\text{O}$	- 121	$\text{K}_2\text{O}$	- 63
$\text{Na}_2\text{O}$	- 76	$\text{K}_2\text{O}_2$	- 81
$\text{Na}_2\text{O}_2$	- 85	$\text{KO}_2$	- 47
$\text{NaO}_2$	- 39		

TABLE 2

PARAMETERS OF THE OXYGEN ELECTRODE REACTION

Solute	Chemical reaction	Electrode reaction	$\frac{\partial \ln(O_2)}{\partial E}$	$\frac{\partial \ln(\text{solute})}{\partial E}$
$\text{O}^{2-}$		$\frac{1}{2}\text{O}_2 + 2e = \text{O}^{2-}$	$RT/4 F$	$- RT/2 F$
$\text{O}_2^{2-}$	$\text{O}_2^{2-} = \frac{1}{2}\text{O}_2 + \text{O}^{2-}$	$\frac{1}{2}\text{O}_2 + 2e = \text{O}^{2-}$	$RT/2 F$	$- RT/2 F$
$\text{OH}^-$	$2\text{OH}^- = \text{H}_2\text{O} + \text{O}^{2-}$	$\frac{1}{2}\text{O}_2 + 2e = \text{O}^{2-}$	$RT/4 F$	$- RT/F$
$\text{O}_2^{2-}$		$\text{O}_2 + 2e = \text{O}_2^{2-}$	$RT/2 F$	$- RT/2 F$
$\text{O}^{2-}$	$\text{O}_2^{2-} = \frac{1}{2}\text{O}_2 + \text{O}^{2-}$	$\text{O}_2 + 2e = \text{O}_2^{2-}$	$RT/4 F$	$- RT/2 F$
$\text{O}_2^{2-}$		$\text{O}_2^{2-} + 2e = 2\text{O}^{2-}$		$+ RT/2 F$
$\text{O}^{2-}$		$\text{O}_2^{2-} + 2e = 2\text{O}^{2-}$		$- RT/F$
$\text{OH}^-$		$\text{H}_2\text{O} + \text{O}_2 + 4e = 4\text{OH}^-$	$RT/4 F$	$- RT/F$
$\text{O}^{2-}$	$\text{O}^{2-} + \text{H}_2\text{O} = 2\text{OH}^-$	$\text{H}_2\text{O} + \text{O}_2 + 4e = 4\text{OH}^-$	$RT/4 F$	$- RT/2 F$
$\text{O}_2^{2-}$	$\text{O}_2^{2-} + 2\text{H}_2\text{O} = 4\text{OH}^-$	$\text{H}_2\text{O} + \text{O}_2 + 4e = 4\text{OH}^-$	$RT/4 F$	$- RT/4 F$

AND MORLOTTI<sup>19</sup> have explained the results of some electrochemical measurements in molten fluorides on the assumption that peroxide ion is formed in the melt. They suggested that the ion was formed electrochemically at the anode:



The stability of peroxides in molten FLiNaK was demonstrated by dissolving Na<sub>2</sub>O<sub>2</sub> in the melt at 600° and carrying out an analysis of the aqueous extract of the solidified melt.

Table 2 gives the values of the Nernst slopes that can be predicted for several oxygen electrode reaction schemes. Possible chemical reactions involving the solute, as well as the actual charge transfer reactions, play a part in determining the Nernst slope. It can be seen that only one reaction scheme gives rise to a slope of  $RT/F$  for the addition of Li<sub>2</sub>O; this is:



The exchange current for this homogeneous reaction is probably much higher than that for the heterogeneous reaction (1). Therefore, the former is more likely to be potential-determining than the latter.

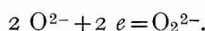
The observations that gold and platinum electrodes take up the same potential can be accounted for on this basis. However the role of the oxide film on the surface of the metal is not explained by this model. The Nernst slopes predicted for models that directly involve stoichiometric surface oxides are all  $RT/2F$ . Presumably the adsorbed oxide film functions as an electronic, rather than as an ionic, conductor. Surface oxides of the type MO<sub>2</sub> have been proposed as intermediates in the cathodic and anodic processes in molten carbonates<sup>20</sup>. Again, however, the Nernst slopes for models involving this type of oxide are  $RT/2F$ .

#### ACKNOWLEDGEMENT

The authors wish to thank the Central Electricity Generating Board for financial assistance.

#### SUMMARY

The results of potentiometric studies in molten lithium chloride-potassium chloride eutectic are reported. The potentials of gold and platinum electrodes were found to respond to variations in the oxide-ion concentration of the melt and to changes in the partial pressure of oxygen above the melt. These changes in potential did not obey the Nernst Equation for a reversible oxygen electrode. It is suggested that the potential-determining reaction is:



#### REFERENCES

- 1 G. J. JANZ AND F. SAEGUSA, *Electrochim. Acta*, 7 (1962) 393.
- 2 H. FLOOD, T. FORLAND AND K. MOTZFIELDT, *Acta Chem. Scand.*, 6 (1952) 257.
- 3 H. LUX, *Z. Elektrochem.*, 45 (1939) 303; *ibid.*, 52 (1948) 220; *ibid.*, 53 (1949) 43.
- 4 G. K. STEPANOV AND A. M. TRUNOV, *Dokl. Akad. Nauk SSSR*, 142 (1962) 866.

- 5 H. A. LAITINEN AND B. B. BHATIA, *J. Electrochem. Soc.*, 107 (1960) 705.
- 6 R. LITTLEWOOD AND E. J. ARGENT, *Electrochim. Acta*, 4 (1961) 114.
- 7 A. A. SHAMS EL DIN AND A. A. EL HOSARY, *J. Electroanal. Chem.*, 6 (1963) 131.
- 8 A. D. GRAVES, D. INMAN AND N. S. WRENCH, in preparation.
- 9 J. BRAVO, *Inorg. Syn.*, 7 (1963) 1.
- 10 J. O'M. BOCKRIS, G. J. HILLS, D. INMAN AND L. YOUNG, *J. Sci. Instr.*, 33 (1956) 438.
- 11 R. L. EVERETT AND R. L. GRIMSLY, *J. Electroanal. Chem.*, 9 (1965) 165.
- 12 N. S. WRENCH AND D. INMAN, in preparation.
- 13 A. M. SHAMS EL DIN AND A. A. GERGES, in *Electrochemistry, Proceedings of 1st Australian Conference on Electrochemistry*, 1963, Pergamon, London, 1964.
- 14 G. DELARUE, Thesis, University of Paris, 1960.
- 15 K. H. STERN, *J. Phys. Chem.*, 66 (1962) 1311.
- 16 H. LUX, R. KUHN AND T. NEIDERMAIER, *Z. Anorg. Allgem. Chem.*, 298 (1959) 285.
- 17 J. GORET, *Bull. Soc. Chim. France*, (1964) 1074.
- 18 J. GORET AND B. TREMILLON, *Bull. Soc. Chim. France*, (1966) 67.
- 19 S. PIZZINI AND R. MORLOTTI, *Electrochim. Acta*, 10 (1965) 1033.
- 20 A. V. SILAKOV, G. S. TYURIKOV AND N. P. VASILISTOV, *Elektrokhimiya*, 1 (1965) 613.
- 21 N. S. WRENCH, Ph.D. Thesis, University of London, 1967.

*J. Electroanal. Chem.*, 17 (1968) 319-325



## HIGH SENSITIVITY COULOMETRIC ANALYSIS IN ACETONITRILE

RUSSELL R. BESETTE\* AND JOHN W. OLVER

*Department of Chemistry, University of Massachusetts, Amherst, Mass. 01002 (U.S.A.)*

(Received September 28th, 1967)

### INTRODUCTION

Acetonitrile has found wide use in analytical and electrochemical studies where an aprotic medium is desired or potentials more negative than available in aqueous media. Metal ions generally have lower solvation energies in acetonitrile than in water and are, therefore, reduced at more positive potentials in this non-aqueous medium<sup>1</sup>.

Cuprous copper is an exception to this rule. In aqueous solution the uncomplexed cuprous ion is unstable and disproportionates into cupric copper and copper metal. The cupric ion gives a single polarographic wave at 0.0 V vs. SCE corresponding to its reduction to the amalgam. In acetonitrile, the cuprous ion is stabilized with the result that two reduction waves are obtained for the cupric ion<sup>2</sup>. The first, corresponding to the reduction of Cu(II) to Cu(I), occurs at a potential more positive than the anodic dissolution of mercury (+0.6 V vs. SCE). The second, corresponding to the reduction to the amalgam, occurs at -0.36 V vs. SCE with alkylammonium perchlorate as supporting electrolyte. Quantitative generation of cuprous ions by controlled-potential coulometry could play a role in such applications as, the determination of terminal alkynes, the elucidation of the stoichiometry involved in the synthesis of Cu(I) complexes, the synthesis of inorganic or organo-metallic compounds, or as a reductant in oxidation-reduction reactions.

In spite of the current interest in high energy density cell systems using light alkali-metal anodes in aprotic solvents, there are few methods available for the quantitative microanalysis of these metal ions with a precision and accuracy of 0.5% or less. The reduction potentials of sodium and lithium are accessible in acetonitrile<sup>1</sup>. COKAL AND WISE<sup>3</sup>, in a brief communication, used controlled-potential anodic stripping to determine a single concentration (1.31 μequiv.) of sodium with moderate success ( $\pm 1.2\%$ ). The quantitative polarographic determination of the alkali-metal ions in this medium is hampered by slightly distorted waves and erratic capillary behavior.

We, therefore, have examined the usefulness of acetonitrile for direct controlled-potential coulometric reduction of copper and some alkali-metal ions.

\* Present address: Olin Mathieson Chemical Corporation, New Haven, Conn.

## EXPERIMENTAL

*A. Reagents*

Acetonitrile (Union Carbide, bulk grade) was purified by Method F of FORCIER AND OLVER<sup>4</sup>. A final check on the purity of the acetonitrile was made by running a polarographic scan between +0.6 and -2.8 V *vs.* SCE. The solvent was used if the current that flowed could be attributed solely to charging current.

Tetraethylammonium perchlorate ( $\text{Et}_4\text{NClO}_4$ ) was prepared in the manner described by KOLTHOFF AND COETZEE<sup>1</sup>.

Tetraethylammonium tetrafluoroborate ( $\text{Et}_4\text{NBF}_4$ ) was prepared as described elsewhere<sup>5</sup>.

Copper perchlorate was prepared by adding dropwise to a slurry of basic cupric carbonate ( $\text{CuCO}_3 \cdot \text{Cu}(\text{OH})_2$ , Fisher Scientific Reagent-Grade), a solution of perchloric acid (B and A Reagent-Grade) until the evolution of carbon dioxide stopped. The solution was filtered to remove any unreacted cupric hydroxide. The copper perchlorate was recrystallized and washed three times with cold water and dried under vacuum for twenty-four hours. Copper perchlorate prepared in the manner described crystallizes as the hexahydrate<sup>6</sup>. The copper content determined by electrodeposition<sup>7</sup> was  $17.16 \pm 0.01\%$ , compared with a theoretical value for per-cent copper in  $\text{Cu}(\text{ClO}_4)_2 \cdot 6\text{H}_2\text{O}$  of 17.15%.

Lithium and sodium perchlorates were prepared as described by WAWZONEK AND RUNNER<sup>8</sup>. Owing to the hygroscopic nature of anhydrous sodium and lithium perchlorates, and to insure their complete dryness, these salts were dried in the manner described by JONES<sup>9</sup> before preparing the standard solutions.

*B. Apparatus and methodology*

The coulometric cell was an all-glass, three-compartment water-jacketed system<sup>10</sup>. The working electrode, central, and auxiliary electrode sections were separated from each other by fine porosity 10-mm glass frits (Ace Glass Co., porosity D). The central and auxiliary compartments were provided with ground-glass joints and sealed with glass caps. Glass inlets were provided in the cap of the working electrode section, for a salt bridge and for the passage of nitrogen above and into the solution. The working electrode was a mercury pool 5 cm in diameter, and the auxiliary electrode was a coil of platinum wire.

The salt bridge contained a 0.1 M acetonitrile solution of the supporting electrolyte used in the working electrode section.

The reference electrode consisted of an aqueous solution containing 1 M  $\text{Me}_4\text{NCl}$  and calomel over a mercury pool<sup>5</sup>. The reference potential was +0.043 V *vs.* SCE and remained constant to within 1 mV.

A Jaissle model 300R potentiostat was used to maintain the potential applied to the working electrode. A provision was included for instantaneously monitoring the current that flowed in the auxiliary electrode–working electrode circuit. The controlled-potentials used to attain 99.9% complete electrochemical reactions were determined as described by DELAHAY<sup>11</sup>.

The coulometer was a conventional resistance–capacitance electronic integrator. The unit was based on the design of the integrator section of the previously described High Sensitivity Controlled-Potential Coulometric Titrator<sup>12</sup>. Modifications in the

JONES, SHULTS AND DALE integrator consisted in changing the values of the feedback resistances in the current-controlling amplifier, and the value of the capacitor in the integrating amplifier. These modifications were needed to make possible the integration of the current values over the time periods relevant during the course of the present experiments.

A further modification based on a design by BOOMAN<sup>13</sup> consisted of introducing a variable 250- $\Omega$  resistor between the input of the current-controlling amplifier and the connection to the working electrode. The variable resistor allowed one to limit the initial current to any desired value in cases where an amplifier-limiting initial current was otherwise obtained. This resistor added the capability to work in highly concentrated solutions of electroactive material.

During the course of the experiments, the current-time function was continuously monitored by attaching a Sargent Model SR recorder with a floating input, to the terminals on the potentiostat provided for that purpose. The chart speed was set at 12 in./h and a variable range switch was used in order to maintain maximum recorder sensitivity throughout the course of the experiment. The recorder range could be varied from 100  $\mu$ A/mm down to 1  $\mu$ A/mm.

The applied potentiostatic potential and the integrator readout potential were measured using a Honeywell Potentiometer model 2730. A Sola constant voltage transformer was used in conjunction with the potentiostat and integrator in order to stabilize the line voltage. A 0.1- $\mu$ F capacitor was inserted across the poles to the reference and auxiliary electrodes in the potentiostat in order to filter out 60 cycle a.c. noise which was otherwise picked up by the unshielded cell. With this capacitor in the circuit, the noise level was reduced to 2 mV peak-to-peak.

Solutions were stirred with a Mag-Mix (Precision Scientific Company) magnetic stirrer and a 7/8-in. glass-enclosed stirring bar.

The solutions were de-aerated for 45 min prior to electrolysis with Airco pre-purified nitrogen. Tank nitrogen was bubbled through an all-glass train consisting of aqueous vanadous chloride followed by two scrubbing towers of concentrated sulfuric acid, and finally an acetonitrile presaturator, before entering the cell.

All experiments were carried out at  $25.0^\circ \pm 0.1^\circ$  using a P.M. Tamson constant temperature bath and circulating pump Model A2.

Blank corrections were made for faradaic impurity, faradaic residual and charging currents. The corrections were evaluated by a pre-electrolysis at the controlled-potential followed by addition of a volume of solvent equal to the sample volume, and a second electrolysis during which the current-time function was integrated over the time period of the experiment (usually 1 h). The bulk solution contained 0.1 M Et<sub>4</sub>NClO<sub>4</sub> as supporting electrolyte.

The stock solution of Cu(ClO<sub>4</sub>)<sub>2</sub>·6H<sub>2</sub>O was prepared by dissolving a quantity of the salt in acetonitrile and diluting to the mark in a volumetric flask. This solution was standardized by electrodeposition<sup>7</sup> and found to contain 1.405 mg of copper/ml of solution.

Stock solutions of sodium or lithium perchlorate were prepared as follows. A quantity of the appropriate salt was added to a previously weighed volumetric flask. The flask and contents were dried in an oven at 250° for at least 10 h. It was then removed, placed in a desiccator over phosphorus pentoxide, allowed to come to room temperature and reweighed. Solvent was added to the mark.

TABLE I  
CONTROLLED-POTENTIAL ELECTROLYSES IN ACETONITRILE

Sample	n	E <sup>a</sup>	Taken (μequiv.)	Found <sup>b</sup> (μequiv.)	Blank (μequiv.)	i <sub>Res.</sub> (μA)	% Error	% S.D.	Time to 99% completion (min)
Cu <sup>2+</sup>	2	-0.600	21.9	0.029	0	0.00	±0.64	45	
	1	-0.100	11.1	11.0	0.00	0	0.90	±0.00	38
Cu(II) → Cu(I)									
Cu(I) → Cu(Hg)	-0.600	11.1	11.3	0.261	0	1.80	±0.88	18	
Na <sup>+</sup>	1	-2.000	102.8	103.4	0.185	2	0.58	±0.81	25
			25.8	26.0	0.185	2	0.78	±0.27	25
			5.16	5.14	0.251	0	0.39	±0.68	23
Li <sup>+</sup>	1	-2.200	99.7	99.3	0.434	2	0.40	±0.58	23
			21.2	21.2	0.156	3	0.00	±0.33	26
			5.00	4.95	0.130	4	1.00	±0.17	23

<sup>a</sup> E vs. Hg, Hg<sub>2</sub>Cl<sub>2</sub>, TMACl (aq, 1.0 M).

<sup>b</sup> All values are averages of at least 3 determinations in solns. with 0.1 M Et<sub>4</sub>NClO<sub>4</sub> as supporting electrolyte.

All sample volumes for analysis were measured with a calibrated 1-ml syringe. The delivered volumes could be reproduced to within 0.002 ml.

## RESULTS AND DISCUSSION

### A. Electrolysis of copper ions

The results for the controlled-potential coulometric studies on copper in acetonitrile are summarized in Table I. The results of a direct reduction of Cu(II) to the amalgam indicated that the potentiostat, integrator, and cell were functioning properly. Linear log current *vs.* time plots were obtained in all cases thus assuring the absence of a catalytic current contribution. The residual current was insignificant.

The data show that the quantitative coulometric generation of cuprous copper in acetonitrile with  $\text{Et}_4\text{NClO}_4$  as supporting electrolyte is feasible. Uncomplexed Cu(I) is relatively stable in acetonitrile since it can be kept in a de-aerated solution for at least 1 h and subsequently reduced quantitatively to the amalgam.

The slightly high results obtained for the reduction of Cu(I) to the amalgam can be attributed to a cumulative error from the previous reduction of Cu(II) to Cu(I) and to the size of the blank correction necessary and the precision involved in its determination. For the reduction of Cu(I), the bulk of solution in the cell was de-aerated and pre-electrolyzed at  $-0.100$  V. Cu(I) was then coulometrically generated from Cu(II). The potential was shifted to  $-0.600$  V and the Cu(I) was reduced to the amalgam. The same procedure was followed in the blank determination. This unavoidable shift of 500 mV between the pre-electrolysis and electrolysis potentials led to the high blank correction and subsequent error in the determination. In all other analyses the pre-electrolysis was performed at the same potential setting used for the analysis.

### B. Electrolysis of alkali-metal ions

This investigation was limited to sodium and lithium perchlorates.

In the initial electrolyses in the  $10\text{--}30 \mu\text{equiv}$ . range, the errors in determinations on successive samples added to the same solvent and electrolyte, drifted in a single direction toward smaller errors rather than scattering about a mean. On consecutive electrolyses of  $100 \mu\text{equiv}$ . samples in a single solution, the first determination was low by 2–3%, but all successive determinations were quantitative and scattered about 0% error. In any subsequent determination at any concentration level, after a pre-electrolysis the solution was pretreated by adding  $100 \mu\text{equiv}$ . of the sample and reducing that to the amalgam.

In using the pretreatment above, the residual current after a pre-electrolysis ( $11 \mu\text{A}$ ) was always approximately 4 times greater than the residual current after a single electrolysis at the  $100\text{-}\mu\text{equiv}$ . level ( $3 \mu\text{A}$ ). The change in the residual current level before and after a solution pretreatment suggested a catalytic current contribution. The possible contributors were residual water, the cationic or anionic portion of the supporting electrolyte, impurities present in the supporting electrolyte and oxygen. No experimentally significant effect on the catalytic current was found on varying the residual water concentration, the concentration of supporting electrolyte, and on changing the supporting electrolyte from  $\text{Et}_4\text{NClO}_4$  to  $\text{Et}_4\text{NBF}_4$ .

To determine the effect of oxygen, a pre-electrolysis was performed without

de-aeration followed by an electrolysis with 99.7  $\mu\text{equiv}$ . of lithium added. These determinations are compared in Fig. 1 with a pre-electrolysis performed after 1-h de-aeration. The residual current level without de-aeration was 80  $\mu\text{A}$  compared with 12  $\mu\text{A}$  residual current for the pre-electrolysis with de-aeration. The results also showed that the lithium did interrupt the catalytic process, since the residual current level decreased from 80  $\mu\text{A}$  to 26  $\mu\text{A}$ . Furthermore, the lithium determination was about 50% low.

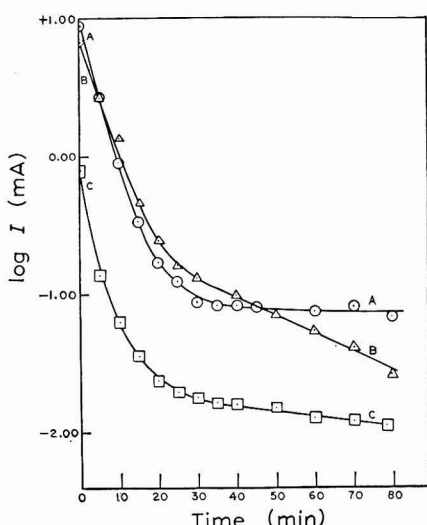


Fig. 1. Log current *vs.* time curves. (A), Pre-electrolysis with no de-aeration; (B), subsequent electrolysis with 99.7  $\mu\text{equiv}$ . of lithium perchlorate added; (C), pre-electrolysis with 1-h nitrogen de-aeration.

SAWYER AND ROBERTS<sup>14</sup> have proposed the production of and the subsequent disproportionation (rate 1–3%/h) of the superoxide ion in dimethylsulfoxide at a mercury electrode with  $\text{Et}_4\text{NClO}_4$  as supporting electrolyte. They also noted that when  $\text{LiClO}_4$  was used as a supporting electrolyte, a film formed on the mercury surface due to insoluble, non-electroactive  $\text{LiO}_2$ .

PEOVER AND WHITE<sup>15</sup> give evidence for the production of the superoxide ion in acetonitrile. They based their conclusion on the observation of an electron spin resonance signal for the superoxide anion. Decay of the radical was indicated by a decrease of the ESR signal with time.

It is reasonable to assume that a very small concentration (only  $2 \cdot 10^{-5} M$  oxygen would be required) of oxygen remained in the electrolysis cell even after a 45-min de-aeration period. This residual oxygen when reduced to the superoxide anion ties up the alkali-metal ions, causes low results, and therefore requires the solution pretreatment already described in order to obtain correct results.

The quantitative controlled-potential coulometric analyses of sodium and lithium at various concentrations are summarized in Table 1. The results agree favorably in precision and accuracy with other microchemical methods of analysis for

these metal ions, such as the determination of sodium as sodium zinc uranyl acetate<sup>16</sup> and the determination of lithium as periodate<sup>16</sup>.

These analyses were better than 99.9% complete in 30 min and the operator need be present for only a fraction of that time. Another time-saving feature is that successive analyses can be performed on the same bulk solution and mercury pool. By adapting the system to stirring with a high speed synchronous motor, the analysis time could be shortened even further.

The upper limit of concentration that can be handled by this method is determined by the solubility of the metal in mercury (0.039 wt% for Li and 0.62 wt% for Na<sup>17</sup>). The lower limit is determined by the error involved in determining the blank correction. The blank determinations could be made with a precision of 10%. Considering the average size of the blank correction and limiting the error to within  $\pm 1\%$ , the lower limit of applicability is 2  $\mu$ equiv.

#### ACKNOWLEDGEMENT

This work was supported in part by the Directorate of Chemical Sciences, AFOSR Grant 777-65, and taken in part from the thesis submitted by R.R.B. in partial fulfilment of requirements for the Ph.D. degree at the University of Massachusetts, 1967.

#### SUMMARY

Cuprous copper was quantitatively coulometrically generated in acetonitrile. No catalytic or induced current contribution was found. Uncomplexed Cu(I) was stable in acetonitrile since it could be kept in solution for at least an hour and subsequently reduced quantitatively to the amalgam.

The slightly high results obtained for the reduction of Cu(I) to the amalgam were attributed to relatively high blank corrections and to any cumulative errors from the previous reductions of Cu(II) to Cu(I).

In the determination of sodium and lithium, a solution pretreatment and electrolysis with 100  $\mu$ equiv. of sodium or lithium perchlorate was necessary to eliminate a catalytic current contribution caused by residual oxygen. The results for the quantitative controlled-potential coulometric analysis of sodium and lithium agreed favorably in precision and accuracy with other microquantitative methods of analysis. Under the conditions employed, the method is applicable between a lower limit of 2  $\mu$ equiv. governed by error in the blank determination and an upper limit governed by solubility of the metals in the pool used.

#### REFERENCES

- 1 I. M. KOLTHOFF AND J. F. COETZEE, *J. Am. Chem. Soc.*, 79 (1957) 870.
- 2 I. M. KOLTHOFF AND J. F. COETZEE, *J. Am. Chem. Soc.*, 79 (1957) 1852.
- 3 E. J. COKAL AND E. N. WISE, *Anal. Chem.*, 35 (1963) 914.
- 4 G. A. FORCIER AND J. W. OLVER, *Anal. Chem.*, 37 (1965) 1447.
- 5 G. A. FORCIER, Ph.D. Thesis, University of Massachusetts, 1966.
- 6 N. V. SIDGWICK, *The Chemical Elements and Their Compounds*, Oxford University Press, London, England, 1950.

- 7 H. H. WILLARD, N. H. FURMAN AND C. E. BRICKER, *Elements of Quantitative Analysis*, Van Nostrand Co., Princeton, N.J., 4th ed., 1956.
- 8 S. WAWZONEK AND M. E. RUNNER, *J. Electrochem. Soc.*, 99 (1952) 457.
- 9 J. H. JONES, *J. Phys. Colloid Chem.*, 51 (1947) 516.
- 10 L. MEITES, *Anal. Chem.*, 27 (1955) 1116.
- 11 P. DELAHAY, *New Instrumental Methods in Electrochemistry*, Interscience Publishers, Inc., New York, N.Y., 1954, p. 274.
- 12 H. C. JONES, W. D. SHULTS AND J. M. DALE, *Anal. Chem.*, 37 (1965) 680.
- 13 G. L. BOOMAN, *Anal. Chem.*, 29 (1957) 213.
- 14 D. T. SAWYER AND J. C. ROBERTS, *J. Electroanal. Chem.*, 12 (1966) 90.
- 15 M. E. PE OVER AND B. S. WHITE, *Chem. Commun. London*, No. 10 (1965) 183.
- 16 I. M. KOLTHOFF AND P. J. ELVING, *Treatise on Analytical Chemistry*, Part II, Vol. I, Interscience Publishers, New York, N.Y., 1961.
- 17 M. HANSEN AND K. ANDERKO, *Constitution of Binary Alloys*, McGraw-Hill Book Co., New York, N.Y., 2nd ed., 1958.

*J. Electroanal. Chem.*, 17 (1968) 327-334

## ELECTRODES “METAL-COMPLEXE”

### III. ELECTRODE Ag | [Ag(Et<sub>2</sub>NH)<sub>2</sub>]<sup>+</sup>, Et<sub>2</sub>NH DANS L’ETUDE DES COMPLEXES DE Zn(II) ET Cd(II) AVEC LA DIETHYLAmine

GRIGORE POPA, VASILE MAGEARU ET CONSTANTIN LUCA

*Laboratoire de Chimie Analytique de la Faculté de Chimie de Bucarest, Bucarest (Roumanie)*

(Reçu le 14 septembre, 1967)

Antérieurement, nous avons étudié les principes du fonctionnement d’un nouveau type d’électrodes réversibles par rapport au ligant<sup>1,2</sup>. Un tel type d’électrode peut-être représenter d’un manière schématique par:



Comme le ligant  $\text{L}^{b-}$  réagit avec l’ion  $\text{Me}^{a+}$  pour former le complexe  $[\text{MeL}_n^{(nb-a)-}]$ , on peut écrire l’expression du potentiel de l’électrode métallique:

$$E = E_{\text{Me}^{a+}}^0 + \frac{RT}{aF} \ln \frac{[\text{MeL}_n^{(nb-a)-}]}{\beta_n [\text{L}^{b-}]^n} \quad (2)$$

$\beta_n$  étant la constante de stabilité du complexe.

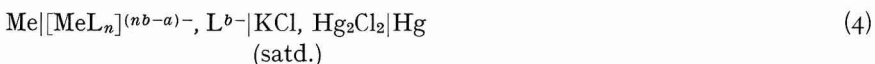
Si la concentration des ions métalliques est très faible par rapport à la concentration du ligant,  $[\text{Me}^{a+}]/[\text{L}^{b-}] < 1/10^6$ , on peut considérer que tous les ions  $\text{Me}^{a+}$  sont pratiquement transformés en complexe. En même temps, si dans une série de déterminations, la concentration des ions  $\text{Me}^{a+}$  reste constante, la concentration du complexe formé reste aussi pratiquement constante.

Dans l’expression (2), la concentration du complexe et la constante de stabilité,  $\beta_n$ , peuvent donc être englobées dans le terme constant:

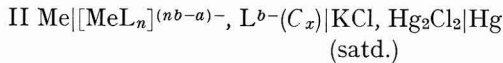
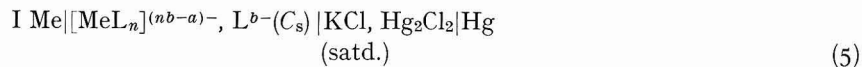
$$E = E_{\text{Me}|\text{MeL}_n^{(nb-a)-}}^0 - (RT/aF) \ln [\text{L}^{b-}]^n \quad (3)$$

Ce type d’électrode réversible par rapport au ligant, a été dénomé “électrode métal-complexe”. Du point de vue de la théorie des solutions électrolytiques, nous pouvons d’ailleurs considérer ce type d’électrode comme analogue à celui des électrodes de deuxième espèce dans lequel le composé insoluble est remplacé par un composé non-dissocié à concentration maintenue fixe.

Nous avons déjà montré<sup>1,2</sup> qu’un tel type d’électrode peut-être utilisé pour déterminer analytiquement la concentration du ligant  $\text{L}^{b-}$  au moyen de la cellule:



mais, le potential de diffusion entre la solution de KCl et la solution de ligant peut-être une source importante d’erreurs. Cet inconvénient peut être éviter en utilisant deux cellules de type:



dans lesquelles les concentrations globales de l'ion  $\text{Me}^{a+}$  sont égales et où l'on connaît la concentration,  $C_s$ , d'une solution standard de ligant.

En présence d'un électrolyte support de force ionique prédominante, la différence des f.e.m. des cellules (5) I et (5) II sera:

$$E_{\text{II}} - E_{\text{I}} = (nRT/aF) \ln [\text{L}^{b-}]_s - (nRT/aF) \ln [\text{L}^{b-}]_x \quad (6)$$

et la concentration inconnue du ligant  $[\text{L}^{b-}]_x$  sera:

$$\log [\text{L}^{b-}]_x = \log [\text{L}^{b-}]_s - a(E_{\text{II}} - E_{\text{I}})/0.05916n \quad (7)$$

Le présent mémoire est destiné à l'étude d'électrode metal-complexe



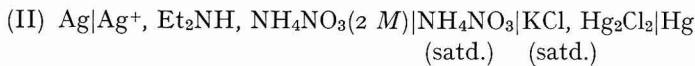
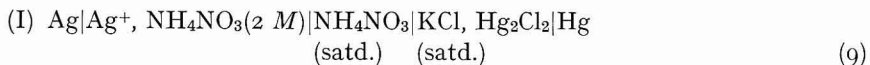
et ses applications à la détermination des constantes de stabilité des autres systèmes de complexation compétitives. Les constantes de stabilité des complexes de zinc et de cadmium avec la diéthylamine ont été déterminées.

#### PARTIE EXPÉRIMENTALE

##### *1. Complexes diéthylaminiques de l'argent*

En vue de vérifier la consistance des résultats, il est intéressant d'établir préalablement (ce qui n'est pas toujours indispensable) les constantes de stabilité des complexes diéthylaminiques de l'argent.

Partant de deux cellules de type:



on peut écrire:

$$E_{\text{I}} - E_{\text{II}} = (RT/F) \ln (C_{\text{Ag}^+}/[\text{Ag}^+]) \quad (10)$$

d'où on peut encore calculer les fonctions  $F([\text{Et}_2\text{NH}])$

$$F([\text{Et}_2\text{NH}]) = \frac{C_{\text{Ag}^+}}{[\text{Ag}^+]} = \sum_0^N \beta_n \cdot [\text{Et}_2\text{NH}]^n \quad (11)$$

Par des extrapolations successives des fonctions:

$$F_n = (F_{n-1} - \beta_{n-1})/[\text{Et}_2\text{NH}] \quad (12)$$

pour lesquelles;

$$\lim_{[\text{Et}_2\text{NH}] \rightarrow 0} F_n = \beta_n \quad (13)$$

on peut déterminer les constantes  $\beta_n$ . Nous avons mis en évidence deux complexes (comme d'ailleurs dans un mémoire antérieur<sup>3</sup>).

Les valeurs des constantes de stabilité, pour les deux complexes ont été trouvées:  $\log \beta_1 = 4.93$  et  $\log \beta_2 = 7.08$ .

Toutes les mesures ont été faites à  $25^\circ \pm 0.1^\circ$  et à la force ionique  $\mu = 2$  ( $\text{NH}_4\text{NO}_3$ ).

Les données expérimentales et les valeurs de la fonction,  $F([\text{Et}_2\text{NH}])$ , pour chaque concentration de ligant sont consignées dans le Tableau I.

TABLEAU I

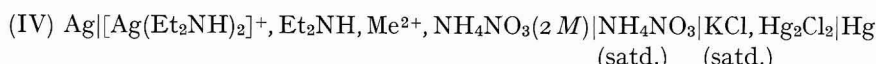
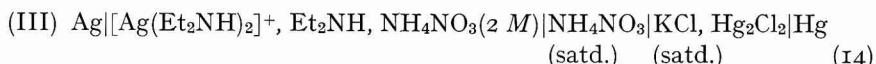
DONNÉES DU SYSTÈME  $\text{Ag}^+ - \text{Et}_2\text{NH}$  $25^\circ, \mu = 2$  ( $\text{NH}_4\text{NO}_3$ )

$C_{\text{Et}_2\text{NH}}$ (M)	$\Delta E = E_I - E_{II}$ (V)	$F \cdot 10^{-4}$	$F_1 \cdot 10^{-5}$	$F_2 \cdot 10^{-7}$
0.02396	0.2295	0.776	3.239	—
0.04745	0.2649	3.095	6.523	—
0.07048	0.2854	6.886	9.770	—
0.11504	0.3081	16.667	14.490	1.257
0.13697	0.3182	24.680	18.045	1.319
0.17925	0.3305	39.920	21.270	1.125
0.21998	0.3393	56.256	25.571	1.162
0.25927	0.3479	78.820	30.400	1.172
0.31564	0.3563	109.300	34.635	1.097

$$\beta_1 = 8.5 \cdot 10^4; \beta_2 = 1.2 \cdot 10^7$$

## 2. Complexes diéthylaminiques du zinc et cadmium

L'on passe ensuite à l'étude des complexes  $\text{Zn}-\text{Et}_2\text{NH}$  et  $\text{Cd}-\text{Et}_2\text{NH}$  en mesurant les f.e.m. d'une série de cellules de type:



dans laquelle la concentration totale de l'ion  $\text{Ag}^+$  a toujours la même valeur. La seule différence des cellules 14(III) et 14(IV) est que la seconde contient en surplus une quantité connue d'ions  $\text{Me}^{2+}$  ( $\text{Zn}^{2+}$  ou  $\text{Cd}^{2+}$ ) réagissant avec le ligant diéthylamine pour former la série des complexes  $[\text{Me}(\text{Et}_2\text{NH})_n]^{2+}$ .

Pour étudier les systèmes  $\text{Me}^{2+}-\text{Et}_2\text{NH}$ , il convient de mesurer la concentration de ligant libre dans la série de cellules 14(IV). On utilise pour cela la relation (7) dans laquelle  $n=1$ ;  $a=1$ ; et  $s$  est la concentration de ligant dans la cellule correspondante 14(III).

On peut écrire (à  $25^\circ$ ):

$$\log [\text{Et}_2\text{NH}]_{IV} = \log [\text{Et}_2\text{NH}]_{III} + (E_{III} - E_{IV}) / 0.11831 \quad (15)$$

On calcule ensuite les valeurs de la fonction de BJERRUM<sup>4</sup>:

$$\bar{n} = (C_{\text{Et}_2\text{NH}} - [\text{Et}_2\text{NH}]) / C_{\text{Me}^{2+}} \quad (16)$$

et les courbes de formation  $\bar{n}-p$   $[\text{Et}_2\text{NH}]$  nous donnent la possibilité de déterminer graphiquement les constantes successives de stabilité,  $k_n$ , par la relation:

$$k_n = ([\text{Et}_2\text{NH}]^{-1})_{\bar{n}=n-\frac{1}{2}} \quad (17)$$

Toutes les valeurs ont été ensuite raffinées à l'aide de la relation de BJERRUM:

$$k_n = ([L]^{-1})_{\bar{n}=n-\frac{1}{2}} \frac{\sum_{t=1}^{t=n-1} \frac{I+2t}{[L]^t \cdot k_{n-1} \cdot k_{n-2} \cdots \cdot k_{n-t}}}{\sum_{t=1}^{t=N-n} (I+2t) \cdot [L]^t \cdot k_{n+1} \cdot k_{n+2} \cdots \cdot k_{n+t}} \quad (18)$$

Les données expérimentales et les valeurs des constantes successives de stabilité pour les deux systèmes sont consignées dans les Tableaux 2, 3 et 6.

Parallèlement, pour vérifier les résultats, nous avons calculé les constantes successives totales de stabilité par une méthode différente, en partant de la courbe  $(\bar{n}/[Et_2NH]) - [Et_2NH]$  qui nous donne la possibilité de déterminer les fonctions:

TABLEAU 2

DONNÉES DU SYSTÈME  $Zn^{2+}$ - $Et_2NH$  $25^\circ, \mu = 2$  ( $NH_4NO_3$ )

$C_{Zn^{2+}}$ (M)	$C_{Et_2NH}$ (M)	$-\Delta E = E_{III} - E_{IV}$ (V)	[ $Et_2NH$ ]	$\phi[Et_2NH]$	$\bar{n}$
0.1237	0.02396	0.1879	0.000611	3.2137	0.189
0.1225	0.04745	0.2044	0.000879	3.0560	0.380
0.1213	0.07048	0.2105	0.001171	2.9316	0.571
0.1190	0.11523	0.2145	0.001753	2.7566	0.953
0.1157	0.17925	0.2180	0.002548	2.5939	1.527
0.1136	0.21998	0.2176	0.003150	2.5017	1.908
0.1116	0.25928	0.2135	0.004022	2.3956	2.287
0.1087	0.31564	0.2054	0.005734	2.2415	2.851
0.1060	0.36913	0.1860	0.010260	1.9889	3.385
0.1040	0.40331	0.1590	0.018544	1.7418	3.699
0.1025	0.43638	0.1250	0.038068	1.4195	3.886
0.1008	0.46841	0.0995	0.067341	1.1717	3.978
0.1000	0.48398	0.0902	0.083255	1.0796	4.006

TABLEAU 3

DONNÉES DU SYSTÈME  $Cd^{2+}$ - $Et_2NH$  $25^\circ, \mu = 2$  ( $NH_4NO_3$ )

$C_{Cd^{2+}}$ (M)	$C_{Et_2NH}$ (M)	$-\Delta E = E_{III} - E_{IV}$ (V)	[ $Et_2NH$ ]	$\phi[Et_2NH]$	$\bar{n}$
0.2450	0.02980	0.2073	0.000523	3.2817	0.119
0.2381	0.07238	0.2238	0.000918	3.0370	0.300
0.2273	0.13818	0.2196	0.001992	2.7211	0.599
0.2273	0.21998	0.2192	0.003053	2.5152	0.954
0.2174	0.31564	0.2008	0.006273	2.2026	1.423
0.2083	0.40331	0.1765	0.012875	1.8901	1.874
0.2000	0.48398	0.1538	0.024071	1.6185	2.299
0.1923	0.55844	0.1329	0.041750	1.3793	2.687
0.1851	0.62741	0.1126	0.069712	1.1576	3.014
0.1786	0.69140	0.0964	0.105391	0.9772	3.281
0.1724	0.75100	0.0829	0.149002	0.8269	3.492
0.1666	0.80663	0.0729	0.194400	0.7113	3.675
0.1613	0.85867	0.0655	0.239210	0.6213	3.840

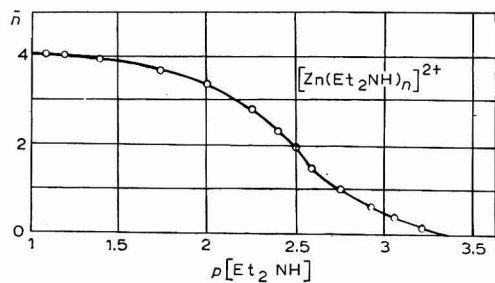
Fig. 1. Courbe de formation du système  $\text{Zn}^{2+}-\text{Et}_2\text{NH}$ .Fig. 2. Courbe de formation du système  $\text{Cd}^{2+}-\text{Et}_2\text{NH}$ .

TABLEAU 4

SYSTÈME  $\text{Zn}^{2+}-\text{Et}_2\text{NH}$ . CALCUL DES CONSTANTES DE STABILITÉ PAR LA MÉTHODE DE FRONAEUS<sup>5</sup>  
 $25^\circ$ ,  $\mu = 2$  ( $\text{NH}_4\text{NO}_3$ )

$[\text{Et}_2\text{NH}]$ (M)	F	$F_1 \cdot 10^{-3}$	$F_2 \cdot 10^{-5}$	$F_3 \cdot 10^{-7}$	$F_4 \cdot 10^{-9}$
0.002	2.0955	0.5477	—	—	—
0.0025	2.7988	0.7195	—	—	—
0.003	3.787	0.929	2.0966	—	—
0.004	6.849	1.462	2.905	5.512	—
0.005	11.888	2.177	3.755	6.110	5.82
0.006	19.78	3.130	4.709	6.688	5.81
0.007	31.59	4.371	5.843	7.347	5.92
0.008	48.44	5.930	7.037	7.921	5.90
0.010	102.3	10.13	9.830	9.130	5.93
0.012	192.1	15.92	13.01	10.25	5.88
0.015	425.3	28.29	18.66	11.97	5.85
0.020	1231	61.49	30.59	14.95	5.87
0.025	2844	113.7	45.36	17.86	5.86
0.030	5656	188.5	62.73	20.67	5.82

$\beta_1 = 3 \cdot 10^2$ ;  $\beta_2 = 7 \cdot 10^4$ ;  $\beta_3 = 3.2 \cdot 10^7$ ;  $\beta_4 = 5.85 \cdot 10^9$ .

TABLEAU 5

SYSTÈME  $\text{Cd}^{2+}-\text{Et}_2\text{NH}$ . CALCUL DES CONSTANTES DE STABILITÉ PAR LA MÉTHODE DE FRONAEUS<sup>5</sup>.  
 $25^\circ$ ,  $\mu = 2$  ( $\text{NH}_4\text{NO}_3$ )

$[\text{Et}_2\text{NH}]$ (M)	F	$F_1 \cdot 10^{-2}$	$F_2 \cdot 10^{-4}$	$F_3 \cdot 10^{-6}$	$F_4 \cdot 10^{-7}$
0.010	9.526	—	—	—	—
0.014	17.620	11.87	—	—	—
0.016	23.015	13.76	—	—	—
0.020	40.767	19.88	7.94	—	—
0.024	61.435	25.17	8.82	—	—
0.030	104.84	34.61	10.20	—	—
0.040	219.70	54.67	12.67	1.972	—
0.050	404.31	80.66	15.34	2.067	1.334
0.060	683.12	113.7	18.28	2.214	1.356
0.070	1082	154.5	21.50	2.357	1.367
0.080	1615	201.8	24.72	2.465	1.331
0.100	3245	324.5	32.05	2.705	1.305
0.120	5916	492.9	40.74	2.978	1.315
0.140	10046	717.4	50.95	3.282	1.344
0.180	24592	1366	75.60	3.922	1.345

$\beta_1 = 4 \cdot 10^2$ ;  $\beta_2 = 5 \cdot 10^4$ ;  $\beta_3 = 1.4 \cdot 10^6$ ;  $\beta_4 = 1.34 \cdot 10^7$ .

TABLEAU 6

VALEURS DES CONSTANTES DE STABILITÉ DES COMPLEXES DE ZINC ET CADMIUM AVEC LA DIÉTHYLAMINE

( $25^\circ$ ,  $\mu = 2$ )

$n$	$[Zn(Et_2NH)_n]^{2+}$			$[Cd(Et_2NH)_n]^{2+}$		
	$\beta[Et_2NH]_{\bar{n}=n-1}$	$\log k_n$ par la méthode de:		$\beta[Et_2NH]_{\bar{n}=n-1}$	$\log k_n$ par la méthode de:	
		BJERRUM	FRONAEUS		BJERRUM	FRONAEUS
1	2.965	2.511	2.477	2.835	2.617	2.602
2	2.598	2.448	2.368	2.141	2.107	2.097
3	2.340	2.529	2.660	1.495	1.516	1.447
4	1.921	2.333	2.262	0.831	1.061	0.983
$\log \beta_4$	9.824	9.821	9.767	7.301	7.302	7.129

$$F = 1 + \beta_1 \cdot [Et_2NH] + \beta_2 \cdot [Et_2NH]^2 + \cdots + \beta_N \cdot [Et_2NH]^N \quad (19)$$

par une intégration graphique basé sur la relation de FRONAEUS<sup>5</sup>:

$$\ln F = \int_0^{[Et_2NH]} \frac{\bar{n}}{[Et_2NH]} d[Et_2NH] \quad (20)$$

On calcule ensuite les constantes successives de stabilité,  $\beta_n$ , pour le système  $Me^{2+}-Et_2NH$  par des extrapolations des fonctions  $F_n = (F_{n-1} - \beta_{n-1})/[Et_2NH]$  (Tableaux 4 et 5).

Les valeurs  $\beta_1 \dots \beta_N$  qui ont été obtenues par la dite méthode sont consignées dans le Tableau 6.

Dans ce tableau on peut constater une bonne concordance des constantes de stabilité obtenues par les deux méthodes.

#### RÉSUMÉ

La stato-potentiométrie directe offre effectivement des possibilités intéressantes de dosage des molécules neutres.

Nous avons mis au point dans le présent mémoire une méthode nouvelle qui permet la détermination de la concentration de la diéthylamine en utilisant une électrode métal-complexe de type:



Nous avons utilisé cette méthode à la base d'une série des mesures destinées à la détermination des constantes de stabilité des complexes de zinc et de cadmium avec la diéthylamine.

#### SUMMARY

Direct potentiometry offers interesting possibilities for quantitative analysis of neutral molecules.

We propose in the present paper a new method for the determination of the concentration of diethylamine using a metal-complex electrode of the type



We have used this method in a series of measurements in which the stability constants for the complexes of zinc and cadmium with diethylamine were determined.

#### BIBLIOGRAPHIE

- 1 C. LUCA, V. MAGEARU ET GR. POPA, *J. Electroanal. Chem.*, 12 (1966) 45.
- 2 V. MAGEARU, C. LUCA ET M. TEODORESCU, *J. Electroanal. Chem.*, 12 (1966) 148.
- 3 GR. POPA, C. LUCA ET V. MAGEARU, *J. Chim. Phys.*, 60 (1963) 355.
- 4 J. BJERRUM, *Metal ammine formation in aqueous solution*, Haase, Copenhagen, 1957.
- 5 S. FRONAEUS, *Acta Chem. Scand.*, 5 (1951) 859.

*J. Electroanal. Chem.*, 17 (1968) 335-341



## KINETICS AND MECHANISM OF THE ADSORPTION OF GLYCOLALDEHYDE ON A SMOOTH PLATINUM ELECTRODE

S. TRASATTI AND L. FORMARO

*Laboratory of Electrochemistry and Metallurgy, University of Milan, Milan (Italy)†*

(Received September 19th, 1967)

### INTRODUCTION

Poisoning phenomena of the electrode surface occur during the oxidation of methanol on platinum<sup>1–3</sup>. Such phenomena were thought<sup>3</sup> to be due to the formation of adsorbed species arising from dimerization of the products of methanol dehydrogenation. According to BIANCHI AND LONGHI<sup>3</sup> these species may be identified as oxalic acid, glyoxal, glycolaldehyde, glycolic acid, glyoxylic acid and ethylene glycol formed from such radicals as ·CHO, ·COOH, ·CH<sub>2</sub>OH. Their experiments showed that glyoxal and glycolaldehyde were the main substances poisoning the platinum surface.

FORMARO AND TRASATTI<sup>4</sup> have reported on the electrochemical behaviour of glyoxal on platinum. The present paper gives the results for glycolaldehyde using smooth platinum electrodes.

### EXPERIMENTAL

#### Materials

Electrodes were prepared with 99.98% platinum wire (Metalli Preziosi, 0.5 mm diam.). Analyzed reagent-grade 60% HClO<sub>4</sub> (Carlo Erba) was used for solutions. The NMR analysis on glycolaldehyde (Fluka) indicated that the crystalline solid was the dimeric form, in agreement with previous results<sup>5</sup>. However, this form was shown<sup>6</sup> to change into the monomer in aqueous solution, the transformation being acid-catalyzed. From the experimental values for the rate constant<sup>6</sup> we have calculated that in 1 M HClO<sub>4</sub> solutions glycolaldehyde is present as the monomer, and we shall always refer to the formula as CH<sub>2</sub>OH-CHO.

#### Methods

Several experimental methods were employed.

Differential capacity curves were used to detect adsorption phenomena. The bridge employed has been described elsewhere<sup>7</sup>. The electrode was activated before each measurement (see later), and the selected potential was applied using a potentiometer. The capacity reading was taken after 3 min.

† This research was sponsored by the Consiglio Nazionale delle Ricerche, Rome, Italy.

The general electrochemical behaviour of glycolaldehyde was studied by means of quasi-stationary potentiostatic  $i/E$  curves according to the method introduced by WILL AND KNORR<sup>8</sup>. The apparatus and experimental procedure adopted have already been described<sup>4</sup>. Each curve was registered after ten complete potential cycles between 60 and 1500 mV (RHE).

The kinetics and amount of adsorption were studied by anodic and cathodic charging curves at high current densities. The apparatus used has been previously described<sup>4</sup>. Electrode activation before each measurement was also carried out in this case.

#### Cell

The cell which has already been described<sup>7</sup> was washed before each experiment with concentrated sulphuric acid, then rinsed and boiled with triple-distilled water. The use of grease on any part of the glass apparatus was avoided.

#### Electrode

Two electrodes were used for the capacity measurements and charging curves. They were prepared by melting the platinum wire in a H<sub>2</sub>-O<sub>2</sub> flame to a small sphere and then sealing the wire into capillary glass tubing. Before use, the electrodes were kept in a vacuum furnace for 3 h at 500° to anneal the metal and eliminate absorbed gases. The electrodes were washed with concentrated H<sub>2</sub>SO<sub>4</sub>, then rinsed and boiled with triple-distilled water before each experiment.

The electrode used for potentiostatic curves was treated similarly. It was prepared by sealing the platinum wire into glass tubing and then sealing a small glass sphere at the other end of the wire to obtain a cylindrical electrode.

#### Electrode real surface area

The real surface areas of the *bead* electrodes were determined by cathodic charging curves as described previously<sup>9</sup>. The areas of the two electrodes were found to be 0.0493 and 0.0394 cm<sup>2</sup>, respectively.

Since the potentiostatic curves were required only for a qualitative analysis of the behaviour of the organic substance, only the geometric (apparent) area of the wire electrode was measured; it was found to be 0.662 cm<sup>2</sup>.

#### Electrode potential

Electrode potentials were measured against a hydrogen electrode<sup>10</sup> in 1 M HClO<sub>4</sub> by means of Keithley electrometers (610 A and 610 B). Potentials quoted in the text and reported in the figures are expressed in RHE scale.

#### Gases

99.999% N<sub>2</sub> with traces of rare gases was used to de-gas solutions. The gas was pre-saturated in traps containing the same base solution as that to be de-gassed. Stirring was provided by the gas bubbling through the solution. Gas entering the pre-electrolysis apparatus was filtered through columns filled with alumina and activated charcoal. Traps at the outlets of the cell and pre-electrolyzer prevented the back-diffusion of oxygen.

### Temperature control

The air temperature was controlled to about  $\pm 0.1^\circ$  and the solution temperature to about  $\pm 0.01^\circ$  by means of an air-thermostat, at all the temperatures used.

### Solutions

1 M HClO<sub>4</sub> solutions were prepared with triple-distilled water, the last distillation being from alkaline permanganate under a nitrogen atmosphere. The resistivity of this water was  $2 \cdot 10^6 \Omega \text{ cm}$ , in air.

HClO<sub>4</sub> solutions were pre-electrolyzed before use, between large platinized-platinum electrodes at a real current density of 80–100  $\mu\text{A}/\text{cm}^2$  for 15–20 h. A slow stream of purified N<sub>2</sub> was maintained through the solution during the pre-electrolysis.

It has been shown previously<sup>7,9</sup> that the organic impurities content in such solutions can be checked by means of cathodic charging curves by measuring the decrease in  $q_H$ , the charge corresponding to atomic hydrogen monolayer formation. In the present case, the platinum electrode was kept after activation at 0.4 V, and showed a decrease in  $q_H$  of 0.8% after 2 min and 4.4% after 5 min. The solutions are conventionally<sup>9</sup> denoted as having an *impurity content of 0.8%*. Only a few measurements of adsorption were made at times longer than 5 min in order to avoid a marked interference<sup>4</sup> by impurities.

### Electrode pre-treatment

It was exhaustively proved in previous papers<sup>4,7,9</sup> that platinum electrodes require an electrochemical treatment before each measurement. This idea was first

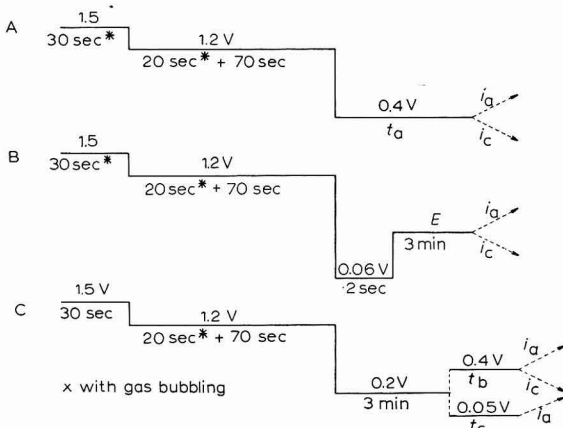


Fig. 1. Potential/time sequences used in this work.

introduced by GILMAN<sup>11</sup>. Figure 1 shows the potential/time sequences used in this work obtained with the aid of a 557 Amel potentiostat. The rise-time between two potential steps is determined by the system (cell + reference electrode) and was found to be negligible (less than  $10 \mu\text{sec}$ ) compared with the duration of the steps.

Sequence A was used for kinetic measurements. At 1.5 V, the adsorbed organic substance (or impurities) are oxidized and the electrode surface becomes covered with a layer of adsorbed oxygen. At 1.2 V, the oxygen layer is retained, whilst stirring of

the solution sweeps away any desorbed species. After 20 sec, gas-stirring was stopped to allow the solution to become quiescent in order to establish the bulk concentration of organic substances at the electrode (glycolaldehyde oxidation rate will be seen later to be negligible at this potential). The electrode was then brought to 0.4 V (kinetic studies were carried out only at this potential) where the oxygen layer is completely reduced within the first few milliseconds so bringing the electrode surface into a clean and reproducible condition. Anodic and cathodic charging curves were then applied to the electrode after a series of times of adsorption, the pre-treatment cycle being repeated for each experiment.

Sequence B was used in the determination of the capacity and the maximum amount of adsorbed material at various potentials. In this case, surface oxide reduction was continued for 2 sec at 60 mV in order to maintain the same reduction step potential for every determination. This potential was low enough for pre-adsorption to be negligible, at least not at very high concentrations.

Sequence C was used to study desorption phenomena. After a pre-treatment as above, the electrode was equilibrated at 200 mV for 3 min. This potential was chosen because adsorption was a maximum (see later) for the concentration used ( $3.3 \cdot 10^{-5} M$ ). The electrode was then brought to 400 mV or 50 mV and desorption was followed by means of anodic and cathodic charging curves, as before.

## RESULTS AND DISCUSSION

### *General aspects of the electrochemical behaviour of glycolaldehyde*

Quasi-stationary potentiostatic curves are one of the most effective methods of obtaining a general description of the behaviour of organic substances. Figure 2 shows four curves obtained at a sweep rate of 50 mV/sec using solutions of different concentrations of glycolaldehyde. Curve (a) was obtained using the base solution. Similar curves have been widely used and discussed by WILL AND KNORR<sup>8</sup> and BREITER<sup>13</sup>. The regions of hydrogen ionization (I), and oxygen adsorption (II), can

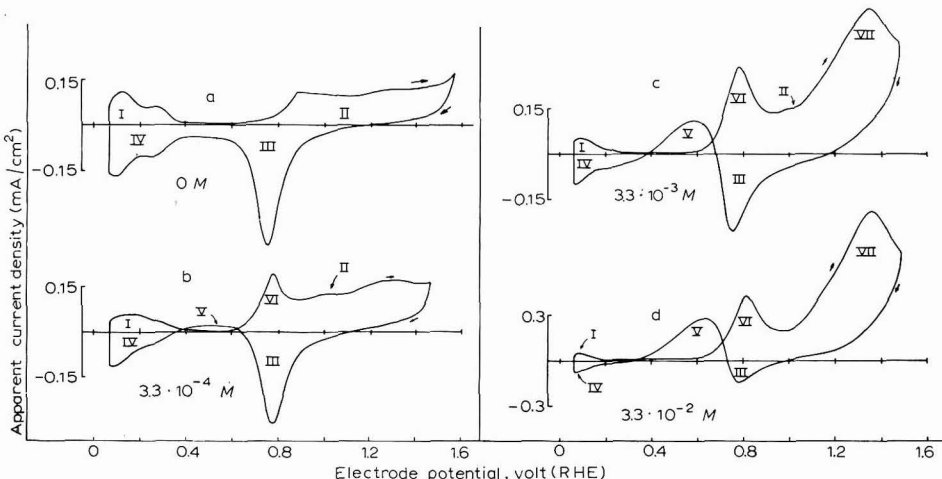


Fig. 2.  $i/E$  curves at 50 mV/sec for different concns. of glycolaldehyde; 25°.

be seen when the potential is becoming increasingly anodic. When the potential is becoming cathodic, the current peak of the reduction of the adsorbed oxygen (III) and the region of atomic hydrogen adsorption (IV), appear.

Some new characteristic regions are seen when the organic substance is present in solution; this may be interpreted as follows. When the potential is becoming cathodic, an anodic current (V) is recorded just after the peak corresponding to oxygen reduction (III), which is due to ionization of the atomic hydrogen detached from the organic molecule by catalytic dehydrogenation on the electrode surface. The organic radicals formed in this way are stabilized by chemisorption on the electrode surface and occupy a fraction of the available sites. The  $i/E$  curves, consequently, show less marked current peaks in the potential region where hydrogen adsorbs on to platinum, because hydrogen can now adsorb only on to the sites free of organic adsorbate.

For  $E > 600$  mV, when the potential becomes anodic the adsorbate is oxidized and this process is responsible for the current peak (VI). The oxygen adsorption is shifted to more anodic potentials and can be observed only at small concentrations of the organic substance (curve (b), small current hump at  $\sim 1.0$  V). At even more anodic potentials, the reaction of direct electrochemical oxidation of glycolaldehyde occurs at a rather high rate giving rise to a current maximum at about 1.35 V.

Glycolaldehyde reacts chemically with the adsorbed oxygen, so lowering the current maximum for the oxygen reduction, the magnitude of which depends on the concentration of the organic substance. At 1.2 V, when the potential is becoming cathodic, the oxidation rate of glycolaldehyde is practically negligible. This justifies the assumption that, during the pre-treatment carried out using the sequences of Figure 1, the concentration of the organic substance at the electrode surface at this potential can be considered to be the same as in the bulk of the solution.

Figure 3 shows the effect of the sweep rate on the  $i/E$  curves at constant concentration of the organic substance ( $3.3 \cdot 10^{-5} M$ ). The general shape of the curves is the same as in Figure 2, but the phenomena relating to the organic substance are less marked the higher the sweep rate. In particular, the sweep rate is so high in curve (C) that the phenomena connected with the presence of the organic substance are small enough to allow even the small current hump due to the formation of ad-

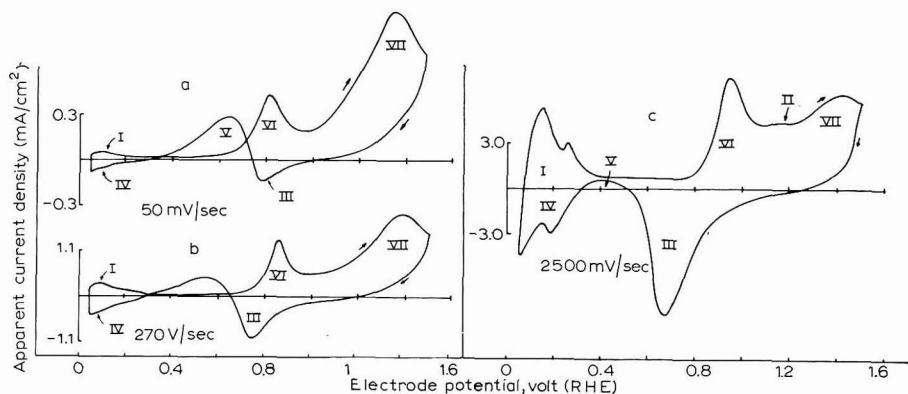


Fig. 3.  $i/E$  curves at different sweep rates for  $3.3 \cdot 10^{-5} M$  glycolaldehyde soln.;  $25^\circ$ .

sorbed oxygen, to appear. Indeed, a high sweep rate causes the magnitude of the adsorption phenomenon, the rate of which is intrinsically slow, to be small. This conclusion is also supported by the fact that the current peaks relating to hydrogen adsorption (IV) and ionization (I) are well marked and outlined in these curves.

It can also be seen that the potential of adsorbate oxidation is shifted to more anodic values with increasing sweep rate. This phenomenon also appears with anodic charging curves where the plateau due to the adsorbate oxidation is at more anodic potentials the higher the current density (see below).

#### Anodic charging curves

Although the method for determining the amount of organic substance adsorbed on a platinum electrode by means of anodic charging curves has been widely used recently, it has been criticized. The method consists of measuring the charge consumed in the oxidation of the adsorbate during a current pulse. Simultaneously with the oxidation of the adsorbed species, oxygen is adsorbed on platinum; obviously this charge must be separated from the former. The way in which this separation is performed and its consequent reliability has been the subject of much discussion.

GILEADI<sup>12</sup> has objected strongly to the method in a recent review on the methods for studying adsorption phenomena. We will attempt to prove here that the various criticisms, justified in principle, can be rejected if the possible errors of the method are thoroughly considered. Some assumptions and approximations are associated with the method, but these can be proved to have a negligible effect on the results. This method is not suitable for all organic substances, but it is, however, reliable for those organic substances that follow a rather simple mechanism of adsorption and give rise to easily oxidizable adsorbed species.

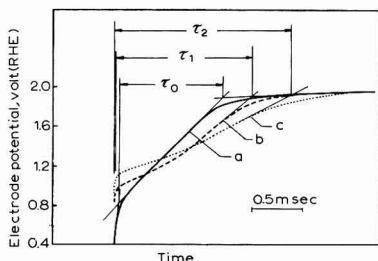


Fig. 4. Anodic charging curves from 0.4 V (RHE) at 486 mA/cm<sup>2</sup> for various glycolaldehyde concns.: (a), 0; (b), 10<sup>-4</sup>; (C), 3.3 · 10<sup>-2</sup> M. t<sub>a</sub> = 3 min; 25°.

Figure 4 shows some typical anodic charging curves obtained at the same current density but using different concentrations of the organic substance. Curve (a) was obtained without glycolaldehyde and shows the characteristic linear region due to the formation of the adsorbed oxygen monolayer. The peculiarities of such curves have already been exhaustively discussed<sup>9</sup>. The transition time during which the formation of the oxygen layer occurs, is denoted as  $\tau_0$ ; the charge consumed in this process is obtained by multiplying the transition time by the pulse current intensity:

$$q_0' = \tau_0 \times I \quad (1)$$

Curves (b) and (c) were recorded using  $10^{-4} M$  and  $3.3 \cdot 10^{-2} M$  glycolaldehyde solutions, respectively. A potential plateau between 1.0 V and 1.1 V appears in both curves; this is due to the oxidation process of the adsorbate. In contrast, the formation of adsorbed oxygen occurs with a linear increase in potential with time, up to the evolution of molecular oxygen. The potential regions relating to the two above processes cannot be clearly distinguished suggesting that some adsorbed oxygen forms during the adsorbate oxidation while a part of the adsorbate is oxidized only at the higher potentials. In other words, owing to the high rate imposed on the process, the oxidation of the organic substance is shifted into the region of electrode oxidation thus hindering any effective graphical separation of the charges relating to the two processes. Therefore,  $q_0'$  must be determined separately from curve (a) and then be subtracted from the total charge determined from curves (b) or (c), for example, using  $\tau_1$  or  $\tau_2$ , respectively, *i.e.*:

$$q_{ox} = q_{tot} - q_0' \quad (2)$$

$q_{ox}$  is here the charge consumed in the process of adsorbate oxidation only.

The above method of calculating  $q_{ox}$  is equivalent to that used by BREITER<sup>13</sup> in the case of formic acid. BRUMMER<sup>14</sup> criticized this procedure and determined the amount of adsorbed oxygen by means of a cathodic pulse following the anodic pulse. Replying to BRUMMER's criticism, BREITER<sup>15</sup> proved that the two techniques are equivalent in the case of formic acid, but that the latter generally leads to errors of unknown magnitude when  $q_{tot}$  is comparable to  $q_0'$ . Omitting any further considerations, we will attempt to demonstrate that the technique we have adopted, which follows BREITER's<sup>12</sup> method, is fundamentally justified as it gives rise to negligible errors only.

Equation (2) is based on the assumption that a complete layer of adsorbed oxygen is actually formed during an anodic pulse in the presence or absence of adsorbate. Figure 4 qualitatively proves this hypothesis. In fact, curves (a), (b) and (c) merge in the region of molecular oxygen evolution irrespective of the concentration of the organic substance and, consequently, also of coverage; it can be seen that  $\theta$  may only affect the overvoltage for adsorbate oxidation. If oxygen evolution takes place either on a partly poisoned surface, or without previous formation of a complete oxygen monolayer, the overvoltage for the process of evolution should be higher the greater the adsorbate coverage, exactly as in the case of hydrogen (see later) which is very similar. Ultimately, an anodic pulse can be reasonably assumed to lead to a fully oxidized surface both in the presence and in the absence of organic adsorption. This justifies eqn. (2), in which the possibility of a small error due to double-layer charging must be taken into consideration.

Equation (2) can be written in the general form:

$$q_{tot} = q_{ox}^{\text{true}} + q_0^{\text{true}} + q_{dl} \quad (3)$$

where  $q_{ox}^{\text{true}}$  is the charge consumed *exclusively* in the process of adsorbate oxidation,  $q_0^{\text{true}}$  is the charge spent *exclusively* for oxygen monolayer formation, and  $q_{dl}$  is the quantity of electricity for double-layer charging *during* the transient. Bearing in mind that the graphical determination of  $q_0'$  according to eqn. (1) also leads to an error for double-layer charging, *i.e.*:

$$q_0' = q_0^{\text{true}} + q_{dl} \quad (4)$$

as a consequence of combining (2), (3), and (4) the value of  $q_{ox}$  as determined graphically may not be the true value. In fact:

$$q_{ox} = q_{ox}^{\text{true}} + q_{dl} - q_{dl}^0 \quad (5)$$

$$q_{ox} = q_{ox}^{\text{true}} + \Delta q_{dl} \quad (6)$$

Practically,  $q_{ox}$  is smaller than  $q_{ox}^{\text{true}}$  as usually  $q_{dl}^0 > q_{dl}$ ; it is well known that the double-layer capacity is reduced by the adsorption of organic substances.

$q_{dl}^0$  and  $q_{dl}$  cannot be evaluated from capacity curves because such curves are always obtained discontinuously, namely point by point, while during the pulse the electrode potential varies continuously and therefore at each moment the electrode surface is affected by its immediate *history*. However, the capacity curves enable us to estimate the *maximum* error described in eqn. (6).

For the highest concentrations of the organic substance, *viz.* in the most unfavourable conditions, the error made by neglecting  $\Delta q_{dl}$  would be about 7% (the capacity curves are not reported completely; the portion relating to a narrower potential range is given later). This error may also be a maximum because the capacity curves refer to almost stationary conditions, while during an anodic pulse the electrode surface progresses (immediately after adsorbate oxidation has commenced) toward the state expected in the absence of organic adsorption, since any re-adsorption phenomenon is avoided at high current density. In other words, the capacity *during* the transient must be higher than that determined from steady-state measurements. In short, the error made by applying eqn. (2) in the most simple way is always less than 7%, but is usually  $\ll 7\%$  and consequently *negligible*.

Finally, a far larger error is created if the correction for  $q_{dl}$  is made directly for each charging curve by drawing the tangent to the curve at its initial portion, as shown elsewhere<sup>9</sup> for the evaluation of  $q_0$ ; this can be concluded from a study of the capacity curves.

#### *Choice of the anodic current density*

The duration of the oxidation processes of both the adsorbate and the electrode, namely the transition time,  $\tau$ , affects the final results because:

(i) oxidation of substance coming from the bulk of the solution can *also* occur during  $\tau$ ;

(ii) the oxidation of the adsorbate may be slow and difficult at high coverages.

In order to find out the experimental conditions in which (i) and (ii) are avoided, we carried out charging curves at several current densities working with  $3.3 \cdot 10^{-2} M$  glycolaldehyde solution in which the electrode surface was saturated with adsorbate. The results are given in Figure 5 (upper curve).  $q_{ox}$  is independent of  $i$  only in the range  $0.25 < i < 0.70 \text{ A/cm}^2$ . At higher densities,  $q_{ox}$  decreases with increasing  $i$ , while at the lowest densities it increases more rapidly with decreasing  $i$ . The range of current density where  $q_{ox}$  is constant spreads out to the left with decreasing concentration and to the right with decreasing coverage.

The above results suggest that:

(i) in the range of  $q_{ox}$  independent of  $i$ , the adsorbate is *completely* removed from the surface by oxidation;

(ii) at small  $i$ , the transition time is long enough for species coming from the

solution to oxidise during the pulse; this agrees with the anodic charging curve data which show a less well defined plateau;

(iii) at very high  $i$ , no complete oxidation of the adsorbate takes place owing to the high rate imposed on the process. Similar results can also be found in GILMAN's data for ethylene<sup>16</sup>.

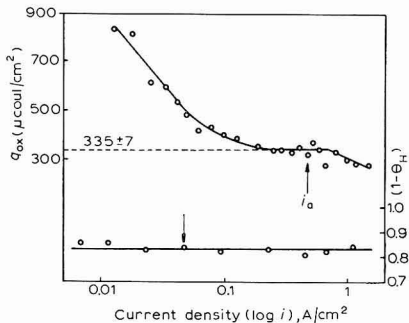


Fig. 5. Dependence of  $q_{\text{ox}}$  and  $(1 - \theta_{\text{H}})$  on pulse current density for  $3.3 \cdot 10^{-2} M$  glycolaldehyde soln. at  $25^\circ$ .  $t_a = 3$  min;  $E = 0.4$  (RHE).

In conclusion, the region of  $i$  where  $q_{\text{ox}}$  is independent of current density is the range where all conditions on which the method is based are almost completely fulfilled. A current density of  $486 \text{ mA/cm}^2$ , denoted in Figure 5 by  $i_a$ , was used therefore for anodic charging curves throughout this work. A charge of  $335 \pm 7 \mu\text{C}/\text{cm}^2$ , calculated on the basis of the real surface area, is required for the oxidation of the adsorbate in the conditions reported in Figure 5.

GILEADI's criticisms of the method<sup>12</sup> are well founded because some assumptions cannot be verified directly, but we think the results cannot be rejected *a priori* without a check on the extent of error that these assumptions may introduce into the final result. We have just proved that the less verifiable assumptions can lead to error, but that this error is so small that the danger of misinterpretation of results is almost non-existent. Finally, the method can *a posteriori* be supported also by the results recently obtained by BRUMMER<sup>17</sup> in the case of propane, and by GILMAN<sup>16</sup> in the case of ethylene and acetylene; GILMAN worked with the potential sweep method which is, in any case, fundamentally similar to the galvanostatic method.

#### Cathodic charging curves

With the anodic charging curves, the amount of adsorbate is determined and expressed as the total quantity of electricity required for its oxidation, but with cathodic charging curves it is possible to evaluate the fraction of surface free of adsorbate by determining the amount of atomic hydrogen deposited on the free sites during the transient. Hence, by means of cathodic charging curves the amount of adsorbed organic substance is expressed in equivalents of atomic hydrogen.

Figure 6 shows three cathodic charging curves at the same current density, for three different concentrations of glycolaldehyde. The transition time relating to the formation of the hydrogen monolayer on the surface free of adsorbate, is denoted in curve (a) as  $\tau_0$ . The curve shows two potential steps, part I and part II, which refer to sites with different heats of atomic hydrogen adsorption. It is well known that

organic substances usually adsorb initially on to the sites with higher adsorption heat<sup>7,9,13</sup>, (part II); this can be seen in Fig. 6.

The method of determining  $\tau$ , used in this work, leads to a partial correction for double-layer charging. However, it has been shown elsewhere<sup>9</sup> that the true value of  $q_{H,s}$ , the charge required to saturate the electrode surface with atomic hydrogen,

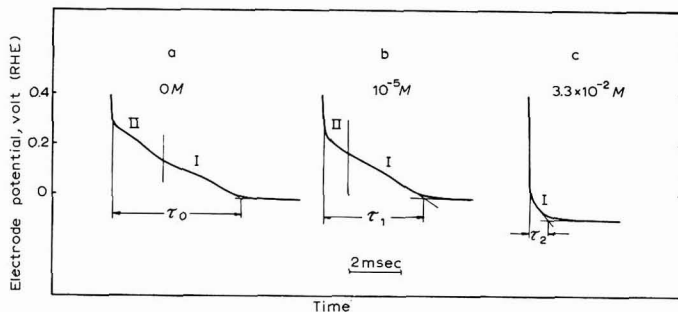


Fig. 6. Cathodic charging curves at 48.4 mA/cm<sup>2</sup> from 0.4 V (RHE) for different glycolaldehyde concns.  $t_a = 3$  min; 25°.

can be determined only after a further correction for double-layer charging. Since this correction is a function of the coverage with adsorbate, it cannot be made easily. Nevertheless, it is possible to prove that no substantial error is caused by neglecting this further correction.

In the absence of the organic substance we can write:

$$q_{H,s} = q_{H,s}^{\text{true}} + q_{dl}^{H,s} \quad (7)$$

Similarly, in the presence of the organic substance:

$$q_H = q_H^{\text{true}} + q_{dl}^H \quad (8)$$

Thus, the calculated coverage is given by:

$$\iota - \theta_H = \iota - (q_H^{\text{true}} + q_{dl}^H) / (q_{H,s}^{\text{true}} + q_{dl}^{H,s})$$

from which:

$$\iota - \theta_H = \{\Delta q_H^{\text{true}} + (q_{dl}^{H,s} - q_{dl}^H)\} / (q_{H,s}^{\text{true}} + q_{dl}^{H,s}) \quad (9)$$

Practically,  $q_{dl}^{H,s}$  is equal<sup>9</sup> to 4.5% of  $q_{H,s}^{\text{true}}$ , while  $q_{dl}^H$  is always  $< q_{dl}^{H,s}$ . Considering, to a first approximation,  $q_{dl}^H$  as a function of the surface free of adsorbate, *viz.*,  $q_{dl}^H/q_{dl}^{H,s} = q_H^{\text{true}}/q_{H,s}^{\text{true}}$ , it follows from eqn. (9) that the possible error is negligible down to  $(\iota - \theta_H) \approx 0.05$  and tends to 4.5% when  $(\iota - \theta_H) \rightarrow 0$ .

#### *Choice of the cathodic current density*

Three of the objections to this technique<sup>12</sup> indicate some valid possibilities of error in the method:

(i) Hydrogen absorption during the pulse, *i.e.*, adsorbed hydrogen has time to dissolve into the metal.

(ii) Reduction (hydrogenation) of adsorbed molecules.

(iii) Desorption of organic molecules during the pulse.

With regard to the first objection, the regions of current density in which an actual absorption of hydrogen can occur have already been indicated<sup>9</sup>. However, for each current density, the corresponding value of  $q_{H,s}$  is used in eqn. (9), thus taking into account any absorption phenomenon.

The occurrence of the other two possible side-reactions can be checked either by means of desorption tests at cathodic potentials (see later) or by determining  $(1 - \theta_H)$  at several current densities. In Fig. 5 the lower curve shows the dependence of  $(1 - \theta_H)$  on  $i$ .  $(1 - \theta_H)$  did not vary over the range examined. If either substantial desorption, or hydrogenation of the organic substance occurred, a variation in  $(1 - \theta_H)$  with  $i$  should appear, most probably a decrease in  $(1 - \theta_H)$  would correspond to a decrease in  $i$ . The absence of any detectable variation in  $(1 - \theta_H)$  suggests that neither desorption nor hydrogenation take place. Desorption and hydrogenation will be seen to be undetected also by sequence C of Fig. 1.

In Fig. 5  $i_c$  is the current density chosen for the cathodic charging curves throughout this work; its exact value is 48.4 mA/cm<sup>2</sup>. From the same figure the fraction of surface covered with adsorbate, when the concentration of glycolaldehyde is  $3.3 \cdot 10^{-2} M$ , can be seen to be about 0.84. This value is the saturation coverage.

#### *Adsorption kinetics at 0.4 V*

Adsorption kinetics were studied using sequence A of Fig. 1. After each pre-treatment the electrode was brought to 0.4 V and, varying  $t_a$ , the progress of adsorption was followed with cathodic and anodic charging curves. However, cathodic charging curves were used far more frequently than anodic charging curves, because the coverage obtained from the latter is unreliable. In fact, at high coverages, the ad-layer consists of differently oxidized species (see later), thus the charge consumed in their oxidation is an average one and cannot be directly referred to the charge determined at lower coverages where the ad-layer consists of only one molecular form. Therefore, anodic data were used to determine only the structure of the ad-layer, while the coverage with adsorbate was *exclusively* calculated from cathodic data.

In the study of adsorption from the gas phase, the coverage is usually defined as:

$$\theta = a/a_{eq} \quad (10)$$

where  $a$  is the amount of gas adsorbed under defined conditions and  $a_{eq}$  is the maximum amount of gas adsorbed under equilibrium conditions and does not necessarily correspond to a monolayer. According to this definition the coverage can be expressed in our case as:

$$\theta = (q_{H,s} - q_H) / (q_{H,s} - q_{H,min}) \quad (11)$$

where  $q_{H,s}$  is proportional to the total number of surface sites,  $q_H$  is proportional to the sites free of adsorbate, and  $q_{H,min}$  is proportional to the number (minimum) of free sites when the surface is saturated with adsorbate. All these quantities are expressed in *equivalents of hydrogen*.  $q_{H,min}$  has been shown to be 16% of  $q_{H,s}$  at 25°.

By dividing eqn. (11) by  $q_{H,s}$  we obtain:

$$\theta = (1 - \theta_H) / (1 - \theta_{H,min}) \quad (12)$$

where  $(1 - \theta_H)_{max} = 1 - \theta_{H,min}$ . Since this quantity is constant and equal to 0.84 at 25°, we shall use  $(1 - \theta_H)$  instead of  $\theta$ .

Figure 7 shows the adsorption kinetics for three different concentrations of glycolaldehyde. There is a semi-logarithmic relationship between the absolute coverage,  $(1 - \theta_H)$ , and the adsorption time for  $(1 - \theta_H) > 0.15$ . The plot is not linear at very long times, when the coverage reaches a stationary value determined by the concentration of glycolaldehyde.

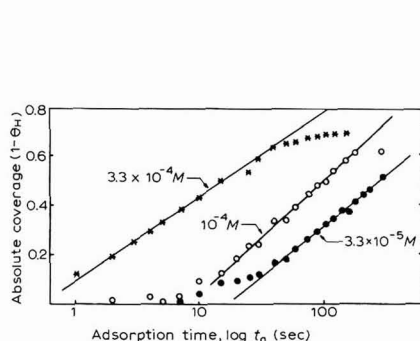


Fig. 7. Glycolaldehyde adsorption as a function of time for different concns. at 25°;  $E = 0.4$  V (RHE).

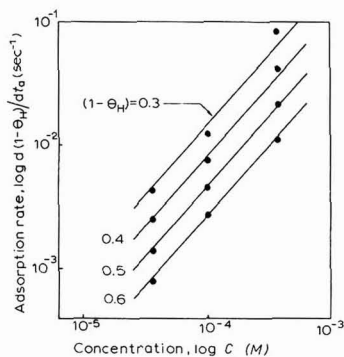


Fig. 8. Dependence of adsorption velocity on glycolaldehyde concn. for different coverages at 25°;  $E = 0.4$  V (RHE).

The experimental law for the adsorption kinetics can be expressed as:

$$(1 - \theta_H) = b \ln t_a / t_0 \quad (13)$$

where  $t_0$  and  $b$  are constants at constant  $T$  and concentration. Equation (13) represents the experimental plot for  $0.15 < (1 - \theta_H) < (1 - \theta_H)_{\text{stat}}$ .

By differentiating eqn. (13) we obtain:

$$d(1 - \theta_H) = b d \ln t_a = b dt_a / t_a \quad (14)$$

Obtaining  $t_a$  from eqn. (13) and substituting into eqn. (14) gives:

$$V_{\text{ads}} = d(1 - \theta_H) / dt_a = (b/t_0) \exp[-(1 - \theta_H)/b] \quad (15)$$

Equation (15) is a form of the *Elovich equation*<sup>18</sup>; thus, glycolaldehyde adsorbs on to platinum according to the kinetics of activated adsorption.

#### Reaction order

In the case of activated adsorption, the adsorption velocity can be written from eqn. (15) in a general form as follows<sup>18</sup>:

$$V_{\text{ads}} = d\theta / dt = K_1 C^x \exp(-E_\theta / RT) \quad (16)$$

where  $\theta$  is the coverage as defined by eqn. (10),  $C$  the concentration of the organic substance and  $E_\theta$  the activation energy which depends on the coverage. By expressing  $\theta$  as in eqn. (12) and summing the constant terms, we obtain:

$$V'_{\text{ads}} = d(1 - \theta_H) / dt_a = K_2 C^x \exp(-E_{(1-\theta_H)} / RT) \quad (17)$$

In eqn. (17), time is denoted by  $t_a$  in order to maintain the symbols of sequence

A (Fig. 1). Introducing logarithms, we have:

$$\ln \{d(\mathbf{1}-\theta_H)/dt_a\} = \ln K_2 + x \ln C - E_{(1-\theta_H)}/RT \quad (18)$$

Both  $x$  and  $E$  can be evaluated from eqn. (18), provided that the adsorption velocity is known. The adsorption velocity can be obtained from the slope of the experimental curves of Fig. 7. From eqn. (14):

$$d(\mathbf{1}-\theta_H)/dt_a = V_{ads}' = b/t_a \quad (19)$$

where  $b$  is the slope. Equation (19) can be used only in the range where eqn. (13) is valid. From eqn. (18) we then obtain, at  $\theta_H = \text{constant}$  and  $T = \text{constant}$ :

$$\ln \{d(\mathbf{1}-\theta_H)/dt_a\} = \text{const.}_1 + x \ln C \quad (20)$$

In this case, eqn. (20) is valid over the whole range of coverage values because the term containing the activation energy is actually constant at constant coverage. Figure 8 shows the experimental plot of the adsorption velocity against the concentration of glycolaldehyde for different values of coverage. The slope of the straight lines is about 1.1, i.e., the adsorption process in *first-order* with respect to glycolaldehyde.

#### *Adsorption activation energy*

From eqn. (18), at constant  $C$  and  $\theta_H$ , we can write:

$$\ln \{d(\mathbf{1}-\theta_H)/dt_a\} = \text{const.}_2 - E_{(1-\theta_H)}/RT \quad (21)$$

From eqn. (21), the activation energy,  $E$ , can be calculated as a function of  $(\mathbf{1}-\theta_H)$  by determining the adsorption velocity at different temperatures for each of the  $(\mathbf{1}-\theta_H)$ -values. The experimental results obtained using  $C = 3.3 \cdot 10^{-5} M$  at four different temperatures are shown in Fig. 9. In this case, the kinetics also follow the Elovich equation as defined by eqn. (15). The adsorption velocity increases with increasing

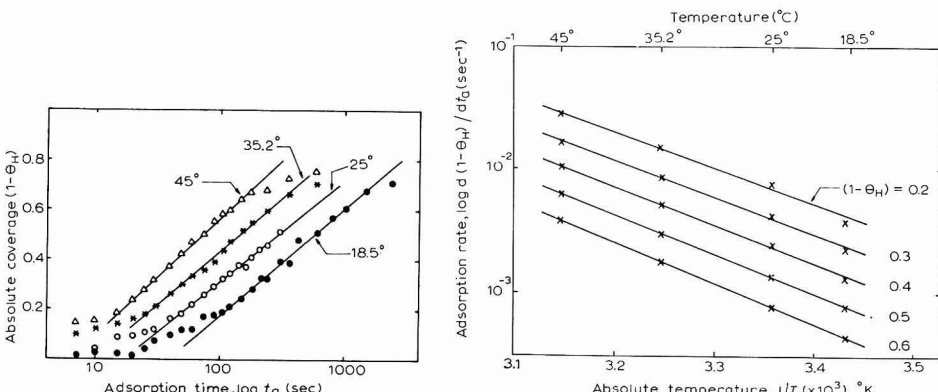


Fig. 9. Glycolaldehyde adsorption as a function of time for  $3.3 \cdot 10^{-5} M$  solution at different temps.;  $E = 0.4$  V (RHE).

Fig. 10. Dependence of velocity of glycolaldehyde adsorption on the reciprocal of absolute temp. in  $3.3 \cdot 10^{-5} M$  soln. for different coverages;  $E = 0.4$  V (RHE).

temperature and the stationary coverage also tends to rise with temperature. For each of these curves, the adsorption velocity at any time can be determined by using eqn. (19).

Figure 10 shows the experimental plot of eqn. (21) using the data derived from Fig. 9. A good linear plot is obtained for each of the coverage values, and from the slopes of the straight lines it is possible to evaluate, by means of eqn. (21), the values of the activation energy at various coverages. Owing to the small difference in slope of the straight lines for various coverages, the best slope for each line was determined using the method of least-squares. The results obtained are shown in Fig. 11. The activation energy increases linearly with increasing surface coverage from  $12.80 \pm 0.05$  kcal/mole at  $(1 - \theta_H) = 0$ , to  $15.95 \pm 0.05$  kcal/mole at  $(1 - \theta_H) = 0.84$ . This value of coverage corresponds to the saturation coverage for glycolaldehyde. The method of least-squares was also used in this case to evaluate the slope of the straight line and to determine the value of  $E_0$ .

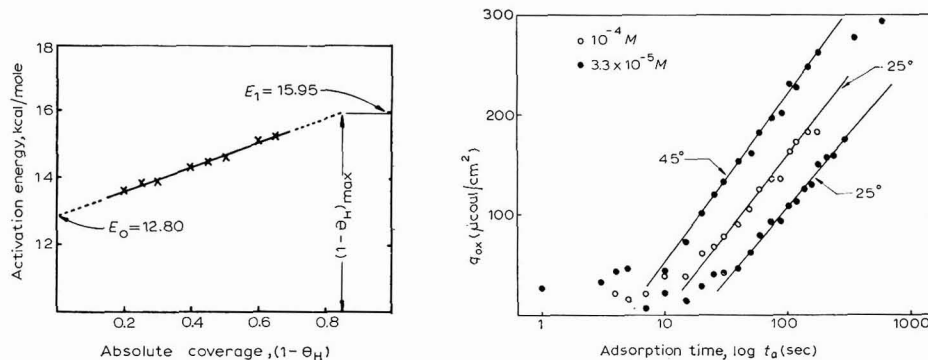


Fig. 11. Dependence of activation energy of glycolaldehyde adsorption on electrode coverage with adsorbate;  $E = 0.4$  V (RHE).

Fig. 12. Glycolaldehyde adsorption as a function of time for different concns. and temps.;  $E = 0.4$  V (RHE).

Obviously, the activation energy so calculated is a differential quantity. However, the dependence of  $E$  on coverage can be represented by the general relationship:

$$E_\theta = E_0 + \alpha\theta \quad (22)$$

where  $\alpha = 3150$  cal/mole. Equation (22) is the dependence to be expected for the kinetics of activated adsorption on a uniformly heterogeneous surface such as a platinum surface. The value of  $E_0 = 12.80$  kcal/mole can be profitably compared with the values of 5.2, 9.5, and 16.4 kcal/mole for the adsorption on to platinum of formic acid, methanol, and ethylene glycol<sup>19</sup>, respectively. It is also interesting to observe that in the particular case of the dehydrogenation of phosphorous acid on palladium, the value of 17.05 kcal/mole was found<sup>20</sup> for the activation energy. The dependence of the activation energy on the structure of the molecule suggests that the rate of the adsorption process may be related to the energy of the bond broken during the adsorption process itself.

### Mechanism and nature of the adsorption

The kinetic measurements show the adsorption of glycolaldehyde on to platinum to be an activated adsorption; the  $i/E$  curves (Fig. 2) and the potential decay curves by BIANCHI AND LONGHI<sup>3</sup> clearly indicate the process to be chemisorption connected with the catalytic dehydrogenation of the molecule on the metal surface. The adsorbed species is therefore different from the species in solution; the problem of determining its structure can be solved by combining the data obtained with cathodic pulses with those obtained with anodic pulses. Similar studies with propane were made by BRUMMER<sup>17</sup>.

Figure 7 shows that there is a linear relationship between coverage and the logarithm of the adsorption time. Also using anodic pulses, as can be seen in Fig. 12, a linear dependence of the amount adsorbed on the adsorption time is obtained. Therefore, the anodic data and the cathodic data at the same temperature and concentration show two aspects of the same phenomenon and so can be compared. Equation (13) is therefore also valid for the anodic data, but it must be expressed using the quantities characteristic of the anodic pulses.

At the same coverage,  $q_{ox}$  is related to  $(1 - \theta_H)$  by the expression:

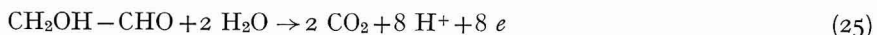
$$q_{ox} = (1 - \theta_H) 210 n/m \quad (23)$$

where  $0.210 \text{ C/cm}^2$  is the charge associated with unit electrode surface when only one electron for each platinum atom is involved in the reaction<sup>9</sup>,  $n$  is the number of electrons needed to oxidize one adsorbate molecule completely, and  $m$  is the number of sites occupied by one adsorbate molecule. Equation (13) becomes therefore:

$$q_{ox} = 210(n/m)b \ln(t_a/t_0) \quad (24)$$

Since  $b$  is the slope of the kinetic curves obtained with cathodic data, and  $210 \cdot n/m \cdot b$  is the slope of the analogous anodic curves, the ratio between the two slopes enables us to determine  $n/m$ . With reference to Fig. 12, we obtain  $n/m = 1.70$  for  $C = 3.3 \cdot 10^{-5} M$  at  $25^\circ$ ,  $n/m = 1.65$  for  $C = 10^{-4} M$  at  $25^\circ$ , and  $n/m = 1.69$  for  $C = 3.3 \cdot 10^{-5} M$  at  $45^\circ$ . The arithmetic mean of these three values gives  $n/m = 1.68$ .

The complete oxidation of the molecule of glycolaldehyde requires 8 electrons according to the reaction:



Assuming that in the adsorption each molecule loses  $m$  hydrogen atoms and forms  $m$  bonds with the surface, *i.e.*, occupies  $m$  sites, we can write:

$$n/m = (8 - m)/m = 1.68 \quad (26)$$

From eqn. (26),  $m = 2.98 \approx 3$  and  $n = 5$ , are obtained. In conclusion, glycolaldehyde adsorbs on to the platinum electrode losing 3 hydrogen atoms and forming 3 bonds with three surface sites.

The value of  $n/m$  can also be determined in a different way by using relationship (23) directly. Actually, the two methods differ only in matters of computation. However, since the ratio  $n/m$  is a determining quantity, we think it is useful to use two different approaches, even using the same data, to make sure of its exact value. On the other hand, the first method allows the ratio  $n/m$  to be straightway evaluated; the second method allows, more than a direct evaluation of  $n/m$ , its graphical compa-

rison with a given or expected value of the ratio. In this respect the latter method is complementary to the former. Figure 13 shows the experimental plot of eqn. (23). The points lie on a straight line and approach very nearly the straight line calculated for  $n=5$  and  $m=3$ . In the same figure the line calculated for  $n/m=1.50$ , is also given. This value was chosen to demonstrate that with such a plot it is possible to distinguish easily between two very similar cases.

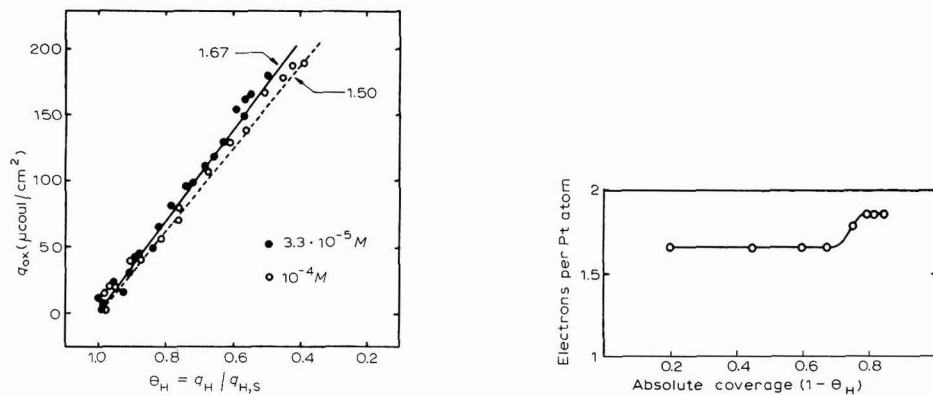
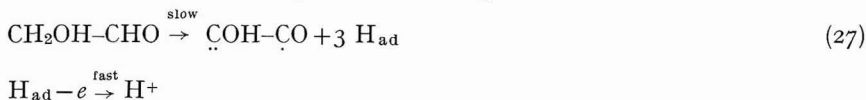


Fig. 13. Relationship between  $q_{\text{ox}}$  and  $q_{\text{H}}$  for different concns. at  $25^{\circ}$ ;  $E = 0.4$  V (RHE). The slopes of the straight lines are expressed as the average number of electrons/covered platinum atom involved in adsorbate oxidation.

Fig. 14. Variation of average number of electrons/covered platinum atom involved in oxidation of the adsorbed glycolaldehyde, with electrode coverage by adsorbate.

The results obtained are also reasonable from a molecular point of view. The projected area of the molecule is about three times as large as the area of a platinum atom; therefore, the possibility that the molecule can occupy more than three sites can be excluded. However, by its structure and the mode of attachment to the surface, the molecule may cover the electrode surface in an unsymmetrical way; this may be why about 16% of sites are still capable of adsorbing hydrogen when the platinum surface is saturated with adsorbate. Finally, partial dehydrogenation (*i.e.*,  $n > 5$ ) is to be considered as unlikely, since methanol, for example, loses all of its hydrogen atoms directly bound to the carbon<sup>19</sup>. Dehydrogenation of the OH-group must also be rejected, as tertiary alcohols do not dehydrogenate<sup>21</sup>. Finally, dehydrogenation of the aldehydic group is a reasonable possibility if we consider that glyoxal, a very similar molecule, undergoes such a reaction<sup>4</sup>.

In conclusion the overall process can be represented as follows:



#### *Structure of the ad-layer at 0.4 V*

At 0.4 V (without any interference by hydrogen or oxygen adsorbed on platinum), the reaction of glycolaldehyde adsorption proceeds, as shown, according to (27), *viz.*, via loss of three hydrogen atoms and formation of three bonds with three platinum atoms. According to this mechanism the molecule adsorbs in a *flat orientation*.

*tion* on to the surface, but it is to be expected that the  $-OH$  and  $=O$  groups are slightly turned towards the solution owing to the bond angles. Complete flattening of the molecule on the electrode surface should require strong interaction between platinum atoms and functional groups that can only result from formation of a chemical bond that would force all the bond directions of the carbon atom towards the electrode surface.

The results obtained do not indicate any breaking of the C–C bond, as in this case two distinct species would form, *i.e.*,  $C-OH$  and  $C=O$ , the former alone occupying three sites as in the case of the methanol dehydrogenation<sup>19</sup>. The C–C bond generally breaks at higher temperatures than those used in this work:  $70^\circ$  for ethylene glycol<sup>19</sup>,  $120^\circ$  for ethane<sup>22</sup>. Also, the platinum surface, by its metallic nature, does not lead to bonds that are strongly localized in one direction, and, therefore, the length of the C–C bond is reasonably consistent with 3-site adsorption without any breaking of the molecule.

With increasing coverage, the 3-site adsorption must lead to steric difficulties that hinder the progress of further adsorption with the same mechanism. For high enough  $(1 - \theta_H)$  values the adsorption is expected to proceed on two sites or even only on one site. Figure 14 proves the validity of such a supposition. As long as the coverage is low, the average number of electrons per platinum atom is 1.67 and is in agreement with the mechanism proposed above. When the coverage exceeds 70%, the average number of electrons tends to rise, and reaches the stationary value of about 1.88 when the surface becomes saturated. This indicates that the adsorbed molecule is less dehydrogenated and covers a smaller number of sites. The most likely hypothesis is that, owing to their sizes, some molecules no longer adsorb in a flat orientation but *vertically* when  $(1 - \theta_H) > 0.7$ . If the structure of the molecule is taken into consideration, it is likely that the molecule adsorbs on to two sites with its alcoholic group losing two hydrogen atoms; adsorption of the aldehyde group would still lead to coverage of two sites but with formation of only one bond with platinum. The first hypothesis is favoured if we take into account the energies connected with the two processes. At  $(1 - \theta_H) > 0.7$  the dehydrogenation mechanism is therefore as follows:



Three electrons for each platinum atom are required, on the average, to oxidize these adsorbed species, because  $n=6$  and  $m=2$ . We will attempt to calculate the average number of electrons per platinum atom in the case of the surface saturated with adsorbate. Up to 70% coverage, the average number is 1.67; when the surface is saturated, the coverage is 0.84; we can then write:

$$(1.67 \times 0.7 + 3 \times 0.14)/0.84 = 1.89 \quad (29)$$

The calculated value is in very good agreement with the experimental value of 1.88 (Fig. 14). In order to check the reliability of such a calculation, we will also determine the average number of electrons for an intermediate coverage. From Fig. 14 the resulting average number is 1.78 at  $(1 - \theta_H) = 0.75$ , and then the calculated value of 1.76 is in very good agreement with the observed value.

#### *Influence of the potential on the structure of the ad-layer*

The results reported above were obtained at 0.4 V because at this potential adsorbed hydrogen or oxygen have no effect<sup>23</sup>. In order to test if the structure

of the ad-layer remains the same at any potential, experiments were also carried out at potentials both anodic and cathodic with respect to 0.4 V. Figures 15 and 16 show the plots of capacity and  $q_{ox}$  as a function of potential, respectively. Both curves were obtained for  $t_a=3$  min in order to avoid any interference due to impurities in the base solution; this is particularly important in capacity measurements<sup>4</sup>. At  $t_a=3$  min, the stationary coverage is reached at almost all high and intermediate concentrations; it is most nearly approached with  $C=3.3 \cdot 10^{-5} M$ ; it is not reached at  $C=10^{-5} M$ . However, this does not at all affect any conclusion that can be drawn from the results.

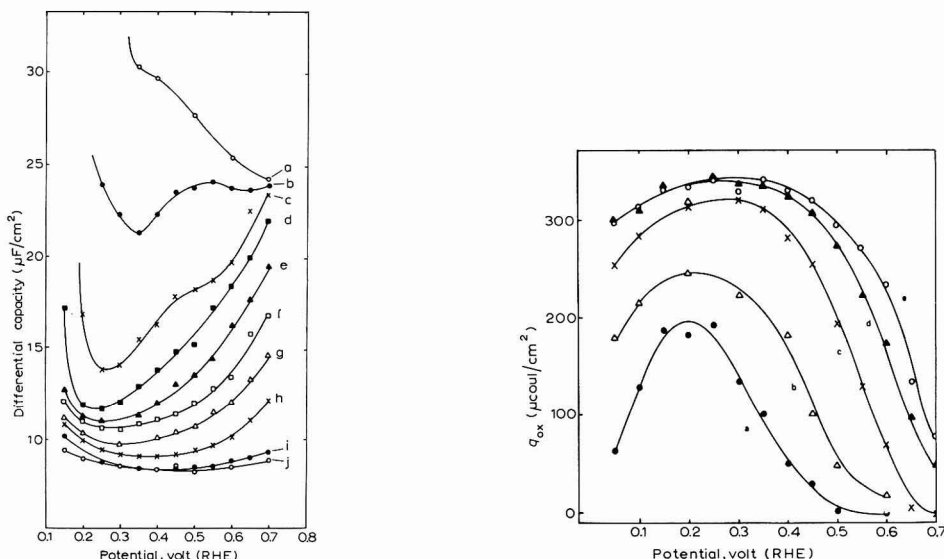


Fig. 15. Capacity/potential curves at 25° for various concns. of glycolaldehyde. Adsorption time, 3 min. Bridge method, 5 kHz. (a), o; (b),  $10^{-5}$ ; (c)  $3.3 \cdot 10^{-5}$ ; (d),  $10^{-4}$ ; (e),  $3.3 \cdot 10^{-4}$ ; (f),  $10^{-3}$ ; (g),  $3.3 \cdot 10^{-3}$ ; (h),  $10^{-2}$ ; (i),  $3.3 \cdot 10^{-2}$ ; (j),  $10^{-1} M$ .

Fig. 16. Dependence of glycolaldehyde adsorption on electrode potential at 25°. Adsorption time, 3 min. (a),  $10^{-5}$ ; (b),  $3.3 \cdot 10^{-5}$ ; (c),  $3.3 \cdot 10^{-4}$ ; (d)  $10^{-2}$ ; (e),  $3.3 \cdot 10^{-2} M$ .

For  $E < 400$  mV, the shapes of the curves in the two figures are very similar; the lower the potential, the smaller the amount of substance adsorbed. This does not mean that the substance is either desorbed or hydrogenated (see later) but only that for  $E < 400$  mV competitive adsorption between hydrogen and the organic substance occurs, and this competition is more in favour of hydrogen the lower the potential.

On the contrary, for  $E > 400$  mV,  $q_{ox}$  decreases with increasing potential much more than capacity increases. This suggests that the organic substance is still strongly adsorbed, but is in a higher state of oxidation depending on the potential, so that  $q_{ox}$ , the charge consumed in oxidizing the adsorbate, appears less even at the same coverage. In reality, capacity and cathodic data show the coverage to decrease with increasing potential, but this decrease is much less than expected when only considering the variation in  $q_{ox}$  with the potential.

In Fig. 17, the average number of electrons per covered platinum atom released

on oxidation of the adsorbate is reported as a function of the potential. It varies from about 1.88 at 0.4 V to about 0.7 at 0.7 V. This indicates that for  $E > 0.4$  V, the ad-layer consists of different species being, on the average, more oxidized than at 0.4 V. This fact may be related to results obtained in the study of oxygen adsorption on platinum<sup>24</sup>. The oxygenated species existing on platinum even at 0.5 V, and arising from the first stage of water oxidation, can interact with the adsorbate, so adding chemical oxidation to the initial oxidation by catalytic dehydrogenation.

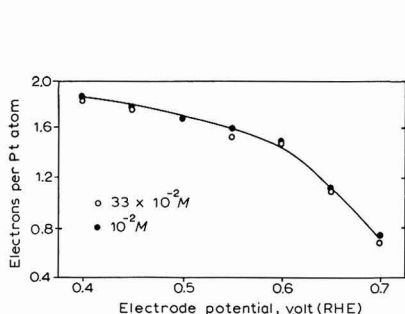


Fig. 17. Variation of average number of electrons/covered platinum atom involved in adsorbate oxidation, with electrode potential.

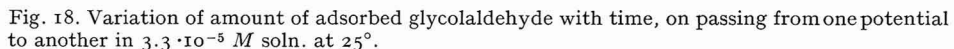


Fig. 18. Variation of amount of adsorbed glycolaldehyde with time, on passing from one potential to another in  $3.3 \cdot 10^{-5} M$  soln. at  $25^\circ$ .

#### Desorption phenomena

Owing to experimental difficulties in diluting solutions with the electrode in place, we used a special potentiostatic sequence to obtain the same effect, in order to study desorption phenomena. Let  $\theta_1$  be the coverage at a particular potential,  $E_1$ , in a specified solution; also let  $\theta_2 > \theta_1$  be the coverage at another potential,  $E_2$ . When the electrode is equilibrated at potential  $E_2$  and then rapidly brought to potential  $E_1$  the corresponding initial coverage at  $E_1$  is not  $\theta_1$  but still  $\theta_2$ , which is equivalent to dilution of the solution.

Sequence C of Fig. 1 was applied to the electrode for these measurements using a  $3.3 \cdot 10^{-5} M$  solution. The electrode was equilibrated at 0.2 V; the coverage is maximum at this potential, as shown by Fig. 16. The potential was then brought to either 0.05 V or 0.4 V to observe desorption on both sides of the maximum. The results obtained with both cathodic and anodic charging curves can be seen in Fig. 18. Passing from 0.2 V to 0.4 V and from 0.2 V to 0.05 V, no variation in  $q_{ox}$  and  $q_H$  is observed. The organic substance adsorbed at 0.2 V seems to be retained on the electrode surface; no evidence could be obtained for hydrogenation, desorption and variation in the number of covered sites. Similar results have been reported for methanol<sup>14</sup> and glyoxal<sup>9</sup>.

At more anodic potentials than 0.4 V, some variation in  $q_{ox}$  and  $q_H$  is actually observed, but it is due only to a higher oxidation state of the adsorbed material, as shown above. In conclusion, for  $E > 0.4$  V the substance is not desorbed but only oxidized or, if there is desorption, it occurs as a result of oxidation. At lower potentials than 0.4 V, on the contrary, the adsorbate appears to be completely stable, which seems *at first sight*, to suggest an *irreversibility* in glycolaldehyde adsorption.

### Nature of the isotherm

The kinetic data clearly show that a definite limiting value of the coverage is reached which depends on the concentration of the organic substance in the solution.

By plotting the final value of  $(1 - \theta_H)$  as a function of the concentration, a well defined relationship is obtained (Fig. 19) which can be identified with the Temkin logarithmic isotherm<sup>18</sup>. Similar relationships have also been found in the case of glyoxal<sup>4</sup>, methanol and ethylene glycol<sup>19</sup> adsorption. It must be mentioned, however, that in all these cases any desorption phenomenon could not be proved experimentally; no desorption of methanol is apparent even at lower potentials than that of hydrogen evolution.

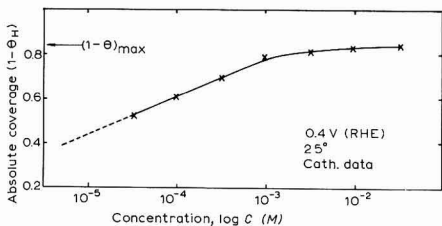


Fig. 19. Relationship between electrode coverage with adsorbate and glycolaldehyde concn. in soln. for conditions specified.

The situation for glycolaldehyde is quite similar. The experimental results show two aspects in opposition to each other. The fact that the Temkin logarithmic isotherm is obeyed can be interpreted as evidence for the establishment of a true equilibrium; on the other hand the absence of detectable desorption gives the phenomenon an apparent aspect of irreversibility. Such a difficulty can also be found in the paper by BAGOTSKY AND VASSILEV<sup>19</sup> and this is the main reason for the discussion arising on this subject at the recent Symposium in Cleveland<sup>25</sup>.

Writing the Temkin isotherm in the form<sup>18</sup>:

$$(1 - \theta_H) = A + f^{-1} \ln C \quad (30)$$

where  $f$  is the inhomogeneity factor of the platinum surface, the slope of the linear portion of the curve in Fig. 19 gives the value of 13.5 for  $f$ . This value is in very good agreement with that calculated (about 14) from the isotherm for hydrogen adsorption on platinum<sup>19</sup>. Also, the inhomogeneity factor is related to the difference between the maximum and minimum values of adsorption heat<sup>18</sup>:

$$f = \alpha' Q_0 / RT = (Q_0 - Q_1) / RT \quad (31)$$

From eqn. (31),  $Q_0 - Q_1 = 7.95$  kcal/mole is thus obtained; this refers to the whole electrode surface because  $f$  has been calculated from eqn. (30) which contains the term  $(1 - \theta_H)$ . By examining the heats of hydrogen adsorption obtained by electrochemical methods<sup>26</sup>, the value calculated from eqn. (31) can be seen to agree very well with that found for hydrogen. This fact suggests that the value of  $Q_0 - Q_1$  is not a property of the substance being adsorbed, *viz.* it is not determined by forces of mutual repulsion between the adsorbed particles, but is indeed determined by the properties of the adsorbing surface. On this point our results and conclusions agree with those of BAGOTSKY AND VASSILEV<sup>19</sup>. Now, writing the dependence of the activation energy on coverage in the form given by these authors<sup>19</sup>:

$$E = E_0 + \alpha'' fRT (1 - \theta_H) \quad (32)$$

but continuing to refer to the whole electrode surface and not only to the surface fraction capable of adsorbing glycolaldehyde, we calculate  $\alpha'' fRT = 3980$  cal/mole using  $f = 13.5$  and assuming  $\alpha'' = 0.5$ .  $\alpha''$  is called the conversion factor<sup>19</sup>, being related to the shape of the energy curve of the reaction path. The value thus calculated is in very good agreement with the experimental value of 3750 cal/mole obtained for  $\alpha$  from eqn. (22) when  $(1 - \theta_H)$  is substituted for  $\theta$ , i.e., when the whole electrode surface is considered.

All the results presented in this section confirm that the adsorption of glycolaldehyde on to platinum follows all the features expected from the theory of activated adsorption on a uniformly heterogeneous surface. This investigation shows the picture for glycolaldehyde adsorption to be similar to that for other organic substances<sup>19</sup>. We agree with BAGOTSKY AND VASSILIEV<sup>19</sup> that only to a first approximation can the distribution of heterogeneous sites on the platinum surface be considered as uniform. The error caused by this approximation is, however, not large enough to cause the results to deviate from the conclusions of the theory.

Any desorption phenomenon is apparently lacking however, and this does not allow conclusive proof on an experimental basis of the establishment of a true equilibrium. All available data suggest that desorption is a very difficult process being most probably characterized by a very high activation energy. This would explain why desorption is not experimentally detectable.

The fact that coverage generally increases with increasing temperature can be explained by considering adsorption as a *replacement reaction* of water molecules on the electrode surface<sup>12</sup>. In this case, even a negative adsorption heat can be expected.

Another difficulty is the way in which desorption can occur. For potentials  $E > 400$  mV, the absence of adsorbed atomic hydrogen makes the supposition concerning recombination of hydrogen and the organic radicals, unlikely. Moreover, no hydrogenation of the radicals is observed even at strongly cathodic potentials. The desorption phenomenon, not detectable macroscopically, might on a molecular scale be considered as detachment of a radical from the surface and its subsequent hydrogenation by water molecules.

However, quite opposite opinions are held. Irreversibility in propane adsorption<sup>17</sup> seems to be due to a transformation reaction that the adsorbate undergoes on the electrode surface. Hypotheses suggesting the isotherm to be not thermodynamic but kinetic in nature have also been put forward; the limiting coverage should be a stationary non-equilibrium state<sup>25</sup>.

In conclusion, the problem of adsorption of organic substances on to platinum requires further study for experimental proof of the attainment of a true equilibrium, but the results so far obtained support the view that adsorption is *only apparently irreversible*.

#### NOTE ADDED IN PROOF

Since this paper was submitted, the authors have learned of the note by S. S. BESKOROVAINAYA, YU. B. VASILEV AND V. S. BAGOTSKII (*Elektrokhim.*, 2 (1966) 1493) in which desorption of particles from the surface of a platinum electrode after



## DEUTUNG DER POLAROGRAPHISCHEN MAXIMA DER ERDALKALIIONEN IN WÄSSRIGER LÖSUNG

L. HOLLECK UND A. M. SHAMS EL DIN

Chemisches Institut der Hochschule, Bamberg (Deutschland)

(Eingegangen am 31 Oktober 1967)

In einer kürzlich veröffentlichten Arbeit berichtete LINGANE<sup>1</sup> über das polarographische Verhalten der Mischungen von  $\text{Ba}^{2+}$  und  $\text{Sr}^{2+}$  in Lösungen mit  $(\text{C}_2\text{H}_5)_4\text{NI}$  als Leitsalz. In den automatisch registrierten Polarogrammen wies die  $\text{Sr}^{2+}$ -Stufe ein scharfes Maximum mit einigen ungewöhnlichen Eigenschaften auf. So fiel die Stromstärke im Anschluss an das Maximum auf ein Minimum und erreichte erst danach den konstanten diffusionsbestimmten Wert. Bei Umkehr der Polarisationsrichtung (Potentialänderung in Richtung auf positivere Werte) wurde das Minimum nicht beobachtet: der  $\text{Sr}^{2+}$ -Diffusionsstrom blieb konstant bis zum plötzlichen Einsetzen des Maximums. Zusatz von 0.01% Gelatine beseitigte das Maximum, verursachte aber einen früheren Grenzanstieg, so dass kein brauchbares Grenzstrom-Plateau ausgebildet wurde. Andererseits zeigte sich, dass Triton X-100, sonst ein kräftig wirkender Maximum-Unterdrücker, ohne Einfluss auf das  $\text{Sr}^{2+}$ -Maximum blieb. Es wurden noch weitere Eigenschaften des Maximums beschrieben<sup>1</sup>, jedoch keine Erklärung hierfür gegeben.

Wir haben nun gefunden, dass das Maximum—wie es oben beschrieben ist—keine Besonderheit der  $\text{Sr}^{2+}$ -Ionen darstellt, sondern auch bei der Reduktion von

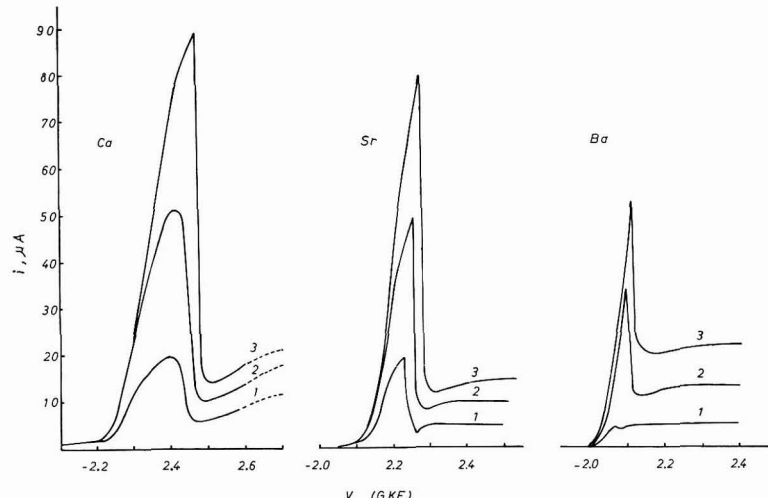


Abb. 1. Polarographische Stufen von  $\text{Ca}^{2+}$ ,  $\text{Sr}^{2+}$  und  $\text{Ba}^{2+}$  in 0.1 M  $(\text{C}_2\text{H}_5)_4\text{NI}$ .  $\text{Ca}^{2+}$ : (1), 1; (2), 2; (3),  $3 \cdot 10^{-3}$  M.  $\text{Sr}^{2+}$ : (1), 1; (2), 2; (3),  $3 \cdot 10^{-3}$  M.  $\text{Ba}^{2+}$ : (1), 1; (2), 2; (3),  $5 \cdot 10^{-3}$  M.

$\text{Ca}^{2+}$ ,  $\text{Ba}^{2+}$  und  $\text{NH}_4^+$  im gleichen Grundelektrolyten zu beobachten ist. Die Ursache dieser Maxima ist in jedem Falle die gleiche, nämlich ein Rühreffekt infolge Auflösung der gebildeten Amalgame.

Abb. 1 zeigt Kurven der polarographischen Reduktion wachsender Mengen von  $\text{Ca}^{2+}$ ,  $\text{Sr}^{2+}$  und  $\text{Ba}^{2+}$  in  $0.1 \text{ M}$   $(\text{C}_2\text{H}_5)_4\text{NI}$ . Die Polarogramme wurden automatisch mit einem Vorschub von  $0.05 \text{ V/min}$  registriert (Potentialänderung zu negativeren Werten). Man sieht hieraus, dass die Reduktionsstufen aller drei Kationen durch ein Maximum eingeleitet werden, auf das ein Minimum folgt, bevor der Grenzstrom eingestellt wird. In Übereinstimmung mit den Beobachtungen LINGANES<sup>1</sup> wurde das Minimum bei Umkehr der Polarisationsrichtung nicht beobachtet. Mit  $\text{Sr}^{2+}$  und  $\text{Ba}^{2+}$  wurden gut ausgebildete, diffusionsbestimmte Grenzstrom-Plateaus erhalten, nicht jedoch mit  $\text{Ca}^{2+}$ ; im letzteren Falle liegt wegen der negativeren Potentiale sehr wahrscheinlich eine Störung durch Zersetzungprodukte des Leitelektrolyten vor. Das Ca-Maximum ist jedoch sowohl in Höhe wie Form in beiden Polarisationsrichtungen gut reproduzierbar. Abb. 1 zeigt weiterhin, dass bei gleicher Konzentration Höhe und Breite der Maxima in der Reihenfolge  $\text{Ca}^{2+}$   $\text{Sr}^{2+}$   $\text{Ba}^{2+}$  abnehmen. Es ist auch bemerkenswert, dass die Polarogramme einer Lösung von  $1 \text{ mM}$   $\text{Ba}^{2+}$  bei normaler Polarisationsrichtung ein kleines, schlecht-ausgebildetes Maximum zeigen, das bei Umkehr der Polarisationsrichtung nicht beobachtet wird. Aus diesem Grunde überrascht es nicht, dass LINGANE bei Anwendung von  $0.8 \text{ mM}$   $\text{Ba}^{2+}$  das Ba-Maximum nicht auffand. Mit geeigneten Konzentrationen tritt das Maximum jedoch sowohl in einfachen Lösungen als auch in Mischungen mit  $\text{Sr}^{2+}$  (Abb. 2) bei normaler und umgekehrter Polarisationsrichtung in Erscheinung.

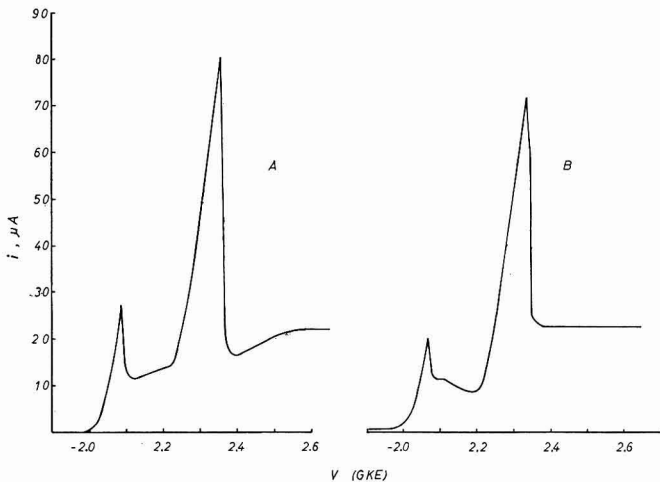


Abb. 2. Polarographische Stufen von  $3 \cdot 10^{-3} \text{ M}$   $\text{Ba}^{2+}$  +  $2 \cdot 10^{-3} \text{ M}$   $\text{Sr}^{2+}$  in  $0.1 \text{ M}$   $(\text{C}_2\text{H}_5)_4\text{NI}$  bei normaler (A) und umgekehrter (B) Polarisationsrichtung.

Die Ursache der Maxima der drei Erdalkali-Metalle lässt sich leicht verstehen, wenn man die Reaktivität der bei ihrer Reduktion in wässriger Lösung gebildeten Amalgame in Betracht zieht. Wegen der hohen Austausch-Stromdichten dieser Metalle kann nämlich bei Potentialen in der Nähe des Abscheidungspotentials der anodische Reoxidationsschritt nicht vernachlässigt werden. Bei diesem Schritt ver-

ursacht das Metall jedoch die Entwicklung von Wasserstoff, die mit einer Strömung des Elektrolyten entlang der Elektrodenoberfläche einhergeht.



Bei der Auflösung des Amalgams ist Reaktion (1a) geschwindigkeitsbestimmend, so dass die Elektrode mit fortschreitend negativerem Potential in den Zustand des "kathodischen Schutzes" gebracht wird, worauf das Maximum verschwindet.

Wie man erwarten muss, wächst die Tendenz eines bestimmten Amalgams zur Wiederauflösung mit steigender Reaktivität des Metalls, d.h. mit der Negativität seines Reduktionspotentials. Dies erklärt, warum sowohl Höhe wie Breite des  $\text{Ca}^{2+}$ -Maximums grösser sind als jene von  $\text{Sr}^{2+}$  und  $\text{Ba}^{2+}$  unter ähnlichen Bedingungen.

Das bei normaler Polarisationsrichtung dem Maximum folgende Minimum wird durch eine Verarmung des Elektrolyten in Umgebung der Elektrode infolge der Strömung verursacht. Diese Erklärung findet dadurch Unterstützung, dass bei umgekehrter Polarisationsrichtung in dem Polarogramm der Mischung von  $\text{Ba}^{2+}$  und  $\text{Sr}^{2+}$  der  $\text{Ba}^{2+}$ -Grenzstrom von kleineren Stromwerten her erreicht wird, da hier die von der vorhergehenden  $\text{Sr}^{2+}$ -Auflösung herrührende Strömung noch wirksam ist (Abb. 2B). In Lösungen der einzelnen Kationen wird bei umgekehrter Polarisationsrichtung demgegenüber ein konstanter Grenzstrom eingestellt, bis das Potential soweit positiv wird, dass der Effekt des kathodischen Schutzes verschwindet und das Maximum plötzlich einsetzt.

Die obige Erklärung der Ursache der Maxima von  $\text{Ca}^{2+}$ ,  $\text{Sr}^{2+}$  und  $\text{Ba}^{2+}$  befindet sich in Übereinstimmung mit den charakteristischen Merkmalen dieser Maxima und klärt einige ihrer Eigenschaften, die bislang keine geeignete Deutung erfuhrten. So wächst z.B. die Höhe des Maximums mit der molaren Lösungskonzentration der Ionen; letztere steigert offensichtlich die Oberflächenkonzentration des Metalls im Quecksilber und damit die Geschwindigkeit der Reaktion (1a). Infolgedessen wächst auch das Ausmass der Strömung, welche durch die Entwicklung von Wasserstoff durch die Komplementärreaktion (1b) verursacht wird. Da die Maxima ferner durch solche Faktoren geregelt werden, die im wesentlichen auf der Elektrodenseite wirksam sind, überrascht es nicht, dass sie sowohl in neutraler als auch in alkalischer Lösung beobachtet werden<sup>1</sup>. Obgleich die drei Maxima durch die Entwicklung von Wasserstoff verursacht werden, werden diese nicht durch Substanzen beeinflusst, die Protonen-Entladungs- oder Protonen-Übertragungs-Prozesse katalysieren, wie etwa N,N-Dimethyl-*p*-phenylenediamin<sup>2,3</sup>.

Die Maxima können jedoch ganz oder teilweise eliminiert werden, wenn die Bedingungen auf der Lösungsseite so gewählt werden, dass die Geschwindigkeit der Amalgam-Auflösung verringert wird oder gegen null geht. ZLOTOWSKI UND KOLTHOFF<sup>4</sup> fanden z.B., dass das grosse  $\text{Ca}^{2+}$ -Maximum in wässriger  $(\text{C}_2\text{H}_5)_4\text{NI}$ -Lösung weniger stark ausgeprägt ist, wenn die Lösung 80% Äthanol enthält. Offensichtlich ist die Auflösungsgeschwindigkeit in äthanolischer Lösung viel geringer als in wässriger. Dieser Schluss wird durch die Tatsache gestützt, dass das Halbstufenpotential der  $\text{Ca}^{2+}$ -Stufe (ebenso wie diejenigen von  $\text{Sr}^{2+}$  und  $\text{Ba}^{2+}$ ) mit wachsendem Äthanolgehalt der Lösung zu positiveren Werten verschoben wird. Auch Spuren von  $\text{Ba}^{2+}$

und  $\text{La}^{3+}$  üben einen unterdrückenden Einfluss auf das  $\text{Ca}^{2+}$ -Maximum aus<sup>4</sup>. Obwohl dies in der vorliegenden Arbeit nicht untersucht wurde, ist es recht wahrscheinlich, dass diese—bereits bei positiveren Potentialen abgeschiedenen—Metalle mit Calcium intermetallische Phasen bilden, deren Auflösungsmerkmale sich von denen des reinen Metalls unterscheiden. In diesem Zusammenhang ist die Arbeit von KEMULA<sup>5</sup> über die Bildung intermetallischer Verbindungen in Quecksilber von besonderem Interesse.

Die Reaktivität der Amalgame der Erdalkalimetalle ist jedoch nicht der einzige Faktor, der für die Metallauflösung verantwortlich ist. Andere Parameter wie die Grösse der Atome sowie Löslichkeit und/oder Bildung intermetallischer Phasen mit Quecksilber scheinen ebenfalls zur Ausbildung einer hohen Oberflächenkonzentration des Metalls im Quecksilber beizutragen. Diese Feststellung wird dadurch gestützt, dass  $\text{Li}^+$ ,  $\text{Na}^+$ , und  $\text{K}^+$ , deren Amalgame nicht weniger reaktiv sind als diejenigen von  $\text{Ca}^{2+}$ ,  $\text{Sr}^{2+}$  und  $\text{Ba}^{2+}$ , in dem gleichen Leitelektrolyten normale Stufen liefern, die nicht durch Maxima gestört werden. Der Unterschied der Ladungen beider Kation-Gruppen ist nicht verantwortlich für das ungleiche polarographische Verhalten, da die Reduktionsstufe des  $\text{NH}_4^+$ -Ions unter gleichen Bedingungen ein wohl ausgebildetes Maximum aufweist (Abb. 3). Tatsächlich ist das Ammonium-Amalgam

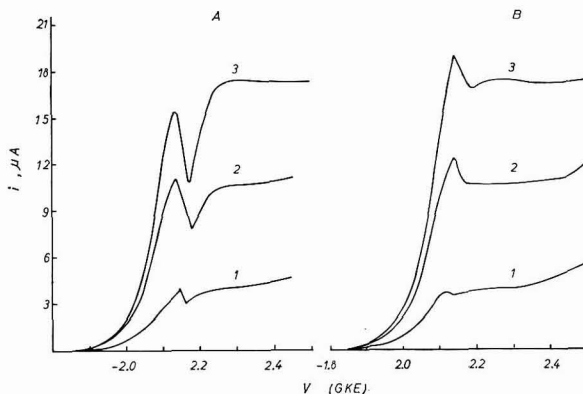


Abb. 3. Polarographische Stufen von  $\text{NH}_4^+$  in  $0.1 \text{ M}$   $(\text{C}_2\text{H}_5)_4\text{NI}$  bei normaler (A) und umgekehrter (B) Polarisationsrichtung. (1), 1; (2), 3; (3),  $5 \cdot 10^{-3} \text{ M}$ .

in wässriger Lösung weniger stabil als diejenigen der Alkalimetalle. Die Form des  $\text{NH}_4^+$ -Maximums hängt in gleicher Weise von der Polarisationsrichtung ab, wie sie oben für die Erdalkalimetalle beschrieben wurde; dies liefert einen weiteren Beweis dafür, dass die Ursache aller vier Maxima die nämliche ist, d.h. die Zersetzung des gebildeten Amalgams.

Der Alexander-von-Humboldt-Stiftung danken wir für das dem einen von uns (A. M. SHAMS EL DIN) gewährte Forschungs-Stipendium.

#### ZUSAMMENFASSUNG

Den polarographischen Reduktionsstufen von  $\text{Ca}^{2+}$ ,  $\text{Sr}^{2+}$ ,  $\text{Ba}^{2+}$  und  $\text{NH}_4^+$  in wässrigen Lösungen mit  $(\text{C}_2\text{H}_5)_4\text{NI}$  als Leitsalz geht ein Maximum voran, dessen

Höhe mit der molaren Konzentration der Depolarisatoren wächst. Beim Registrieren der Polarogramme mit gewöhnlicher Polarisationsrichtung durchläuft die Stromstärke ein Minimum, bevor der Grenzstrom eingestellt wird. Dieses Minimum, das auf einem Verarmungseffekt beruht, wird bei umgekehrter Polarisationsrichtung (Potentialvorschub in positiver Richtung) nicht beobachtet.

Die Maxima werden auf eine Strömung der Lösung zurückgeführt, welche durch die Reaktion des amalgam-bildenden Metalls mit Wasser verursacht wird. Diese Deutung ist in Übereinstimmung mit den experimentellen Befunden und erklärt einige Besonderheiten der Maxima, die bislang nicht in geeigneter Weise interpretiert wurden.

#### SUMMARY

The polarographic reduction waves of  $\text{Ca}^{2+}$ ,  $\text{Sr}^{2+}$ ,  $\text{Ba}^{2+}$  and  $\text{NH}_4^+$  in aqueous  $(\text{C}_2\text{H}_5)_4\text{NI}$  solutions are preceded by maxima the height of which increases with the molar concentration of the depolarizer. Following the maxima in "forward" polarization experiments, the current passes through a dip before the limiting value is established. The dip, which is due to the impoverishment of the electrolyte, is not recorded upon "backward" polarization.

The development of the four maxima is related to a streaming motion of the solution, brought about by the dissolution of the amalgams formed. This explanation is in harmony with the experimental findings and clarifies some of the characteristics of the maxima not hitherto properly accounted for.

#### LITERATUR

- 1 J. J. LINGANE, *J. Electroanal. Chem.*, 15 (1967) 211.
- 2 M. VON STACKELBERG, W. HANS UND W. JENSCH, *Z. Elektrochem.*, 62 (1958) 839.
- 3 D. JANNAKOUDAKIS, A. WILDENAU UND L. HOLLECK, *J. Electroanal. Chem.*, 15 (1967) 83.
- 4 I. ZLOTOWSKI UND I. M. KOLTHOFF, *J. Am. Chem. Soc.*, 66 (1944) 1431.
- 5 W. KEMULA, *Advances in Polarography*, I. S. LONGMUIR (Edt.), Pergamon Press, 1960, p. 105.



PROPRIETES EN SOLUTION DANS LE TETRACHLOROALUMINATE  
DE SODIUM FONDU\*

I. SYSTEMES "ACIDE-BASE"

BERNARD TRÉMILLON ET GÉRARD LETISSE

*Laboratoire de Recherches de Chimie Analytique de la Faculté des Sciences, associé au CNRS,  
ENSCP, Paris, 5ème (France)*

(Reçu le 9 octobre, 1967)

Le mélange équimoléculaire de chlorure d'aluminium et de chlorure de sodium conduit par fusion à la formation d'un composé défini, le tétrachloroaluminate de sodium,  $\text{NaAlCl}_4$ . Nous avons envisagé d'utiliser ce composé comme solvant, d'une façon analogue à ce qui a été réalisé avec d'autres sels fondus, et d'en déterminer les principales propriétés, dans cette optique. C'est ainsi qu'il nous a paru intéressant et fructueux d'introduire la notion généralisée d'"acidité selon le système du solvant", dont la définition est due à FRANKLIN<sup>1</sup>, et qui permet une description systématique d'un certain nombre de propriétés en solution dans ce milieu.

Il est tout d'abord utile de rappeler quelques-unes des propriétés essentielles (physiques et physico-chimiques) des mélanges  $\text{AlCl}_3 + \text{NaCl}$ .

BUNSEN<sup>2</sup> a, le premier, fait mention de l'existence du composé défini  $\text{NaAlCl}_4$ . Mais celle-ci apparaît plus sûrement sur le diagramme de phases des mélanges  $\text{AlCl}_3 + \text{NaCl}$ , dont la détermination a fait l'objet de plusieurs travaux<sup>3-6</sup>.

La température de fusion de  $\text{NaAlCl}_4$ —qui fond sans décomposition à la limite de la congruence, l'eutectique  $\text{NaCl}-\text{NaAlCl}_4$  ayant une composition très proche de celle de  $\text{NaAlCl}_4$  et n'en pouvant être distingué—est 151° d'après ref. 6, 155° d'après ref. 5; nous avons pour notre part déterminé une température de cristallisation égale à 154°, ce qui est en accord avec les valeurs précédentes.

A partir de ce composé défini, la branche du liquidus du côté  $\text{NaCl}$  est très abrupte, ce qui implique une faible solubilité du chlorure de sodium dans  $\text{NaAlCl}_4$  fondu, entre la température de fusion de celui-ci et des températures de l'ordre de 350–400°. Nous verrons que ce fait intervient lors de notre étude des propriétés de solvant du tétrachloroaluminate fondu.

Du côté  $\text{AlCl}_3$  existe par contre un eutectique, dont la température de fusion est voisine de 110° et qui comprend environ 39 moles % de chlorure de sodium et 61 moles % de chlorure d'aluminium (à signaler que l'eutectique ternaire  $\text{AlCl}_3 + \text{NaCl} + \text{KCl}$  fond à 89°). Par ailleurs, une zone de démixtion—en  $\text{AlCl}_3$  saturé de  $\text{NaAlCl}_4$  (faible solubilité) et  $\text{NaAlCl}_4$  saturé de  $\text{AlCl}_3$ —apparaît aux fortes proportions (>80%) de chlorure d'aluminium, marquant une limite de solubilité de  $\text{AlCl}_3$  dans  $\text{NaAlCl}_4$ . Cette limite est toutefois suffisamment élevée pour que nous n'ayons pas à la faire

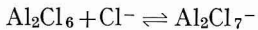
\* Etude effectuée dans le cadre de la recherche coopérative sur programme du CNRS, RCP No. 20, *Solvants et Sels Fondus*.

intervenir lors de notre étude, qui ne concerne que des solutions relativement diluées dans NaAlCl<sub>4</sub> fondu.

NaAlCl<sub>4</sub> fondu est un liquide ionisé constitué d'une part de cations Na<sup>+</sup> et d'autre part d'anions complexes AlCl<sub>4</sub><sup>-</sup>. Ces anions complexes sont stables puisqu'ils existent jusqu'à la température d'ébullition<sup>5</sup> et même à l'état de vapeur<sup>7</sup>. Le liquide utilisé comme solvant est donc, à l'état pur, très conducteur du courant électrique; c'est ainsi que le mélange AlCl<sub>3</sub> 51.7% + NaCl 40.4% + KCl 7.9% (en moles), proche de celui que nous utilisons, possède à 180°, selon MIDORIKAWA<sup>8</sup>, une conductance spécifique de 0.352 Ω<sup>-1</sup> cm<sup>2</sup>. La structure (tétraédrique) des anions AlCl<sub>4</sub><sup>-</sup> a été établie par spectroscopie Raman<sup>9</sup>.

Le chlorure de sodium se dissout dans NaAlCl<sub>4</sub> fondu vraisemblablement à l'état ionique Na<sup>+</sup>+Cl<sup>-</sup>, la grande différence de dimension entre Cl<sup>-</sup> et AlCl<sub>4</sub><sup>-</sup> expliquant la faible solubilité jusqu'à 400–500°.

Quant à la structure de l'espèce résultant de la dissolution de chlorure d'aluminium dans NaAlCl<sub>4</sub> fondu, elle a fait l'objet de plusieurs études<sup>3,10–14</sup>. Il semble qu'il se forme l'anion complexe Al<sub>2</sub>Cl<sub>7</sub><sup>-</sup>. On sait déjà, par des études de diffraction des rayons X<sup>15</sup>, que le chlorure d'aluminium fondu pur est constitué de molécules Al<sub>2</sub>Cl<sub>6</sub> (et non AlCl<sub>3</sub>), deux des six ions chlorure se trouvant associés en commun avec deux ions aluminium(III). OYE ET GRUEN<sup>11</sup> ont, en particulier, lors d'une étude par spectroscopie d'absorption, montré que l'addition de chlorure à Al<sub>2</sub>Cl<sub>6</sub> conduit probablement à la formation d'un complexe avec un ion Cl<sup>-</sup> supplémentaire, selon :



avant la formation du complexe supérieur, AlCl<sub>4</sub><sup>-</sup>.

Des constantes d'équilibre à 1000°K ont été déterminées par MOORE, MORREY ET VOILAND<sup>12,13</sup>.

Nous pensons donc que la dissolution de chlorure d'aluminium dans NaAlCl<sub>4</sub> fondu (solution diluée) conduit ainsi à la formation de l'espèce Al<sub>2</sub>Cl<sub>7</sub><sup>-</sup>. Celle-ci peut être considérée comme étant la molécule AlCl<sub>3</sub> "solvatée" par AlCl<sub>4</sub><sup>-</sup>, puisqu'il s'agit de AlCl<sub>3</sub>+AlCl<sub>4</sub><sup>-</sup>.

Plusieurs mémoires publiés font état de la détermination de quelques propriétés en solution dans NaAlCl<sub>4</sub>: potentiels normaux d'oxydo-réduction<sup>16,20</sup> (dont les valeurs sont pour la plupart rassemblées et classées dans le livre de CHARLOT ET TRÉMILLON<sup>21</sup>), potentiels de décomposition<sup>22</sup> et autres propriétés oxydo-réductrices<sup>12,13,23,24</sup>, degrés d'oxydation intermédiaires de certains cations métalliques<sup>25</sup>.

Signalons aussi toutes les études qui ont été effectuées dans les mélanges ternaires AlCl<sub>3</sub>+KCl+NaCl fondus (plus riches en chlorure d'aluminium que le composé NaAlCl<sub>4</sub>)<sup>26–36</sup> et plus particulièrement la thèse de LEROY<sup>33</sup>, dans laquelle diverses propriétés mettant en jeu les ions oxyde O<sup>2-</sup> sont décrites.

Comme le fait remarquer LEROY, l'activité des ions chlorure se trouve fixée dans l'eutectique liquide, en raison d'un effet tampon dû à la présence simultanée en proportions voisines des deux constituants du couple donneur-accepteur de chlorure AlCl<sub>4</sub><sup>-</sup>/AlCl<sub>3</sub> (ou Al<sub>2</sub>Cl<sub>7</sub><sup>-</sup>). Par contre, dans NaAlCl<sub>4</sub> fondu, cette activité peut en principe varier, en se plaçant soit en excès de chlorure de sodium (jusqu'à saturation) soit en excès de chlorure d'aluminium par rapport à la composition du composé défini. Il devient alors possible de définir, dans ce milieu particulier, des propriétés d'échange de l'ion chlorure, caractérisées par le potentiel d'ions chlorure pCl<sup>-</sup>, et de

faire apparaître une grande analogie de raisonnement avec les propriétés acides-bases (échange de proton) en solution aqueuse. Cette analogie conduit à l'introduction de la notion d'"acidité" généralisée (selon le système du solvant), dont nous allons établir la théorie dans le cas qui nous intéresse ici.

#### A. DÉFINITION DE L'"ACIDITÉ" ET DE LA "BASICITÉ" DANS LE TÉTRACHLOROALUMINATE FONDU

##### 1. Système du solvant

Du fait de l'existence possible, en présence de AlCl<sub>4</sub><sup>-</sup>, soit des ions chlorure, Cl<sup>-</sup>, soit des ions heptachlorodialuminate, Al<sub>2</sub>Cl<sub>7</sub><sup>-</sup>, on peut considérer que les anions AlCl<sub>4</sub><sup>-</sup> du solvant à l'état pur et fondu subissent une dissociation partielle selon l'équilibre :



Cet équilibre constitue le "système du solvant", selon la définition de FRANKLIN<sup>1</sup>. On peut, en appliquant la loi d'action de masse, le caractériser par la constante :

$$K_1^0 = \alpha_{(\text{Al}_2\text{Cl}_7^-)} \cdot \alpha_{(\text{Cl}^-)} / [\alpha_{\text{AlCl}_4^-}]^2 \quad (\text{A-2})$$

Dans l'hypothèse où le solvant est stable, c'est-à-dire où l'équilibre (A-1) n'est que très faiblement déplacé vers la droite, on admet que l'activité de AlCl<sub>4</sub><sup>-</sup> est très voisine de l'unité (selon la convention de TEMKIN-FÖRLAND pour les mélanges de sels ionisés), et qu'il en restera ainsi dans toutes les solutions diluées où NaAlCl<sub>4</sub> joue le rôle de solvant. On a donc en première approximation :

$$K_1^0 = \alpha_{(\text{Al}_2\text{Cl}_7^-)} \cdot \alpha_{(\text{Cl}^-)}$$

Le produit des activités des ions Cl<sup>-</sup> et Al<sub>2</sub>Cl<sub>7</sub><sup>-</sup> reste constant.

D'une façon plus pratique, nous utiliserons par la suite non pas les activités mais les concentrations, que nous désignerons par leur symbole classique : deux barres encadrant la formule chimique de l'espèce considérée. Nous pouvons alors remarquer que les coefficients d'activité vont rester constants en solution diluée, de sorte que non seulement le produit des activités de Cl<sup>-</sup> et Al<sub>2</sub>Cl<sub>7</sub><sup>-</sup> reste constant, mais aussi celui des concentrations de ces espèces chimiques. Ce produit va jouer le rôle d'une constante d'équilibre "apparente", que nous désignerons par K<sub>i</sub>:

$$K_i = [\text{Al}_2\text{Cl}_7^-][\text{Cl}^-] \quad (\text{A-4})$$

Nous appellerons aussi :

$$\text{p}K_i = -\log K_i \quad (\text{A-5})$$

Cette grandeur s'avère être d'un plus grand intérêt pratique (pour les calculs de bilans réactionnels) que la constante thermodynamique pK<sub>i</sub><sup>0</sup> = -log K<sub>i</sub><sup>0</sup>.

##### 2. Définition des "acides" et des "bases" en solution dans NaAlCl<sub>4</sub>

D'une façon générale, la définition de l'"acidité selon le système du solvant" consiste à considérer, dans un solvant moléculaire, que les donneurs de l'anion libéré par la dissociation ionique d'une molécule de solvant sont des "bases", tandis que les accepteurs de cet anion (donneurs du cation antagoniste) sont des "acides".

Cette définition est compatible avec la définition classique de BRØNSTED. Dans l'eau, en effet, les bases sont donneurs de l'anion OH<sup>-</sup> et accepteurs du cation antagoniste H<sub>3</sub>O<sup>+</sup> ( $2\text{H}_2\text{O} \rightleftharpoons \text{H}_3\text{O}^+ + \text{OH}^-$ ), les acides sont donneurs de H<sub>3</sub>O<sup>+</sup> et accepteurs de OH<sup>-</sup>. De la même manière, dans l'ammoniac liquide<sup>1</sup>,  $2\text{NH}_3 \rightleftharpoons \text{NH}_4^+ + \text{NH}_2^-$ , et les bases sont donneurs de l'anion amidure NH<sub>2</sub><sup>-</sup> et accepteurs du proton "solvaté" NH<sub>4</sub><sup>+</sup>, tandis que les acides sont donneurs de NH<sub>4</sub><sup>+</sup> et accepteurs de NH<sub>2</sub><sup>-</sup>.

La généralisation et la scission avec la définition de BRØNSTED apparaissent pour les solvants moléculaires non protoniques, comme l'oxychlorure de phosphore POCl<sub>3</sub> par exemple. La dissociation ionique postulée étant  $\text{POCl}_3 \rightleftharpoons \text{POCl}_2^+ + \text{Cl}^-$ , les "bases" sont ici les donneurs de l'anion Cl<sup>-</sup> (accepteurs du cation POCl<sub>2</sub><sup>+</sup>) et les acides les accepteurs de Cl<sup>-</sup> (et donneurs de POCl<sub>2</sub><sup>+</sup>), dont en particulier le cation H<sup>+</sup> et les acides au sens de BRØNSTED.

Cette généralisation a été prolongée au cas des solvants ionisés (sels fondus), essentiellement dans le cas des complexes "oxyde" (avec l'ion O<sup>2-</sup>) (voir la revue de cette question<sup>21,37</sup>). Par exemple, dans les nitrates fondus, le système du solvant étant  $\text{NO}_3^- \rightleftharpoons \text{NO}_2^+ + \text{O}^{2-}$ , les "bases" sont les donneurs de l'anion oxyde (accepteurs de NO<sub>2</sub><sup>+</sup>), les "acides" sont les accepteurs de O<sup>2-</sup> (H<sup>+</sup> en particulier). De même, dans les hydroxydes alcalins fondus, le système du solvant est  $2\text{OH}^- \rightleftharpoons \text{H}_2\text{O} + \text{O}^{2-}$  et les "bases" sont les donneurs de O<sup>2-</sup> et accepteurs de H<sub>2</sub>O, les "acides" sont les donneurs de H<sub>2</sub>O et accepteurs de O<sup>2-</sup>. GORET ET TRÉMILLON<sup>38</sup> ont souligné le fait que, comme dans l'eau, la conception généralisée se confond, dans les hydroxydes fondus, avec la conception restreinte de BRØNSTED, puisque H<sub>2</sub>O joue le rôle du proton "solvaté" par les anions du solvant.

Dans les autres cas, les termes "solvo-acides" et "solvo-bases" ont été quelquefois utilisés pour éviter la confusion possible avec les acides et les bases au sens défini par BRØNSTED.

Dans le cas qui nous intéresse, la dissociation de l'anion du solvant fait apparaître deux anions, mais la logique et la conciliation avec l'ensemble de la théorie imposent de choisir l'anion chlorure Cl<sup>-</sup> pour établir la définition des "acides" et des "bases". Nous considérerons donc comme:

— "bases": les donneurs de Cl<sup>-</sup> (donc accepteurs de Al<sub>2</sub>Cl<sub>7</sub><sup>-</sup>);

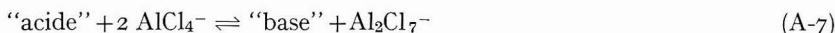
— "acides": les accepteurs de Cl<sup>-</sup> (donc donneurs de Al<sub>2</sub>Cl<sub>7</sub><sup>-</sup>).

Les couples "acide-base" sont ainsi les couples accepteur-donneur de Cl<sup>-</sup>:



Lorsqu'on va dissoudre un "acide" ou une "base" dans NaAlCl<sub>4</sub> fondu, il s'établira un équilibre d'échange de Cl<sup>-</sup> avec les anions AlCl<sub>4</sub><sup>-</sup>, conduisant à la notion, comme pour les acides et les bases en solution aqueuse, d'"acide" fort et d'"acide" faible, de "base" forte et de "base" faible.

Avec un "acide":



Nous définissons la constante d'"acidité" (constante apparente):

$$K_A = [\text{"base"}][\text{Al}_2\text{Cl}_7^-]/[\text{"acide"}] \quad (\text{A-8})$$

(l'activité de AlCl<sub>4</sub><sup>-</sup> étant supposée rester voisine de l'unité).

Si l'équilibre (A-7) est pratiquement totalement déplacé vers la droite, l'"acide"

est fort (solvolyse complète avec formation de Al<sub>2</sub>Cl<sub>7</sub><sup>-</sup>; la "base" est un complexe chlorure plus stable que AlCl<sub>4</sub><sup>-</sup>). Sinon, l'"acide" est faible et sa force est mesurée par la valeur de pK<sub>A</sub> = -log K<sub>A</sub>, d'autant plus grande que l'"acide" est plus faible.

Les chlorures entièrement dissociés, et tout particulièrement le chlorure de sodium, se comportent en "bases" fortes. Les chlorures à caractère de complexes, non entièrement dissociés, sont des "bases" faibles, dont la force est mesurée par leur constante de dissociation (qui est ici une constante de "basicité") ou par la constante d'"acidité" de l'"acide" conjugué. Par exemple, pour un composé "basique" du type MCl:



(M<sup>+</sup> est l'"acide" conjugué de MCl, accepteur de Cl<sup>-</sup>):

$$K_B = [\text{M}^+] [\text{Cl}^-] / [\text{MCl}] \quad (\text{A-10})$$

ou



$$K_A = [\text{MCl}] [\text{Al}_2\text{Cl}_7^-] / [\text{M}^+] \quad (\text{A-12})$$

On démontre la relation:

$$\text{p}K_A + \text{p}K_B = \text{p}K_i \quad (\text{A-13})$$

Les raisonnements sont identiques à ceux effectués pour les hydroxydes en solution aqueuse.

D'autres espèces chimiques pourront avoir des propriétés "basiques", c'est-à-dire faire apparaître des ions Cl<sup>-</sup> libres par solvolyse; elles seront "bases" fortes si la solvolyse est complète, "bases" faibles dans le cas contraire. Nous décrirons plus loin le cas des anions oxyde, mais il y a sans doute aussi d'autres anions (F<sup>-</sup> par exemple) et des molécules coordinatives qui présentent un caractère basique.

### 3. Potentiel d'ions chlorure pCl<sup>-</sup>. Echelle d'"acidité"

Puisque l'anion chlorure Cl<sup>-</sup> est la particule sur laquelle est fondée la définition de l'"acidité" — comme H<sup>+</sup> est celle qui sert à l'établissement de la définition de BRØNSTED —, nous ferons appel, pour mesurer l'"acidité" des solutions dans NaAlCl<sub>4</sub> fondu, au potentiel d'ions chlorure défini par:

$$\text{pCl}^- = -\log a_{(\text{Cl}^-)} \quad (\text{A-14})$$

(anologue à pH = -log a<sub>(H<sup>+</sup>)</sub>.

C'est cette grandeur dont nous envisagerons la mesure expérimentale potentiométrique.

Pour les calculs pratiques, il est souvent plus commode de se servir d'une grandeur "opérationnelle", que nous relions à la concentration, et non à l'activité, des ions Cl<sup>-</sup>:

$$\text{pCl}^- = -\log |\text{Cl}^-| \quad (\text{A-15})$$

C'est sur cette dernière que nous allons raisonner.

(a) On a en principe pCl<sup>-</sup> = 0 pour une solution de chlorure de sodium 1 M. Cette concentration est en fait inaccessible, puisque la solubilité de NaCl dans

$\text{NaAlCl}_4$  à  $175^\circ$  est faible, de l'ordre de  $5 \cdot 10^{-2}$ , comme nous le verrons dans les résultats expérimentaux.

(b) On a  $\text{pCl}^- = \text{p}K_i$  pour une solution de chlorure d'aluminium  $1\text{ M}$  (concentration réalisable, bien que la solution ne soit pas très stable, le chlorure d'aluminium pouvant s'échapper à l'état de vapeur).

(c) Pour du tétrachloroaluminate fondu rigoureusement pur, la règle de dissociation de  $\text{AlCl}_4^-$  impose que  $[\text{Cl}^-] = [\text{Al}_2\text{Cl}_7^-]$ , de sorte que:

$$\text{pCl}^- = \frac{1}{2}\text{p}K_i \quad (\text{A-16})$$

C'est la *neutralité* des solutions dont  $\text{NaAlCl}_4$  est le solvant.

(d) Le domaine  $\text{pCl}^- < \frac{1}{2}\text{p}K_i$  définit les solutions "*basiques*" (excès de  $\text{Cl}^-$  par rapport à  $\text{Al}_2\text{Cl}_7^-$ ). Le domaine  $\text{pCl}^- > \frac{1}{2}\text{p}K_i$  définit les solutions "*acides*" (excès de  $\text{Al}_2\text{Cl}_7^-$  par rapport à  $\text{Cl}^-$ ).

Ainsi, tout mélange pour lequel le rapport moléculaire  $\text{NaCl}/\text{AlCl}_3$  est supérieur à l'unité constitue, par rapport au tétrachloro-aluminate fondu, un milieu "*basique*". Inversement, tout mélange plus riche en  $\text{AlCl}_3$  qu'en  $\text{NaCl}$  (rapport  $\text{AlCl}_3/\text{NaCl}$  supérieur à l'unité) constitue un milieu "*acide*"; c'est en particulier le cas de l'eutectique fondu utilisé par LEROY et d'autres, pour lequel  $\text{pCl}^-$  est un peu supérieur à  $\text{p}K_i$ .

(f) Les valeurs de  $\text{pCl}^-$  caractérisant l"*"acidité"* des solutions d"*"acides"* ou des "*bases*" sont calculables selon les mêmes modes que le pH en solution aqueuse.

Remarquons que les bases les plus fortes, ajoutées au tétrachloroaluminate fondu, font apparaître un précipité de chlorure de sodium dès que  $\text{pCl}^-$  atteint la valeur minimale, égale au cologarithme de la solubilité de  $\text{NaCl}$  à la température de l'expérience.

## B. SYSTÈME OXYDO-RÉDUCTEUR DE L'ALUMINIUM ET "*ACIDITÉ*". DÉTERMINATION EXPÉRIMENTALE DE LA CONSTANTE $\text{p}K_i$ DE DISSOCIATION DES ANIONS TÉTRACHLOROALUMINATE

Tout système oxydo-réducteur mettant en jeu des ions chlorure a ses propriétés modifiées par variation de  $\text{pCl}^-$ . Cette modification est en principe exploitable pour déterminer des propriétés "*acides-bases*".

Nous avons voulu commencer par étudier les systèmes oxydo-réducteurs du solvant, qui limitent le domaine d'électroactivité dans  $\text{NaAlCl}_4$  fondu: le système de l'aluminium, d'une part:



(limitation vers la réduction par la réaction  $\text{Al}^{\text{III}} + 3 e \rightarrow \text{Al}\downarrow$ ), et le système du chlore, d'autre part:



(limitation vers l'oxydation par la réaction de formation du chlore). Nous décrivons en premier lieu les résultats obtenus pour le système de l'aluminium. L'étude des courbes intensité-potentiel à une micro-électrode d'aluminium tournante a fourni un moyen précis de détermination de la constante de dissociation  $\text{p}K_i$  des ions  $\text{AlCl}_4^-$ , donnant ainsi l'étendue du domaine d"*"acidité"*.

Pour le couple  $\text{Al}/\text{Al}^{\text{III}}$  dans le tétrachloroaluminate fondu, deux systèmes

oxydo-réducteurs peuvent être écrits selon que le milieu est "basique" (présence d'ions Cl<sup>-</sup> libres) ou "acide" (présence d'ions Al<sub>2</sub>Cl<sub>7</sub><sup>-</sup>).

(a) En milieu "basique":



(b) En milieu "acide":



Dans les deux cas, la réduction de Al<sup>III</sup> conduit directement à la formation d'aluminium métal; des dendrites apparaissent à la cathode. Inversement, l'oxydation de l'aluminium conduit d'abord aux ions Al<sup>3+</sup>, qui se combinent à des ions Cl<sup>-</sup>, soit libres (en milieu "basique"), soit prélevés sur les anions du solvant AlCl<sub>4</sub><sup>-</sup>.

Il est apparent que l'oxydation de l'aluminium est plus aisée (thermodynamiquement) si des ions Cl<sup>-</sup> libres sont présents au contact du métal que si ces ions Cl<sup>-</sup> doivent être arrachés à AlCl<sub>4</sub><sup>-</sup>, donc si l'on a affaire à un milieu "basique" que si l'on a affaire à un milieu "acide". En sens inverse, la réduction de Al<sub>2</sub>Cl<sub>7</sub><sup>-</sup>, présent seulement en milieu "acide", est plus aisée que celle de AlCl<sub>4</sub><sup>-</sup>, composé dans lequel Al<sup>3+</sup> se trouve plus fortement complexé. En somme, d'après les lois d'équilibre, les potentiels auxquels la réaction (B-3) se produit sont inférieurs à ceux où a lieu la réaction (B-4).

Le potentiel d'équilibre d'une électrode d'aluminium plongeant dans le tétra-chloroaluminate fondu est exprimé par les formules:

—en milieu "basique":

$$E = (E_0^0)_{\text{Al}} - (4 RT/3 F) \ln [\text{Cl}^-] \quad (\text{B-5})$$

Soit, à 175°:

$$E = (E_0^0)_{\text{Al}} - 0.120 \log [\text{Cl}^-] \quad (\text{B-6})$$

Nous avons pris par convention  $E=0$  pour la solution de chlorure de sodium saturé à 175°. C'est d'ailleurs le potentiel de l'électrode de référence qui a été adoptée pour effectuer toutes les mesures (voir technique expérimentale). Remarquons en outre que ce potentiel correspond à des activités thermodynamiques toutes égales à l'unité pour les constituants du système: AlCl<sub>4</sub><sup>-</sup> (anion du solvant), Al (solide) et NaCl (saturé, solide en présence); il s'agit donc du potentiel normal thermodynamique.

—en milieu "acide":

$$E = (E_1^0)_{\text{Al}} + (4 RT/3 F) \ln [\text{Al}_2\text{Cl}_7^-] \quad (\text{B-7})$$

Soit, à 175°:

$$E = (E_1^0)_{\text{Al}} + 0.120 \log [\text{Al}_2\text{Cl}_7^-] \quad (\text{B-8})$$

$(E_1^0)_{\text{Al}}$  et  $(E_0^0)_{\text{Al}}$  sont reliés par:

$$(E_1^0)_{\text{Al}} - (E_0^0)_{\text{Al}} = 0.120 \text{ p}K_1 \quad (\text{B-9})$$

Il est pratiquement impossible d'obtenir le solvant NaAlCl<sub>4</sub> à l'état rigoureusement pur, neutre, puisqu'il est préparé par mélange de quantités en principe équimoléculaires de chlorure d'aluminium et de chlorure de sodium. En fait, utilisant la très faible solubilité (à 175°) du chlorure de sodium dans NaAlCl<sub>4</sub> fondu, nous avons toujours constitué au départ une solution saturée de NaCl, grâce à un léger excès de

ce sel par rapport à la quantité équimoléculaire de  $\text{AlCl}_3$ . Après élimination du chlorure de sodium solide résiduel, nous disposons ainsi d'une solution très bien définie et parfaitement reproductible, mais qui se trouve à la limite de "basicité" accessible ( $p\text{Cl}^-$  minimal). Pour revenir à un milieu neutre, puis éventuellement "acide", nous avons opéré par ré-introduction de quantités connues de chlorure d'aluminium pur; nous décrirons plus loin par quel processus électrochimique. La technique expérimentale sera décrite dans le mémoire suivant.

Nous avons d'abord déterminé les courbes voltampérométriques à une micro-électrode d'aluminium tournante (régime de diffusion stationnaire), dans le but de vérifier la concordance entre les phénomènes expérimentaux et la théorie des courbes intensité-potentiel des systèmes rapides, pour lesquels le courant d'électrolyse reste contrôlé uniquement par la diffusion stationnaire des espèces mises en jeu dans la réaction électrochimique. Ces courbes sont représentées sur la Fig. I.

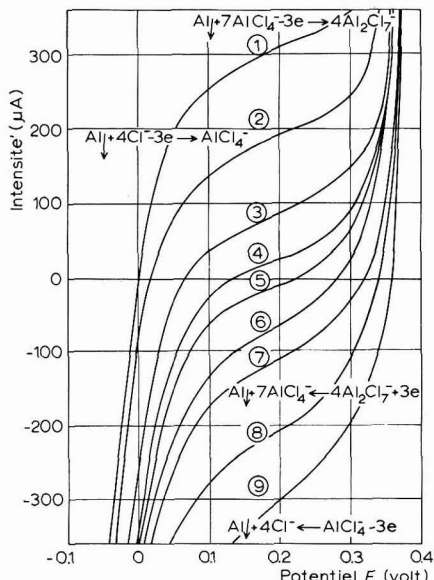


Fig. I. Courbes intensité-potentiel à une micro-électrode d'aluminium tournante (vitesse de rotation 300 t/min) dans  $\text{NaAlCl}_4$  fondu. (1),  $\text{NaCl}$  saturé; (2),  $\text{Cl}^- 2.9 \cdot 10^{-2}$ ; (3),  $1.35 \cdot 10^{-2}$ ; (4),  $3.5 \cdot 10^{-3}$ ; (5),  $\text{Al}_2\text{Cl}_7^- 3.5 \cdot 10^{-3}$ ; (6),  $1.2 \cdot 10^{-2}$ ; (7)  $2 \cdot 10^{-2}$ ; (8),  $3 \cdot 10^{-2}$ ; (9),  $4 \cdot 10^{-2} M$ .

La première courbe, 1, est obtenue avec la solution saturée de chlorure de sodium. L'oxydation de l'aluminium se produit d'abord selon la réaction:



Mais l'intensité de cette réaction est limitée par la diffusion des ions  $\text{Cl}^-$  qui sont consommés à l'électrode. En raison de leur faible concentration, le courant-limite est peu intense. D'où le palier qui apparaît sur la courbe.

L'oxydation se poursuit, environ 300 mV plus loin, selon la réaction:



Le courant dû à cette dernière réaction n'est pas limité par diffusion (les ions

AlCl<sub>4</sub><sup>-</sup> consommés étant ceux du solvant); il y a production de l'anion "acide" fort Al<sub>2</sub>Cl<sub>7</sub><sup>-</sup>.

L'addition de chlorure d'aluminium fait diminuer la concentration de Cl<sup>-</sup>, par suite de la réaction "base" forte—"acide" fort:



d'où l'abaissement du palier d'oxydation (courbes 2-4).

Quand tous les ions Cl<sup>-</sup> présents initialement ont été neutralisés, l'excès d'ions Al<sub>2</sub>Cl<sub>7</sub><sup>-</sup> provoque l'apparition d'un palier de réduction (courbes 5-9) correspondant à la réaction:



dont l'intensité est limitée par la diffusion de Al<sub>2</sub>Cl<sub>7</sub><sup>-</sup>.

Ces différentes courbes présentent tous les caractères des courbes intensité-potentiel dues à un système "rapide" et, s'étant ainsi assurés de l'établissement rapide de l'équilibre entre l'électrode d'aluminium et les solutions "acides" ou "basiques", nous avons pu nous servir de cette électrode comme indicatrice de pCl<sup>-</sup>, puisque son potentiel doit alors suivre la loi simple:

$$E = (E_0^0)_{\text{Al}} + 0.120 \text{ pCl}^- \quad (\text{B-14})$$

aussi bien en milieu "acide" qu'en milieu "basique". Nous avons alors déterminé la variation de ce potentiel d'équilibre lorsque, partant de la solution saturée de chlorure de sodium, nous avons ajouté des quantités croissantes d'"acide" fort.

#### *Introduction coulométrique de l'"acide" fort*

Selon le système (B-4), l'oxydation de l'aluminium conduit à la production de 4 anions Al<sub>2</sub>Cl<sub>7</sub><sup>-</sup> pour 3 électrons arrachés, soit 4 ions-grammes d'"acide" fort pour 3 faradays consommés. Aucune limitation du courant correspondant à cette réaction n'apparaissant, la production électrochimique de Al<sub>2</sub>Cl<sub>7</sub><sup>-</sup> peut être effectuée à intensité constante.

Pour une production suffisamment rapide de Al<sub>2</sub>Cl<sub>7</sub><sup>-</sup>, la valeur de l'intensité imposée a été de 100 mA, et, pour ne pas atteindre ainsi de trop fortes densités de courant, l'électrode consommable était un disque d'aluminium de 1-2 cm<sup>2</sup> de surface.

La contre-électrode était un disque analogue placé dans un compartiment séparé rempli de tétrachloroaluminate fondu. Il s'y passe évidemment une réduction, c'est-à-dire un dépôt important d'aluminium (dendrites); en même temps, selon (B-3), il y a production de Cl<sup>-</sup> libre, d'où précipitation de chlorure de sodium quand la solution est saturée. Il en résulte que le potentiel de cette contre-électrode reste constant.

Remarquons aussi que, si l'oxydation de l'aluminium est effectuée dans une solution initialement "basique", le système (B-3), Al $\downarrow$  + 4 Cl<sup>-</sup> - 3 e  $\rightarrow$  AlCl<sub>4</sub><sup>-</sup> est également mis en jeu. Mais 4 ions-grammes de chlorure ("base" forte) y sont consommés en même temps que 3 faradays, ce qui revient au même que d'introduire 4 ions-grammes d'"acide" fort.

#### *Courbe potentiométrique d'équilibre*

En interrompant à intervalles réguliers l'introduction coulométrique d'"acide"

fort, la mesure du potentiel d'équilibre d'une micro-électrode indicatrice d'aluminium a été effectuée (par rapport à une électrode de référence  $\text{Al}/\text{AlCl}_4^- + \text{NaCl}$  saturé,  $E=0$ ). Les valeurs expérimentales et la courbe qui en résulte sont représentées sur la Fig. 2.

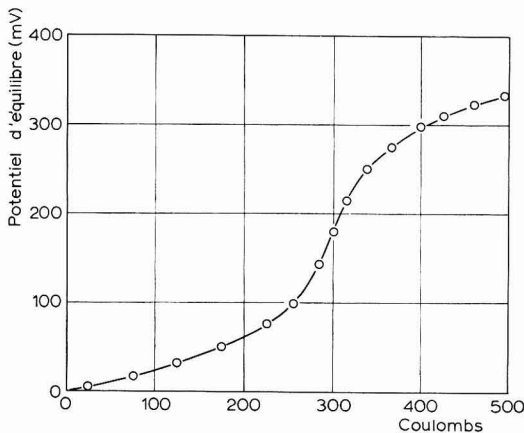


Fig. 2. Courbe potentiométrique de titrage coulométrique (à intensité constante,  $i_0 = 100 \text{ mA}$ ) de la "base" forte  $\text{Cl}^-$  par l'"acide" fort  $\text{Al}_2\text{Cl}_7^-$ .

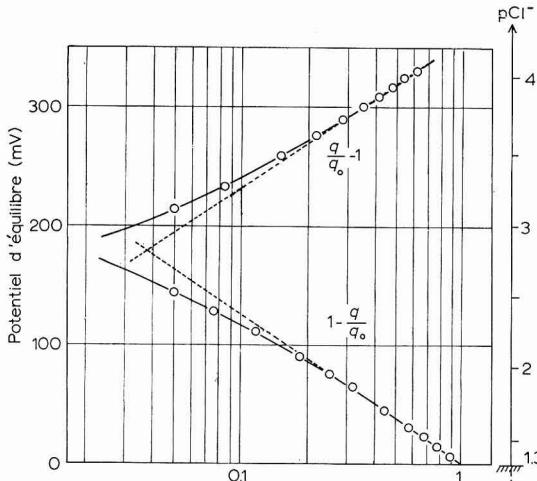


Fig. 3. Titrage coulométrique de la "base" forte  $\text{Cl}^-$  par l'"acide" fort  $\text{Al}_2\text{Cl}_7^-$  (cf. figure précédente).

Il s'agit de la courbe de titrage potentiométrique de la "base" forte  $\text{Cl}^-$ , dont la concentration initiale est celle de la solution saturée de chlorure de sodium dans  $\text{NaAlCl}_4$  fondu à  $175^\circ$ , par l'"acide" fort  $\text{Al}_2\text{Cl}_7^-$ . Celui-ci étant introduit coulométriquement, nous avons porté en abscisse le nombre  $q = i_0 t$  de coulombs consommés lors de cette production électrolytique.

Le point équivalent, correspondant au milieu rigoureusement neutre, est

atteint après 300 ( $\pm 10$ ) °C, pour 85( $\pm 0.5$ ) g de solvant. La solubilité du chlorure de sodium dans NaAlCl<sub>4</sub> fondu, à 175°, est ainsi évaluée à  $4.9 (\pm 0.2) \cdot 10^{-2}$  mole kg<sup>-1</sup>.

La courbe de titrage expérimentale présente bien la forme en "S" classique de la courbe de titrage d'une base forte par un acide fort. Théoriquement, en appelant  $q$  la quantité d'électricité introduite et  $q_0$  celle nécessaire pour atteindre le point équivalent, le potentiel d'équilibre de l'électrode d'aluminium doit varier selon la relation :

$$E = -0.120 \log(1 - q/q_0) \quad (\text{B-15})$$

(puisque  $E=0$  pour  $q=0$ ), dans le domaine où la réaction de neutralisation (B-12) peut être considérée comme pratiquement quantitative ( $q \ll q_0$ ), et selon la relation :

$$E = \text{constante} + 0.120 \log(q/q_0 - 1) \quad (\text{B-16})$$

lorsque la neutralisation de Cl<sup>-</sup> est pratiquement achevée, en présence d'un excès suffisant de Al<sub>2</sub>Cl<sub>7</sub><sup>-</sup> ( $q \gg q_0$ ).

Les deux relations (B-15) et (B-16) ont été testées à partir des valeurs expérimentales (Fig. 3). La linéarité de  $E$  en fonction de  $\log(1 - q/q_0)$  ou de  $\log(q/q_0 - 1)$  est satisfaisante, avec une pente voisine de la valeur théorique 0.120.

Aux alentours du point équivalent, les relations (B-15) et (B-16) ne peuvent être vérifiées, car la dissociation de AlCl<sub>4</sub><sup>-</sup> intervient notablement et [Cl<sup>-</sup>] est du même ordre de grandeur que [Al<sub>2</sub>Cl<sub>7</sub><sup>-</sup>]. Il y a incurvation des variations de  $E$  sur la Fig. 3, les deux courbes tendant asymptotiquement vers la valeur du potentiel au point équivalent, 180 mV. Ce potentiel correspond à  $p\text{Cl} = \frac{1}{2} pK_i$ .

#### Conclusion. Valeur de $pK_i$

Tous les essais expérimentaux démontrent la validité de l'utilisation de l'électrode d'aluminium comme électrode de mesure de pCl<sup>-</sup>. De la courbe potentiométrique, nous déduisons les grandeurs suivantes, caractéristiques du solvant (à 175°) :

(a)  $p\text{Cl}^-$  minimal (milieu le plus "basique" accessible). La solubilité du chlorure de sodium ayant été déterminée égale à  $(4.9 \pm 0.2) \cdot 10^{-2} M$ , nous en déduisons la valeur minimale de pCl<sup>-</sup>, que nous désignerons par  $p\text{Cl}^-_0$ :

$$p\text{Cl}^-_0 = -\log[(4.9 \pm 0.2) \cdot 10^{-2}] = 1.31 \pm 0.02 \quad (\text{B-17})$$

(b) Valeur de  $pK_i$ . Celle-ci est déductible des deux droites de la Fig. 3:

$$pK_i = 5.48 \pm 0.05 \quad (\text{B-18})$$

Soit, pour le produit  $K_i$ :

$$K_i = [\text{Cl}^-][\text{Al}_2\text{Cl}_7^-] = (3.4 \pm 0.4) \cdot 10^{-6} \quad (\text{B-19})$$

(échelle des molalités). Au point équivalent du titrage,  $p\text{Cl}^- = 2.75$ .

La correspondance entre l'échelle de pCl<sup>-</sup> et l'échelle de potentiel (étalonnage de l'électrode d'aluminium indicatrice de pCl<sup>-</sup>) est ainsi représentée sur la droite de la Fig. 3. L'échelle de pCl<sup>-</sup> accessible, à 175°, va de  $p\text{Cl}^-_0 = 1.3$  à des valeurs de l'ordre de 5.5 en présence de chlorure d'aluminium concentré.

Remarque. Le titrage en sens inverse du chlorure d'aluminium ("acide" fort), ajouté en excès, par du chlorure de sodium ("base" forte) a été aussi effectué, mais

non coulométriquement (addition progressive de NaCl solide, dissolution assez lente). Il est expérimentalement moins commode que le titrage coulométrique.

Il nous a cependant permis de vérifier que la loi de proportionnalité entre le potentiel de l'électrode d'aluminium et  $p\text{Cl}^-$  restait valable jusqu'à des concentrations de chlorure d'aluminium au moins 1 M (Fig. 4).

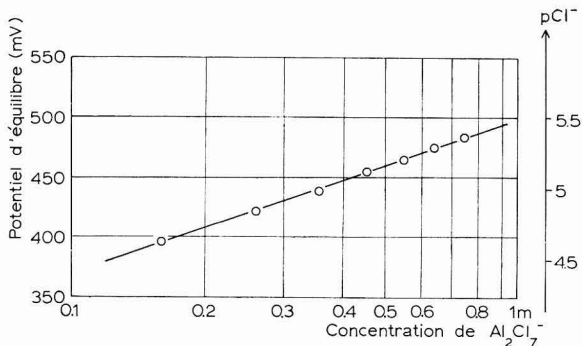


Fig. 4. Étalonnage de l'électrode indicatrice de  $p\text{Cl}^-$  en milieu "acide" fort concentré.

### C. SYSTÈME OXYDO-RÉDUCTEUR DU CHLORE

Des raisonnements similaires à ceux effectués pour le système de l'aluminium sont valables pour le système correspondant à l'oxydation du solvant, c'est-à-dire le système chlorure-chlore. Les propriétés de ce système, qui met naturellement en jeu les ions chlorure, sont variables avec l'"acidité" du milieu. L'étude a été conduite comme dans le cas de l'aluminium, avec une électrode à chlore: détermination des courbes intensité-potentiel pour justifier le fonctionnement de l'électrode, exploitation des variations de potentiel d'équilibre.

C'est le graphite qui est généralement utilisé pour constituer les électrodes à chlore en milieu sel fondu (voir notamment refs. 23, 39-46). Pour notre part, nous avons obtenu les résultats les plus satisfaisants avec une électrode de carbone vitrifié (surface 8 mm<sup>2</sup>). Les conditions de fabrication et d'utilisation de cette électrode seront décrites dans la partie Technique Expérimentale à la fin du mémoire suivant.

Le chlore a été introduit dilué par de l'azote, avec un rapport constant des débits de chlore et d'azote.

1. La Fig. 5 représente les courbes d'oxydation obtenues en l'absence de chlore. En présence de chlorure libre, apparaît une vague correspondant à la réaction:



Le courant est limité par la diffusion des ions  $\text{Cl}^-$  vers l'électrode; c'est pourquoi se produit un palier dont la hauteur est en principe proportionnelle à la concentration des ions  $\text{Cl}^-$ .

Lorsqu'on neutralise ces ions  $\text{Cl}^-$  par addition progressive de chlorure d'aluminium, le palier s'abaisse et finalement disparaît. On obtient enfin, en milieu neutre et "acide", la courbe 5 correspondant à la réaction d'oxydation de  $\text{AlCl}_4^-$ :



2. La Fig. 6 représente les courbes d'oxydo-réduction obtenues en présence de chlore.

La partie oxydation se présente de la même manière. Il apparaît ici en outre des vagues correspondant à la réduction du chlore, et limitée par la diffusion de cette espèce chimique dissoute.

En milieu "basique", le chlore est réduit en ions Cl<sup>-</sup>. La courbe globale présente les caractéristiques d'un système rapide, où le courant est uniquement contrôlé par la diffusion stationnaire.

Le passage en milieu "acide" doit provoquer le déplacement de la vague de

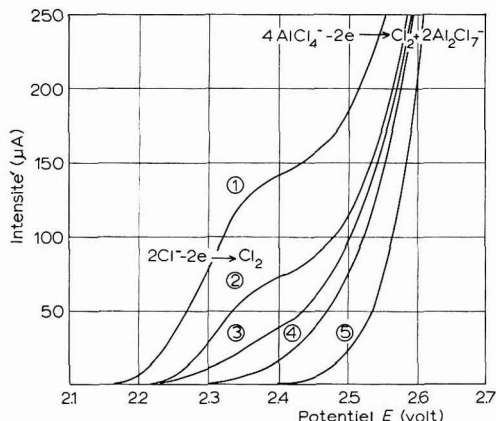


Fig. 5. Courbes intensité-potentiel à une micro-électrode de carbone vitrifié (surface 8 mm<sup>2</sup>) dans NaAlCl<sub>4</sub> fondu. pCl<sup>-</sup>: (1), 1.66; (2), 1.99; (3), 2.30; (4), 2.80; (5), 4.06.

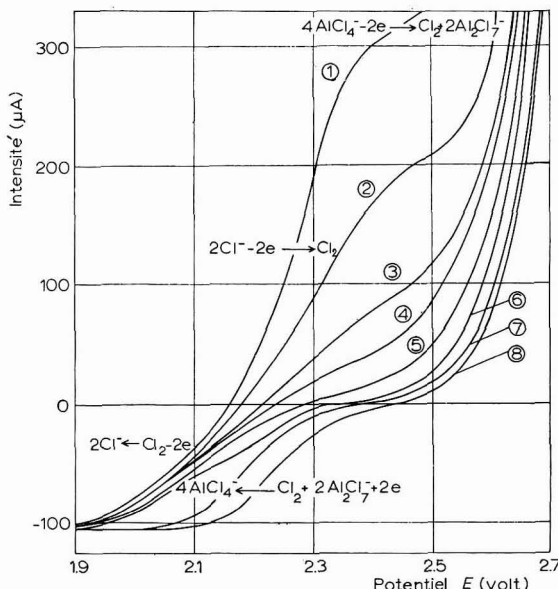


Fig. 6. Courbes intensité-potentiel à une micro-électrode de carbone vitrifié dans NaAlCl<sub>4</sub> fondu, en présence de chlore. pCl<sup>-</sup>: (1), 1.3; (2), 1.5; (3), 1.8; (4), 2.05; (5), 2.7; (6), 3.5; (7), 3.8; (8), 4.5.

réduction du chlore vers les potentiels plus élevés, selon le système :



L'expérience vérifie cette hypothèse, mais il s'avère que la courbe globale en milieu "acide" (courbes 6-8) ne présente plus les caractéristiques d'un système où le courant est contrôlé par la diffusion, le potentiel de demi-vague de réduction étant inférieur d'environ 200 mV à ce qu'il devrait être pour qu'il en soit ainsi. Une étude approfondie—que nous n'avons pas entreprise—du mécanisme des réactions électrochimiques eut été nécessaire pour déterminer si cette anomalie est dûe à une faible vitesse d'échange d'électrons en milieu "acide", ou à des phénomènes physiques au niveau de l'électrode (adsorption, en particulier).

En raison de cette anomalie des courbes intensité-potentiel en milieu "acide", nous ne sommes pas certains que le potentiel à courant nul indiqué par l'électrode en présence d'un excès de  $\text{Al}_2\text{Cl}_7^-$  soit le véritable potentiel d'équilibre de l'électrode à chlore, obéissant à la formule de NERNST. Néanmoins, ce potentiel est suffisamment bien défini pour pouvoir le mesurer avec certitude et suivre sa variation lors de la réaction de neutralisation "base" forte—"acide" fort.

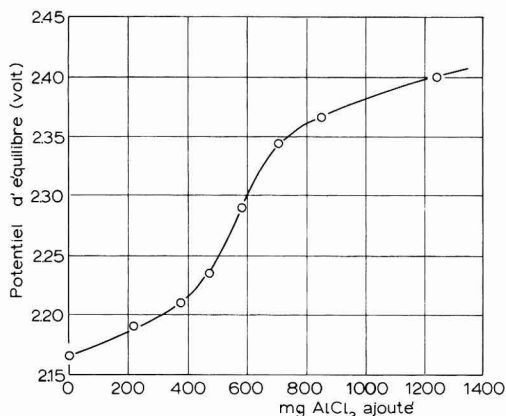


Fig. 7. Courbes de titrage potentiométrique, à l'électrode à chlore, de la "base" forte  $\text{Cl}^-$  par le chlorure d'aluminium.

La courbe potentiométrique représentée Fig. 7 présente l'allure que l'on pouvait attendre d'après la théorie. Le point équivalent est en accord avec la valeur de la solubilité du chlorure de sodium, que nous connaissons d'après l'étude précédente. La courbe permet aussi de déterminer une valeur de la constante  $pK_1$  du solvant, égale à 5.2. Cette valeur est un peu plus faible que celle obtenue par l'étude de l'électrode d'aluminium. En raison des imperfections de l'électrode à chlore, elle est certainement moins sûre; mais, compte tenu de cette difficulté, nous estimons que l'accord est satisfaisant.

#### CONCLUSION

Les deux couples oxydo-réducteurs du solvant, qui limitent son domaine d'électroactivité, sont donc soumis, tout à fait comme dans le cas de l'eau, à l'influence

de l'“acidité”. Il ne s’agit pas ici de l’acidité au sens donné par BRØNSTED, mais d’une “acidité” généralisée, basée sur le système du solvant, en l’occurrence système d’échange des ions chlorure.

L’étude expérimentale, meilleure dans le cas du système de l’aluminium, a fourni l’étendue du domaine d’“acidité” accessible. L’électrode à chlore en a fourni une confirmation.

Pour les applications électrochimiques, il est intéressant de noter que la force électromotrice d’une pile (Al↓|NaAlCl<sub>4</sub> fondu, saturé de NaCl à 175°||NaAlCl<sub>4</sub> fondu, saturé de NaCl et de chlore|graphite) sera de l’ordre de 2,2 V. Du fait de la faible solubilité de NaCl, la tension tombera à 1,7 V environ lors du débit d’un courant intense.

#### RÉSUMÉ

La notion d’acidité généralisée (échange de Cl<sup>-</sup>) dans le tétrachloroaluminate de sodium fondu—mélange équimoléculaire de chlorure d’aluminium et de chlorure de sodium—a été développée. L’équilibre de dissociation des anions du solvant:



constitue le système du solvant sur lequel repose la définition des “acides” (accepteurs de Cl<sup>-</sup>) et des “bases” (donneurs de Cl<sup>-</sup>). On mesure l’acidité du milieu par la grandeur  $p\text{Cl}^- = -\log[\text{Cl}^-]$ .

L’étude voltampérométrique du système oxydo-réducteur de l’aluminium a montré qu’une électrode de ce métal est indicatrice de pCl<sup>-</sup>. La courbe potentiométrique de titrage de Cl<sup>-</sup>, par l’“acide” fort Al<sub>2</sub>Cl<sub>7</sub><sup>-</sup> produit coulométriquement, a permis de déterminer la valeur de la constante apparente de l’équilibre (1), à 175°:

$$K_i = [\text{Al}_2\text{Cl}_7^-][\text{Cl}^-] = (3.4 \pm 0.4) \cdot 10^{-6} \text{ mole}^2 \text{ kg}^{-2}$$

L’étude voltampérométrique d’une électrode à chlore, qui est en principe également indicatrice de pCl<sup>-</sup>, a permis d’effectuer une seconde détermination de la constante  $K_i$ , compatible avec la première, compte tenu des imperfections des caractéristiques de l’électrode à chlore.

#### SUMMARY

The conception of generalized acidity (exchange of Cl<sup>-</sup>) in molten sodium tetrachloroaluminate—equimolar mixture of aluminium chloride and sodium chloride—has been developed.

The dissociation equilibrium of the solvent anions:

$2 \text{ AlCl}_4^- \rightleftharpoons \text{Al}_2\text{Cl}_7^- + \text{Cl}^-$ , constitutes the solvent system upon which is based the definition of “acids” (Cl<sup>-</sup> acceptors) and “bases” (Cl<sup>-</sup> donors). The acidity of the medium is measured by the value of  $p\text{Cl}^- = -\log[\text{Cl}^-]$ .

The electrochemical study of the aluminium redox system showed that an aluminium electrode can be used as pCl<sup>-</sup> indicator. The potentiometric titration curve of Cl<sup>-</sup> by the strong “acid” Al<sub>2</sub>Cl<sub>7</sub><sup>-</sup> produced coulometrically, enabled the apparent equilibrium constant to be determined:

$$K_i = [\text{Al}_2\text{Cl}_7^-][\text{Cl}^-] = (3.4 \pm 0.4) \cdot 10^{-6} \text{ mole}^2 \text{ kg}^{-2}, \text{ at } 175^\circ$$

The electrochemical study of the chlorine electrode, which is theoretically also a pCl<sup>-</sup> indicator, gave another value for  $K_1$  which is in accordance with the first, if the imperfections of the electrode characteristics are taken into account.

## BIBLIOGRAPHIE

- 1 E. C. FRANKLIN, *The Nitrogen System of Compounds*, Reinhold, 1935.
- 2 R. BUNSEN, *Pogg. Ann.*, 92 (1854) 648.
- 3 J. KENDAL, E. D. CRITTENDEN ET H. K. MILLER, *J. Am. Chem. Soc.*, 45 (1923) 963.
- 4 I. WASILEWSKY, I. KACZOROWSKY ET M. DYNKIN, *Przemysl. Chem.*, 18 (1934) 608.
- 5 A. CHRETIEN ET E. LOUS, *Compt. Rend.*, 217 (1963) 451.
- 6 W. FISCHER ET A. L. SIMON, *Z. Anorg. Allgem. Chem.*, 306 (1960) 1.
- 7 E. W. DEWING, *J. Am. Chem. Soc.*, 77 (1955) 2639.
- 8 R. MIDORIKAWA, *J. Electrochem. Soc. Japan*, 24 (1956) 83.
- 9 H. GERDING ET H. HOUTGRAAF, *Rec. Trav. Chim.*, 30 (1953) 381.
- 10 L. AMBROZ ET Z. ZLAMAL, *J. Polymer Sci.*, 30 (1958) 381.
- 11 H. OYE ET D. M. GRUEN, *Inorg. Chem.*, 3 (1964) 386.
- 12 R. H. MOORE, J. R. MORREY ET E. E. VOILAND, *J. Phys. Chem.*, 67 (1963) 744.
- 13 J. R. MORREY ET R. H. MOORE, *J. Phys. Chem.*, 67 (1963) 748.
- 14 V. A. KOPTYUG, V. G. SHUBIN ET A. I. REZVUKHIN, *Izv. Akad. Nauk SSSR, Ser. Khim.*, 1 (1965) 201.
- 15 P. L. HARRIS, R. E. WOOD ET H. L. RITTE, *J. Am. Chem. Soc.*, 73 (1951) 3151.
- 16 V. A. PLOTNIKOV, E. I. KIRICHENKO ET N. S. FORTUNATOV, *Zap. Inst. Khim. Akad. Nauk. SSSR*, 7 (1940) 159.
- 17 Y. K. DELIMARSKII, E. M. SKOBETS ET L. S. BEREMBLYUM, *Zh. Fiz. Khim.*, 22 (1948) 1108.
- 18 Y. K. DELIMARSKII, *Ukrn. Khim. Zh.*, 16 (1950) 414.
- 19 Y. K. DELIMARSKII, L. S. BEREMBLYUM ET I. N. SHEIKO, *Zh. Fiz. Khim.*, 25 (1951) 398.
- 20 Y. K. DELIMARSKII, *Zh. Fiz. Khim.*, 29 (1955) 28.
- 21 G. CHARLOT ET B. TRÉMILLON, *Les Réactions Chimiques dans les Solvants et les Sels Fondus*, Gauthier-Villars, Paris, 1963.
- 22 H. G. KHER ET P. S. MENE, *Indian J. Chem.*, 1 (1963) 185.
- 23 H. J. VANDERBROELE, *Rev. Fac. Cien. Quim. Univ. Nac. La Plata*, 34 (1964) 215.
- 24 G. L. GROSHEV, *Tr. Prokhim. i Khim. Tekhnol.*, 1 (1964) 64.
- 25 T. C. F. MUNDAY ET J. D. CORBETT, *Inorg. Chem.*, 5 (1966) 1263.
- 26 W. D. TREADWELL ET L. TEREBEST, *Helv. Chim. Acta*, 18 (1935) 103.
- 27 W. H. WADE, G. O. TWELLMAYER ET L. F. YNTEMA, *Trans. Electrochem. Soc.*, 78 (1940) 77.
- 28 E. E. MARSHALL ET L. F. YNTEMA, *J. Phys. Chem.*, 45 (1941) 353.
- 29 R. G. VERDIECK ET L. F. YNTEMA, *J. Phys. Chem.*, 46 (1942) 344.
- 30 R. G. VERDIECK ET L. F. YNTEMA, *J. Phys. Chem.*, 48 (1944) 268.
- 31 R. H. MOSS, *Dissertation Abst.*, 15 (1955) 1325.
- 32 R. GUT, *Helv. Chim. Acta*, 43 (1960) 830.
- 33 M. LEROY, Thèse, Paris, 1963.
- 34 R. MARTIN DE FREMONT, R. ROSSET ET M. LEROY, *Bull. Soc. Chim. France*, (1964) 706.
- 35 T. HAYASHI, Y. KIWA, M. YOSHIDA ET N. KIKUMOTO, *Denki Kagaku*, 33 (1965) 8, 567.
- 36 P. C. GOOD, M. O. BUTTLER ET L. A. YERKES, *U.S. Bur. Mines, Rept. Invest.*, 6785 (1966).
- 37 B. TRÉMILLON, *Rev. Chim. Min.*, 3 (1966) 767.
- 38 J. GORET ET B. TRÉMILLON, *Bull. Soc. Chim. France*, (1964) 1074; (1966) 67 et 2872.
- 39 W. TRZEBIATOWSKI ET A. KISZA, *Bull. Acad. Polon. Sci., Ser. Sci. Chim.*, 9 (1961) 605.
- 40 M. F. LANTRATOV ET T. N. SHEVLYAKOVA, *Zh. Prikl. Khim.*, 35 (1962) 1964.
- 41 M. BRUNEAUX, S. ZIOLKIEWICZ ET G. MORAND, *Compt. Rend.*, 257 (1963) 3591.
- 42 B. F. MARKOV ET S. V. VOLKOV, *Ukr. Khim. Zh.*, 30 (1964) 906.
- 43 B. F. MARKOV ET S. V. VOLKOV, *Ukr. Khim. Zh.*, 30 (1964) 341.
- 44 M. V. SMIRNOV ET A. P. KHAIMENTOV, *Dokl. Akad. Nauk SSSR*, 158 (1964) 1172.
- 45 S. ZIOLKIEWICZ ET G. MORAND, *J. Chim. Phys.*, 62 (1955) 312.
- 46 R. S. SETHI ET H. L. JINDAL, *Current Sci. India*, 34 (1965) 284.

PROPRIETES EN SOLUTION DANS LE TETRACHLOROALUMINATE  
DE SODIUM FONDU

II. COMPORTEMENT DES PROTONS ET DES IONS OXYDE

GÉRARD LETISSE ET BERNARD TRÉMILLON

*Laboratoire de Recherches de Chimie Analytique de la Faculté des Sciences, associé au CNRS, ENSCP,  
Paris, 5ème (France)*

(Reçu le 9 octobre, 1967)

Le comportement des ions  $H^+$  et des ions oxyde  $O^{2-}$  est d'une importance primordiale dans le milieu qui nous intéresse. Ces deux ions sont les constituants de l'eau, le principal corps qui puisse se trouver comme soluté dans le tétrachloroaluminate fondu. En effet, lors des manipulations du chlorure d'aluminium, une contamination par l'humidité atmosphérique se produit très aisément à moins de prendre des précautions extrêmes. Le rôle que peut jouer l'eau ou ses produits de décomposition dans le milieu fondu doit donc être précisé pour prévoir les interférences possibles avec d'autres solutés.

Nous avons pu constater que l'eau introduite dans  $NaAlCl_4$  fondu se trouvait décomposée en ses ions, en raison du fort pouvoir accepteur de  $Al^{III}$  vis-à-vis des ions  $O^{2-}$ , d'une part, et de celui de  $Cl^-$  vis-à-vis de  $H^+$ , d'autre part.

Il était intéressant de pouvoir situer les comportements de  $H^+$  et de  $O^{2-}$  dans le cadre des propriétés "acides-bases" telles que nous les avons définies. Toutes les définitions de l'"acidité" étant compatibles entre elles, les ions  $H^+$  doivent nécessairement présenter un caractère "acide", tandis que les ions  $O^{2-}$  doivent avoir les caractères de "base".

A. COMPORTEMENT "ACIDE" ET OXYDANT DES PROTONS

(1) L'ion  $H^+$  est accepteur de  $Cl^-$ , avec lequel il forme la molécule d'acide chlorhydrique  $HCl$ . Cette propriété correspond bien à un caractère "acide" tel que nous l'avons défini; il en résulte, en solution dans  $NaAlCl_4$  fondu, l'établissement de l'équilibre:



par lequel on rend compte de l'apparition d'"acide" fort  $Al_2Cl_7^-$  lors de l'introduction de protons.

Si cet équilibre est pratiquement complètement déplacé vers la droite, cela signifie selon notre terminologie que l'ion  $H^+$  est "acide" fort dans  $NaAlCl_4$  fondu, et ne peut exister en solution qu'à l'état d'acide chlorhydrique  $HCl$ .

Sinon, il s'agit d'un "acide" faible, pouvant exister sous forme  $H^+ AlCl_4^-$  en milieu "acide", et sous forme  $HCl$  en milieu basique ( $HCl$  serait alors une "base", donneur de  $Cl^-$ ). Cette dernière hypothèse est peu vraisemblable.

(2) Par ailleurs,  $H^+$  (ou ses composés) est un oxydant, réductible avec formation d'hydrogène. Pour  $H^+$  à l'état libre, s'il peut exister, le couple oxydo-réducteur est:



Pour  $HCl$ :

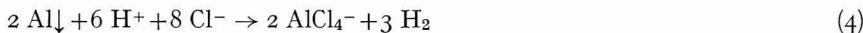


L'oxydation d'hydrogène dissous conduit en sens inverse à la formation de  $H^+$  ou de  $HCl$ .

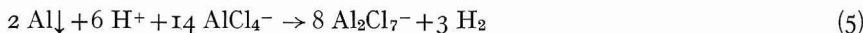
#### *Courbes intensité-potentiel expérimentales du système $H^+/H_2$*

Nous avons réalisé une électrode à hydrogène avec une microélectrode de platine (surface  $0.5 \text{ mm}^2$ ) tournant à 600 tours/min. Cette électrode n'a pas besoin d'être platinée, le système  $H^+/H_2$  étant à  $175^\circ$  suffisamment rapide sur platine poli pour que le courant correspondant soit contrôlé par la diffusion stationnaire; d'autres études à des températures du même ordre de grandeur l'ont déjà prouvé<sup>1,2</sup>.

Les protons ont été introduits sous forme d'eau, qui se trouve entièrement dissociée. Pour introduire l'hydrogène, nous avons préféré éviter un barbotage de gaz et produire l'hydrogène *in situ* par réduction partielle des protons au moyen de poudre d'aluminium<sup>3</sup>; en milieu "basique":



et en milieu "acide":



Nous avons constaté que l'hydrogène ainsi produit était assez soluble dans  $NaAlCl_4$  fondu et y subsistait pendant un temps suffisant pour permettre la détermination de courbes intensité-potentiel. La concentration d'hydrogène est toutefois difficilement reproductible par ce procédé, ce qui se traduit par des différences de hauteur des paliers d'oxydation.

Les courbes expérimentales sont reproduites sur la Fig. 1, pour un milieu "basique", A, et pour un milieu "acide", B.

On note l'existence de la vague d'oxydation de  $H_2$  de hauteur en principe proportionnelle à la concentration de cette substance, et de la vague de réduction des protons, ayant également une hauteur proportionnelle à leur concentration. Toutes les courbes présentent les caractéristiques correspondant à un système rapide, ce qui valide l'utilisation de l'électrode à hydrogène pour l'étude quantitative du comportement des protons. On note aussi qu'une différence de potentiel notable sépare les courbes obtenues en milieu "acide" de celles obtenues en milieu "basique", ce qui correspond nécessairement aux propriétés "acides" du proton.

Le potentiel d'équilibre de l'électrode à hydrogène, mesurable sur les courbes intensité-potentiel (à intensité nulle), doit répondre à la formule de Nernst appliquée au couple oxydo-réducteur réel. En milieu "basique", tout au moins, le couple est (3); la formule de Nernst donne:

$$E = (E_0^0)_H + (RT/2F) \ln ([HCl]^2/[H_2][Cl^-]^2) \quad (6)$$

Soit encore, à 175°:

$$E = (E_0^0)_H - 0.045 \log [H_2] + 0.090 \log ([HCl]/[Cl^-]) \quad (7)$$

$$E = (E_0^0)_H - 0.045 \log [H_2] + 0.090 \log [HCl] + 0.090 pCl^- \quad (8)$$

Dans l'hypothèse où H<sup>+</sup> est "acide" fort, le système oxydo-réducteur reste le même (c'est-à-dire met toujours en jeu HCl) et le potentiel d'équilibre reste donné par la formule (8). La différence de potentiel d'équilibre correspond ainsi à la différence de pCl<sup>-</sup> (compte tenu des variations possibles de concentrations de HCl et de l'hydrogène, dont les hauteurs des paliers de réduction et d'oxydation fournissent les valeurs).

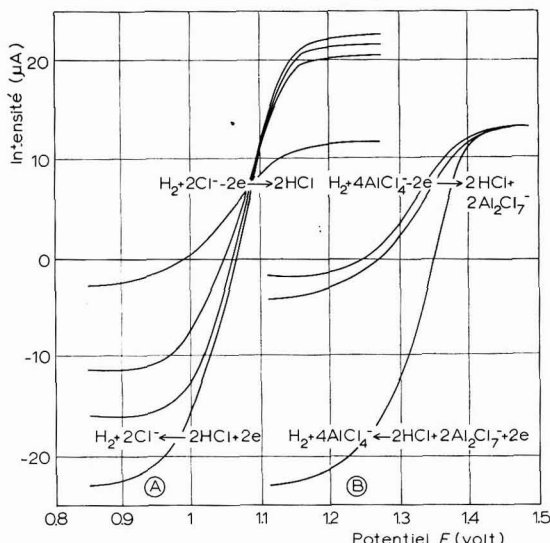


Fig. 1. Courbes intensité-potentiel, à une micro-électrode de platine tournante, du système H<sup>+</sup>/H<sub>2</sub>. (A), En milieu "basique", pCl<sup>-</sup> = 1.3. (NaCl saturé); (B), en milieu "acide", pCl<sup>-</sup> = 4.4 (concн de Al<sub>2</sub>Cl<sub>7</sub><sup>-</sup> égale à 8.10<sup>-2</sup> M). Courbes obtenues pour différentes concns. de HCl et de H<sub>2</sub>.

Les courbes expérimentales de la Fig. 1 ont été déterminées d'une part à pCl<sup>-</sup> = 1.3 (A), d'autre part à pCl<sup>-</sup> = 4.4 (B), soit pour une différence de pCl<sup>-</sup> égale à 3.1. Il y correspond une différence de potentiel théorique de 278 mV. Or, en se ramenant à des valeurs de [H<sub>2</sub>] et de [HCl] identiques, la différence de potentiel d'équilibre expérimentale est égale à 280 ± 5 mV. L'accord de ces valeurs nous permet d'affirmer que l'hypothèse initiale est valable: H<sup>+</sup> est un "acide" fort et ne peut exister en solution qu'à l'état d'acide chlorhydrique.

#### B. COMPORTEMENT "BASIQUE" DES IONS OXYDE

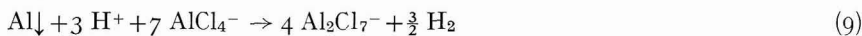
L'ion oxyde O<sup>2-</sup> possède un fort pouvoir de combinaison avec les cations Al<sup>3+</sup>, qui a été souvent mis en évidence lors d'études de complexes oxyde. Il est donc susceptible de réagir aussi bien avec l'anion du solvant AlCl<sub>4</sub><sup>-</sup> qu'avec l'anion "acide" fort Al<sub>2</sub>Cl<sub>7</sub><sup>-</sup>. Dans ce dernier cas, la réaction correspond à un caractère "basique" des ions oxyde (selon notre terminologie); dans le premier cas, la réaction entraînant vraisemblablement une libération d'ions Cl<sup>-</sup>, il s'agit encore de l'effet caractéristique

d'une "base" (donneur de chlorure). La question est de déterminer si  $O^{2-}$  est une "base" forte ou faible, et s'il s'agit d'une mono-"base", d'une di-"base", d'une tri-"base", etc.

Le caractère "basique" pourra être mis expérimentalement en évidence, ici, grâce aux mesures de  $pCl^-$  avec l'électrode indicatrice d'aluminium. Contrairement au cas précédent des protons, les ions oxyde dissous dans  $NaAlCl_4$  fondu ne sont pas électroactifs (oxydables) et une électrode à oxygène n'est pas envisageable.

Un problème technique a été posé par l'introduction d'ions oxyde dans le milieu fondu, malgré que ces ions soient fortement solvatés. Les oxydes métalliques vieillis ou calcinés ont refusé toute dissolution; ce fut le cas de l'alumine, de  $Na_2O$ ,  $Li_2O$ , et aussi des carbonates, dont nous avions envisagé l'emploi comme donneurs d'ions  $O^{2-}$  par dissociation de  $CO_3^{2-}$ . Nous avons dû faire appel, pour introduire commodément des ions oxyde en quantités bien connues (par pesée), à de l'hydroxyde de baryum,  $Ba(OH)_2$ , pur et anhydre. C'est donc en fait l'ion hydroxyde  $OH^-$  qui a été introduit, soit simultanément un ion "basique"  $O^{2-}$  et un ion "acide"  $H^+$ .  $H^+$  n'étant que mono-"acide", le milieu devient "basique" si  $O^{2-}$  est une poly-"base"; ce qui fut le cas.

Mais les ions  $H^+$  sont gênants car ils oxydent l'aluminium et viennent attaquer l'électrode indicatrice d'aluminium, réaction qui a pour effet des modifications d'acidité puisque:



Il nous a donc paru préférable, pour l'obtention d'un effet bien défini, de

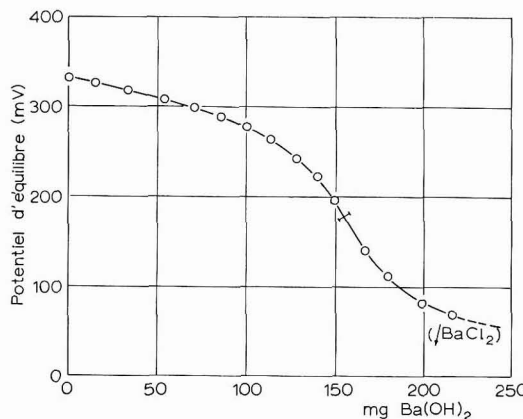


Fig. 2. Titrage potentiométrique (électrode indicatrice d'aluminium) d'une solution d'"acide" fort  $Al_2Cl_7^-$  par la baryte.

rendre complète la réduction des protons au moyen de poudre d'aluminium ajoutée préalablement à l'introduction de baryte. Selon (9), chaque  $H^+$  correspond à la libération de  $\frac{4}{3} Al_2Cl_7^-$  dont l'"acidité" se déduit de la "basicité" des ions oxyde.

Nous avons utilisé cet excédent de "basicité" pour doser une solution rendue préalablement "acide" par production coulométrique de  $Al_2Cl_7^-$ . Nous avons ajouté des quantités connues croissantes de baryte et nous avons mesuré après chaque

addition le potentiel d'équilibre d'une électrode indicatrice d'aluminium. La courbe potentiométrique est représentée Fig. 2.

Nous pouvons constater qu'il s'agit de la courbe de titrage de l'"acide" fort Al<sub>2</sub>Cl<sub>7</sub><sup>-</sup> par une "base" forte et non par une "base" faible, car la courbe est identique à celle obtenue lors du titrage de Al<sub>2</sub>Cl<sub>7</sub><sup>-</sup> par Cl<sup>-</sup>. Les ions O<sup>2-</sup> constituent donc une "base" forte. Vers la fin de la courbe se produit une précipitation de BaCl<sub>2</sub>, moins soluble que NaCl, empêchant d'atteindre les milieux les plus basiques, mais ce phénomène ne se produit que loin après le point équivalent de la réaction.

La position du point équivalent permet de calculer le nombre d'ions oxyde nécessaires pour neutraliser l'ion "acide" fort, Al<sub>2</sub>Cl<sub>7</sub><sup>-</sup>. D'une façon générale, un bilan est à effectuer de la façon suivante. Appelons *n* le nombre de "basicité" de l'ion oxyde (*n* = 1 si O<sup>2-</sup> est mono-"base", *n* = 2 si di-"base", etc.). Chaque mole de Ba(OH)<sub>2</sub> introduite va donc pouvoir neutraliser un nombre d'ions-grammes d'"acide" fort égal à:

$$2n - 2 \times \frac{4}{3} = 2n - \frac{8}{3} \quad (10)$$

La correspondance entre la quantité connue d'"acide" fort initial et la quantité de baryte nécessaire pour atteindre le point équivalent nous fournit ainsi la valeur de *n*. Plusieurs expériences renouvelées nous ont conduits à la valeur:

$$n = 3.2 \pm 0.2 \quad (11)$$

Nous pouvons ainsi conclure que l'ion oxyde est, en solution dans NaAlCl<sub>4</sub> fondu, une tri-"base" forte.

Une preuve supplémentaire que O<sup>2-</sup> est plus qu'une di-"base" nous a été fournie par le comportement de l'eau. Si O<sup>2-</sup> était di-"basique", H<sup>+</sup> étant "mono-acide", 2 H<sup>+</sup> et un ion O<sup>2-</sup> se neutraliseraient et l'introduction d'eau laisserait inchangée l'"acidité" du tétrachloroaluminate fondu. Au contraire, si O<sup>2-</sup> est "tri-basique", sa "basicité" l'emporte sur l'"acidité" de H<sup>+</sup>, de sorte que l'eau doit alors rendre le milieu plus "basique". C'est bien ce que l'expérience confirme, un barbotage de vapeur d'eau conduisant à une diminution importante du potentiel de l'électrode indicatrice d'aluminium. De plus, on observe le même phénomène en présence de poudre d'aluminium; dans ce cas, un bilan analogue aux précédents conduit à *n* >  $\frac{8}{3}$  (un ion H<sup>+</sup> correspondant à la libération de  $\frac{4}{3}$  Al<sub>2</sub>Cl<sub>7</sub><sup>-</sup>).

Nous pouvons essayer, d'après ce résultat, de préciser la nature de l'espèce chimique en solution qui englobe l'ion oxyde. Le fait que celui-ci soit une "tri-base" forte implique que la réaction, pratiquement quantitative, de O<sup>2-</sup> sur les ions du solvant AlCl<sub>4</sub><sup>-</sup> libère 3 ions Cl<sup>-</sup> par ions O<sup>2-</sup>. Nous pouvons ainsi écrire:



Ou plutôt, pour des raisons structurales:



L'espèce chimique englobant O<sup>2-</sup> aurait ainsi la formule Al<sub>2</sub>OCl<sub>5</sub><sup>-</sup> (AlOCl + AlCl<sub>4</sub><sup>-</sup>, structure analogue à celle de Al<sub>2</sub>Cl<sub>6</sub>, un ion O<sup>2-</sup> remplaçant un ion Cl<sup>-</sup> pour effectuer le pont entre deux atomes d'aluminium). La "tri-basicité" de O<sup>2-</sup> exclut la possibilité des espèces AlOCl<sub>2</sub><sup>-</sup> et Al<sub>2</sub>OCl<sub>6</sub><sup>2-</sup> (correspondant à une "di-basicité").

Enfin,  $O^{2-}$  étant une "base" forte, l'espèce  $Al_2OCl_5^-$  résultant de sa dissolution ne présente pas de propriétés "acides-bases". Sa présence ne pouvait donc être gênante pour l'étude primitive du domaine d'"acidité": même si le chlorure d'aluminium utilisé n'est pas rigoureusement pur, il n'en résulte aucune intervention lors de la variation coulométrique de  $pCl^-$ .

Finalement, la réaction globale représentant l'action de l'eau sur le tétra-chloroaluminate de sodium fondu doit s'écrire, d'après ces résultats:



#### TECHNIQUE EXPÉRIMENTALE

Pour constituer le solvant, nous avons utilisé le chlorure d'aluminium anhydre, sublimé et exempt de fer (produit Fluka) sans autre traitement. Les manipulations jusqu'à l'obtention du solvant fondu ont été effectuées sous atmosphère d'azote sec.

On constate au bout de plusieurs heures de fusion un brunissement de la solution qui empêche toute observation visuelle. Ce phénomène est dû, d'après MUNDAY ET CORBETT<sup>4</sup>, à la décomposition d'impuretés organiques contenues dans le chlorure d'aluminium. On s'en débarrasse en chauffant la solution à 450° pendant plusieurs heures, jusqu'à obtenir une flocculation. Après décantation, on peut éliminer ces impuretés par filtration ou séparation mécanique à l'état solide, et on obtient alors une solution parfaitement limpide. Nous avons préféré à cette méthode un procédé plus simple: une plaque d'aluminium de 2 cm<sup>2</sup> de surface adsorbe les produits de décomposition et maintient la solution limpide pendant plusieurs jours.

La pollution par l'humidité ambiante lors des différentes opérations préparatoires, peut, comme nous l'avons vu, introduire des protons (qui n'existent dans le chloroaluminate de sodium fondu que sous forme HCl dissous). L'acide chlorhydrique est électroactif et le courant résiduel à différentes électrodes indicatrices présente une vague polarographique de réduction due à cette espèce. Par ailleurs, les protons sont susceptibles d'oxyder les différentes électrodes en aluminium, éventuellement présentes, et ainsi de modifier l'acidité de la solution selon la réaction (9). Il convient donc en premier lieu d'éliminer l'acide chlorhydrique. Ceci a été réalisé par un barbotage d'azote sec. Le courant-limite de réduction de HCl à une micro-électrode de platine tournante de 1 mm<sup>2</sup> atteint ainsi une intensité minimale de 1.5  $\mu A$  en 3 h. Nous avons pu obtenir une élimination plus complète par addition de poudre d'aluminium, qui réduit l'acide chlorhydrique restant<sup>3</sup>. L'intensité du courant-limite précédent est alors abaissée à 0.2  $\mu A$ .

Les électrodes d'aluminium ont été réalisées à l'aide de lames ou de fils à 99.99% de pureté.

Le carbone vitrifié provient de la Société Vitreous Carbons Ltd.

#### Instrumentation

Tout l'appareillage (cellule de mesure étanche, maintenue à la température de 175 ( $\pm 1$ )° par un thermostat à circulation d'huile de silicium, montage potentiostatique à trois électrodes pour l'enregistrement des courbes intensité-potentiel, dispositif de coulométrie à intensité constante) est classique et ne nécessite aucune description particulière. La constitution des électrodes présente plus d'intérêt.

*(a) Electrode de référence*

L'électrode de référence a été constituée d'un fil d'aluminium plongeant dans une solution de chlorure de sodium saturé dans NaAlCl<sub>4</sub> fondu, contenue dans un compartiment séparé. Celui-ci était un tube de verre fermé à une extrémité par une paroi de verre fritté de porosité 3 en contact avec le milieu à étudier. Le remplissage du compartiment a été effectué par aspiration.

L'électrode de référence n'atteignait un potentiel fixe et reproductible qu'au bout d'un certain temps variant d'un quart d'heure à une heure et demie. Au début, le potentiel était plus positif et devait correspondre au potentiel mixte de la réduction de HCl résiduel par l'aluminium. Nous avons en effet constaté un établissement plus rapide de l'équilibre lorsque le solvant était soigneusement débarrassé au préalable de HCl.

*(b) Electrode indicatrice d'aluminium*

L'électrode proprement dite a été constituée par un fil d'aluminium pur, de 1 mm de diamètre et plongeant dans la solution sur une longueur d'environ 3 mm.

Le fil d'aluminium a été collé au verre d'enrobage par de l'araldite. Les polarogrammes les plus satisfaisants ont été obtenus en faisant tourner l'électrode à 300 tours/min.

*(c) Electrode indicatrice de carbone vitrifié et électrode à chlore*

Elle a été réalisée par soudure d'un barreau cylindrique de 3,2 mm de diamètre à un tube de verre pyrex de diamètre intérieur voisin. Nous avons étudié l'influence de la vitesse de rotation d'une telle électrode sur les polarogrammes obtenus, mais il s'est avéré que les résultats les plus satisfaisants étaient obtenus en maintenant l'électrode immobile.

Pour réaliser l'électrode à chlore, ce gaz a été mélangé à de l'azote, dans le rapport  $\frac{1}{3}$  à  $\frac{1}{2}$ , puis desséché par passage dans l'acide sulfurique pur, avant d'aller barboter dans la cellule de mesure autour de l'électrode de carbone.

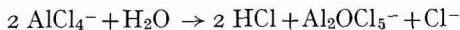
L'ouverture de la cellule en cours de manipulation doit évidemment être prohibée. Par conséquent, nous avons introduit AlCl<sub>3</sub> solide en faisant basculer des petites nacelles placées au préalable à des ajutages latéraux du couvercle de la cellule et contenant des quantités connues de substance. Le dispositif permet, en utilisant trois rodages du couvercle, de faire six additions.

## RÉSUMÉ

Suite à l'étude du mémoire précédent, le comportement des protons et des ions oxyde O<sup>2-</sup> dans NaAlCl<sub>4</sub> fondu a été déterminé électrochimiquement. H<sup>+</sup> est un "acide" fort et ne peut exister que sous forme d'acide chlorhydrique, quelle que soit l'"acidité" du milieu. O<sup>2-</sup> est une "tribase" forte et doit exister sous forme du complexe Al<sub>2</sub>OCl<sub>5</sub><sup>-</sup>.

Le comportement des protons a été déduit de la mesure de variation de potentiel de l'électrode à hydrogène. Celui de O<sup>2-</sup> de la courbe potentiométrique de titrage (électrode indicatrice d'aluminium) de l'"acide" fort Al<sub>2</sub>Cl<sub>7</sub><sup>-</sup>, par de la baryte.

Il en a été déduit que l'eau réagit complètement avec le tétrachloroaluminate fondu selon la réaction :



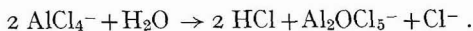
L'hydrolyse amenant ainsi toujours une plus grande "basicité".

#### SUMMARY

Following the results reported in the previous paper, the behaviour of protons and O<sup>2-</sup> ions in molten NaAlCl<sub>4</sub> has been studied electrochemically. H<sup>+</sup> is a strong "acid" and can only exist in the form of HCl irrespective of the "acidity" of the melt. O<sup>2-</sup> is a strong "tribase" and probably exists in the complex form Al<sub>2</sub>OCl<sub>5</sub><sup>-</sup>.

The behaviour of protons has been deduced from the measure of hydrogen electrode potentials and the behaviour of O<sup>2-</sup> ions from the potentiometric titration curve of the strong acid, Al<sub>2</sub>Cl<sub>7</sub><sup>-</sup>, and Ba(OH)<sub>2</sub> (with an aluminum electrode as indicator).

It has been found that water reacts completely with the molten tetrachloroaluminate according to the reaction :



Thus, addition of water always leads to a higher "basicity".

#### BIBLIOGRAPHIE

- 1 J. GORET, *Bull. Soc. Chim. France*, (1964) 1074.
- 2 J. VEDEL ET B. TRÉMILLON, *Bull. Soc. Chim. France*, (1966) 220.
- 3 G. L. GROSHEV, *Tr. Prokhim. i. Khim. Tekhnol.*, 1 (1964) 64.
- 4 T. C. F. MUNDAY ET J. D. CORBETT, *Inorg. Chem.*, 5 (1966) 1263.

*J. Electroanal. Chem.*, 17 (1968) 387-394

## DETERMINATION OF BISMUTH CONTENT OF URINE. POLAROGRAPHIC METHOD

PIETRO LANZA, VITTORIO CONCIALINI AND AUGUSTA BENATI

*Istituto Chimico "G. Ciamician", Università di Bologna*

*Scuola di Specializzazione in Chimica Analitica, Centro di Polarografia (C.N.R.), Sezione di Bologna (Italy)*

(Received September 26th, 1967)

### INTRODUCTION

The determination of the bismuth content of urine is of particular interest in that numerous pharmaceutical products containing bismuth in various forms are frequently used in therapy. In clinical and pharmacological experiments, the methods commonly used for the observation of drug absorption or the course of drugs transfer from the gastroenteric system to the blood stream, provide for the substance to be determined in urine. Colorimetric, spectrophotometric and polarographic methods have been proposed for dealing with the problem. TORLOTIN<sup>1</sup> compiled a critical summary of these methods, which can be used for reference.

Polarography, because of its sensitivity and precision, is particularly suitable for the determination of traces of metals in various media and many workers have used polarographic analysis for this purpose, *e.g.*, TORLOTIN, GORDON AND TANKLEVSKAYA<sup>2</sup>, and PROCTOR AND OESTER<sup>3</sup>. Except for the methods of atomic absorption and emission spectroscopy with which WILLIS<sup>4</sup> obtained excellent results, all the methods proposed present a common problem, *i.e.*, the necessity of preliminary elimination of interfering ions, and in particular, copper and lead ions which strongly affect both the colorimetric method using dithizone, and the polarographic determination. Although generally efficacious, the use of base solutions with particular complexing action for the separation of bismuth and copper, presents other difficulties<sup>1</sup>. On the other hand, quite apart from the interference due to the presence of other metal ions, many types of organic matter can also affect the polarographic determination. Even in the absence of other metals, bismuth (particularly at low concentrations) cannot be detected in urine polarographically because the step is badly distorted, or even completely suppressed, by the presence of interfering substances. Therefore, before the polarographic determination can be carried out, a sample is usually prepared by destruction of all organic matter in the urine. This preparatory phase, as with other instrumental methods such as colorimetry, spectrophotometry etc., is generally the longest and most delicate part of the procedure. It was, therefore, of interest to develop a practical polarographic determination that would permit the easy evaluation of bismuth (in  $\mu\text{g}/\text{ml}$ ) with sufficient precision, without preliminary evaporation of urine and treatment with inorganic acids.

The principle of the method is to fix the bismuth in a given volume of urine, to an ion-exchange resin; this is followed by a careful washing of the resin and then finally

by the polarographic determination of the metal in the eluate. It is well known that bismuth is easily fixed as a chloride complex,  $\text{BiCl}_4^-$ , to anionic resins<sup>5</sup> in a wide pH-range. This property allows it to be easily separated from many other metals of the same analytical group<sup>6</sup>; on washing the resin, the interfering organic matter is thus eliminated.

The systematic examination of various parameters has shown the best working conditions for (i) quantitative fixing of bismuth, (ii) efficient washing, (iii) elution with a minimum amount of solvent and the most favourable composition of the base solution for the polarographic determination.

#### PROCEDURE

##### *Materials and apparatus*

*Ion-exchange resins.* The anionic resins used were: British Drug House (B.D.H) type IRA 400 (50–60 mesh) and Zerolit FF (50–100 mesh), Dow Chemical Co. type Dowex (100–200 mesh).

*Apparatus for the continuous polarographic recording of the chromatographic eluate.* The apparatus (see Fig. 1) consists of a chromatographic column (a), an heli-

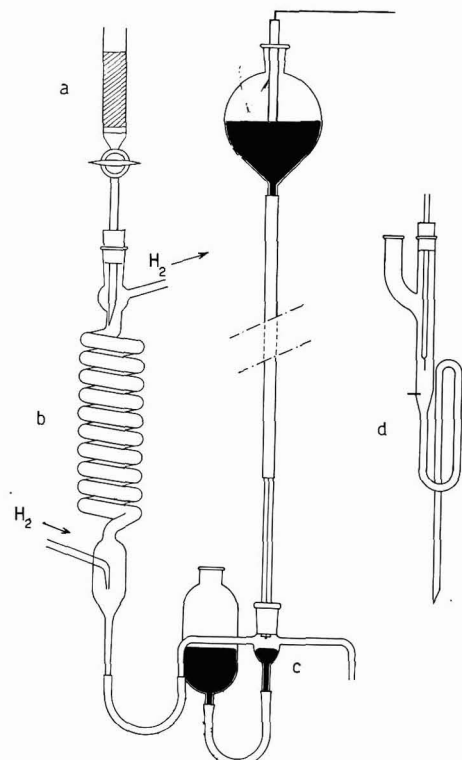
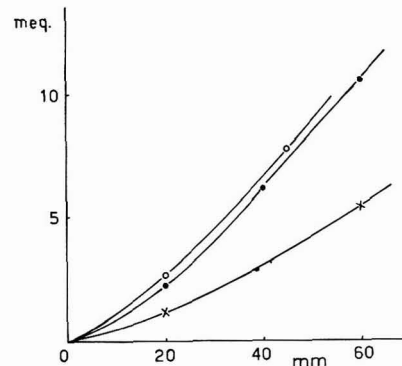


Fig. 1. Chromato-polarographic apparatus

Fig. 2. Capacity of the chromatographic columns used. (○) Dowex 1; (×) IRA-400; (●) Zerolit FF.



coidal condenser (b) of 100 cm total length on the walls of which the eluate forms a thin layer which is freed from air by means of a countercurrent of saturated hydrogen, the eluent solution, and an approximately 0.5-ml microcell (c) connected to an external reference anode (SCE) by means of a fourth tube filled with agar, not visible in the figure. To maintain the volume of the liquid in the cell fairly constant, the mercury flowing from the capillary is collected into a reservoir of suitable diameter. The solution flowing out of the cell is discharged into a 3-ml syphon (d) fitted with platinum electrodes which interrupt the electric circuit when contact is made and thus allow the recording on a polarographic chart, of the volume of the eluate. A current type of polarograph was employed. It was maintained at constant potential during the recording of the continuous stream of eluate, and the device for the marking of the potential was used to indicate the volume. Thus, a mark appeared on the chart each time the syphon was emptied.

The continuous analysis of the eluate was found to be very useful for systematic research into the best conditions for the analytical procedure.

#### *Test for the resin capacity*

Chromatographic columns of different lengths and of 10 mm internal diameter were prepared with the anionic resins, IRA-400, Zerolit FF, and Dowex-1. For the preparation of the columns, the resins were thoroughly washed with 2 N sulphuric acid solution until the washings gave a negative result on the polarographic test, then washed freely with water and finally with 2 N hydrochloric acid solution. A 0.1 N  $\text{BiCl}_3$  solution in 2 N HCl was then conveyed through the prepared column at a rate of 0.8 ml/min. The appearance of bismuth in the eluate, indicating saturation of the column, was recorded by the apparatus described above.

The results of the tests are shown in Fig. 2 which gives the practical capacity of the columns (in mequiv.) in relation to their length.

#### *Elution of bismuth*

In order to develop a practical method of test, it is necessary to choose operating conditions that will permit complete elution of bismuth with a minimum amount of eluate, and complete elimination of interfering matter without loss of bismuth. To limit the amount of the eluent to an acceptable value (25 ml), the most suitable column length was determined by preparing several columns of various lengths (10–120 mm) with the different resins fixed with the same quantity of bismuth (350  $\mu\text{g}$  in 25 ml of urine). After a washing with 100 ml of a 1:2 hydrochloric acid-acetone mixture and then with water until neutrality was reached, the bismuth was eluted with 2 N sulphuric acid solution, and the first 25 ml of eluate collected into one-mark volumetric flasks. The bismuth contained in the eluate was determined polarographically using the method described below. Figure 3 shows the percentage of bismuth recovered from 25 ml of eluate in relation to the column length and the type of resin.

In order to determine the best conditions for the complete elimination of interfering organic matter, a number of washing mixtures were tested; the quantity of bismuth recovered was determined for each and, by examination of the polarograms, the presence or absence of interfering matter was evaluated. All the experimental tests were carried out using a 40-mm column packed with Zerolit FF resin and 25

ml of urine having a constant bismuth content of 350 µg. The results obtained are given in Table I which shows that the most efficient washing is obtained with the hydrochloric acid-acetone mixture in the ratio, 1:2. This mixture has also given satisfactory results with larger amounts of urine. In experiments carried out with 50–75–100 ml of urine containing 350 µg of bismuth, recovery was always complete. These results clearly indicate that the method can be used for the analysis of urine even when the bismuth content is very low, provided that a sufficient amount of the test sample is available.

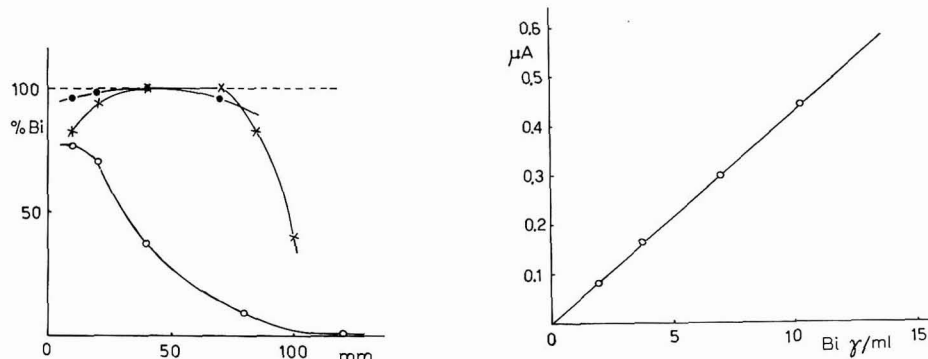


Fig. 3. Percentage of bismuth found in 25 ml of eluate, in relation to the column length and type of resin used. (○) IRA-400; (✕) Zerolit FF; (●) Dowex 1.

Fig. 4. Bismuth calibration curve.

TABLE I  
RESULTS OBTAINED WITH DIFFERENT WASHING MIXTURES

Composition of mixture	Quantity used (ml)	Bi found (%)
10 N HCl soln.	50	83.0
	100	17.0
	200	0.0
6 N HCl soln.	50	97.2
	100	93.6
	120	85.0
1:1 HCl-acetone	60	98.0
	100	89.5
1:2 HCl-acetone	65	100.0
	100	100.0
	200	93.6
1:9 HCl-acetone	100	98.0
	200	91.5
Acetone	100	85.0

During the washing with hydrochloric acid-acetone mixture, it was observed that the resin becomes dark; this colouration remains even after a prolonged washing and treatment with 2 N sulphuric acid solution. The ion-exchange column can be regenerated after the elution of bismuth, by washing it with 2 N hydrochloric acid

solution until complete disappearance of  $\text{SO}_4^{2-}$  ions. However, the darkening seems to limit the efficiency of the resin and consequently, a column cannot be used for more than three tests.

#### *Polarographic test*

The sulphuric medium of the chromatographic eluate containing bismuth causes a reduction step to  $E_{\frac{1}{2}} = -0.06$  V (SCE), which is not easily measurable, especially at low concentrations. It has been observed that bismuth gives more suitable steps on complexation with EDTA in alkaline medium. A suitable solution is 0.1 M EDTA (sodium salt) solution and 0.5 M sodium hydroxide solution. A well developed step is obtained in this case with  $E_{\frac{1}{2}} = -0.65$  V. Under these conditions it is possible to evaluate bismuth contents of approximately 1  $\mu\text{g}/\text{ml}$  and obtain a good calibration curve (Fig. 4).

#### *Possible interference from other metals*

In the present study only interferences from copper and lead have been considered, as these are the most likely metals to be present in urine. Checks were carried out by adding to samples of urine, amounts of copper and lead, respectively, that were twice the amount of bismuth present. The samples were tested following the procedure described above; under these conditions it was noted that copper is not fixed on the resin and is completely eliminated during the washing operation. Lead, although less firmly fixed than bismuth, as a chloride-complex<sup>5</sup>, is not completely eliminated by washing and is found partly in the eluate together with bismuth. It does not however interfere; in the EDTA solution under the conditions described, it gives a reduction step ( $E_{\frac{1}{2}} = -1.22$  V SCE) completely separated from that of bismuth ( $E_{\frac{1}{2}} = -0.65$  V SCE).

#### *Proposed procedure*

On the basis of the experimental results the following procedure was finalized:

A given volume of urine, containing not less than 40–50  $\mu\text{g}$  of bismuth, was acidified with hydrochloric acid to pH 1. The sample was then passed through the column at a 0.8 ml/min flow rate. The column was washed with 100 ml of freshly prepared 1:2 hydrochloric acid-acetone mixture for approximately one hour and then

TABLE 2

## EXPERIMENTAL RESULTS

Quantity of urine (ml)	Bismuth ( $\mu\text{g}/\text{ml}$ )	Total bismuth ( $\mu\text{g}$ )	Quantity found ( $\mu\text{g}$ )	Bi found (%)
25	28.0	700	700	100.0
25	16.8	420	408	97.0
25	14.0	350	350	100.0
50	7.0	350	347	99.0
75	4.7	350	350	100.0
100	3.5	350	350	100.0
25	2.7	70	68.5	98.0
50	1.35	70	69.0	98.5
50	1.0	50	49.0	98.0

with water until neutrality was reached. The bismuth is then fixed to the resin as a complex anion, while the interfering organic matter has been eliminated by the washing. The fixed bismuth is eluted with 2 N sulphuric acid solution at a 0.5 ml/min flow rate and the eluate is received into a 25 ml one-mark volumetric flask.

5 ml of 0.1 M EDTA solution in 4.5 N NaOH solution are then added to 10 ml of the sulphuric eluate in a polarographic cell (giving the alkaline solution of the complex). The solution is freed from air and examined polarographically, recording at 0 to -1.0 V. Some experimental results are shown in Table 2.

We were able to test this procedure on a considerable number of samples of human urine from patients who were undergoing treatment with bismuth-containing drugs, as well as on urine from rats treated with bismuth products.

This method is suitable for routine tests.

#### ACKNOWLEDGEMENT

We wish to thank Professor T. BERTI of the Pharmacological Institute of the University of Bologna for the active interest he showed in this work and for supplying us with the numerous samples of urine used in the tests.

#### SUMMARY

A polarographic method for the determination of bismuth in urine is described. A preliminary purification of the sample by means of ion-exchange resins in order to eliminate interfering matter, is proposed. Several tests carried out on samples of urine with different bismuth contents, have shown that it is possible to determine the bismuth content of urine in micrograms per milliliter with a 2% margin of error.

#### REFERENCES

- 1 J. C. TORLOTIN, *Ann. Biol. Chim.*, 23 (1965) 7-9, 905.
- 2 B. E. GORDON AND R. M. TANKLEVSKAYA, *Teoriya i Prakt. Polyarogr. Analiza, Akad. Nauk MoldavskSSR, Materialy Pervogo Vses. Soveshch.*, (1962) 58-62; *C.A.* 59 (1963) 15839c.
- 3 C. D. PROCTOR AND Y. T. OESTER, *J. Forensic Med.*, 5 (1958) 89.
- 4 J. B. WILLIS, *Anal. Chem.*, 34 (1962) 614.
- 5 F. NELSON AND K. A. KRAUS, *J. Am. Chem. Soc.*, 76 (1954) 5916.
- 6 O. SAMUELSON, *Ion-Exchange Separations in Analytical Chemistry*, J. Wiley, New York, 1963.

## ÜBER DIE KATALYTISCHE UND INHIBIERENDE WIRKUNG VON GELATINE AUF POLAROGRAPHISCHE REDUKTIONSSTUFEN IN SAUEREN LÖSUNGEN

L. HOLLECK, J. M. ABD EL KADER UND A. M. SHAMS EL DIN

*Chemisches Institut der Hochschule, Bamberg (Deutschland)*

(Eingegangen am 31 Oktober, 1967)

Die Adsorbierbarkeit von Gelatine über einen breiten Potentialbereich begünstigt ihre Anwendung bei polarographischen Arbeiten als Unterdrücker sowohl positiver als auch negativer Maxima. Unter wohldefinierten Bedingungen übt dieser Zusatzstoff auch einen katalytischen Effekt aus. So rufen z.B. geringe Mengen von Gelatine in saueren gepufferten Lösungen einen um etwa 150 mV zu positiveren Potentialen vorverlagerten Grenzanstieg hervor<sup>1</sup>. Nach HANS UND JENSCH wird die Wasserstoff-Stufe in HCl/KCl-Lösungen durch Spuren von Gelatine zu positiveren Potentialen verlagert und zeigt einen steileren Verlauf<sup>2</sup>. Grössere Gelatine-Konzentrationen wirkten jedoch inhibierend und verursachten zugleich eine Abnahme des Grenzstromes. Diese Erscheinungen wurden durch eine Blockierung der Elektrodenoberfläche bzw. durch die Bindung eines Teils der H<sup>+</sup>-Ionen durch die Gelatine gedeutet. HOLLECK UND HOLLECK haben kürzlich nachgewiesen, dass Protonenübertragungen auf organische Depolarisatoren durch geringe Zusätze an Gelatine katalysiert werden können<sup>3</sup>.

In Zusammenhang mit einer Untersuchung des polarographischen Verhaltens von Aluminium in saueren Lösungen<sup>4</sup> wurde der Einfluss wachsenden Gelatine-Gehaltes der Lösung auf die Wasserstoff-Stufe im einzelnen untersucht. Die dabei erhaltenen Ergebnisse wiesen auf einige interessante neue Gesichtspunkte, so dass die Untersuchungen nunmehr zu noch höheren Zusatz-Konzentrationen ausgedehnt wurden, wie sie bei polarographischen Arbeiten gewöhnlich nicht angewandt werden (bis zu 0.5 Gew.-%). Auch der Einfluss dieser hohen Gelatine-Konzentrationen auf die Reduktion von Pb<sup>2+</sup>, Cd<sup>2+</sup> und Zn<sup>2+</sup> in saurer und neutraler Lösung wurde untersucht. Es zeigte sich, dass kleine Mengen Gelatine, welche die Wasserstoff-Stufe katalysieren, in derselben Lösung eine ausgeprägte Inhibitionswirkung auf die Cd<sup>2+</sup>- und Zn<sup>2+</sup>-Stufe ausüben. Ein Mechanismus der Wirkung der Gelatine, der das beobachtete Verhalten erklärt, wird vorgeschlagen.

### EXPERIMENTELLES

Als sauerer Leitelektrolyt diente eine Lösung von 0.2 M Li<sub>2</sub>SO<sub>4</sub> + 5 · 10<sup>-3</sup> M H<sub>2</sub>SO<sub>4</sub>, für die Pb<sup>2+</sup>-Reduktion entsprechend 0.2 M KNO<sub>3</sub> + 5 · 10<sup>-3</sup> M HNO<sub>3</sub>. Als Substanzen dienten CdSO<sub>4</sub> · 8/3H<sub>2</sub>O, ZnSO<sub>4</sub> · 7H<sub>2</sub>O, Pb(NO<sub>3</sub>)<sub>2</sub>, H<sub>2</sub>SO<sub>4</sub> und HNO<sub>3</sub> der Firma Merck, "pro analysi", ohne weitere Reinigung. Zur Herstellung der Lösungen diente doppelt destilliertes Wasser. Die Gelatine-Stammlösung wurde täglich frisch

hergestellt. Die Lösungen wurden in der polarographischen Zelle mit reinem Stickstoff entlüftet. Die Messungen erfolgten bei Raumtemperatur,  $20 \pm 2^\circ$ . Die Potentialangaben beziehen sich auf eine zugleich als Anode dienende grossflächige gesättigte Kalomelektrode.

#### ERGEBNISSE UND DISKUSSION

In einem Leitelektrolyten der Zusammensetzung  $0.2\text{ M Li}_2\text{SO}_4 + 5 \cdot 10^{-3}\text{ M H}_2\text{SO}_4$  wird eine wohldefinierte, diffusionsbestimmte polarographische Stufe registriert. Ihr geht jedoch ein scharfes negatives Maximum vorauf (Abb. 1, Kurve 1), das durch Gelatine-Zusatz unterdrückt werden kann. In Gegenwart von  $2 \cdot 10^{-4}$  Gew.-% Gelatine ist die Höhe des Maximums stark herabgesetzt; bei  $4 \cdot 10^{-4}$  Gew.-% nimmt es die Form eines kleinen Absatzes im ansteigenden Teil der Stufe an (Abb. 1, Kurven 2 und 3). Eine vollständige Beseitigung des Maximums wird erreicht, sobald die Lösung  $10^{-3}$  Gew.-% des Zusatzes enthält. Bei grösseren Gelatine-Konzentrationen

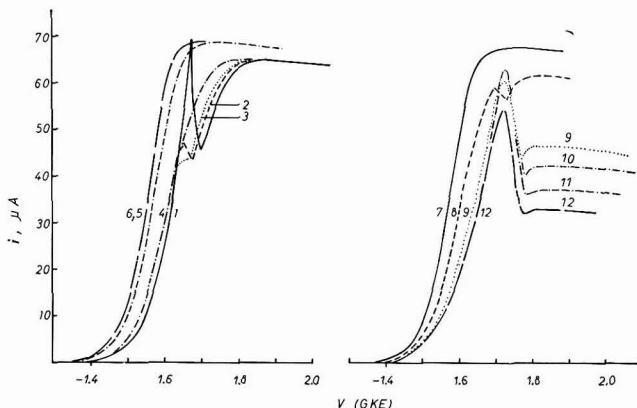


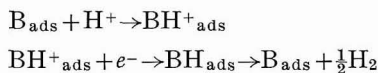
Abb. 1. Wirkung von Gelatine-Zusatz auf die Wasserstoff-Stufe von  $5 \cdot 10^{-3}\text{ M H}_2\text{SO}_4$  in  $0.2\text{ M Li}_2\text{SO}_4$ . (1), 0; (2),  $2 \cdot 10^{-4}$ ; (3),  $4 \cdot 10^{-4}$ ; (4),  $10^{-3}$ ; (5),  $4 \cdot 10^{-3}$ ; (6),  $8 \cdot 10^{-3}$ ;  $10^{-2}$  und  $1.4 \cdot 10^{-2}$ ; (7),  $2 \cdot 10^{-2}$ ; (8),  $10^{-1}$ ; (9),  $2 \cdot 10^{-1}$ ; (10),  $3 \cdot 10^{-1}$ ; (11),  $4 \cdot 10^{-1}$ ; (12),  $5 \cdot 10^{-1}$  Gew.-% Gelatine.

wird die gesamte Stufe zu positiveren Potentialen vorverlagert (Katalyse) und nimmt eine steilere Form an. Die Katalyse erreicht jedoch einen Grenzwert bei  $8 \cdot 10^{-3}$  Gew.-%, der auch in Gegenwart von  $10^{-2}$  und  $1.4 \cdot 10^{-2}$  Gew.-% aufrechterhalten bleibt. In diesen letzteren Lösungen steigt der Grenzstrom etwas über den in zusatzfreier Lösung gemessenen an.

Bei weiterer Steigerung des Gelatine-Gehaltes der Lösung kehrt sich die oben beschriebene Folge der Effekte um. Zunächst verschiebt sich die ganze Stufe wieder zu negativeren Potentialen (Inhibition) und wird flacher, und der Grenzstrom nimmt wieder etwas ab. Bei  $8 \cdot 10^{-2}$  Gew.-% Gelatine erscheint ein kleines Maximum, das mit wachsender Konzentration des Zusatzes ausgeprägter wird. Im Anschluss an den plötzlichen Abbruch des Maximums durchläuft die Stromstärke ein flaches Minimum, bevor das Grenzstrom-Plateau erreicht wird (Abb. 1). In diesen konzentrierten Gelatine-Lösungen ist der Grenzstrom erheblich geringer als derjenige in zusatzfreier Lösung.

Die beiden Maxima der Wasserstoff-Stufe—beobachtet in Abwesenheit bzw. in Gegenwart hoher Gelatine-Konzentration—zeigen charakteristische Unterschiede. Während in ersterem Falle das Maximum durch den Zusatz eines anderen grenzflächenaktiven Stoffes, z.B. Tylose SL 600, vollständig eliminiert werden kann, bleibt es in letzterem Falle praktisch unbeeinflusst. Dies beruht, wie weiter unten gezeigt wird, darauf, dass die Elektrodenoberfläche bereits durch Gelatine belegt ist. Ferner bleibt bei Umkehrung der Polarisationsrichtung nach Erreichen des Grenzstroms das Minimum der Stromspannungskurve in den zusatzfreien Lösungen erhalten, während das Maximum etwas kleiner wird. In Gegenwart von Gelatine jedoch verschwindet das Minimum bei Polarisationsumkehr, während das Maximum praktisch unverändert gegenüber den Kurven mit normaler Polarisationsrichtung bleibt. Man kann hieraus die Folgerung ziehen, dass die Ursache beider Maxima verschieden ist.

VON STACKELBERG und Mitarbeiter<sup>1,2</sup> haben die Befähigung der Gelatine zur Katalyse der Wasserstoffentwicklung aus wässrigen Lösungen einwandfrei nachgewiesen. Diese Eigenschaft der Gelatine, die sie mit anderen Stickstoff enthaltenden Verbindungen teilt, wird in Beziehung gebracht zur Leichtigkeit, mit der ein Proton der Lösung an das freie Elektronenpaar des N-Atoms unter Bildung der protonisierten Form  $\text{BH}^+$  (B ist das Katalysator-Molekül) gebunden wird. Die Entladung des Wasserstoffions erfolgt über das Kation  $\text{BH}^+$  nach dem allgemeinen Schema<sup>1</sup>:



Die Reduktion des Kations  $\text{BH}^+$  erfolgt leichter als diejenige von  $\text{H}_3\text{O}^+$ , so dass eine Abnahme der Wasserstoff-Überspannung beobachtet wird. Die Stärke des katalytischen Effekts hängt von der Adsorptionsfähigkeit und der Säurestärke des Kations  $\text{BH}^+$  ab.

In neutralen Lösungen, in denen die Konzentration freier Wasserstoffionen begrenzt ist, bewirkt Gelatine nur einen geringen katalytischen Effekt, der sich in einer schwachen Positivierung des Grenzanstiegs-Potentials äussert (s. weiter unten), während in saueren Lösungen geringe Zusatz-Konzentrationen eine merkliche Verschiebung der Wasserstoff-Stufe zu positiveren Potentialen bewirken und die Stufe steiler wird (Abb. 1). Beurteilt man die katalytische Wirkung jedoch nach dem Ausmass der grössten Positivierung der Stufe (etwa 50 mV in bezug auf die Stufe bei  $10^{-3}$  Gew.-% Gelatine, wo das Maximum erstmals eliminiert ist), so ist sie nur schwach im Vergleich zu derjenigen anderer Substanzen, die die gleiche Wirkung zeigen, z.B. N,N-Dimethyl-*p*-phenyleniamin<sup>1,5</sup>. In einer Konzentration von  $10^{-4} M$  verschiebt letztere Verbindung die Wasserstoff-Stufe um etwa 220 mV zu positiveren Potentialen<sup>4</sup>.

Oberhalb von  $1.4 \cdot 10^{-2}$  Gew.-% wirkt sich Gelatine nicht mehr als Katalysator aus, sondern als Inhibitor. Die gesamte Wasserstoff-Stufe wird zu negativeren Potentialen zurückverschoben; bei noch höheren Konzentrationen erscheint ein neues Maximum und der Grenzstrom nimmt beträchtlich ab. Zum besseren Verständnis der Inhibitorwirkung gröserer Gelatinemengen sei zunächst ihr Einfluss auf die Reduktionsstufen von  $\text{Cd}^{2+}$ ,  $\text{Zn}^{2+}$  und  $\text{Pb}^{2+}$  geschildert.

In neutralem Medium zeigen  $\text{Cd}^{2+}$  und  $\text{Pb}^{2+}$  reversible Reduktionsstufen, die durch Gelatine-Zusätze bis zu 0.5 Gew.-% nicht erheblich beeinflusst werden (Abb.

2A). Dagegen ist die  $Zn^{2+}$ -Stufe in neutraler Sulfat-Lösung tatsächlich irreversibel und wird durch Gelatine merklich beeinflusst; ein Zusatz von z.B. 0.2 Gew.-% verursacht eine Verschiebung des Halbstufenpotentials um etwa 100 mV zu negativeren Werten, und die Stufe wird zugleich flacher (Abb. 3A). Der Diffusions-Grenzstrom der drei Kationen wird durch Gelatine-Zusätze bis zu 0.5 Gew.-% kaum beeinflusst, woraus zu schliessen ist, dass die Viskosität im Innern der Lösung sich nicht erheblich von derjenigen zusatzfreier Lösungen unterscheidet. Der Gelatine-

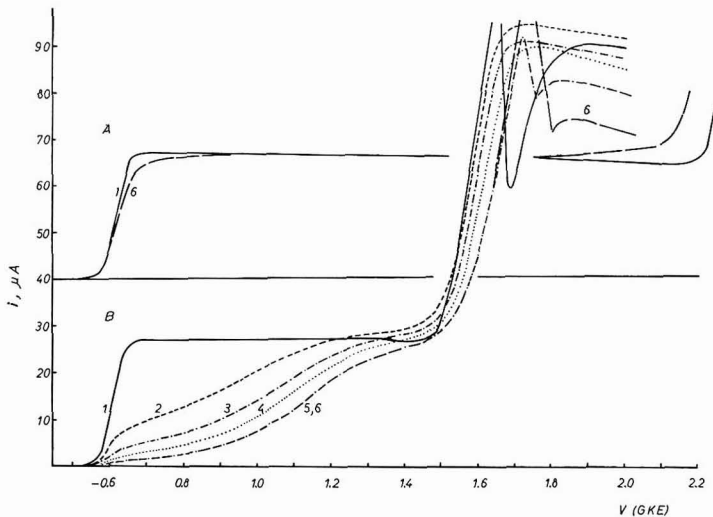


Abb. 2. Wirkung von Gelatine-Zusatz auf die Reduktionsstufe von  $5 \cdot 10^{-3} M$   $Cd^{2+}$  in neutralem (A) und sauerem (B) Leitelektrolyten. (1), 0; (2),  $2 \cdot 10^{-2}$ ; (3),  $3 \cdot 10^{-2}$ ; (4),  $5 \cdot 10^{-2}$ ; (5),  $2 \cdot 10^{-1}$ ; (6),  $4 \cdot 10^{-1}$  Gew.-% Gelatine.

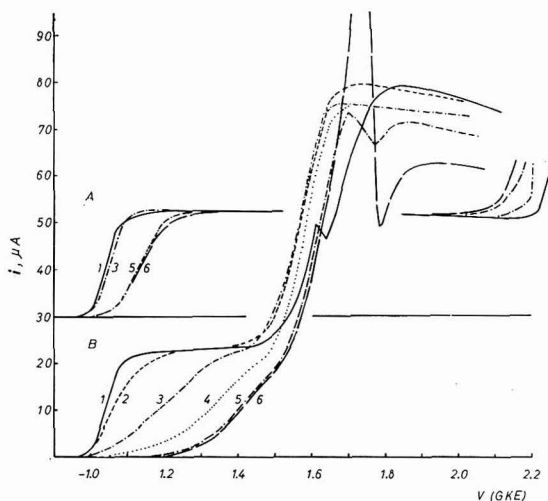


Abb. 3. Wirkung von Gelatine-Zusatz auf die Reduktionsstufe von  $5 \cdot 10^{-3} M$   $Zn^{2+}$  in neutralem (A) und sauerem (B) Leitelektrolyten. (1), 0; (2),  $5 \cdot 10^{-3}$ ; (3),  $10^{-2}$ ; (4),  $2 \cdot 10^{-2}$ ; (5),  $10^{-1}$ ; (6),  $2 \cdot 10^{-1}$  Gew.-% Gelatine.

zusatz bewirkt jedoch einen früheren Grenzanstieg der Stromstärke infolge des katalytischen Einflusses auf die Wasserstoff-Entwicklung. Dieser Effekt wächst mit steigendem Gelatine-Gehalt der Lösungen.

Eine ganz andere Wirkung zeigt Gelatine jedoch auf die Reduktionsstufen von  $\text{Cd}^{2+}$  und  $\text{Zn}^{2+}$  in *sauerer* Lösungen. Die  $\text{Cd}^{2+}$ -Stufe, die in neutralem Medium vom Gelatine-Zusatz fast völlig unbeeinflusst blieb, wird in Gegenwart von  $5 \cdot 10^{-3} M$   $\text{H}_2\text{SO}_4$  schon durch nur  $2 \cdot 10^{-2}$  Gew.-% Gelatine stark verzerrt. Obwohl das Stufenfuss-Potential dasselbe bleibt wie in zusatzfreier Lösung, wächst der Strom nun über einen Potentialbereich von etwa 0.6 V fast linear mit der angelegten Spannung (Abb. 2B). Eine weitere Steigerung der Gelatine-Konzentration verschiebt die ganze verformte Stufe zu negativeren Potentialen. Die Inhibition erreicht ihr maximales Ausmass in Gegenwart von 0.2 Gew.-% Gelatine; eine weitere Negativierung wird nicht beobachtet. In Gegenwart von  $\text{Cd}^{2+}$  ist die Wirkung der Gelatine auf die nachfolgende Wasserstoff-Stufe praktisch gleich derjenigen in Abwesenheit von  $\text{Cd}^{2+}$ . In Abb. 2B erkennt man die gleiche Abfolge der Effekte mit steigender Gelatine-Konzentration—Maximum-Unterdrückung, Katalyse, Inhibition, Ausbildung des neuen Maximums, Verminderung des Grenzstromes—wie in  $\text{Cd}^{2+}$ -freien Lösungen.

Praktisch das gleiche Verhalten, wie oben für  $\text{Cd}^{2+}$  beschrieben, wird bei der Reduktion von  $\text{Zn}^{2+}$  in saureren Elektrolyten beobachtet (Abb. 3B). Da die  $\text{Zn}^{2+}$ -Reduktion jedoch empfindlicher auf eine Inhibition anspricht, sind in diesem Falle geringere Gelatine-Konzentrationen für eine vollständige Inhibition erforderlich als bei der  $\text{Cd}^{2+}$ -Reduktion. Bemerkenswerterweise wirken  $10^{-2}$  Gew.-% Gelatine, die einen starken Inhibitionseffekt auf die  $\text{Zn}^{2+}$ -Stufe ausüben, als Katalysator der nachfolgenden  $\text{H}^+$ -Reduktion. Eine Inhibition der letzteren tritt erst bei höheren Gelatine-Konzentrationen auf. Ferner zeigen die Kurven der Abb. 2 und 3, dass der Grenzstrom der inhibierten  $\text{Cd}^{2+}$ - und  $\text{Zn}^{2+}$ -Stufen nur wenig vom Gelatine-Gehalt beeinflusst werden. Dies führt wiederum zu dem Schluss, dass nicht eine Viskositätsänderung des Lösungsmittels für die Verzerrung der Stufen verantwortlich ist.

Im Gegensatz zu ihrem Einfluss auf die  $\text{Cd}^{2+}$ - und  $\text{Zn}^{2+}$ -Stufe übt Gelatine in saurerer Lösung keine merkliche inhibierende Wirkung auf die  $\text{Pb}^{2+}$ -Stufe aus. In geringen Konzentrationen unterdrückt der Zusatz das Maximum der  $\text{Pb}^{2+}$ -Stufe, während grössere Mengen eine schwache Abnahme der Grenzstromstärke zur Folge haben, die sicherlich einer Änderung der Lösungsviskosität zugeschrieben werden kann.

Der Unterschied der Wirkung von Gelatine einerseits in neutraler, andererseits in saurerer Lösung auf die  $\text{Cd}^{2+}$ - und  $\text{Zn}^{2+}$ -Stufe zeigt deutlich, dass die inhibierenden Eigenschaften des Zusatzstoffes beim Übergang zu sauerem Medium radikal geändert und verstärkt werden. Da die Inhibition (ebenso wie die Katalyse) ein Oberflächeneffekt ist, muss man der Grenzfläche Metall/Lösung bei sauerem Elektrolyten eine Struktur zuschreiben, die anders ist als diejenige in neutralem Medium. Dies wird leicht verständlich, wenn man die katalytischen Eigenschaften der Gelatine in Betracht zieht, nämlich die Fähigkeit, Protonen an das freie Elektronenpaar der N-Atome zu binden. Als Folge der hierdurch der Gelatine erteilten positiven Ladung wächst ihre Adsorbierbarkeit bei Potentialen negativ vom elektrokapillaren Nullpunkt an und übertrifft diejenige der unprotonisierten Form. In relativ konzentrierten Lösungen muss man erwarten, dass ein dicht gepackter Gelatinefilm die Elektrodenoberfläche blockiert. Infolge der dichten Struktur—and wahrscheinlich auch infolge elektrostatischer Effekte—übt der protonisierte Gelatinefilm einen inhibierenden

Einfluss auf die Reduktion von Kationen aus, deren Reduktionspotentiale auf der negativen Seite des Ladungs-Nullpunktes liegen. Die Inhibition äussert sich in der Ausbildung verflachter Stufen, jedoch ohne erhebliche Beeinflussung des Grenzstromes. In dieser Beziehung ähnelt die Wirkung der Gelatine derjenigen eines hohen Widerstandes, den man in den Stromkreis einführt. Da die Adsorption der protonisierten Gelatine erst zu erwarten ist, wenn die Elektrodenoberfläche negativ geladen ist, kann es nicht überraschen, dass ein ähnlicher Inhibitionseffekt, wie er in saueren Lösungen bei  $\text{Cd}^{2+}$  und  $\text{Zn}^{2+}$  beobachtet wird, bei der Reduktion von  $\text{Pb}^{2+}$  nicht vorliegt; das Reduktionspotential des letzteren Ions liegt auf der positiven Seite der Elektrokapillarkurve.

Die Blockierung der Elektrodenoberfläche durch hohe Gelatine-Zusätze wirkt auch inhibierend auf die Wasserstoff-Stufe und verschiebt sie zu negativeren Potentialen. Ein deutlicher Widerstandseffekt, wie er im Falle der  $\text{Cd}^{2+}$ - und  $\text{Zn}^{2+}$ -Stufe vorliegt, wird hier jedoch nicht beobachtet, da auch die an Gelatine-Moleküle gebundenen Protonen reduziert werden können.

Bei der Entladung der in unmittelbarem Kontakt mit der Elektrode befindlichen Protonen bleibt die unprotonisierte Gelatine an der Grenzfläche zurück. Als Folge von Unterschieden der Adsorptionsenergie bzw. dem Ausmass der Adsorption beider Gelatine-Formen ergeben sich Änderungen der Grenzflächenspannung am Quecksilbertropfen, die eine Strömung der anhaftenden Elektrolytschicht in Gang bringt, was sich in Form eines Strommaximums äussert. Infolge der Reduktion der Grenzflächen-Protonen setzt ferner ein Transportmechanismus ein, der dem Grothus-Mechanismus der Protonen-Leitung in wässriger Lösung ähnlich ist, wobei die Protonenübertragung im vorliegenden Falle über die Stickstoff-Gruppen der Gelatine erfolgt. In diesem Zusammenhang sind die Arbeiten von NIVEN<sup>7</sup> und RIEHL<sup>8</sup> zu erwähnen; diese Autoren erklären die Leitfähigkeit in Gelatinefolien durch einen Mechanismus, bei dem eine Protonenübertragung über Wasserstoff-Brücken erfolgt. Nach Abbruch des Maximums verringert sich der polarographische Strom auf einen Wert, der beträchtlich geringer als derjenige in zusatzfreier Lösung ist. HANS UND JENSCH<sup>2</sup> erklären diese Erscheinung durch die Bindung eines Teiles der Wasserstoff-Ionen an Gelatine. Im Konzentrationsbereich ihrer Untersuchungen (bis zu  $8 \cdot 10^{-2}$  Gew.-%) wurde die Abnahme der Wasserstoffionen-Konzentration,  $\Delta c$ , durch die Beziehung

$$\Delta c = 0.08 \cdot 10^{-3} \cdot c_g$$

ausgedrückt, worin  $c_g$  die Konzentration der Gelatine in 0.01% bedeutet. Bei den hier mitgeteilten Untersuchungen, insbesondere aber in dem von uns untersuchten Gebiet noch höherer Gelatinekonzentration, zeigte sich keine reine Linearität in der Beziehung. Sehr wahrscheinlich wird der Stofftransport zur Elektrode durch die Geschwindigkeit des Protonentransports durch den Gelatinefilm an der Grenzfläche bestimmt. Diese Annahme wird dadurch gestützt, dass—in Gegenwart geringen Gelatine-Zusatzes—die gebundenen Protonen leichter reduziert werden als die freien. Weitere Untersuchungen sind vorgesehen, die die Gültigkeit dieser Annahme prüfen sollen.

Trotz ihrer hervorstechenden Erscheinung bei diesen Untersuchungen wurden die Maxima der Wasserstoff-Stufe bei hohen Gelatine-Konzentrationen von HANS UND JENSCH<sup>2</sup> nicht beobachtet, wohl aber die Verringerung des Grenzstromes. Der

Grund für diesen Unterschied der Ergebnisse der hier berichteten Untersuchungen und derjenigen von HANS UND JENSCH scheint in einer verschiedenen Technik beim Registrieren der Stromspannungskurven zu liegen. Bei der Konstruktion ihrer Kurven verwendeten HANS UND JENSCH die polarometrische Methode, bei der der Strom durch den Spannungsabfall ( $iR$ ) über einen Präzisionswiderstand (in ihrem Falle  $100\text{ k}\Omega$ ) gemessen wird. Obgleich die Grenzströme und die Potentiale im ansteigenden Teil der polarographischen Stufen mit dieser Methode genauer gemessen werden können als mittels automatisch registrierter Polarogramme, vermag der relativ grosse Widerstand im Stromkreis scharfe Maxima stark zu verringern<sup>9,10</sup>. Dass dies tatsächlich der Fall ist, wurde im Rahmen der vorliegenden Untersuchungen nachgewiesen. Abb. 4 zeigt Polarogramme, die mit sauerem Elektrolyten und 0.4

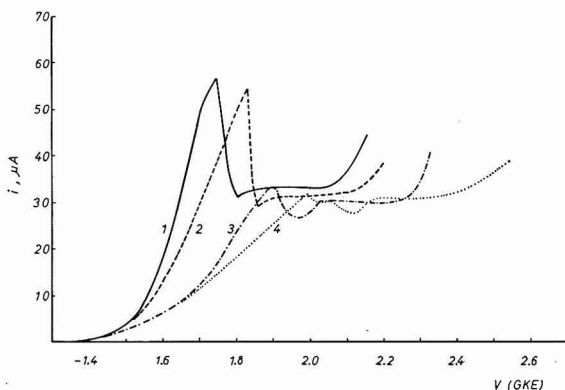


Abb. 4. Wirkung eines zusätzlichen Serien-Widerstandes auf das Maximum der Wasserstoffstufe in Gegenwart von 0.4 Gew.-% Gelatine. (1), 0; (2), 2; (3), 4; (4),  $10\text{ k}\Omega$ .

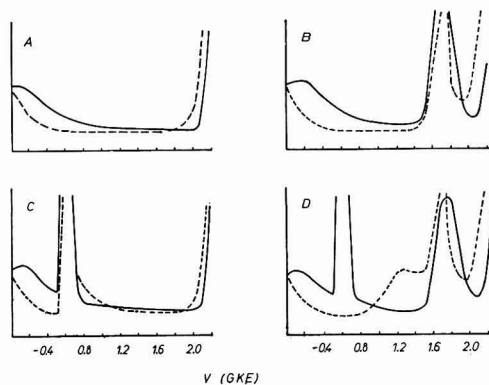
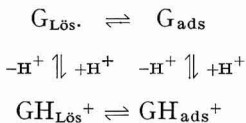


Abb. 5. Wechselstrom-Polarogramme in Abwesenheit (—) und in Gegenwart (---) von 0.4 Gew.-% Gelatine. (A und B), Grundstrom in neutraler bzw. saurer Lösung; (C und D), desgl. in Gegenwart von  $5 \cdot 10^{-3} M \text{ Cd}^{2+}$ .

Gew.-% Gelatine beobachtet wurden, wobei Widerstände von 2, 4 und  $10\text{ k}\Omega$  in Serie zur polarographischen Zelle eingeschaltet wurden. Man sieht deutlich, wie die Höhe des Maximums mit wachsendem Serienwiderstand abnimmt. Da man bei der manuellen Methode ein ziemlich hoch gedämpftes Galvanometer benutzt und den

Mittelwert seiner Schwingungen mit dem Auge feststellt und da das Potential der Tropfelektrode stufenweise geändert wird, kann hierbei die wahre Natur einer polarographischen Stufe leicht übersehen werden<sup>11</sup>.

Dass Gelatine in saurerer Lösung eine stärkere Inhibitionswirkung zeigt als in neutralem Medium, wurde auch mittels Wechselstrom-Polarogrammen nach der Methode von BREYER und Mitarbeiter<sup>12</sup> nachgewiesen. Während die ausgezogenen Kurven der Abb. 5A und B die Änderungen der Doppelschichtkapazität als Funktion des Elektrodenpotentials im reinen neutralen bzw. saueren Leitelektrolyten darstellen, sind die entsprechenden gestrichelten Kurven bei Zusatz von 0.4 Gew.-% Gelatine erhalten. Dieser Zusatz verursacht in beiden Medien eine beträchtliche Verminderung der Doppelschichtkapazität über den ganzen Potentialbereich. Dass Gelatine in saurerer Lösung auch auf der positiven Seite der Elektrokapillarkurve eine Kapazitätserniedrigung hervorruft, lässt sich leicht mittels der Gleichgewichte zwischen den protonisierten ( $\text{GH}^+$ ) und unprotonisierten (G) Formen der Gelatine in Lösung und denjenigen auf der Elektrodenoberfläche erklären. Diese können schematisch folgendermassen dargestellt werden:



In neutraler Lösung ist das Gleichgewicht  $\text{G}_{\text{Lös.}} \rightleftharpoons \text{G}_{\text{ads}}$  wirksam, ebenso in saurerer Lösung bei Potentialen positiver als der Ladungs-Nullpunkt. Auf der negativen Seite der Elektrokapillarkurve stellt sich in saurerer Lösung das Gleichgewicht  $\text{GH}_{\text{Lös.}}^+ \rightleftharpoons \text{GH}_{\text{ads}}^+$  ein. Demgemäß ist das Gleichgewicht  $\text{G}_{\text{ads}} \rightleftharpoons \text{GH}_{\text{ads}}^+$  potentialabhängig. Der Übergang von dem einen Zustand der Adsorption zum anderen erfolgt jedoch ohne entsprechendes tensammetrisches Maximum.

In neutralem Leitelektrolyten verursacht die  $\text{Cd}^{2+}$ -Reduktion ein scharfes Maximum, das nur wenig von Gelatine beeinflusst wird und daher einen hohen Grad von Reversibilität der Elektrodenreaktion anzeigt (Abb. 5C). In Abwesenheit von Gelatine gibt  $\text{Cd}^{2+}$  auch in sauerem Elektrolyten ein Maximum bei vergleichbaren Potentialen und von vergleichbarer Höhe wie in neutraler Lösung. Die Zugabe von 0.4 Gew.-% Gelatine verschiebt aber das Reduktionspotential zu negativeren Werten und der reversible Charakter des Wechselstrom-Maximums geht verloren; die Reduktion gibt sich durch eine breite buckel-artige Welle zu erkennen (Abb. 5D). Die Ergebnisse der wechselstrom-polarographischen Untersuchungen sind demnach in Übereinstimmung mit denjenigen der Gleichstrom-Messungen, indem sie auch hier die verstärkte inhibierende Wirkung der Gelatine in sauerem Medium deutlich machen.

Der Alexander-von-Humboldt-Stiftung danken wir bestens für ein dem einen von uns (A.M.S.) gewährtes Stipendium, dem Bundesministerium für Wirtschaft für finanzielle Unterstützung (J.M.K.).

#### ZUSAMMENFASSUNG

Die Wirkung von Gelatine auf die Wasserstoff-Stufe von  $5 \cdot 10^{-3} M \text{ H}_2\text{SO}_4$  in

0.2 M Li<sub>2</sub>SO<sub>4</sub> wird über einen weiten Konzentrationsbereich untersucht. Bis zu 1.4 · 10<sup>-2</sup> Gew.-% katalysiert der Zusatzstoff die Elektrodenreaktion und die Stufe nimmt eine steilere Form an. Größere Konzentrationen wirken jedoch inhibierend, wobei ein neues, nicht-unterdrückbares Maximum ausgebildet wird zugleich mit einer merklichen Verminderung des Grenzstromes.

In neutralen Lösungen werden die Reduktionsstufen von Pb<sup>2+</sup> und Cd<sup>2+</sup> praktisch nicht durch Gelatine-Zusatz beeinflusst, während diejenige von Zn<sup>2+</sup> etwas inhibiert wird. Vergleichbare Zusatz-Konzentrationen in sauerem Medium haben eine starke Verformung der Cd<sup>2+</sup>- und Zn<sup>2+</sup>-Stufen zur Folge, während diejenige von Pb<sup>2+</sup> unbeeinflusst bleibt.

Es wird ein Mechanismus für die Wirkung der Gelatine in saurerer Lösung vorgeschlagen, der den experimentellen Befunden Rechnung trägt.

#### SUMMARY

The effect of gelatin on the hydrogen wave of 5 · 10<sup>-3</sup> M H<sub>2</sub>SO<sub>4</sub> in 0.2 M Li<sub>2</sub>SO<sub>4</sub> is examined over a wide range of concentration. Up to 1.4 · 10<sup>-2</sup> wt.-%, the additive catalyzes the electrode reaction and the wave acquires a steeper form. Larger concentrations act, however, as inhibitor, causing the development of a new maximum which cannot be eliminated, together with a marked decrease in the limiting current.

In neutral solutions both the Pb<sup>2+</sup>- and Cd<sup>2+</sup>-waves are practically unaffected by gelatin-additions up to 0.4 wt.-%, that of Zn<sup>2+</sup> is, however, somewhat inhibited. Comparable additive concentrations in acid media cause a strong deformation of the Cd<sup>2+</sup>- and Zn<sup>2+</sup>-waves, while that of Pb<sup>2+</sup> remains unchanged.

A mechanism of the action of gelatin in acid solutions accounting for the experimental findings, is presented.

#### LITERATUR

- 1 M. VON STACKELBERG, W. HANS UND W. JENSCH, *Z. Elektrochem.*, 62 (1958) 839.
- 2 W. HANS UND W. JENSCH, *Z. Elektrochem.*, 56 (1952) 648.
- 3 G. HOLLECK UND L. HOLLECK, *Naturwiss.*, 51 (1964) 433.
- 4 Unveröffentlichte Ergebnisse.
- 5 D. JANNAKOUDAKIS, A. WILDENAU UND L. HOLLECK, *J. Electroanal. Chem.*, 15 (1967) 83.
- 6 J. KORYTA, *Electrochim. Acta*, 6 (1962) 67.
- 7 C. D. NIVEN, *Trans. Faraday Soc.*, 54 (1957) 441.
- 8 N. RIEHL, *Kolloid-Z.*, 151 (1957) 66.
- 9 R. BRDIČKA, *Collection Czech. Chem. Commun.*, 8 (1936) 419.
- 10 J. J. LINGANE, *J. Am. Chem. Soc.*, 62 (1940) 1665.
- 11 J. J. LINGANE, *J. Electroanal. Chem.*, 15 (1967) 221.
- 12 B. BREYER, F. GUTMAN UND S. HACOBIAN, *Austr. J. Sci. Res.*, A3 (1950) 558; B. BREYER UND S. HACOBIAN, *ibid.*, A3 (1952) 500.



## THE ELECTROCHEMICAL REDUCTION OF RIBOFLAVIN IN DIMETHYLSULFOXIDE

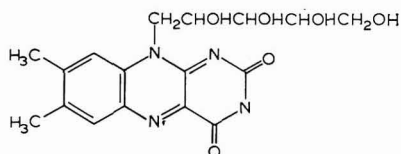
SHANKAR V. TATWAWADI, K. S. V. SANTHANAM AND ALLEN J. BARD

*Department of Chemistry, The University of Texas, Austin, Texas, 78712 (U.S.A.)*

(Received October 23rd, 1967)

### INTRODUCTION

Interest in the possible involvement of intermediate free radicals (semiquinones) of flavin compounds in biological oxidation processes has been evident since the pioneering studies of MICHAELIS and coworkers<sup>1</sup>. Confirming evidence of intermediate radicals has been obtained by numerous electron spin resonance (ESR) spectroscopic studies of chemically-reduced riboflavin (6,7-dimethyl-9-[D-1'-ribityl]-isoalloxazine).



and related compounds in aqueous solutions<sup>2</sup>. Electrochemical studies in aqueous solutions have also provided evidence of a reduction involving two successive one-electron steps to the intermediate radical and a completely reduced (leuco) form<sup>3</sup>. However, studies in aqueous solutions are complicated by the existence of a number of protonated and deprotonated forms of the oxidized, semiquinone, and reduced forms at different pH-values and by the strong adsorption of the various forms at the mercury-solution interface<sup>3,4</sup>. Furthermore, the potentials for the two reduction steps are very near one another, so that clear differentiation of the two waves is difficult and preparation of the radical in the absence of appreciable amounts of either the oxidized or leuco-form is not possible. Finally, the low solubility of riboflavin in aqueous solutions (about 0.3 mM at 25°) makes many types of electrochemical studies difficult.

This study of the electrochemistry of riboflavin in the aprotic solvent dimethylsulfoxide (DMSO) was undertaken with the hope that the reduction path would be similar to that found with aromatic hydrocarbons and related compounds, where a clear separation of the reduction waves is obtained in the absence of a protonation reaction following the first electron-transfer step. Electrochemistry in DMSO, in which riboflavin is easily soluble, has been reviewed recently<sup>5</sup>.

## RESULTS

*Voltammetric methods*

The polarographic reduction of riboflavin in DMSO solutions containing  $\text{NaClO}_4$  as a supporting electrolyte showed three reduction waves (Fig. 1). The first wave was very well-defined with a half-wave potential ( $E_{\frac{1}{2}}$ ) of  $-0.71$  V vs. an aqueous saturated calomel electrode (SCE). The height of this wave was directly proportional to con-

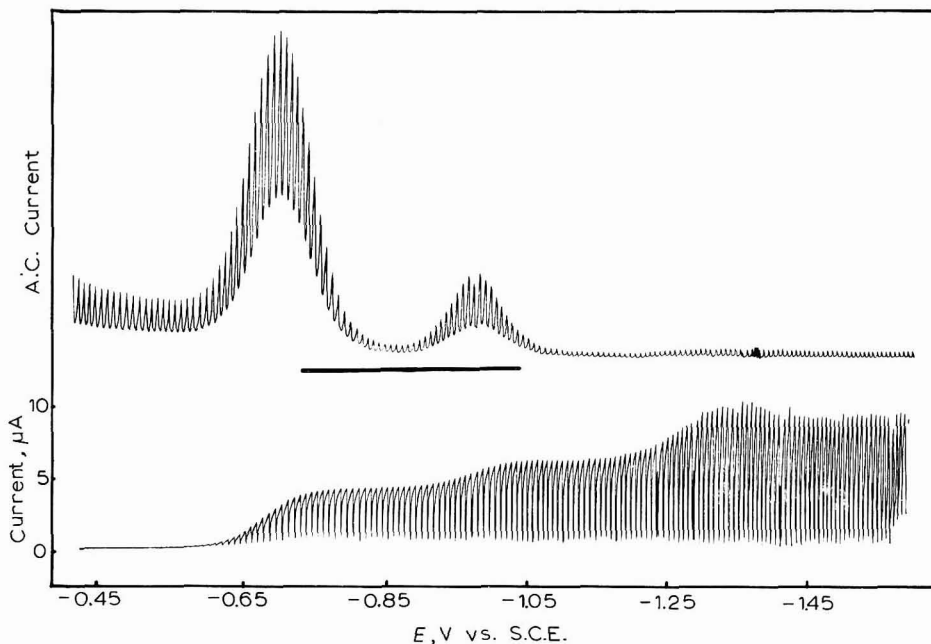


Fig. 1. Polarograms for the reduction of riboflavin (3 mM) in DMSO containing 0.8 M  $\text{NaClO}_4$ . Upper curve, a.c. polarogram, with 10 mV, 200 c/sec superimposed; lower curve, d.c. polarogram.

centration (0.2–4 mM) and varied as the square root of the head of the dropping mercury electrode (DME). The diffusion current constant for this wave was 0.89 in 0.8 M  $\text{NaClO}_4$ , yielding a polarographic diffusion coefficient, (Ilkovic equation),  $D$ , of about  $1.6 \cdot 10^{-6}$   $\text{cm}^2/\text{sec}$ , assuming this step to be a one-electron reduction. This value agrees with the  $D$ -value obtained in aqueous solutions,  $4 \cdot 10^{-6}$   $\text{cm}^2/\text{sec}^{3,4}$ , since the viscosity of DMSO is about twice that of water ( $\eta_{\text{DMSO}} = 1.96$  cps). The second and third waves were smaller and less well-defined than the first, with  $E_{\frac{1}{2}}$ -values of  $-1.02$  and  $-1.25$  V vs. SCE. The second wave became more pronounced and relatively larger at higher riboflavin concentrations, with the total height of waves 2 and 3 about equal to wave 1 at all concentrations. Because wave 2 was rather drawn out, and wave 3 was obscured by a maximum, often with rather erratic current fluctuations on its plateau, reliable quantitative data on these waves by polarography was difficult.

The adsorption prewave which occurs in aqueous solutions is absent in DMSO. Electrocatalytic curves, taken by measuring the drop-time at various potentials and

converting these to surface tension measurements, show no appreciable changes in surface tension of the mercury-DMSO solution interface at potentials of  $-0.3$  and  $-1.0$  V when increasing amounts of riboflavin are added to a DMSO- $0.1\text{ M}$   $\text{NaClO}_4$  solution; a slight increase in surface tension is noticed on going from DMSO- $0.1\text{ M}$   $\text{NaClO}_4$  to a solution containing  $1\text{ mM}$  riboflavin.

When a.c. polarography was carried out by imposing a small a.c. voltage on the d.c. voltage scan, a.c. peaks at potentials corresponding to waves 1 and 2 were obtained (Fig. 1). Clear a.c. peaks were given for wave 2 even under conditions where its d.c. wave was very drawn out and hard to observe.

The cyclic voltammogram of a  $1.4\text{ mM}$  riboflavin solution in a  $0.1\text{ M}$   $\text{NaClO}_4$ -DMSO solution at a hanging mercury drop electrode (HMDE) shown in Fig. 2, is

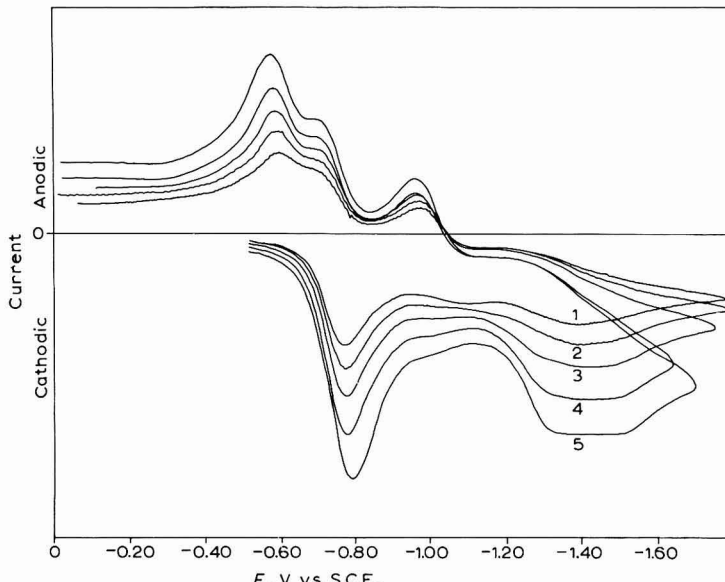


Fig. 2. Cyclic voltammetry of riboflavin. The soln. contained  $0.1\text{ M}$   $\text{NaClO}_4$  and  $1.4\text{ mM}$  riboflavin in DMSO. Scan rates: (1),  $152$ ; (2),  $222$ ; (3),  $312$ ; (4),  $476$ ; (5),  $714$  mV/sec.

characterized by a well-defined reduction peak, with a cathodic peak potential ( $E_{pc}$ ) of  $-0.77$  V and a rather broad peak with an  $E_{pc}$  of  $-1.3$  V. At higher concentrations of riboflavin, e.g.,  $3.2\text{ mM}$ , another peak, corresponding to the second polarographic wave, with an  $E_{pc}$  of about  $-1.07$  V, becomes more distinct. Typical cyclic voltammetric data for these reductions are given in Table 1. The constancy of the current function (proportional to  $i_p/v^{1/2}$ , where  $i_p$  is the peak current and  $v$  is the scan rate) for the first peak suggests a diffusion-controlled limiting current, in agreement with the polarographic results. The current function of the second peak is strongly dependent upon scan rate, decreasing with increasing scan rate. This suggests that this wave is caused by reduction of a substance formed by a homogeneous chemical reaction of a product produced during the first reduction wave.

When the scan direction is reversed  $80$ - $90$  mV past the first cathodic peak, two anodic peaks, with  $E_{pa}$ -values of  $-0.72$  V and  $-0.57$  V, appeared (Fig. 3). Typical data for these reversal peaks is given in Table 2. Because the anodic peaks

TABLE 1

CYCLIC VOLTAMMETRIC DATA FOR THE REDUCTION OF RIBOFLAVIN<sup>a</sup>

Sweep rate (mV/sec)	Peak I		Peak II		Peak III	
	-E <sub>pc</sub> <sup>b</sup>	i <sub>pc</sub> /v <sup>1/2</sup> <sup>c</sup>	-E <sub>pc</sub> <sup>b</sup>	i <sub>pc</sub> /v <sup>1/2</sup> <sup>c</sup>	-E <sub>pc</sub> <sup>b</sup>	i <sub>pc</sub> /v <sup>1/2</sup> <sup>c</sup>
Concn. = 1.06 mM						
67	0.77	0.38	1.08	0.03	1.30	0.15
152	0.77	0.39	—	—	1.30	0.23
222	0.77	0.38	—	—	1.31	0.23
312	0.77	0.41	—	—	1.31	0.25
476	0.77	0.40	—	—	1.32	0.24
714	0.77	0.39	—	—	1.32	0.23
Concn. = 3.2 mM						
67	0.77	1.10	1.05	0.17	1.35	0.13
152	0.78	1.10	1.07	0.15	1.37	0.23
222	0.78	1.10	1.07	0.12	1.38	0.24
312	0.78	1.10	1.07	0.07	1.38	0.23
476	0.78	1.20	1.07	0.01	1.39	0.23
714	0.79	1.10	—	—	1.39	0.30

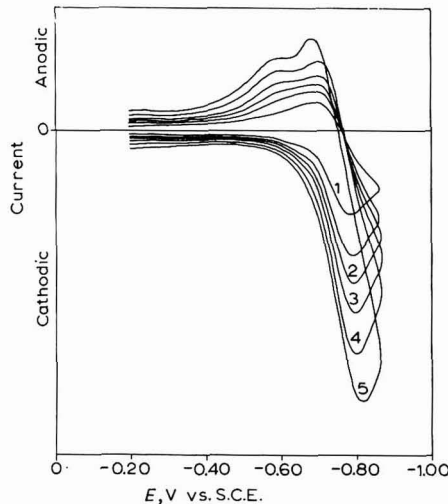
<sup>a</sup> The soln. contained 0.1 M NaClO<sub>4</sub> in DMSO.<sup>b</sup> Potentials in V vs. aq. SCE.<sup>c</sup> In  $\mu\text{A sec}^{1/2} \text{mV}^{-1/2}$ .

Fig. 3. Cyclic voltammetry of riboflavin for reversal following first peak. Scan rates: (1), 67; (2), 222; (3), 312; (4), 476; (5), 714 mV/sec.

are not well-resolved and it is rather difficult to make adequate correction for the baseline of these peaks (the decaying cathodic current, corrected for residual and charging current), the reported magnitudes must be considered as somewhat arbitrary. The data indicate that the current function of the first anodic peak obtained on scan reversal is almost independent of scan rate and that  $i_{pa}/i_{pc}$  is slightly less than one. The second anodic peak increases with increasing scan rate, and is almost absent at

TABLE 2

CYCLIC VOLTAMMETRIC DATA FOR REVERSAL AT FIRST PEAK OF RIBOFLAVIN<sup>a</sup>

Sweep rate (mV/sec)	$i_{pc}$ <sup>b</sup> $v^{\frac{1}{2}}$	$i_{pa_{II}}$ <sup>b,c</sup> $v^{\frac{1}{2}}$	$i_{pa_{III}}$ <sup>b,d</sup> $v^{\frac{1}{2}}$
Concn. = 1.06 mM			
67	0.38	0.33	0.02
152	0.40	0.33	0.02
222	0.41	0.33	0.06
312	0.41	0.34	0.08
476	0.43	0.36	0.10
714	0.42	0.37	0.11
Concn. = 3.2 mM			
67	1.26	1.1	—
152	1.26	1.0	0.02
222	1.27	1.0	0.03
312	1.28	1.0	0.04
476	1.28	1.0	0.08
714	1.27	1.1	0.13

<sup>a</sup> The soln. contained 0.1 M NaClO<sub>4</sub> in DMSO.<sup>b</sup>  $\mu$ A sec $^{\frac{1}{2}}$  mV $^{-\frac{1}{2}}$ .<sup>c</sup> Scan reversed 80–90 mV more negative than  $E_{pc}$ . Measured using procedure of NICHOLSON<sup>6</sup>.<sup>d</sup> Measured from baseline obtained by approximate extrapolation of current from  $i_{par}$ .

very slow scan rates; this suggests that the substance giving rise to this wave is decomposing by a homogeneous chemical reaction.

The addition of a large excess of the proton donor, hydroquinone (HQ) (4.4 mM riboflavin–0.57 M HQ), resulted in the height of the first cathodic wave doubling and the disappearance of the third cathodic wave. The second wave, or a new wave in the same potential region, was present. The anodic waves, which appeared to be at about the same potentials as before HQ addition, were very distorted by a stirring effect in the presence of HQ.

#### Controlled potential coulometry

Coulometric experiments at a mercury pool electrode controlled at a potential on the diffusion plateau of the first wave ( $-0.80$  V vs. SCE) showed that one ( $0.99 \pm 0.01$ ) faraday per mole of electroactive material is consumed in a complete reduction. Examination of the solution after reduction, by polarographic or cyclic voltammetric techniques, showed an anodic wave (sometimes complicated by stirring at the electrode surface?) at about  $-0.7$  V. The polarographic wave height for this anodic wave was about 30–40% smaller than the original height of the first cathodic polarographic wave before reduction. For a cathodic cyclic voltammetric sweep in this solution, two reduction peaks with  $E_p$ -values at  $-1.05$  V and  $-1.37$  V, appear. These peaks are better defined than the corresponding peaks obtained during cyclic voltammetry of the original solution. The current functions of these peaks were constant with varying scan rate. Examination of the solution after reduction, by ESR spectroscopy, shows a rather poorly resolved spectrum (Fig. 4) which is stable with time, and which is generally very similar to that observed from riboflavin semiquinone species in aqueous media<sup>2</sup>.

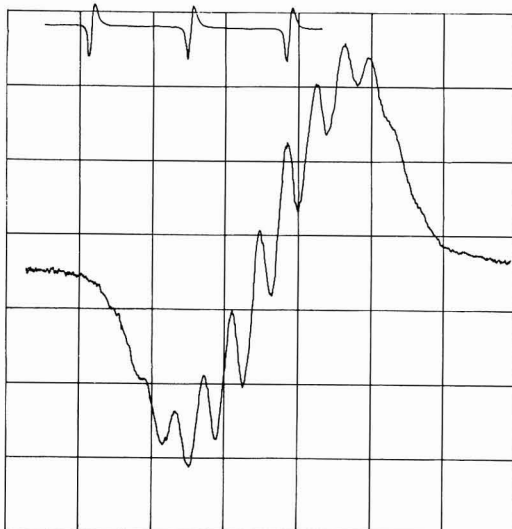


Fig. 4. ESR spectrum for soln. containing 1.1 mM riboflavin and 0.8 M NaClO<sub>4</sub> in DMSO following reduction. Upper signal is of potassium peroxyxylamine disulfonate with 13.0 gauss splitting.

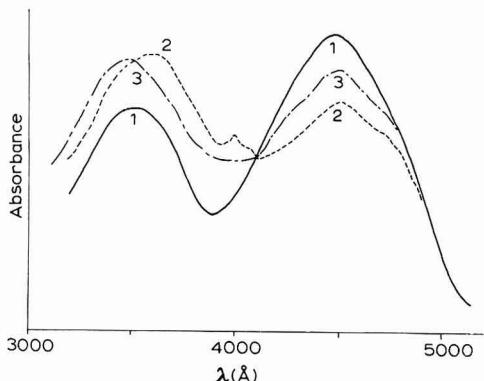


Fig. 5. Visible spectra during riboflavin reduction. The soln. contained 4.5 mM riboflavin and 0.8 M NaClO<sub>4</sub> in DMSO. Reduction carried out at -0.8 V vs. SCE. (1), Before reduction; (2), partially reduced; (3), almost complete reduction.

Reversal coulometry<sup>8</sup> was employed to obtain information about the stability of the reduced species. The number of coulombs recovered on the oxidation ( $Q_b$ ) was always less than that for the reduction ( $Q_f$ ). For short electrolysis times (2 min reduction followed by complete oxidation),  $Q_b/Q_f$  was about 0.7. For longer electrolysis times (5–15 min),  $Q_b/Q_f$  was 0.4–0.6. The values of  $Q_b/Q_f$  did not depend upon the initial concentration of riboflavin, but were not reproducible enough to gain any quantitative kinetic data about the reduction product. When the solution resulting from the oxidation was examined by voltammetric techniques, voltammetric waves at the same potentials as the original solution were observed, with the second cathodic wave ( $E_p = 1.05$  V) being somewhat more prominent than the one found in the original solution.

Continued coulometric reduction of the solution at  $-1.3$  V vs. SCE following exhaustive reduction at the first wave, showed the consumption of approximately two additional faradays per mole, and the disappearance of all anodic and cathodic waves on polarographic examination of the reduced solution.

A spectrophotometric analysis of the solution during the course of the reduction was also performed. This was accomplished by pumping solution from the electrolysis cell through a quartz flow cell contained in a spectrophotometer and then back into the electrolysis cell. Typical curves during the course of the electrolysis are shown in Fig. 5. Initially, the riboflavin solution shows two absorption maxima, one at  $448\text{ m}\mu$  and another at  $350\text{ m}\mu$ , with a ratio of peak heights of about 1 to 0.78. These values are very close to those found in other non-aqueous solvents<sup>9</sup>. During the reduction, at  $-0.80$  V, the band at  $448\text{ m}\mu$  decreased in height, while that at  $350\text{ m}\mu$  increased and shifted to about  $360\text{ m}\mu$ . A new small peak appeared at about  $400\text{ m}\mu$ . With continued electrolysis at the same potential, however, the band at  $450\text{ m}\mu$  increases again while that at  $360\text{ m}\mu$  shifts back to  $350\text{ m}\mu$ , with a ratio of peak heights of the  $450\text{ m}\mu$  to  $350\text{ m}\mu$  bands of about 1 to 1.1; the peak at  $400\text{ m}\mu$  has disappeared. Visually, the electroreduction is characterized by a change in the solution from a bright yellow to a deep orange-red. All solutions show an isosbestic point at  $410\text{ m}\mu$ . These results tend to confirm the previous electrochemical data and suggest the formation of an intermediate upon electroreduction which undergoes a following chemical reaction.

#### DISCUSSION

Clearly the mechanism of the reduction of riboflavin in DMSO is more complicated than that of simpler organic compounds (*e.g.*, aromatic hydrocarbons, azo-compounds, quinones) in aprotic solvents. The first step (the reduction wave with  $E_p = -0.78$  V vs. SCE) is clearly a one-electron reduction to the riboflavin anion radical:



All the results indicate, however, that this anion radical,  $\text{Rf}^-$ , is *not stable*. The experimental results are best explained by assuming that the decomposition of  $\text{Rf}^-$  occurs by parallel reactions such as



where A is a substance which is reduced at potentials of the second cathodic wave ( $E_p \sim -1.07$  V) and  $\text{B}^-$  is an anion radical of a substance B whose electrochemical properties are very similar to that of riboflavin itself. This explanation then implies that the radical observed by ESR spectroscopy is  $\text{B}^-$  rather than  $\text{Rf}^-$ . The third cathodic wave during the reduction may be composed of the reductions of Rf,  $\text{Rf}^-$ , B, and  $\text{B}^-$  to the dianions, followed by some following reaction, *e.g.*, protonation. In fact, close observation of the third cathodic wave (Fig. 2) shows that it may be composed of two closely spaced waves.

The anodic waves on reversal of scan in voltammetry may be ascribed to

oxidation of  $B^-$  and  $Rf^-$ , and perhaps another species produced as a product of reactions (2) or (3).

This mechanism also satisfactorily explains the bulk electrolysis, coulometric results. In these long duration experiments, the solution resulting from coulometric reduction will contain A and  $B^-$ , although  $Rf^-$  may appear for a time and may be responsible for the transient spectrophotometric peak at  $400\text{ m}\mu$ . The solution upon oxidation will show a  $Q_b/Q_f$  less than one, since only  $B^-$  will be oxidized, and it will be present in smaller concentrations than the amount of riboflavin originally present. For very short electrolysis times, the oxidation is of  $Rf^-$  and  $B^-$  and  $Q_b/Q_f$  is close to one; at longer times a limiting value is reached.

Electrolysis at  $-1.3\text{ V}$  probably yields reduced forms which rapidly undergo irreversible reactions with the solvent to produce non-electroactive species. This type of behavior is observed in the reduction of aromatic hydrocarbons<sup>7</sup>, where formation of the dianion is followed by a rapid protonation reaction. The cyclic voltammetry experiments in the presence of a proton donor (HQ) indicate that the radical anions can also undergo a protonation reaction when excess acid is present.

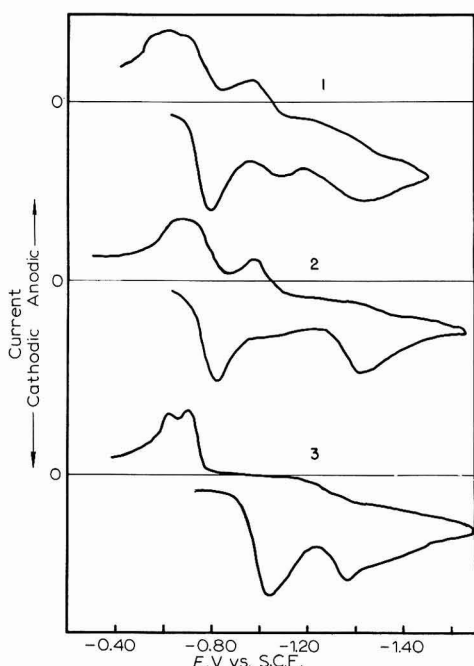


Fig. 6. Cyclic voltammograms of: (1), riboflavin; (2), lumiflavin; (3), lumichrome in DMSO.

In an attempt to identify the species A and B, a brief study of compounds related to riboflavin was undertaken. Lumiflavin (riboflavin with the ribityl at the 9-position replaced by a methyl group), and lumichrome (complete dealkylation at the 9-position, with the molecule in the alloxazine form), known as photochemical decomposition products of riboflavin, were investigated. Typical cyclic voltammo-

grams of these species and riboflavin are shown in Fig. 6. As expected, the electrochemical behavior of lumiflavin is very similar to that of riboflavin. The coulometric reduction of lumiflavin at potentials of the first reduction wave consumes one faraday per mole and produces a solution which shows a strong ESR signal similar to that of riboflavin, but with somewhat better resolution. Lumichrome shows reduction peaks at about -1.1 V and -1.4 V vs. SCE. Another possibility for a product of the reaction of riboflavin anion radical is a dimer of riboflavin. MICHAELIS AND SCHWARZENBACH<sup>10</sup> have reported dimerization reactions in aqueous solutions and the apparent concentration-dependence of the second cathodic wave is suggestive of this kind of reaction. To eliminate the electrode material, supporting electrolyte or solvent as major reactants in the chemical reactions following electron transfer, some experiments were performed using a platinum rather than a mercury electrode, using tetra-*n*-butylammonium iodide or perchlorate rather than NaClO<sub>4</sub> as supporting electrolyte, or using N,N-dimethylformamide rather than DMSO as solvent. The general electrochemical behavior of riboflavin was the same in these experiments. A definite assignment of the products and mechanisms of the following chemical reactions must await better product analysis and further electrochemical studies.

#### EXPERIMENTAL

Riboflavin was obtained from Eastman Organic Chemicals and used without further purification. Its purity was checked by melting point, and coulometry in aqueous solution. Lumiflavin was obtained from Professor DAVID METZLER and Professor GORDON TOLLIN. Lumichrome was obtained from Aldrich Chemical Company. Sodium perchlorate was G. Frederick Smith reagent-grade, and was dried at 120° before use. Dimethylsulfoxide was obtained from Matheson, Coleman and Bell and was purified by treating with anhydrous alumina overnight and then distilling under vacuum. Solutions of riboflavin were protected from light by covering volumetric ware and electrochemical cells with black vinyl tape. Photochemical reactions of riboflavin in DMSO were shown to occur when the solutions were exposed to sunlight or strong ultraviolet light.

The procedures and apparatus for the electrochemical studies were generally as described previously<sup>7</sup>. In some experiments, the solutions were de-aerated with purified nitrogen, and in others vacuum line techniques<sup>7</sup> were employed with no difference in electrochemical behavior. Spectrophotometry was carried out by pumping solution from the electrolysis cell through Tygon tubing to a quartz flow cell contained in a Cary Model 14 spectrophotometer. A Varian V-4502-14 spectrometer was employed for ESR studies.

#### ACKNOWLEDGEMENTS

The support of this research by the National Science Foundation (GP-1921) and the Robert A. Welch Foundation is gratefully acknowledged. We are indebted to Professors DAVID METZLER and GORDON TOLLIN for providing samples of lumiflavin. The ESR instrument was purchased from funds provided by the National Science Foundation (Grant No. GP-2090).

## SUMMARY

The electroreduction of riboflavin in dimethylsulfoxide solutions at a mercury electrode was studied by polarographic, cyclic voltammetric and coulometric techniques. The solutions produced upon reduction were examined by electron spin resonance spectroscopy and spectrophotometry. A mechanism for the reaction, based on an initial one-electron transfer to form the riboflavin radical anion which decomposes by two parallel reactions, is proposed.

## REFERENCES

- 1 L. MICHAELIS, M. P. SHUBERT AND C. V. SMYTHE, *J. Biol. Chem.*, **116** (1936) 587; L. MICHAELIS AND G. SCHWARZENBACH, *ibid.*, **123** (1938) 527.
- 2 A. EHRENBURG, *Electronic Aspects of Biochemistry*, Academic Press, Inc., New York, N.Y., 1964, pp. 379-396; A. V. GUZZO AND G. TOLLIN, *Arch. Biochem. Biophys.*, **105** (1964) 380 and references contained therein.
- 3 R. BRDIČKA, *Z. Elektrochem.*, **47** (1948) 721; *ibid.*, **48** (1942) 278, 686; B. KE, *Arch. Biochem. Biophys.*, **68** (1957) 339.
- 4 B. BREYER AND T. BIEGLER, *Collection Czechoslov. Chem. Commun.*, **25** (1960) 3348; S. V. TATWAWADI AND A. J. BARD, *Anal. Chem.*, **36** (1964) 2; A. M. HARTLEY AND G. S. WILSON, *ibid.*, **38** (1966) 686; T. BIEGLER AND H. A. LAITINEN, *J. Phys. Chem.*, **68** (1964) 2374.
- 5 J. N. BUTLER, *J. Electroanal. Chem.*, **14** (1967) 89; C. K. MANN, *Electroanalytical Chemistry. A Series of Advances*, Vol. III, edited by A. J. BARD, Marcel Dekker, Inc., New York, N.Y., in press.
- 6 R. S. NICHOLSON, *Anal. Chem.*, **38** (1960) 1406.
- 7 K. S. V. SANTHANAM AND A. J. BARD, *J. Am. Chem. Soc.*, **88** (1964) 2676.
- 8 A. J. BARD AND S. V. TATWAWADI, *J. Phys. Chem.*, **68** (1964) 2676.
- 9 J. KOZIOL, *Photochem. and Photobiol.*, **5** (1966) 41.
- 10 L. MICHAELIS AND G. SCHWARZENBACH, *J. Biol. Chem.*, **123** (1938) 527.

*J. Electroanal. Chem.*, **17** (1968) 411-420

## SHORT COMMUNICATIONS

### The differential capacitance of zinc in aqueous solution

#### Introduction

The kinetics of exchange of zinc in alkali have recently been investigated<sup>1,2</sup> using both polycrystalline and single crystal (0001) electrodes. The very high value obtained for the frequency-independent capacity ( $C_0$ ) shunting the double layer has been attributed in part to the adsorption of  $\text{OH}^-$  on to the electrode surface.

Russian workers<sup>3,4</sup> have independently reported differential capacitance curves for single crystal and polycrystalline surfaces of zinc in aqueous  $\text{KCl}$  (pH 7) and  $\text{Na}_2\text{SO}_4$  (pH 3) electrolytes; however, the Russian reports differ from each other in the values of the p.z.c. (point of zero charge) obtained from the capacitance minima, in the shapes of the curves, and in the extent of the observed regions of polarizability.

Previously<sup>5,6</sup>, differential capacitance measurements on  $\text{Ag}$  and  $\text{Cd}$  in aqueous solution have been reported. The results of similar measurements on polycrystalline and single crystal (0001) zinc surfaces are reported in the present paper.

#### Experimental

Details of the electrolytic cell, electrode construction, electrolyte purification and electrical circuit (by which the electrode impedance is matched as a series combination of resistive,  $R_E$ , and capacitive,  $C_L$ , components) have been described previously<sup>1,5</sup>. Electrodes were mechanically polished (on roughened glass lubricated with water) and/or chemically etched (10%  $\text{HClO}_4$ ): single crystal electrodes were chemically etched only. Electrochemical etching was found to be unsatisfactory as electrode pre-treatment; with acid etching media, the frequent observation of low  $C_L$ -values indicated the possible presence of a film on the electrode (cf.  $\text{Ag}^5$ ).

Differential capacitance curves corresponding to single crystal electrodes were determined in aqueous  $\text{KCl}$  and  $\text{NaClO}_4$ ; similar experiments with polycrystalline electrodes were conducted in aqueous  $\text{KCl}$ ,  $\text{NaClO}_4$ ,  $\text{KNO}_3$  and  $\text{Na}_2\text{SO}_4$ .

#### Results

*Single crystal electrodes.* Electrometric measurements indicated that a small polarizable region was located near  $-0.9$  V (NHE). Figure 1 shows differential capacitance curves for single crystal electrodes in  $\text{KCl}$  electrolytes; the polarizable region extended from  $-0.8$  to  $-1.20$  V (similar values were obtained with the other electrolytes). The dashed curve in Fig. 1 shows the variation of  $R_E$  with potential. Hydrogen evolution was observed from the (0001) basal plane at  $-1.47$  V. On returning the potential to the polarizable region after an excursion beyond  $-1.02$  V (even to  $-1.5$  V),  $C_L$ -values characteristic of the polarizable region were rapidly re-established. On certain single crystal electrodes which had exposed higher index planes at the edge, hydrogen evolution was observed from this edge at potentials less cathodic than  $-1.47$  V. Notable features of the behaviour of the single crystal electrode was the reproducibility ( $\sim \pm 5\%$  variation between replicate electrodes) and the relatively

short time (30 min) of electrode/electrolyte contact required initially for the time stability of the impedance.

*Polycrystalline electrodes.* Figure 2 shows differential capacitance (and  $R_E$ ) for polycrystalline electrodes in KCl electrolytes. Reproducibility was  $\sim \pm 10\%$  of the typical mean results illustrated. The inserted curve illustrates the extent of polarizability, the polarizable region extended from about -0.8 to -0.98 V. Hydrogen evolution was observed at -1.3 V. A small shift in the minima of these curves to more positive values at greater dilution was noticed. The shapes of the curves obtained with  $\text{Na}_2\text{SO}_4$ ,  $\text{KNO}_3$ ,  $\text{NaClO}_4$  and KCl were similar. In the region of the capacitance minima, all the curves were broad and flat.

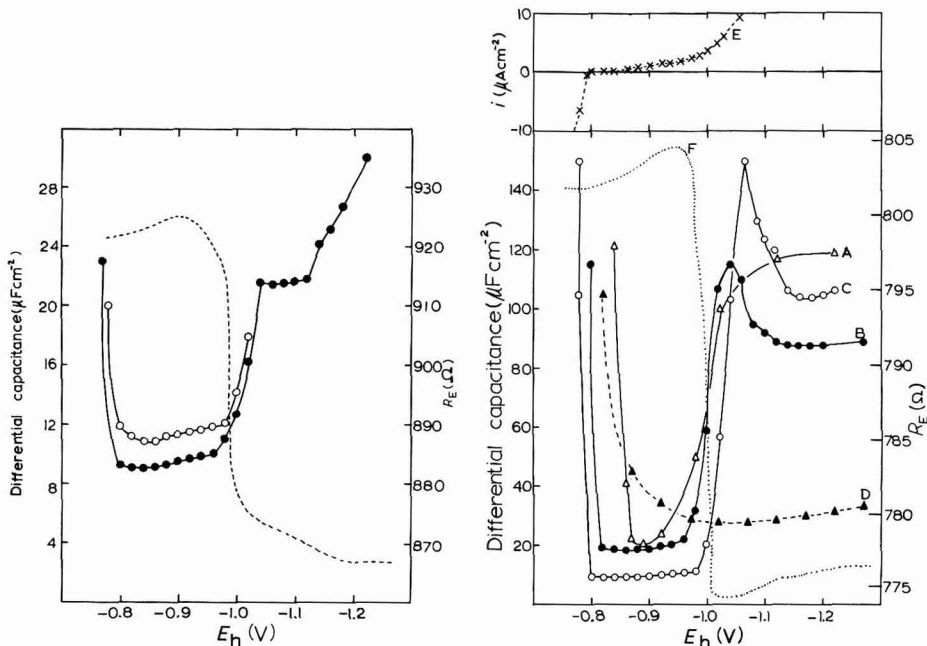


Fig. 1. Differential capacitance curves for single crystal zinc electrodes in aq. KCl electrolytes.  $25^\circ$ ; 1 kc/sec; chemical etch (10%  $\text{HClO}_4$ ); superficial area,  $11.3 \cdot 10^{-2} \text{ cm}^2$ . (○), 0.1 M KCl; (●), 0.01 M KCl; (---),  $R_E$  for 0.01 M KCl.

Fig. 2. Differential capacitance curves for polycrystalline zinc electrodes in aq. KCl electrolytes.  $25^\circ$ ; 1 kc/sec; chemical etch (10%  $\text{HClO}_4$ ); superficial area,  $9.1 \cdot 10^{-2} \text{ cm}^2$ . (A), 1.0 M KCl; (B), 0.1 M KCl; (C), 0.01 M KCl; (D), 1.0 M KCl, electrode polarized at potentials more anodic than -0.8 V; (E), faradaic current curve corresponding to C; (F),  $R_E$  for electrode corresponding to C (mean value).

A dispersion of capacitance with frequency was observed at all electrodes even within the polarizable region; this was greatest in the case of polycrystals (Fig. 3). Electrodes polarized more cathodically than -1.25 V exhibited a greater frequency-dependence of capacitance than those corresponding to Fig. 3.

Polycrystalline electrodes required a long electrode/electrolyte contact time for equilibration particularly if etching had been omitted. In concentrated (1 M) electrolyte, stabilization of chemically etched electrodes was observed after the initial 12 h; for dilute electrolytes (0.01 M) the requirement was reduced to 2 h.

Electrodes dipped in NaOH ( $1\text{ M}$ ) and thoroughly washed with water or electrolyte out of contact with air showed very high capacitances,  $\sim 150\ \mu\text{Fcm}^{-2}$ , which persisted for long times. The effect could be removed by lightly etching the electrode in  $\text{HClO}_4$  (10%) when, after washing, the characteristic capacitance was observed; normal capacitances were found on electrodes treated initially with neutral and acid electrolytes.

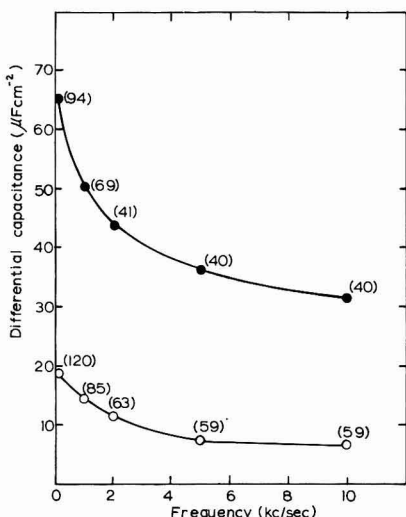


Fig. 3. Dispersion of capacitance for polycrystalline and single crystal zinc electrodes.  $0.5\text{ M KCl}$ ;  $25^\circ$ ; chemical etch (10%  $\text{HClO}_4$ );  $-0.98\text{ V}$ . (●), Polycrystalline electrode; (○), Single crystal electrode.  $R_E$ -values are given in parenthesis ( $\Omega$ ).

### Discussion

Differential capacitance curves characteristic of the surface at the instant of electrode/electrolyte contact were not feasible because of changes in  $C_L$  during the time required to make bridge measurements. A process of surface stabilization is indicated by the smaller time-dependence of  $C_L$  on the most stable, basal, plane. The small time-dependence on this face is possibly connected with the removal of atoms in the double-layer charging process. It might be expected that more extensive recrystallization would ensue at the surface of a polycrystalline electrode. It is interesting that a shorter time is required for electrodes to stabilize in dilute than in concentrated electrolytes. A recrystallization taking some hours might be thought to penetrate many atomic layers. The observed dependence on electrolyte concentration suggests the operation of local cells.

Some frequency dispersion was observed by previous workers<sup>3,4</sup>; the present work has confirmed the order of frequency dispersion reported at different types of electrode. Various explanations are possible, it should be remembered that the electrode is not ideally polarizable (Fig. 2). The results of polarizability experiments indicate clearly that the close-packed (0001) plane is less effective for the discharge of hydrogen ions than the polycrystalline surface.

Figure 2 includes a capacitance curve, D, corresponding to an electrode previously polarized anodically. The difference between this curve and curve A is due to

a film on the electrode, which could be clearly seen. The higher value of the capacitance observed within the polarizable region is probably due to pseudo-capacitance associated with adsorbed OH<sup>-</sup> produced during the anodic excursion (*cf.* low capacitance caused by electrolytically etching in acid conditions). The observation of high capacitances when OH<sup>-</sup> ions are associated with zinc electrodes confirms recent work on the a.c. impedance of zinc in alkali. OH<sup>-</sup> is strongly adsorbed on zinc as indicated by the persistence of high electrode capacitances of electrodes treated in NaOH. It has been suggested<sup>2</sup> that in the presence of OH<sup>-</sup>, adatoms (atoms of low coordination number on the surface of the electrode) are stabilized by OH<sup>-</sup> bonding. Increases in the resistive component of the electrode impedance as the electrode potential is swept anodically over the range -1.4 to -1.2 V indicate interaction of anions (probably OH<sup>-</sup>) and the electrode surface.

Crossing of  $C_L-E_h$  curves at high negative potentials (Fig. 2) is probably due to small pH differences (1 M—pH 7; 0.01 M—pH 6.6).

#### Acknowledgement

One of us (D.L.) thanks the Science Research Council for a grant. Professors R. F. PHILLIPS and E. C. ROLLASON are thanked for their interest.

*Department of Chemistry,  
Loughborough University of Technology,  
Leicestershire (England)*

D. S. BROWN
J. P. G. FARR*
N. A. HAMPSON
D. LARKIN
C. LEWIS

- 1 J. P. G. FARR AND N. A. HAMPSON, *Trans. Faraday Soc.*, 62 (1966) 3493.
- 2 J. P. G. FARR AND N. A. HAMPSON, *J. Electroanal. Chem.*, 13 (1967) 433.
- 3 B. S. KRASIKOV AND V. A. SYSOEVA, *Dokl. Akad. Nauk SSSR*, 114 (1957) 826.
- 4 C.-S. TZA AND Z. A. IOFA, *Dokl. Akad. Nauk SSSR*, 131 (1960) 137.
- 5 N. A. HAMPSON, D. LARKIN AND J. R. MORLEY, *J. Electrochem. Soc.*, 114 (1967) 817.
- 6 N. A. HAMPSON AND D. LARKIN, *J. Electrochem. Soc.*, 114 (1967) 933.

Received October 23rd, 1967

---

\* Joseph Lucas Fellow, Department of Industrial Metallurgy, University of Birmingham, England.

### Courants d'induction électromagnétique en solutions d'électrolytes

Un champ magnétique constant appliqué à une solution d'électrolyte se trouvant dans un champ électrique peut produire soit un déplacement de certaines particules ou molécules neutres en suspension dans l'électrolyte (effet électromagnétophorétique)<sup>1</sup> soit le déplacement de la masse même de la solution d'électrolyte (effet magnétohydrodynamique)<sup>2</sup>.

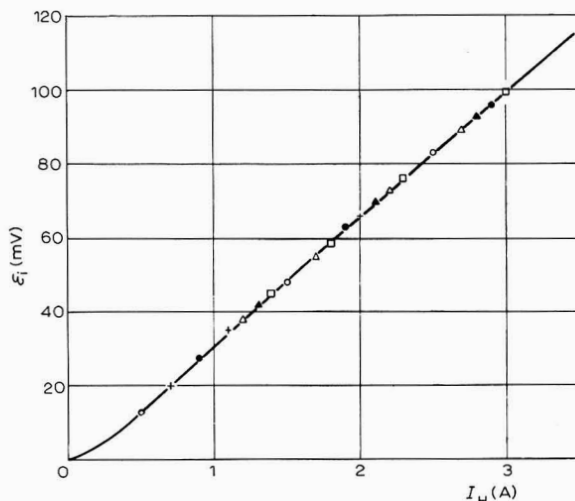


Fig. 1. Variation de la force électromotrice induite,  $\varepsilon_i$ , en fonction du courant d'alimentation du champ magnétique,  $I_H$ , pour quelques solutions de natures et de résistances différentes; 25°.  
 $\text{H}_2\text{SO}_4$ : (○), 64  $\Omega$ ; (●), 13.000  $\Omega$ ,  $\text{CoCl}_2$ : (△), 540  $\Omega$ ; (▲), 33.500  $\Omega$ ,  $\text{K}_2\text{SO}_4$ : + 1.850  $\Omega$ ,  $\text{NaOH}$ : (□), 4.900  $\Omega$ .

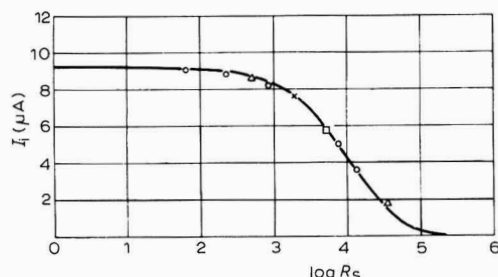


Fig. 2. Variation du courant alternatif induit,  $I_i$ , débité sur une résistance fixe de 10.5 k $\Omega$ , en fonction de la valeur de la résistance de la solution d'électrolyte. (○),  $\text{H}_2\text{SO}_4$ ; (△),  $\text{CoCl}_2$ ; (×),  $\text{K}_2\text{SO}_4$ ; (□),  $\text{NaOH}$ .  $I_H = 3$  A.

L'effet d'un champ magnétique variable est tout à fait différent. Sous l'action d'un champ magnétique alternatif, une solution d'électrolyte se comporte d'une manière analogue à celle d'un conducteur métallique. Quelques résultats sont montrés dans les Figs. 1 et 2 et dans le Tableau 1. Les déterminations ont été faites sur un

conducteur électrolytique sous la forme d'une colonne de solution de 23 cm de longueur dont le diamètre,  $\phi = 10$  mm, placée horizontalement dans l'entrefer d'un électro-aimant à pièces polaires de 20 mm de diamètre. L'électro-aimant était alimenté par un réseau de courant alternatif à 50 Hz.

TABLEAU 1

Solution	$R(\Omega)$	$R_i(\Omega)$
NaCl	172	213
KCl	175	209
CoCl <sub>2</sub>	170	212
HNO <sub>3</sub>	170	209
H <sub>2</sub> SO <sub>4</sub>	170	217
Constantan	171	209

Dans la Fig. 1 on a représenté la variation de la force électromotrice induite,  $\varepsilon_i$ , dans la colonne d'électrolyte collectée aux bornes de la colonne par l'intermédiaire de deux électrodes inertes, en fonction de l'intensité du courant d'alimentation de l'électro-aimant,  $I_H$ . On a travaillé avec des solutions de nature et de résistance différentes à 25°. Les valeurs mesurées sont représentées par des points; la ligne continue représente la variation de  $\varepsilon_i$  pour un fil de nickéline (longueur 25 cm,  $\phi = 0.2$  mm) de  $R = 1.2 \Omega$ . On y voit clairement, que conformément à la loi de l'induction électromagnétique, la valeur  $\varepsilon_i$  est indépendante de la nature et des propriétés du conducteur du circuit induit.

Dans la Fig. 2 on a représenté la variation du courant  $I_i$  débité par le générateur de courant alternatif sur une résistance fixe de 10.5 kΩ, en fonction de la résistance ohmique de la solution d'électrolyte, à la même valeur du champ magnétique, correspondant au courant  $I_H = 3$  A. Les points expérimentaux se placent pratiquement sur la ligne continue qui représente la même variation pour quelques conducteurs métalliques (nickéline  $\phi = 0.2$  mm, et constantan  $\phi = 0.02$  mm et  $\phi = 0.12$  mm).

Enfin, les déterminations de résistance intérieure du générateur du courant alternatif aux conducteurs métalliques et aux conducteurs ioniques (par le tracé de la caractéristique extérieure) présentées dans le Tableau 1 montrent la même identité de comportement. La résistance intérieure  $R_i$  a pratiquement la même valeur, indifféremment de la nature du conducteur,  $R_i = 212 \pm 3 \Omega$  pour la même valeur de la résistance ohmique des conducteurs  $R \cong 170 \Omega$ . Les expériences ont été faites avec un champ magnétique correspondant au courant de  $I_H = 3$  A.

*Institut de Physique Atomique,  
Section de Cluj (Roumanie)*

R. V. BUCUR  
V. MORARIU

<sup>1</sup> D. LEENOV ET A. KOLIN, *J. Chem. Phys.*, 22 (1954) 683.

<sup>2</sup> E. Z. GAK ET G. R. RIK, *Dokl. Akad. Nauk SSSR*, 175 (1967) 856.

Reçu le 24 octobre 1967

## La réaction déterminante de potentiel à l'électrode $\beta$ -(Pd-H)/H<sub>2</sub>

La réaction déterminante de potentiel aux électrodes palladium-hydrogène, est analogue avec celle des électrodes réversibles à hydrogène



avec la particularité que la pression partielle du gaz est déterminée par l'équilibre thermodynamique entre l'hydrogène dissous dans le métal et la couche d'hydrogène moléculaire adsorbé sur la surface<sup>1</sup>. Pour les électrodes  $\alpha$ -(Pd-H)/H<sub>2</sub><sup>2</sup> et  $(\alpha + \beta)$ -(Pd-H)/H<sub>2</sub><sup>1</sup> cela a déjà été prouvé expérimentalement en utilisant les données thermodynamiques, mesurées à l'équilibre dans la phase gazeuse, au calcul du potentiel des électrodes.

Les électrodes  $\beta$ -(Pd-H)/H<sub>2</sub> présentent le même comportement pendant l'absorption du gaz de la solution. En effet, la variation du potentiel d'une électrode palladium-hydrogène, mesurée par rapport à une électrode réversible à hydrogène dans la même solution, a pour expression l'équation de Nernst<sup>1</sup>

$$\varepsilon(t) = (RT/nF) \ln P_{\text{H}_2} - (RT/nF) \ln p_e(t) \quad (2)$$

où  $P_{\text{H}_2}$  est la pression de l'hydrogène sur l'électrode réversible, et  $p_e(t)$  la pression correspondante sur l'électrode palladium-hydrogène. Comme  $P_{\text{H}_2} = \text{const.}$ , il en résulte que dans la représentation graphique des paires de valeurs  $\varepsilon(t)$  et  $\ln p_e(t)$ , prises à des différents moments, on doit obtenir une dépendance linéaire. Du moment que l'équilibre thermodynamique entre l'hydrogène à l'interface et celui dissous en palladium est réalisé, en dépit du fait que l'équilibre d'absorption n'est pas encore établi, la pression  $p_e(t)$  peut-être exprimée à l'aide de l'isotherme d'équilibre de la phase gazeuse<sup>3,4</sup>.

$$p_e(t) = K_\beta r(t) / \{r_\infty - r(t)\} \quad (3)$$

où  $r(t)$  représente la composition de la phase  $\beta$  exprimée par le rapport atomique H/Pd. En combinant l'éqn. (2) avec (3) on obtient

$$\varepsilon(t) = \frac{RT}{nF} \ln P_{\text{H}_2} - \frac{RT}{nF} \ln K_\beta - \frac{RT}{nF} \ln \frac{r(t)}{r_\infty - r(t)} \quad (4)$$

Dans la Fig. 1 on a représenté par des points, les valeurs correspondantes aux paires de grandeurs mesurées à une électrode  $\beta$ -(Pd-H)/H<sub>2</sub> en solution H<sub>2</sub>SO<sub>4</sub> 2 N, 25°. La détermination du contenu d'hydrogène dans le palladium a été faite avec la méthode de l'oxydation anodique à tension linéairement variable, décrite dans un travail antérieur<sup>5</sup>. À cause de la difficulté d'une détermination précise de la pesanteur de l'électrode de palladium et par conséquent du rapport atomique  $r$ , on a porté sur l'abscisse de la Fig. 1, le logarithme du rapport des intégrales des courbes courant-temps;  $S_\infty$  a été mesuré à l'équilibrage de l'électrode avec l'hydrogène de la source extérieure, à la pression  $P_{\text{H}_2} (\varepsilon=0)$ .

Sur la même figure on a tracé les droites théoriques calculées avec l'éqn. (4), à  $P_{\text{H}_2} = 0.987 - \log P_{\text{H}_2\text{o}}(\text{atm})^*$  et avec l'expression de la constante d'équilibre

\*  $P_{\text{H}_2\text{o}}$  est la pression partielle de l'eau à la température respective.

$\ln K_\beta = 4.915 - 2140/T^3$ , pour  $n=1$  et  $n=2$ . On constate que l'expression de l'isotherme d'absorption pour la phase  $\beta$  calculée en conditions d'équilibre dans la phase gazeuse, peut-être utilisée avec des bons résultats dans des calculs électrochimiques. Cela prouve également que dans le cas des électrodes  $\beta$ -(Pd-H)/H<sub>2</sub> *en régime d'absorption* il y a une équilibre thermodynamique entre l'hydrogène qui se trouve dans la couche superficielle et celui de l'intérieur du palladium. De même il est évident que, aussi sur ces électrodes, l'hydrogène participe en état moléculaire à la réaction déterminante de potentiel ( $n=2$ ).

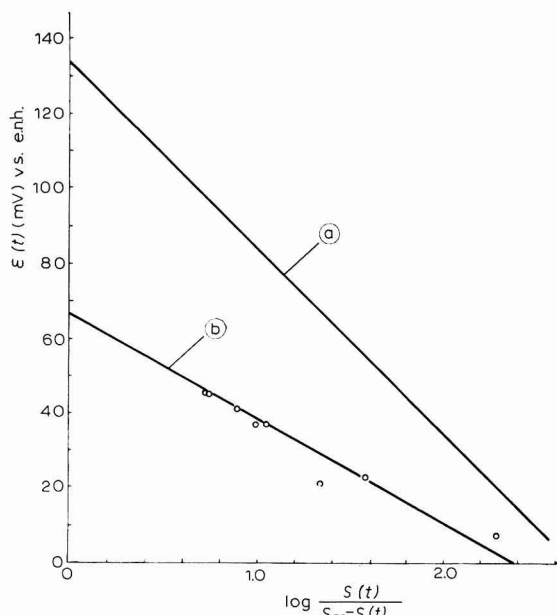


Fig. 1. La dépendance du potentiel de l'électrode  $\beta$ -(Pd-H)/H<sub>2</sub> du contenu d'hydrogène dissous en palladium, H<sub>2</sub>SO<sub>4</sub> 2 N, 25°. (a)  $n=1$ ; (b),  $n=2$ .

### Remerciements

J'adresse des remerciements à Mme. LIVIA STOICOVICIU pour ses observations regardant la rédaction de ce travail.

*Institut de Physique Atomique,  
Section de Cluj (Roumanie)*

R. V. BUCUR

- 1 R. V. BUCUR, *Rev. Phys. Acad. Rep. Populare Romine*, 6 (1961) 269, 571; *Acad. Rep. Populare Romine Studii. Cercetari Chim.*, 12 (1964) 171.
- 2 M. J. VASILE ET C. G. ENKE, *J. Electrochem. Soc.*, 112 (1965) 865.
- 3 R. V. BUCUR, *Rev. Phys. Acad. Rep. Populare Romine*, 6 (1961) 583.
- 4 R. V. BUCUR ET M. CRISAN, *J. Phys. Chem. Solids*, 28 (1967) 995.
- 5 R. V. BUCUR, *J. Electroanal. Chem.*, 10 (1965) 8.

Reçu le 3 octobre 1967

## Potentiometrischer Isotopieeffekt an der Pd/H-Elektrode in deuterierter essigsaurer Lösung

Der Isotopieeffekt des Potentials der  $(\text{Pd}-\text{H})_{\alpha\beta}$ -Elektrode beträgt in vollständig deuterierter Lösung nach Messungen von SCHULDINER UND HOARE<sup>1</sup> sowie FLANAGAN<sup>2</sup> etwa 20 mV. Im Hinblick auf eine eventuelle analytische Anwendung wäre eine Vergrösserung des messbaren Effektes wünschenswert, wie sie unter Ausnutzung des Isotopieeffektes der Dissoziation in Lösungen schwacher Säuren erreicht werden kann. Wir arbeiteten in essigsaurer Lösung, wobei die der maximalen Leitfähigkeit entsprechende Konzentration ( $2.92 \text{ M}$ ) gewählt wurde. Als Referenzelektrode diente eine gesättigte Kalomelektrode. Nach jeweils einer anodischen Oxydation sollte die spontane Wasserstoffaufnahme der Palladiumelektrode potentiometrisch verfolgt werden, bis der dem Koexistenzgebiet von  $\alpha$ - und  $\beta$ -Phase entsprechende konstante Wert erreicht war. In essigsaurer Lösung ergab sich jedoch keine völlige Konstanz, sondern es verblieb ein geringer zeitlicher Potentialanstieg. Die zehn Minuten nach "Plateau" beginn registrierten Potentialwerte waren ziemlich gut reproduzierbar und wurden—etwas willkürlich—in Beziehung zu der relativen D-Häufigkeit der Lösung gesetzt. Die erhaltenen Werte sind in folgender Tabelle zusammengestellt:

rel. Häufigkeit des Deuteriums (Atom-%)	Isotopieeffekt (mV)
22.6	1.2
39.8	4.8
67.2	12.0
93.6	25.0
100 (extr.)	30

Neben der erwarteten Vergrösserung des Isotopieeffekts in vollständig deuterierter Lösung von 20–30 mV überrascht vor allem, dass sich ein nennenswerter Effekt erst oberhalb von 25 Atom-% D bemerkbar macht. Die Ursachen hierfür sind noch ungeklärt.

Für die zur Durchführung dieser Versuche gewährte Gastfreundschaft im Institut für Atomphysik in Cluj/Rumänien sei herzlich gedankt, besonders auch Frau L. STOICOVICI und Herrn Dr. BUCUR.

Institut für stabile Isotope,  
Leipzig (DDR)

K. MAUERSBERGER

<sup>1</sup> S. SCHULDINER UND J. P. HOARE, *J. Electrochem. Soc.*, 105 (1958) 278.  
<sup>2</sup> T. B. FLANAGAN, *J. Phys. Chem.*, 65 (1961) 280; R. V. BUCUR, *Rev. Phys. Akad. Rep. Populaire Roumaine*, 6 (1961) 269.

Eingegangen am 20. November 1967

### Elimination of formaldehyde, prior to the polarographic determination of aromatic carbonyl compounds

The presence of formaldehyde may in some cases interfere with the determination of other carbonyl compounds but this can be avoided, as far as aromatic carbonyl compounds are concerned, by using 0.1 M HCl as supporting electrolyte<sup>1,2</sup> as it is well known<sup>3</sup> that formaldehyde does not give a wave at low pH-values. However, some compounds (*e.g.*, salicylaldehyde) give a wave that precedes the H<sup>+</sup>-wave too closely for exact measurements of their wave height at this pH.

An alternative method is the dimedon method<sup>4,5</sup> although it may be objected that the condensation between formaldehyde and dimedon is only complete within a narrow pH-range ( $\pm 4.5$ )<sup>6,7</sup> that is unfavourable for good polarograms because of doubling of the wave<sup>8,9</sup>. Therefore, it is necessary after a reaction time of about 16 min to make the solution alkaline and de-aerate before running the polarogram.

Compared with this method the cyanohydrin reaction is simpler. The reaction velocity<sup>10–12</sup>, as well as the equilibrium constant<sup>13</sup>, depend strongly on the nature of the compounds considered. Aldehydes generally react faster than ketones, and aromatic ketones should not react at all. Formaldehyde appears to be especially highly reactive so that its elimination from a mixture seems feasible. A closer examination

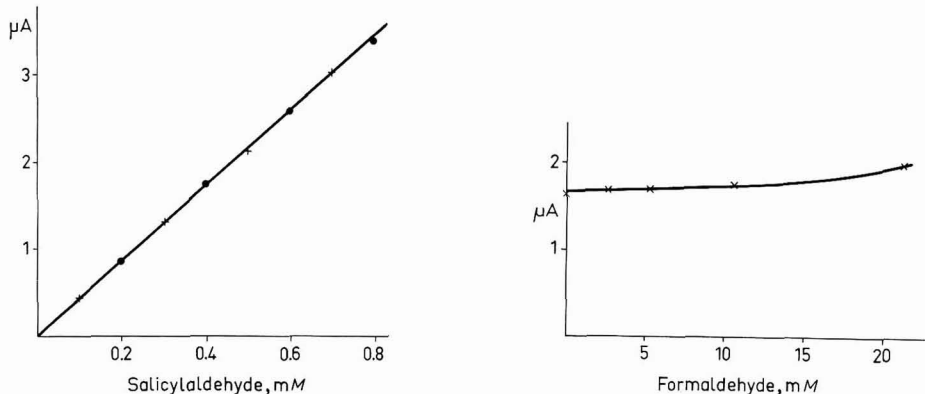


Fig. 1. Calibration curve for salicylaldehyde. (+), Original concn. of formaldehyde  $10^{-2}$  M; (●), formaldehyde absent.

Fig. 2. Limiting current of  $4 \cdot 10^{-4}$  M salicylaldehyde as function of formaldehyde concn.

shows that the statement regarding the non-reactivity of aromatic ketones should not be taken in the absolute sense, for in the medium used, the wave height of acetophenone decreased 0.2%/min. This necessitates the standardization of the time between the addition of cyanide and starting the polarograph. This period, which may be used for expelling oxygen, was fixed at 20 min.

The composition of the medium was: 10 ml 0.2 M KOH, 0.1 ml 0.1% gelatine,  $x$  ml formaldehyde,  $y$  ml carbonyl solution,  $9 - x - y$  ml H<sub>2</sub>O, and finally, 5 ml 0.2 M KCN.

Figure 1 shows that the calibration curve for salicylaldehyde, the half-wave potential of which almost coincides with that for formaldehyde, is not affected by the presence of the latter. According to Fig. 2, a ratio of 15 between the formaldehyde and salicylaldehyde concentrations, expressed in molarities, does not affect the results.

*Laboratory of Analytical Chemistry,  
Technological University,  
Delft (Netherlands)*

H. L. KIES

- 1 I. A. KORSHUNOV AND L. N. SAZANOVA, *J. Phys. Chem. USSR*, 23 (1949) 202.
- 2 T. A. KRJUKOWA, S. I. SINJAKOWA AND T. W. AREFJEWA, *Polarographische Analyse*, VEB Verlag, Leipzig, 1963, p. 435.
- 3 K. VESELÝ AND R. BRDIČKA, *Collection Czech. Chem. Commun.*, 12 (1947) 313.
- 4 S. SANDLER AND Y. H. CHUNG, *Anal. Chem.*, 30 (1958) 1252.
- 5 M. B. NEIMAN AND M. I. GERBEN, *Zh. Anal. Khim.*, 2 (1947) 135.
- 6 N. D. CHERONIS AND I. S. MA, *Organic Functional Group Analysis*, Interscience Publishers, New York, 1964, p. 147.
- 7 J. H. YOE AND L. C. REID, *Ind. Eng. Chem., Anal. Ed.*, 13 (1941) 238.
- 8 R. PASTERNAK, *Helv. Chim. Acta*, 31 (1948) 753.
- 9 M. ASHWORTH, *Collection Czech. Chem. Commun.*, 13 (1948) 229.
- 10 A. J. ULTÉE, *Rec. Trav. Chim.*, 28 (1909) 1, 248.
- 11 A. J. ULTÉE, *Ber.*, 39 (1906) 1856.
- 12 G. G. GUILBAULD AND D. N. KRAMER, *Anal. Chem.*, 38 (1966) 834.
- 13 P. ZUMAN AND F. SANTAVÝ, *Collection Czech. Chem. Commun.*, 19 (1954) 174.

Received November 16th, 1967

*J. Electroanal. Chem.*, 17 (1968) 430-431

## BOOK REVIEW

---

*The Kinetics of Proton Transfer Processes, Discussions of the Faraday Society*, 39 (1965); 278 pages; price 75 sh.

The Faraday Society Discussion on the *Kinetics of Proton Transfer Processes* held at Newcastle in 1965 was a memorable and exciting conference. The papers were generally of a high standard and delivered by authorities of international reputation. The selection of topics to mention in a review is therefore an invidious and possibly dangerous task, but I would single out firstly the introductory paper by EIGEN in which he puts forward the co-operative mechanism to explain why certain proton transfer reactions obey the Brønsted catalysis law too well.

An interesting group of papers showed how much one can find out about the transition state from a study of isotope effects (BELL), from proton tunnelling (CALDIN AND KASPARIAN), and from the solvent isotope effect (GOLD AND KESSICK). CHALLIS AND LONG described detailed work on the rates of proton transfer to and from azulene which supports a two-step mechanism for isotopic exchange. In the field of more rapid reactions, GRUNWALD AND COCIVERA described the elegant work that has been done with NMR on proton transfers in amine systems, WELLER and co-authors dealt with proton transfers in excited molecules studied by fluorescence, and KREEVOY

AND MEAD reported results of the relatively new technique of Raman broadening on trifluoroacetate ion.

Various themes recurred throughout the conference, some of the most important being the detailed information that a sophisticated use of deuterium and tritium can obtain, the role of the solvent in providing "bridges" for proton transfers, the effect of proton tunnelling and the comparison between homogeneous proton transfers and discharge of  $H^+$  at an electrode.

All in all, twenty papers were delivered. Each group of two or three papers was followed by discussion, most of which was useful, and some of which was pretty lively. Almost twenty pages of what was said at the time and what was communicated afterwards are devoted to the controversy between BOCKRIS and CONWAY on the role of tunnelling in the discharge of protons at an electrode; one realises now what it was like to have Popes both at Avignon and Rome.

This account of the conference costs only 75/- and is worth every penny of it.

W. J. ALBERY, Oxford University

*J. Electroanal. Chem.*, 17 (1968) 431-432

## ERRATUM

---

### ERRATUM

H. C. GAUR AND H. L. JINDAL, On the applicability of the Heyrovský-Ilkovič equation in the polarography of molten salts using solid microelectrodes, *J. Electroanal. Chem.*, 16 (1968) 437-439.

In eqn. (1),  $E_{\frac{1}{2}}$  should be replaced by  $E_{\text{const.}}$

*J. Electroanal. Chem.*, 17 (1968) 432

## ANNOUNCEMENT

---

### DIGITAL COMPUTERS IN CHEMICAL INSTRUMENTATION SHORT COURSE, PURDUE UNIVERSITY, JUNE 9-28, 1968

The course is designed to provide a sound introduction to the use of the small digital computer in the laboratory. The principles and practices involved in the application of digital techniques will be discussed. Three weeks of intensive lectures will deal with the elements of digital logic, digital data acquisition techniques, and the use of the on-line digital computer in chemical instrumentation. In addition, there will be ample opportunity for laboratory experience with the designing of digital logic circuits, interfacing chemical instrumentation to the digital computer, and programming the small digital computer.

*J. Electroanal. Chem.*, 17 (1968) 432

JOURNAL OF ELECTROANALYTICAL CHEMISTRY AND INTERFACIAL  
ELECTROCHEMISTRY, VOL. 17 (1968)

AUTHOR INDEX

ABD EL KADER, J. M.	401	KORYTA, J.	167, 177, 185
ANDRZEJCZAK, J.	101	KUMAR, A.	201
ATREYI, M.	227	LANZA, P.	393
BARD, A. J.	411	LETISSE, G.	371, 387
BAUER, H. H.	299	LEWIS, C.	420
BENATI, A.	393	LUCA, C.	335
BESSETTE, R. S.	327	LYKLEMA, J.	267
BINDER, H.	111	MAGEARU, V.	335
BIRKE, R. L.	1	MARZLUFF, JR., W. F.	1
BOMBI, G. G.	95	MAUERSBERGER, K.	428
BOS, P.	21	MAZZOCCHIN, G. A.	95
BROWN, D. S.	420	MEITES, L.	253
BURGHARDT, H.	191	MICHLAYR, M.	153
BUTLER, J. N.	309	MITRA, R. P.	227
CONCIALINI, V.	393	MINC, S.	101
COUEIGNOUX, J. M.	245	MORARIU, V.	424
BUCUR, R. V.	241, 424, 426	MORCOS, I.	7
Cox, J. A.	81	OLVER, J. W.	327
DALEN, E. VAN	21	PEYCHAL-HEILING, G.	153
DELAHAY, P.	69, 289	POPA, G.	335
DESIDERI, P. G.	129	PRADÁČ, J.	167, 177, 185
DOLEŽAL, J.	87	RANGARAJAN, S. K.	61
DOSS, K. S. G.	145	RARKIN, D.	420
EL HOSARY, A. A.	137, 238	RICKERT, H.	161
ELVING, P. J.	299	ROFFIA, S.	13
FARR, J. P. G.	420	ROW, R.	161
FIORANI, M.	95	SANDSTEDE, G.	111
FISCHER, H.	7	SANTHANAM, K. S. V.	411
FISCHER, O.	233	SAWYER, D. T.	207
FORMARO, L.	343	SCHUHmann, D.	45, 245
GOUDA, T.	137	SCHULTZ, F. A.	207
GAUR, J. N.	201	SHAMS EL DIN, A. M.	137, 238, 365, 401
GUPTA, R. C.	227	SPRITZER, M. S.	299
GUTMANN, V.	153	STACKELBERG, M. VON	191
HAMPSON, N. A.	420	ŠTĚPÁNEK, J.	233
HARTLEY, A. M.	81	ŠTULÍK, K.	87
HEYROVSKÝ, M.	293	SUSBIELLES, G. G.	289
HIEBERT, A. G.	81	TADROS, T. F.	267
HOLLECK, L.	293, 365, 401	TATWAWADI, S.	411
HOLUB, K.	69, 277	TESSARI, G.	69
INDIRA, K. S.	145	TOSTMANN, K. H.	161
INMAN, D.	319	TRASATTI, S.	343
JÄGER, H.	191	TRÉMILLON, B.	371, 387
JAIN, D. S.	201	VAVŘÍČKA, S.	293
KARP, S.	253	VIANELLO, E.	13
KIES, H. L.	429	VRIES, W. T. DE	31
KIŠOVÁ, L.	233	WRENCH, N. S.	319
KÖHLING, A.	111		

JOURNAL OF ELECTROANALYTICAL CHEMISTRY AND INTERFACIAL  
ELECTROCHEMISTRY, VOL. 17 (1968)

SUBJECT INDEX

Acetonitrile,		Pradac) . . . . .	185
high-sensitivity coulometry in —		Cystine,	
(Bessette, Olver) . . . . .	327	— at Pt and Au electrodes (Koryta,	
Acid-base titrations,		Pradac) . . . . .	167, 177
Pt and C indicator electrodes for —		DAE, see dropping amalgam electrode	
(Doležal, Štulík) . . . . .	87	Deuterated acetic acid solution,	
Acid solutions,		isopic effect on the Pd-H electrode	
effect of gelatin on polarography in		in — (Mauersberger) . . . . .	429
— (Holleck <i>et al.</i> ) . . . . .	401	<i>p</i> -Diacetylbenzene,	
Adatom transport,		reactions preceding the reduction of	
faradaic impedance measurement		— (Fischer <i>et al.</i> ) . . . . .	233
and — (Rangarajan) . . . . .	61	N,N-Dimethylacetamide,	
Alkali-earth metal ions,		polarography of alkali-earth ions in	
polarography of — in aq. solns.		— (Gutmann <i>et al.</i> ) . . . . .	153
(Holleck, Shams El Din) . . . . .	365	<i>p</i> -Dinitrobenzene,	
polarography of — in N,N-dimethyl-		<i>i-V</i> curves of — (Holleck <i>et al.</i> ) . .	293
acetamide (Gutmann <i>et al.</i> ) . . . . .	153	Double-layer capacity,	
Anaesthetics, see local a.		— and impedance measurement	
Aromatic carbonyl compounds,		with DME or DAE (Tessari <i>et al.</i> ) . .	69
elimination of HCHO in detn. of —		— at the pyrolytic graphite electrode	
(Kies) . . . . .	430	(Bauer <i>et al.</i> ) . . . . .	299
Arsenates, basic,		Double-layer charging,	
formation of — in molten KNO <sub>3</sub>		simultaneous consideration of — and	
(Shams El Din, El Hosary) . . . . .	238	faradaic current (Holub) . . . . .	277
Bismuth,		(Susbielles, Delahay) . . . . .	289
polarographic detn. of urine in —		Dropping amalgam electrode,	
(Lanza <i>et al.</i> ) . . . . .	393	double-layer capacity and impedance	
Cadmium complexes,		measurements with — (Tessari <i>et al.</i> )	69
detn. of stability constants of —		Dropping mercury electrode,	
with metal-complex electrodes (Popa		double-layer capacity and impedance	
<i>et al.</i> ) . . . . .	335	measurements with — (Tessari <i>et al.</i> )	69
Calcium amalgam electrode,		EDTA, see molybdenum-EDTA com-	
standard potential of — (Butler) . .	309	plexes	
Carbon indicator electrode,		Electrode processes,	
use of — for acid-base titrations		relaxation of — (Holub) . . . . .	277
(Doležal, Štulík) . . . . .	87	(Susbielles, Delahay) . . . . .	289
Carbon monoxide,		Electrolyte solutions,	
adsorption and oxidation of — on Pt		electromagnetic induction currents in	
with and without adsorbed S (Binder		— (Bucur, Morariu) . . . . .	425
<i>et al.</i> ) . . . . .	111	Electromagnetic induction currents,	
Carbonyl compounds, see aromatic c.c.		— in electrolyte solns. (Bucur, Mor-	
Catalytic current expression,		raru) . . . . .	425
a closed-form — for a 2nd-order reac-		Equilibrium interfacial tension,	
tion (Birke, Marzluff) . . . . .	1	detn. of — with HMDE (Roffia, Vi-	
Constant-current chronopotentiometry,		anello) . . . . .	13
— with current reversal at a Hg-film		Ethylenediaminetetraacetic acid, see	
electrode (Bos, van Dalen) . . . . .	21	molybdenum-EDTA complexes	
distortion of — by double-layer		Faradaic current,	
charging (de Vries) . . . . .	31	simultaneous consideration of — and	
Controlled-potential electrolysis,		double-layer charging (Holub) . . . . .	277
<i>i-t</i> curves in — (Karp, Meites) . .	253	(Susbielles, Delahay) . . . . .	289
Cysteine,		Faradaic impedances(s),	
— at Au and Pt electrodes (Koryta,			

— including resistances and inductances, at an interface (Schuhmann) . . . . .	45	<i>et al.</i> ) . . . . .	227
— measurement and adatom transport (Rangarajan) . . . . .	61	Molybdenum-EDTA complexes (Schultz, Sawyer) . . . . .	307
Formaldehyde, elimination of — in detn. of aromatic carbonyl compounds (Kies) . . . . .	430	Nernst equation, error due to — in a transient system at the RDE (Coueignoux, Schuhmann) . . . . .	245
Formic acid, adsorption and oxidation of — on Pt with and without adsorbed S (Binder <i>et al.</i> ) . . . . .	111	Nitrates, molten, solubility of $\text{Ag}_2\text{O}$ in — (Shams El Din <i>et al.</i> ) . . . . .	137
Gas mixtures, detn. of $\text{H}_2\text{S}/\text{H}_2$ ratio in — at high temperatures (Rickert <i>et al.</i> ) . . . . .	161	standard potentials of Hg electrodes in — (Mazzocchin <i>et al.</i> ) . . . . .	95
Gelatin, effect of — on polarography in acidic soln. (Holleck <i>et al.</i> ) . . . . .	401	Organic polarography, effects of variables in — (Holleck <i>et al.</i> ) . . . . .	293
Glycolaldehyde, adsorption of — at smooth Pt electrode (Trasatti, Formaro) . . . . .	343	Oxalate, see lead-oxalate complexes	
Hanging mercury drop electrode, detn. of equilibrium interfacial tension with — (Roffia, Vianello) . . . . .	13	Oxygen electrode, potentiometric studies with — in molten salts (Wrench, Inman) . . . . .	319
Hydrochloric acid solution, reduction of $\text{IO}_3^-$ in — (Desideri) . . . . .	129	Palladium-hydrogen electrode, isopic effect on the — in deuterated acetic acid soln. (Mauersberger) . . . . .	429
Hydrogen sulfide : hydrogen ratio, detn. of — in gas mixtures at high temperatures (Rickert <i>et al.</i> ) . . . . .	161	potential-determining reaction at the $\beta$ — (Bucur) . . . . .	427
Induction currents, see electromagnetic i.c.		Platinum, adsorption of $\text{HCOOH}$ and CO on — (Binder <i>et al.</i> ) . . . . .	111
Interfacial tension, see equilibrium i.t.		Platinum electrode, smooth, adsorption of glycolaldehyde at — (Trasatti, Formaro) . . . . .	343
Intermediates, reaction rates of — in controlled-potential electrolysis (Karp, Meites) . . . . .	253	Platinum indicator electrode, use of — for acid-base titrations (Doležal, Štulík) . . . . .	87
Iodate, reduction of — in $\text{HCl}$ soln. (Desideri) . . . . .	129	Potential-determining ions, adsorption of — at the $\text{SiO}_2$ -electrolyte interface (Tadros, Lyklema) . . . . .	267
Lead-oxalate complexes, composition and stability constants of — (Jain <i>et al.</i> ) . . . . .	201	Potential of zero charge, detn. of — from capillary liquid rise on metal plates (Morcos, Fischer) . . . . .	7
Local anaesthetics, polarographic detn. of important — (Burghardt <i>et al.</i> ) . . . . .	191	Pyrolytic graphite, disk electrode, double-layer capacity at — (Bauer <i>et al.</i> ) . . . . .	299
Mercury, adsorption of $\text{NCS}^-$ on — (Minc, Andrzejczak) . . . . .	101	RDE, see rotating disk electrode	
standard electrode potentials of — metal and salts in molten nitrates (Mazzocchin <i>et al.</i> ) . . . . .	95	Riboflavin, reduction of — in DMSO (Tatwawadi <i>et al.</i> ) . . . . .	411
Mercury-film electrode, constant-current chronopotentiometry at — (Bos, van Dalen) . . . . .	21	Rotating disk electrode, the Nernst eqn. in a transient system at the — (Coueignoux, Schuhmann) . . . . .	245
preparation and properties of a Pt-based — (Hartley <i>et al.</i> ) . . . . .	81	Second-order reaction, a closed-form catalytic current expression for — (Birke, Marzluff) . . . . .	1
Metal-complex electrodes, — for the study of Zn and Cd complexes (Popa <i>et al.</i> ) . . . . .	335	Silica-aqueous electrolyte interface, adsorption of potential-determining ions at — (Tadros, Lyklema) . . . . .	267
Methacrylic acid, zwitterion formation in copolymers of — and 2-vinylpyridine (Mitra		Silver chloride films, $\text{Ag}:\text{Cl}^-$ in — with an Ag(Hg) cathode (Indira, Doss) . . . . .	145

- Silver-diethylamine complex, see metal-complex electrodes
- Silver oxide,  
solubility of — in molten nitrates (Shams El Din *et al.*) . . . . . 137
- Sodium aluminium chloride, molten, acid-base system in — (Trémillon, Lettise) . . . . . 371  
behavior of protons and O<sup>2-</sup> in — (Trémillon, Lettise) . . . . . 387
- Sodium tetrachloroaluminate, see sodium aluminium chloride
- Sulphydryl-disulfide system, electrode processes of — (Pradáč, Koryta) . . . . . 167, 177, 185
- Thiocyanate ion, adsorption of — on Hg from aq. soln. (Minc, Andrzejczak) . . . . . 101
- Urine, polarographic detn. of Bi in — (Lanza *et al.*) . . . . . 393
- 2-Vinylpyridine, zwitterion formation in copolymers of — and methacrylic acid (Mitra *et al.*) . . . . . 227
- Voltammetry with linear-variable voltage, detn. of overall electrode reaction in — (Bucur) . . . . . 241
- Zinc, differential capacitance of — in aq. soln. (Brown *et al.*) . . . . . 421
- Zinc complexes, detn. of stability constants of — with metal-complex electrodes (Popa *et al.*) . . . . . 335

## CONTENTS

Sur la validité de l'approximation de Nernst en régime transitoire linéaire pour une électrode à disque tournant J. M. COUEIGNOUX ET D. SCHUHMANN (La Plaine Saint-Denis et Bellevue, France) . . . . .	245
Current-time curves in controlled-potential electrolysis and the rates of reactions of intermediates S. KARP AND L. MEITES (Brooklyn, N.Y., U.S.A.) . . . . .	253
Adsorption of potential-determining ions at the silica-aqueous electrolyte interface and the role of some cations T. F. TADROS AND J. LYKLEMA (Wageningen, Netherlands) . . . . .	267
Relaxation of electrode processes with simultaneous consideration of double-layer charging and faradaic current. Part I K. HOLUB (New York, N.Y., U.S.A.) . . . . .	277
Part II G. G. SUSBIELLES AND P. DELAHAY (New York, N.Y., U.S.A.) . . . . .	289
Bermerkungen zur Methodik der organischen Polarographie L. HOLLECK, M. HEYROVSKÝ UND S. VAVŘÍČKA (Bamberg, Deutschland) . . . . .	293
Double-layer capacity at a pyrolytic graphite disk electrode H. H. BAUER, M. S. SPRITZER AND P. J. ELVING (Ann Arbor, Mich., U.S.A.) . . . . .	299
The standard potential of the calcium amalgam electrode J. N. BUTLER (Waltham, Mass., U.S.A.) . . . . .	309
The oxygen electrode in molten salts. Potentiometric measurements N. S. WRENCH AND D. INMAN (London, Great Britain) . . . . .	319
High sensitivity coulometric analysis in acetonitrile R. R. BESETTE AND J. W. OLVER (Amherst, Mass., U.S.A.) . . . . .	327
Electrodes "métal-complexe". III. Electrode $\text{Ag}[[\text{Ag}(\text{Et}_2\text{NH})_2]^+, \text{Et}_2\text{NH}]$ dans l'étude des complexes de Zn(II) et Cd(II) avec la diéthylamine G. POPA, V. MAGEARU ET C. LUCA (Bucarest, Roumanie) . . . . .	335
Kinetics and mechanism of the adsorption of glycolaldehyde on a smooth platinum electrode S. TRASATTI AND L. FORMARO (Milan, Italy) . . . . .	343
Deutung der polarographischen Maxima der Erdalkalionen in wässriger Lösung L. HOLLECK UND A. M. SHAMS EL DIN (Bamberg, Deutschland) . . . . .	365
Propriétés en solution dans le tétrachloroaluminate de sodium fondu I. Systèmes "acide-base" . . . . .	371
II. Comportement des protons et des ions oxyde . . . . .	387
B TRÉMILLON ET G. LETISSE (Paris, France)	
Determination of bismuth content of urine. Polarographic method P. LANZA, V. CONCIALINI AND A. BENATI (Bologna, Italy) . . . . .	395
Über die katalytische und inhibierende Wirkung von Gelatine auf polarographische Reduktionsstufen in saueren Lösungen L. HOLLECK, J. M. ABD EL KADER UND A. M. SHAMS EL DIN (Bamberg, Deutschland) .	401
The electrochemical reduction of riboflavin in dimethylsulfoxide S. V. TATWAWADI, K. S. V. SANTHANAM AND A. J. BARD (Austin, Texas, U.S.A.)	411

*(Continued on the next page)*

*Short communications*

The differential capacitance of zinc in aqueous solution

- D. S. BROWN, J. P. G. FARR, N. A. HAMPSON, D. LARKIN AND C. LEWIS (Loughborough, Great Britain) . . . . . 421

Courants d'induction électromagnétique en solution d'électrolytes

- R. V. BUCUR ET V. MORARIU (Cluj, Roumanie) . . . . . 425

La réaction déterminante de potentiel à l'électrode  $\beta$ -(Pd-H)/H<sub>2</sub>

- R. V. BUCUR (Cluj, Roumanie) . . . . . 427

Potentiometrischer Isotopieeffekt an der Pd/H-Elektrode in deuterierter essigsaurer Lösung

- K. MAUERSBERGER (Leipzig, Deutschland) . . . . . 429

Elimination of formaldehyde, prior to the polarographic determination of aromatic carbonyl compounds

- H. L. KIES (Delft, Netherlands) . . . . . 430

*Book review* . . . . . 431

*Erratum* . . . . . 432

*Announcement* . . . . . 432

*Author index* . . . . . 433

*Subject index* . . . . . 434

